Universidad de Valladolid

OPTIMISATION OF THE ABLATION PROFILES IN CUSTOMISED TREATMENTS FOR LASER CORNEAL REFRACTIVE SURGERY

ANNEX

Published Resources

Research Group “Grupo de Investigación Reconocido (GIR) de Técnicas ópticas de Diagnóstico (TOD)”. Universidad de Valladolid

Preceptor and Director: Jesús M. Merayo-Lloves MD, PhD, MBA

by **Samuel Arba Mosquera**, MSc in Physics, MSc in Environmental Protection, MSc in Sciences of Vision, Student at the postgraduate program “Doctorado en Investigación en Ciencias de la Visión” Instituto de Oftalmobiología Aplicada (IOBA). University of Valladolid, Valladolid, December 14, 2010

TABLE OF CONTENTS
(Índice)

TABLE OF CONTENTS (Índice) iii

Topic A ANALYSIS OF THE CORNEAL ASPHERICITY (Análisis de la asfericidad corneal) 5

Topic B MODEL OF AN ABERRATION-FREE PROFILE (Modelo de un perfil libre de aberraciones) 7

Topic C DECISION TREE ANALYSIS SYSTEM TO OPTIMISE REFRACTIVE SURGERY OUTCOMES (Análisis por árbol de decisión para la optimización de resultados en cirugía refractiva) 9

Topic D ANALYSIS OF THE LOSS OF ABLATION EFFICIENCY AT NON-NORMAL INCIDENCE (Análisis de la pérdida de eficiencia de ablación para incidencia no-normal)..... 11

Topic E CLINICAL EFFECTS OF CYCLOTORSIONAL ERRORS DURING REFRACTIVE SURGERY (Efectos clínicos de los errores de ciclotorsión durante cirugía refractiva)..... 13

Topic F THE EFFECTIVE OPTICAL ZONE AFTER REFRACTIVE SURGERY (La zona óptica efectiva tras cirugía refractiva) 15

Topic G METHOD TO OBJECTIVELY MINIMISE THE ABLATED TISSUE OF A CUSTOMISED ABLATION BASED ON THE ZERNIKE EXPANSION OF THE WAVEFRONT ABERRATION (Método para minimizar objetivamente la cantidad de tejido resecado en una ablación personalizada basada en la expansión de Zernike de la aberración del frente de onda) 17

Topic A ANALYSIS OF THE CORNEAL ASPHERICITY
(Análisis de la asfericidad corneal)

1. de Ortueta D, Arba Mosquera S. Mathematical properties of asphericity: a method to calculate with asphericities. J Refract Surg; 2008; 24: 119-121

2. Arba-Mosquera S, Merayo-Lloves J, de Ortueta D. Asphericity analysis using corneal wavefront and topographic meridional fits. Journal of biomedical optics 2010;15(2):028003

AUTHOR CONTRIBUTIONS

Study concept and design (S.A.M.); data collection (D.O.); analysis and interpretation of data (S.A.M.); drafting (D.O., S.A.M.); critical revision (T.M., J.M.); statistical expertise (S.A.M.).

the IntraLase laser and Hansatome. Microkeratome eyes had a significant increase in higher order aberrations whereas the IntraLase eyes did not. Montés-Micó et al[10] compared contrast sensitivity following myopic LASIK with the IntraLase laser and microkeratome (Carriazo-Barraquer; SCHWIND eye-tech-solutions, Kleinostheim, Germany). IntraLase eyes demonstrated better contrast sensitivity at high spatial frequencies compared to microkeratome eyes under both photopic and mesopic conditions.

Our discussion of corneal biomechanics illustrates the importance of thin LASIK flaps. There is no doubt that mechanical microkeratomes can produce thin LASIK flaps. However, more collagen fibers are cut with a meniscus-shaped flap measuring 110 µm centrally and 140 µm peripherally compared to a 110-µm planar flap. Thus, biomechanical strength of a cornea with a meniscus-shaped flap is likely weaker than a planar-shaped flap even with both measuring 110 µm centrally. In addition, the risk of buttonhole flaps is greater when creating thin microkeratome flaps due to their meniscus shape. If a thin planar flap can be created with a microkeratome, this should result in improved biomechanics as well. We are currently performing a similar Visante OCT study on Hansatome flaps to evaluate the flap shape, predictability, and reproducibility of flap thickness. As our understanding of corneal biomechanics increases, it is our belief that for each individual patient we will be customizing flap creation including shape, thickness, and diameter to maximize visual outcomes and corneal biomechanical strength.

Jason E. Stahl, MD
Daniel S. Durrie, MD
Frank J. Schwendeman, OD
Allen J. Boghossian, DO
Overland Park, Kansas

REFERENCES

1. Stahl JE, Durrie DS, Schwendeman FJ, Boghossian AJ. Anterior segment OCT analysis of thin IntraLase femtosecond flaps. *J Refract Surg.* 2007;23:555-558.
2. Sarayba MA, Ignacio TS, Binder PS, Tran DB. Comparative study of stromal bed quality by using mechanical, IntraLase laser 15- and 30-kHz microkeratomes. *Cornea.* 2007;26:446-451.
3. Hu MY, McCulley JP, Cavanagh HD, Bowman RW, Verity SM, Mootha VV, Petroll WM. Comparison of the corneal response to laser in situ keratomileusis with flap creation using the FS15 and FS30 femtosecond lasers. *J Cataract Refract Surg.* 2007;33:673-681.
4. Binder PS. One thousand consecutive IntraLase laser in situ keratomileusis flaps. *J Cataract Refract Surg.* 2006;32:962-969.
5. Li Y, Netto M, Shekhar R, Krueger RR, Huang D. A longitudinal study of LASIK flap and stromal thickness with high-speed optical coherence tomography. *Ophthalmology.* 2007;114:1124-1132.
6. Abunto MTA. Clinical report: validation of corneal pachymetry and LASIK flap measurement with the anterior chamber OCT. Dublin, Calif: Carl Zeiss Meditec Inc; 2005.
7. Kezirian GM, Stonecipher KG. Comparison of the IntraLase femtosecond laser and mechanical microkeratomes for laser in situ keratomileusis. *J Cataract Refract Surg.* 2004;30:804-811.
8. Durrie DS, Kezirian GM. Femtosecond laser versus mechanical microkeratome flaps in wavefront-guided laser in situ keratomileusis: prospective contralateral eye study. *J Cataract Refract Surg.* 2005;31:120-126.
9. Tran DB, Sarayba MA, Bor Z, Garufis C, Duh YJ, Soltes CR, Juhasz T, Kurtz RM. Randomized prospective clinical study comparing induced aberrations with IntraLase and Hansatome flap creation in fellow eyes: potential impact on wavefront-guided laser in situ keratomileusis. *J Cataract Refract Surg.* 2005;31:97-105.
10. Montés-Micó R, Rodríguez-Galietero A, Alió JL, Cervino A. Contrast sensitivity after LASIK flap creation with a femtosecond laser and a mechanical microkeratome. *J Refract Surg.* 2007;23:188-192.

Mathematical Properties of Asphericity: A Method to Calculate With Asphericities

To the Editor:

We read with interest the analysis by Calossi[1] investigating various descriptors used for corneal asphericity and its influence on spherical aberration. Many articles report asphericity measurements[2] and average values[3] using different descriptors (Q-factor, eccentricity (*e*), p-factor, shape-factor [SF]), or deal with the effects that refractive treatments have on corneal asphericity, either theoretically[4] or empirically.[5]

The article by Calossi provided useful data, however, we do not agree with the definition provided for the negative values of eccentricity.

"Classical" relationships between the different asphericity descriptors are:

$$p \equiv Q + 1 \equiv 1 - SF = 1 - e^2$$

$$Q \equiv p - 1 \equiv -SF = -e^2$$

$$SF \equiv 1 - p \equiv -Q = e^2$$

$$e = \sqrt{1-p} \equiv \sqrt{-Q} \equiv \sqrt{SF}$$

where:

$p<0$; $Q<-1$; $SF>1$; $e>1 \Rightarrow$ Hyperbola

$p=0$; $Q=-1$; $SF=1$; $e=1 \Rightarrow$ Parabola

$0<p<1$; $-1<Q<0$; $0<SF<1$; $0<e<1 \Rightarrow$ Prolate ellipse

$p=1; \quad Q=0; \quad SF=0; \quad e=0 \Rightarrow$ Sphere

$p>1; \quad Q>0; \quad SF<0 \Rightarrow$ Oblate ellipse

One option is to use an elliptical model, where eccentricity is defined as:

$$e \equiv \sqrt{1-\frac{b^2}{a^2}}$$

where a represents the major semi-axis and b the minor semi-axis. Thus, eccentricity is always defined positively (ie, $e<0$ does not exist).

As mentioned by Calossi, negative values of ε are purely conventional to describe oblate ellipses. Prolate ellipses have values of ε ranging from 0 to 1. If we describe oblate ellipses by means of negative values of e, they would be expected to range from -1 to 0. The definition provided by Calossi (Eq.[6] in the original article) fails to fulfill this requirement:

$$e = \sqrt{-Q}, \forall Q \leq 0$$

$$e = -\sqrt{Q}, \forall Q > 0$$

All positive values of Q (from 0 to $+\infty$) represent oblate ellipses. With the definition used by Calossi, oblate ellipses would have values of e ranging from $-\infty$ to 0.

As ellipses are possible for both negative and positive values of Q, but only the negative Q are covered by the elliptical definition, we can also redefine ε as a function of Q:

$$e = \sqrt{1-\frac{b^2}{a^2}} \Rightarrow Q \equiv -(e^2) \equiv \frac{b^2}{a^2} - 1$$

$$e = \sqrt{-Q}, \forall Q \leq 0 \Rightarrow Q = -(e^2), \forall e \geq 0$$

$$e = -\sqrt{Q/Q+1}, \forall Q > 0 \Rightarrow Q = \frac{e^2}{1-e^2}, \forall e < 0$$

With this definition, prolate ellipses having values of Q ranging from -1 to 0 correspond to values of e ranging from 1 to 0, whereas oblate ellipses having values of Q ranging from 0 to $+\infty$ correspond to values of e ranging from -1 to 0, as expected. (This affects Table 3 in the article by Calossi).

We would also like to bring attention to the fact that asphericity is a dependant magnitude with "non-linear" behavior, having no physical meaning if it is not considered together with paraxial curvature, therefore simple arithmetic using asphericity descriptors might lead to erroneous interpretations and confusion when using different asphericity descriptors. Simple arithmetics to convert from one asphericity descriptor to another, and to average asphericity descriptors, may lead to ambiguous results, depending on the sequence of the calculations.

In corneal surgery, it is has long been known that refractive treatments induce changes in corneal asphericity,[4] and recently it has been argued that preserving preoperative corneal asphericity might be desirable, thus, asphericity-based profiles have been developed.

Asphericity can be computed from the corneal elevation Zernike expansion:

$$p \approx \left(\frac{48(C_4^0\sqrt{5} - 5C_6^0\sqrt{7} + 15C_8^0 3)}{R\,(1-n)} \left(\frac{2R}{OZ}\right)^4 \right)$$

The average of the corneal elevation Zernike expansion can then be used to calculate the "average" asphericity:

$$p_\Sigma \approx \frac{48(\Sigma(C_4^0)_i\sqrt{5} - 5\Sigma(C_6^0)_i\sqrt{7} + 15\Sigma(C_8^0)_i 3)}{1-n} \left(\frac{2}{OZ}\right)^4$$

$$\frac{1}{(\Sigma c_i)^3} = \frac{\Sigma p_i c_i^3}{(\Sigma c_i)^3}$$

$$p_\Sigma \approx \frac{48(\Sigma \bar{C}_4^0\sqrt{5} - 5\Sigma(\bar{C}_6^0)_i\sqrt{7} + 15\Sigma(\bar{C}_8^0)_i 3)}{1-n} \left(\frac{2}{OZ}\right)^4$$

$$\frac{1}{(\Sigma \bar{c})^3} = \frac{48m(\bar{C}_4^0\sqrt{5} - 5\bar{C}_6^0\sqrt{7} + 15\bar{C}_8^0)3}{1-n} \left(\frac{2}{OZ}\right)^4 \frac{1}{m^3\bar{c}^3}$$

$$p_\Sigma \approx \frac{\bar{p}}{m^2}$$

$$p_\Sigma \approx \frac{\Sigma p_i c_i^3}{(\Sigma c_i)3} \approx \frac{\bar{p}}{m^2}$$

$$\bar{p} \approx \frac{\Sigma p_i c_i^3}{(\Sigma c_i)^3} m^2$$

This result is different from a simple arithmetic averaging of asphericities.

Alternatively, how to calculate asphericity considering the curvature of the meridians.

Again, to average the corneal asphericity of a series of individual corneal asphericities:

$$p \approx \frac{\Sigma \overline{pc}^3}{(\Sigma \bar{c})^3} = \frac{m\overline{pc}^3}{m^3\bar{c}^3} = \frac{\bar{p}}{m^2}$$

$$\bar{p} \approx \frac{\Sigma p_i c_i^3}{(\Sigma c_i)^3} m^2$$

This is identical to the previous result based on Zernike expansion.

This can be applied to average corneal asphericity of a series of individual corneal asphericities, or to compute average asphericity of a single cornea, by

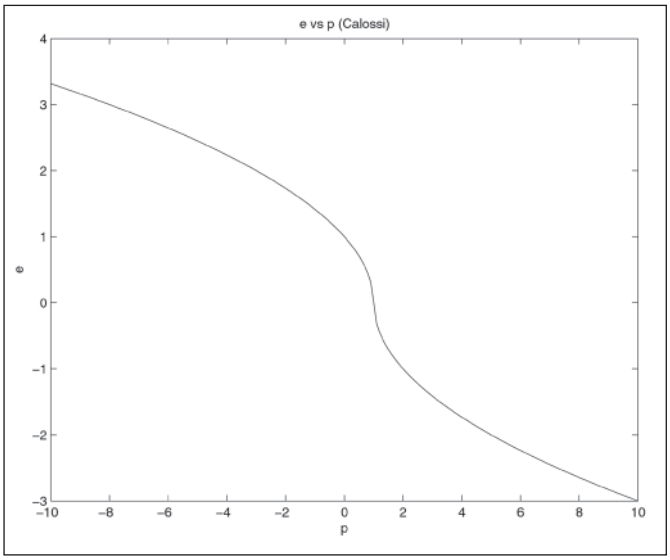

Figure 1. Eccentricity (e) in function of p value following Calossi proposed convention.

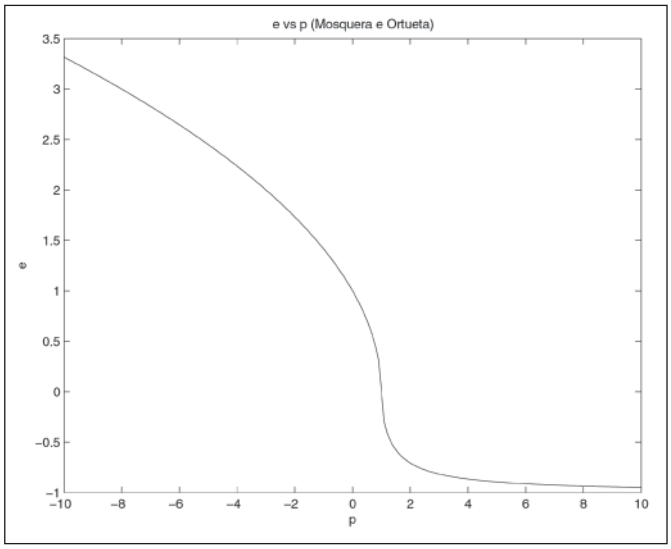

Figure 2. Eccentricity (e) in function of p value following Mosquera and de Ortueta proposed convention.

averaging its two principal meridian asphericities considering their respective curvatures.

For subtracting asphericities, simply add the sign reversed magnitude:

$$p_\Delta \approx \frac{\frac{p_2}{R_2^3} - \frac{p_1}{R_1^3}}{\left(\frac{1}{R_2} - \frac{1}{R_1}\right)^3} = \frac{p_2 {c_2}^3 - p_1 {c_1}^3}{(c_2 - c_1)^3}$$

This can be applied to calculate the asphericity of the average change of a series of individual corneal asphericities or to compute the asphericity of the change in a single cornea.

Following the above described methods, converting from one asphericity descriptor to another and to average asphericity descriptors, will lead to systematic results, independent of the chosen asphericity descriptor and the sequence of the calculi.

Diego de Ortueta, MD
Recklinghausen, Germany
Samuel Arba Mosquera, MS
Kleinostheim, Germany

REFERENCES

1. Calossi A. Corneal asphericity and spherical aberration. *J Refract Surg.* 2007;23:505-514.
2. Kiely PM, Smith G, Carney LG. The mean shape of the human cornea. *Optica Acta.* 1982;29:1027-1040.
3. Sheridan M, Douthwaite WA. Corneal asphericity and refractive error. *Ophthal Physiol Opt.* 1989;9:235-238.
4. Gatinel D, Hoang-Xuan T, Azar DT. Determination of corneal asphericity after myopia surgery with the excimer laser: a mathematical model. *Invest Ophthalmol Vis Sci.* 2001;42:1736-1742.
5. Anera RG, Jiménez JR, Jiménez del Barco L, Bermúdez J, Hita E. Changes in corneal asphericity after LASER in situ keratomileusis. *J Cataract Refract Surg.* 2003;29:762-768.

Reply:

In response to de Ortueta and Mosquera, negative values of e to describe oblate ellipses are purely conventional. I proposed a convention, and they proposed another convention.

We started from this point: the existence domain for p is $(-\infty, +\infty)$. Do we want to associate a value of e to all values of p?

If not, the standard formula must be used:

$$e = \sqrt{1-p} = \sqrt{1-\frac{b^2}{a^2}} \text{ where } p = \frac{b^2}{a^2} \text{ and } b<a.$$

If so:

$$e = \begin{cases} \sqrt{1-p}, & p<1 \\ -\sqrt{p-1}, & p \geq 1 \end{cases}$$

Figure 1 shows a symmetrical pattern in respect to $p = 1$, ie, the sphere.

This is a proposal that allows associating one, and only one, value of e to each value of p. This definition does not produce any ambiguity.

Figure 2 shows how the range $p \geq 1$ is compressed in $-1 \leq e \leq 0$, using Mosquera and Ortueta's definition.

Antonio Calossi, DipOptom
Certaldo (FI), Italy

Asphericity analysis using corneal wavefront and topographic meridional fits

Samuel Arba-Mosquera
University of Valladolid
Instituto de Oftalmobiología Aplicada
Refractive Surgery and Quality of Vision
Valladolid, E-47004 Spain
and
SCHWIND eye-tech-solutions
Research and Development
Mainparkstrasse 6-10
Kleinostheim, D-63801 Germany

Jesús Merayo-Lloves
University of Valladolid
Instituto de Oftalmobiología Aplicada
Refractive Surgery and Quality of Vision
Valladolid, E-47004 Spain

Diego de Ortueta
Augenzentrum Recklinghausen
Recklinghausen, Germany

Abstract. The calculation of corneal asphericity as a 3-D fit renders more accurate results when it is based on the corneal wavefront aberrations rather than on the corneal topography of the principal meridians. A more accurate prediction could be obtained for hyperopic treatments compared to myopic treatments. We evaluate a method to calculate corneal asphericity and asphericity changes after refractive surgery. Sixty eyes of 15 consecutive myopic patients and 15 consecutive hyperopic patients ($n=30$ each) are retrospectively evaluated. Preoperative and 3-month-postoperative topographic and corneal wavefront analyses are performed using corneal topography. Ablations are performed using a laser with an aberration-free profile. Topographic changes in asphericity and corneal aberrations are evaluated for a 6-mm corneal diameter. The induction of corneal spherical aberrations and asphericity changes correlates with the achieved defocus correction. Preoperatively as well as postoperatively, asphericity calculated from the topography meridians correlates with asphericity calculated from the corneal wavefront in myopic and hyperopic treatments. A stronger correlation between postoperative asphericity and the ideally expected/predicted asphericity is obtained based on aberration-free assumptions calculated from corneal wavefront values rather than from the meridians. In hyperopic treatments, a better correlation can be obtained compared to the correlation in myopic treatments. Corneal asphericity calculated from corneal wavefront aberrations represents a 3-D fit of the corneal surface; asphericity calculated from the main topographic meridians represents a 2-D fit of the principal corneal meridians. Postoperative corneal asphericity can be calculated from corneal wavefront aberrations with higher fidelity than from corneal topography of the principal meridians. Hyperopic treatments show a greater accuracy than myopic treatments. [DOI: 10.1117/1.3382910]

Keywords: asphericity; wavefront; topography; aberration; Zernike.

Paper 09474RRR received Oct. 19, 2009; revised manuscript received Feb. 11, 2010; accepted for publication Feb. 22, 2010; published online Apr. 12, 2010.

1 Introduction

A strong tendency toward the use of asphericity parameters in refractive surgery can be observed[1,2] in reporting measurements[3,4] and mean values,[5–7] and using different descriptors (asphericity quotient Q, conic constant K, eccentricity e, p value p, or shape factor E) or measuring the effects of refractive treatments on corneal asphericity.[8,9]

Topographically guided treatments,[10] wavefront-driven treatments,[11] wavefront-optimized treatments,[12] asphericity-preserving treatments,[13] and Q-factor profiles[14] have been proposed as solutions to provide patients with the best possible functional vision. All these approaches behave differently and exert different effects on the postoperative asphericity.

An analysis of corneal topography involves fitting the measured data to geometric models, usually by inclusion of a simple regular surface and a polynomial adjustment of the extra components not covered by the simple regular surface basis.

In this paper, two simple methods to calculate corneal asphericity—based on the corneal wavefront and on the asphericity of the two principal meridians—are compared and the question of whether the corneal wavefront alone is a useful metric to evaluate the corneal asphericity in refractive surgery is addressed. For the purpose of this study, the methods presented were applied to a patient population treated with laser *in situ* keratomileusis (LASIK).

Address all correspondence to: Samuel Arba-Mosquera, SCHWIND eye-tech-solutions, Research and Development, Mainparkstrasse 6-10, Kleinostheim, D-63801 Germany. Tel: 496027508274; Fax: 496027508208; E-mail: sarbamo@cofis.es

1083-3668/2010/15(2)/028003/9/$25.00 © 2010 SPIE

2 Materials and Methods

Retrospective analysis of 60 eyes, including 15 consecutive patients each with myopia and hyperopia, treated at Augenzentrum Recklinghausen (Recklinghausen, Germany) was performed. Preoperative and 3-month-postoperative data are reported.

All operations were performed by one surgeon (DdO). LASIK flaps were created with a Carriazo-Pendular microkeratome[15] (SCHWIND eye-tech-solutions GmbH, Kleinostheim, Germany). An ESIRIS system[16] (SCHWIND eye-tech-solutions GmbH) set for an optical zone of 6.25 mm was used to perform the ablations with aberration-free profiles[17] without nomogram adjustments. This profile does not deliver wavefront-guided ablation targeting zero aberrations after surgery. Rather, the ablation profile itself is aberration free, which means that no aberration is induced by the ablation, so that the preexisting aberrations are preserved.

Preoperative findings as well as outcomes at 3 months postoperatively included manifest refraction, topography, corneal aberrometry, and complications.

Using Keratron-Scout[18] (Optikon2000, Rome, Italy) topographical analysis of the radii of curvature and asphericities of the principal meridians and the corneal wavefront aberrations to the seventh Zernike order was performed preoperatively and 3 months postoperatively.

Classical relationships between different asphericity descriptors[19] were calculated using the formulas

$$p \equiv Q + 1 \equiv 1 - E = 1 - e^2,$$

$$Q \equiv p - 1 \equiv -E = -e^2,$$

$$E \equiv 1 - p \equiv -Q = e^2,$$

$$e = \sqrt{1-p} \equiv \sqrt{-Q} \equiv \sqrt{SF},$$

where

$$p < 0 \Rightarrow \text{hyperbola},$$

$$p = 0 \Rightarrow \text{parabola},$$

$$0 < p < 1 \Rightarrow \text{prolate ellipse},$$

$$p = 1 \Rightarrow \text{sphere},$$

$$p > 1 \Rightarrow \text{oblate ellipse}.$$

However, asphericity is a dependent parameter with "nonlinear" behavior, i.e., it has no meaning, if the apical curvature is not taken into consideration. Any asphericity descriptor can be used, however, to obtain consistent results and interpretations, but the computing cannot be reduced to linear arithmetic. The asphericity descriptor used throughout the study was the p value (p).

Topographic asphericity was computed using two methods. The first was the topographic method based on the principal meridians.[20] Considering the mean corneal asphericity of a series of corneal asphericities, the mean asphericity[20] was computed as

$$\bar{p} = \frac{\sum_{i=1}^{m}(p_i/R_i^3)}{\left[\sum_{i=1}^{m}(1/R_i)\right]^3} m^2, \tag{1}$$

where $\bar{p}$ is the mean asphericity, p_i are the asphericity factors, R_i are the apical radii of curvature, and m is the sample size.

To average the asphericity of the two main meridians under consideration of their curvature, Eq. (1) reduces to

$$p = 4\frac{p_s/R_s^3 + p_f/R_f^3}{(1/R_s + 1/R_f)^3}, \tag{2}$$

where p is the corneal p value; p_s and p_f are the p values of the steep and flat principal meridians, respectively; and R_s and R_f are the apical radiis of curvature of the steep and flat principal meridians.

This method represents a calculation of mean asphericity derived from m meridional radii and asphericities obtained from 2-D fits of the corneal meridians.

The second method investigated was the corneal wavefront method:[20]

$$p = \frac{768R^3(C_4^0\sqrt{5} - 5C_6^0\sqrt{7} + 45C_8^0)}{OZ^4(1-n)}, \tag{3}$$

where p is the corneal p value; $C[4,0]$, $C[6,0]$, and $C[8,0]$ are the radially symmetric terms of the corneal Zernike expansion; R is the apical radius of the corneal curvature; n is the corneal refractive index; and OZ is the analyzed diameter of the corneal Zernike expansion.

This method represents a calculation of the mean asphericity derived from corneal wavefront data obtained from a 3-D fit of the corneal surface. The radially symmetric terms of the corneal Zernike expansion, $C[4,0]$, $C[6,0]$, and $C[8,0]$, were calculated from the radially symmetric terms of the corneal Zernike expansion[21] of the surface elevation of a Cartesian oval ($C_{co}[4,0]$, $C_{co}[6,0]$, and $C_{co}[8,0]$) plus the radially symmetric terms of the corneal wavefront aberration, as provided by the videokeratoscope ($C_{cw}[4,0]$ and $C_{cw}[6,0]$).

Also, the ideally expected topographic asphericity assumed from aberration-neutral conditions was calculated using two methods. First, the ideally expected principal meridians of the topographic method,

$$p_{exp} = p_{co} + \frac{p_{pre} - p_{co}}{[1 + (R\mathrm{SE}q_{cp}/n - 1)]^3}, \tag{4}$$

where p_{exp} is the predicted corneal p value; p_{co} and p_{pre} are the p values of a Cartesian oval and the preoperative cornea, respectively; R is the apical radius of curvature of the preoperative cornea; and $\mathrm{SE}q_{cp}$ is the spherical equivalent to be corrected at the corneal plane.

In this paper, the term "ideally expected" is understood to mean "predicted values" if the aberration-free condition were strictly fulfilled.

The second method employed was the ideally expected corneal wavefront method, again using Eq. (3), with R as the postoperative predicted apical radius of curvature.

Table 1 Preoperative and postoperative data.

	Myopic Group	Hyperopic Group	All Treatments
No. of treated eyes (patients)	30 (15)	30 (15)	60 (30)
Preoperative SEq ± StdDev (D)	−3.18 ± 1.21	+2.48 ± 1.41	−0.32 ± 3.15
Preoperative cylinder ± StdDev (D)	0.50 ± 0.48	0.65 ± 0.79	0.58 ± 0.66
Postoperative SEq ± StdDev (D)	+0.19 ± 0.28	+0.04 ± 0.35	+0.11 ± 0.32
Postoperative cylinder ± StdDev (D)	0.05 ± 0.08	0.11 ± 0.15	0.08 ± 0.13
Predictability <0.50 D (%)	90%	100%	95%
Predictability <1.00 D (%)	100%	100%	100%

Note that the ideally expected corneal wavefront method using Eq. (3) can easily be further applied to any target condition, simply by setting the radially symmetric terms of the corneal wavefront aberration ($C_{cw}[4,0]$ and $C_{cw}[6,0]$) to the desired value.

Optical errors, represented by wavefront aberrations, as described by Zernike polynomials[22] and coefficients in the Optical Society of America (OSA) standard[23] were analyzed for 6-mm diameters.

2.1 *Clinical Evaluation*

Each cornea underwent four consecutive measurements preoperatively as well as at the 3-month follow-up examination, summing up to a total of 240 measurements. For every cornea, the four corresponding topographies were analyzed using both methods, and the corresponding mean value according to Eqs. (1) or (3) was used as representative asphericity of that cornea with each method.

2.2 *Repeatability of Methods*

Following preoperative calculation of the p values with both methods, a global analysis of the behavior of the term pR^{-3} was performed. According to Eqs. (1) and (3), it constitutes a term to be operated on in a simple linear manner. The four corresponding values of each cornea were averaged for both methods, and a global standard deviation value was calculated across the 240 measurements for each method using the formula

$$\mathrm{StdDev}_{\mathrm{Global}} = \left\{ \frac{\sum_{a=1}^{A}\sum_{b=1}^{B}\left[p_{a,b}R_{a,b}^{-3} - \left(\sum_{c=1}^{B} p_{a,c}R_{a,c}^{-3}\right)/B\right]^2}{AB-1} \right\}^{1/2}, \tag{5}$$

where a runs over the number of corneas of the sample ($A=60$), and b and c run over the number of corresponding measurements for each cornea ($B=4$).

2.3 *Statistical Analysis*

We used t tests for statistical analysis, with $P<0.05$ considered as significant.

3 Results

3.1 *Refractive Outcomes*

In both myopic and hyperopic eyes, spherical equivalent (SEq) and cylinder were reduced to subclinical values at 3 months postoperatively (range −0.50 to +0.75 D for defocus and 0.00 to 0.75 D for astigmatism), and 95% of eyes ($n=57$) were within ±0.50 D of the attempted correction (Table 1 and Fig. 1).

3.2 *Corneal Spherical Aberrations*

In the myopic group, the preoperative primary corneal spherical aberration ($C[4,0]$) was $+0.243 \pm 0.098$ μm (mean ± standard deviation), and changed to $+0.319 \pm 0.132$ μm at 3 months postoperatively ($P<0.01$). In the hyperopic group, $C[4,0]$ was $+0.201 \pm 0.118$ μm and changed to -0.006 ± 0.139 μm at 3 months postoperatively ($P<0.001$) (Table 2).

Induced corneal spherical aberration, defined as the difference in postoperative corneal spherical aberration minus the preoperative value, was significant for primary and secondary spherical aberrations ($P<0.001$ for both) and significantly correlated with the achieved defocus correction for primary and secondary spherical aberrations ($r^2=0.65$, $P<0.001$ for primary spherical aberration and $r^2=0.59$, $P<0.001$ for secondary spherical aberration). The rate of induced corneal spherical aberration per defocus (regression slope) was -0.045 μm/D for primary spherical aberration and -0.001 μm/D for secondary spherical aberration at 6 mm (Fig. 2).

3.3 *Corneal Asphericity*

In the myopic group, the mean preoperative corneal asphericity calculated from the principal meridians was +0.79, whereas the mean corneal asphericity calculated from the corneal wavefront was +0.89. In the hyperopic group, the mean preoperative corneal asphericity calculated from the principal meridians was +0.81, whereas the mean corneal asphericity calculated from the corneal wavefront was +0.82 (Table 3).

The preoperative corneal asphericity calculated from the corneal wavefront significantly correlated with the corneal asphericity calculated from the principal meridians in both the

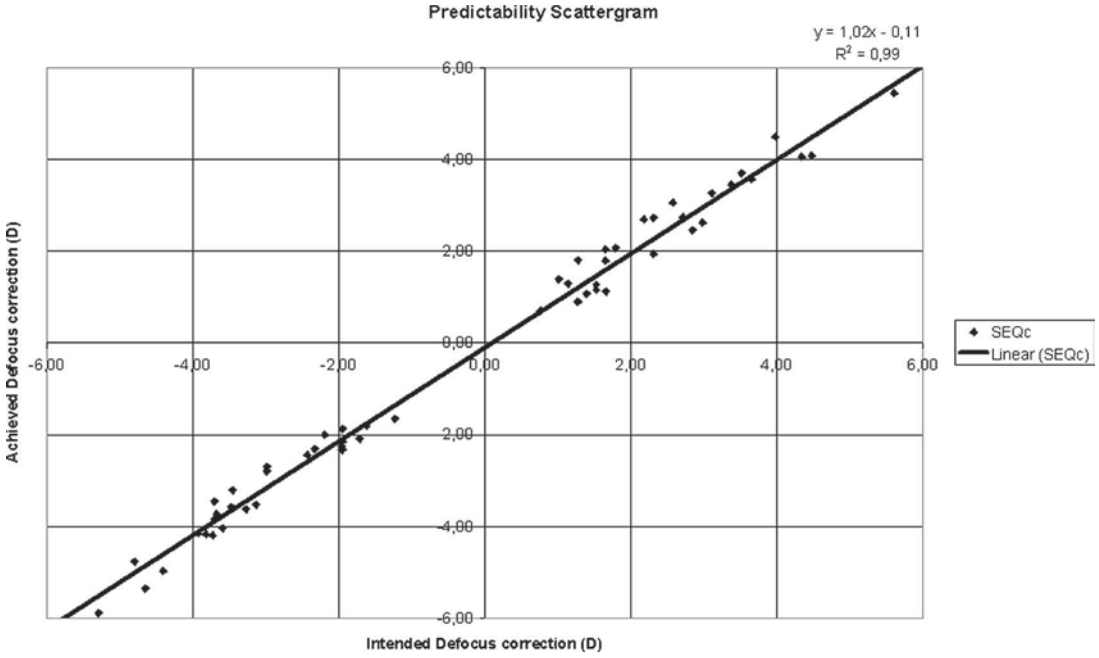

Fig. 1 Predictability scattergram.

myopic and the hyperopic group ($r^2=0.84$, $P<0.001$ for the myopic group; $r^2=0.87$, $P<0.001$ for the hyperopic group). Further, the regression slope was 1.01 for the myopic group and 1.09 for the hyperopic group (Fig. 3).

In the myopic group, the mean postoperative corneal asphericity calculated from the principal meridians was +1.24, whereas the mean corneal asphericity calculated from the corneal wavefront was +1.13. In the hyperopic group, the mean postoperative corneal asphericity calculated from the principal meridians was +0.39, whereas the mean corneal asphericity calculated from the corneal wavefront was +0.47 (Table 3).

Postoperatively, the corneal asphericity calculated from the corneal wavefront values significantly correlated with the corneal asphericity calculated from the principal meridians in both the myopic and the hyperopic group ($r^2=0.81$, $P<0.001$ for the myopic group; $r^2=0.85$, $P<0.001$ for the hyperopic group). Further, the regression slope was 0.51 for the myopic group and 0.88 for the hyperopic group (Fig. 4).

3.4 *Corneal Asphericity Changes*

For myopia, the ideally expected postoperative p value calculated from the principal meridians was +0.87, compared to +0.98 in the wavefront-based calculation (Table 3). The postoperative asphericity did not correlate with the predicted asphericity when calculated from the meridians ($r^2=0.07$, $P=0.2$), and showed a weak but significant correlation with the ideally expected asphericity when calculated from the wavefront ($r^2=0.12$, $P=.05$). Further, the regression slope was +0.68 in a corneal wavefront-based calculation.

For hyperopia, the predicted postoperative asphericity calculated from the principal meridians was +0.76, compared to +0.75 in a wavefront-based calculation (Table 3). The postoperative asphericity was significantly correlated with the ideally expected asphericity when calculated from the meridians ($r^2=0.39$, $P<0.001$), and strongly correlated with the predicted asphericity when calculated from the wavefront

Table 2 Corneal wavefront aberration data reported for 6-mm analysis diameter.

	Myopic Group	Hyperopic Group	All Treatments
Preoperative primary SphAb ± StdDev (μm)	+0.243 ± 0.098	+0.201 ± 0.118	+0.221 ± 0.111
Preoperative secondary SphAb ± StdDev (μm)	0.000 ± 0.003	0.000 ± 0.002	0.000 ± 0.002
Postoperative primary SphAb ± StdDev (μm)	+0.319 ± 0.132	−0.006 ± 0.139	+0.154 ± 0.214
Postoperative secondary SphAb ± StdDev (μm)	+0.003 ± 0.003	−0.004 ± 0.004	−0.0001 ± 0.005
Induced primary SphAb per diopter (μm)	−0.031	−0.048	−0.043
Induced secondary SphAb per diopter (μm)	−0.001	−0.001	−0.001

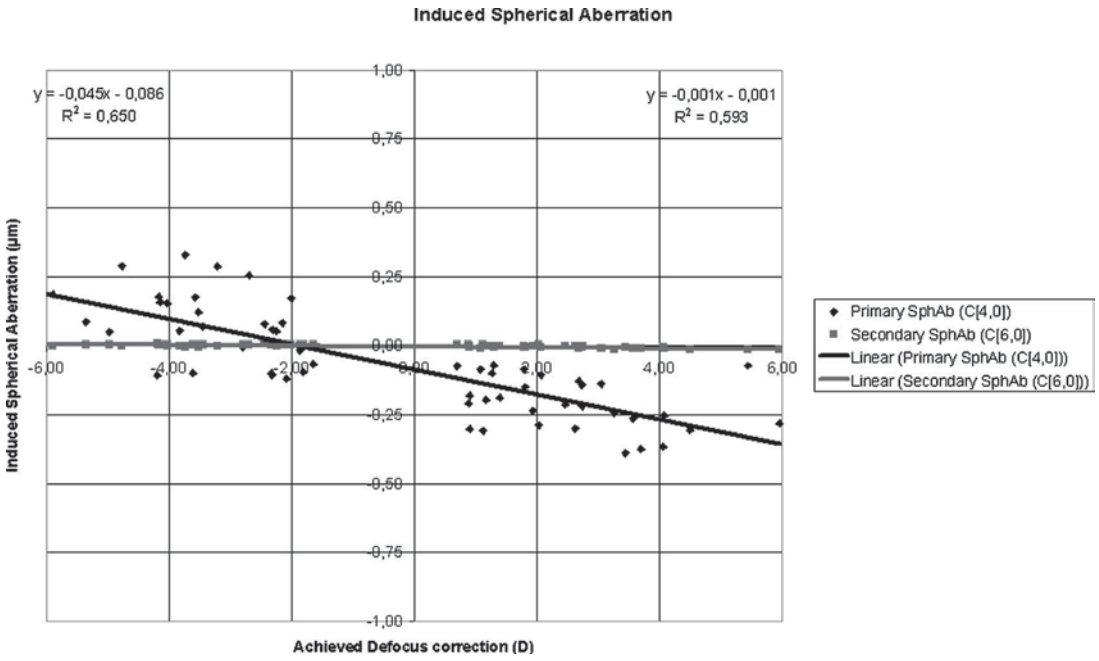

Fig. 2 Induced spherical aberration.

(r^2=0.51, $P<0.001$). Further, the regression slope was +0.67 when calculated from the principal meridians and +0.71 when calculated from the corneal wavefront.

Combining the results of both groups, the ideally expected postoperative asphericity calculated from the principal meridians was +0.81 and that calculated from the corneal wavefront +0.85 (Table 3). The postoperative asphericity was significantly but weakly correlated with the predicted asphericity when calculated from the principal meridians (r^2=0.17, $P<0.05$), and showed a strong correlation with the ideally expected corneal asphericity when calculated from the corneal wavefront (r^2=0.37, $P<0.001$). Further, the regression slope was +1.44 in a principal-meridian-based calculation and +1.19 in a corneal-wavefront-based calculation (Fig. 5).

3.5 *Repeatability of the Corneal Asphericity*

The global standard deviation was 0.0003 mm^{-3} for the meridional method, compared to 0.0001 mm^{-3} for the corneal wavefront method ($P<0.05$).

4 Discussion

We used the p value as the asphericity descriptor throughout this study. The reason for this choice was not a preference for the p value over other asphericity descriptors. In fact, using the identities and equalities described, similar equations could have been derived for any asphericity descriptor. Our aim was the consistent use of one descriptor and to use the classical relationships between descriptors combined with Eqs. (1) and (3), or (4) to derive descriptor-specific equations for computing the mean values, asphericity out of the corneal wavefront, or estimation of the postoperative asphericity, respectively. Note that using simple arithmetic, the average of a parabola (p=0) with an apical curvature of 7 mm and a sphere (p=1) with a radius of curvature of 8 mm would be p=0.5 (i.e., e=0.71). For the same surfaces, however, an averaged parabola (e=1) and an averaged sphere (e=0) would be e=0.5 (i.e., p=0.75) and not 0.71. Using our model, the result would always be p=0.41 or e=0.77.

Table 3 Asphericity data.

	Myopic Group	Hyperopic Group	All Treatments
Preoperative *p* value from meridians	+0.79	+0.81	+0.80
Preoperative *p* value from corneal wavefront	+0.89	+0.82	+0.85
Postoperative *p* value from meridians	+1.24	+0.39	+0.73
Postoperative *p* value from corneal wavefront	+1.13	+0.47	+0.74
Expected/predicted *p* value from meridians	+0.87	+0.76	+0.81
Expected/predicted *p* value from corneal wavefront	+0.98	+0.75	+0.85

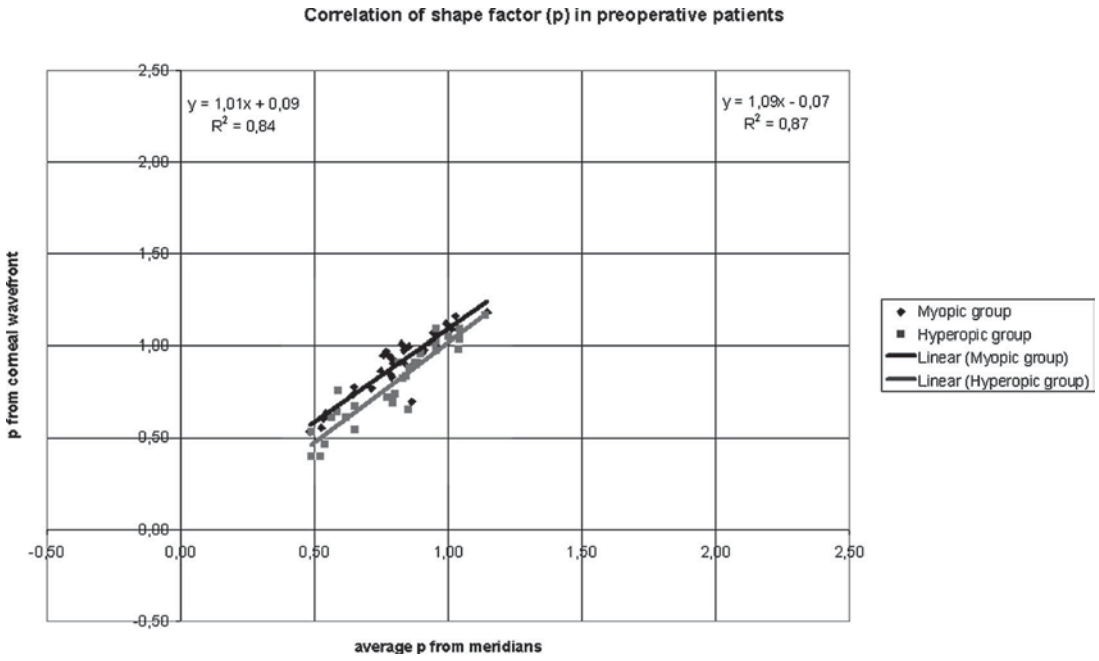

Fig. 3 Preoperative asphericity.

In particular, the corneal wavefront method benefits from avoidance of complicated nonlinear effects in the analysis. Once the Zernike expansion of the corneal wavefront aberration is known, the corresponding coefficients can be linearly averaged, added, or subtracted, or any other linear operation can be performed, and finally the asphericity value can be computed in the desired descriptor.

By analyzing topographic changes, a highly significant correlation between the asphericity calculated from corneal wavefront and from the principal meridians could be observed in both the myopic and the hyperopic group preoperatively as well as postoperatively (Figs. 3 and 4).

To assess the agreement between the methods, a Bland-Altman plot was created[24] (Fig. 6) that showed that the asphericity calculation with the two methods does not produce equivalent results. Corneal-wavefront-based calculation showed an asphericity with an average of 0.05 units higher compared to the calculation based on the principal meridians.

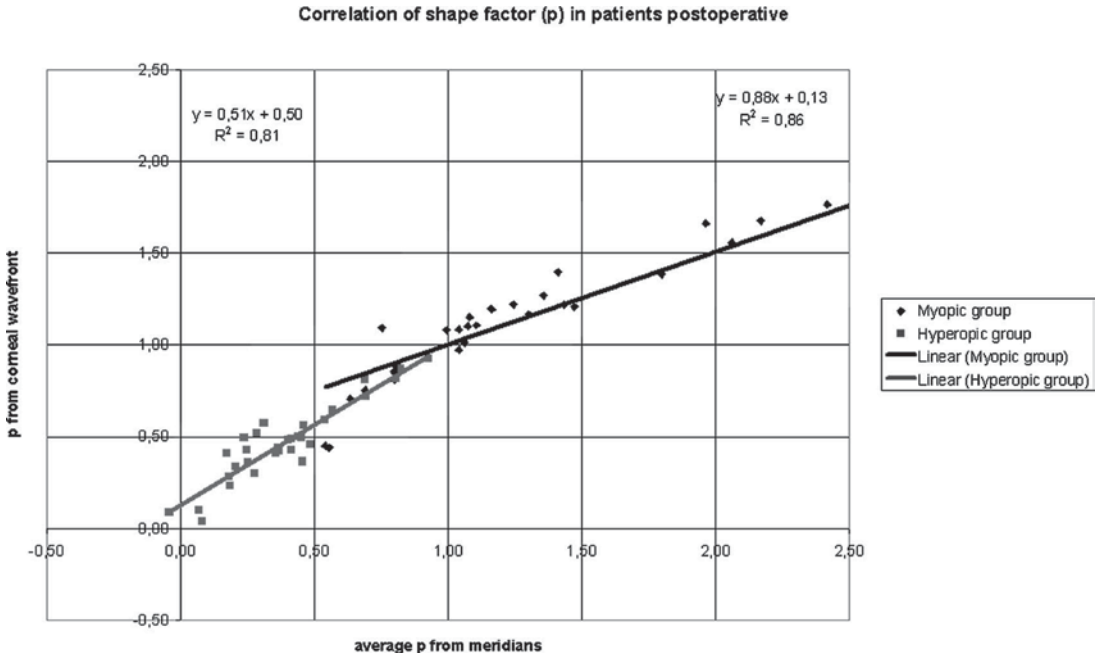

Fig. 4 Postoperative asphericity.

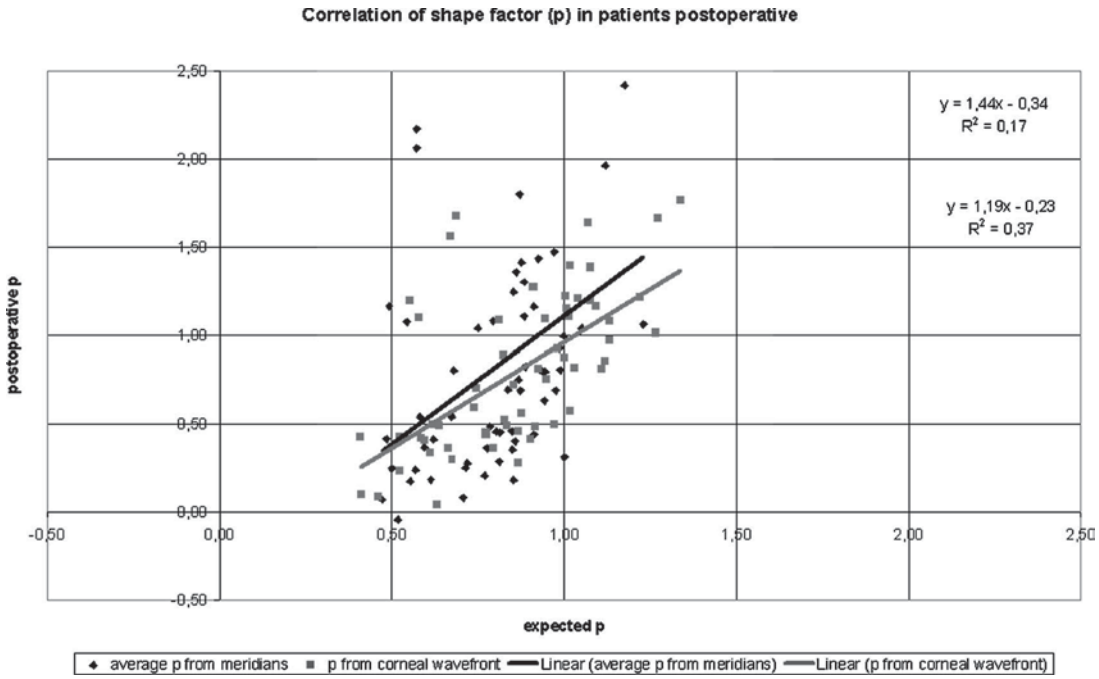

Fig. 5 Ideally expected postoperative asphericity.

Moreover, the difference between the two methods correlated weakly but significantly with the measured value ($r^2=0.11$; $P<0.05$).

The wavefront method proved to be superior to the meridional method, since the aberration coefficients were computed from much denser data sampling (all corneal points within a disk with a 6-mm diameter), and not only from two meridians. However, the conclusion that if many meridians were included in the "meridional" method, the results would approach those of the "wavefront" method is misleading.

Another weakness of the "two-meridians method" is that both meridians are usually selected based on their respective curvature, i.e., the main origin of astigmatism. These two meridians closely represent the highest and lowest meridional curvatures of a cornea, but their corresponding asphericities

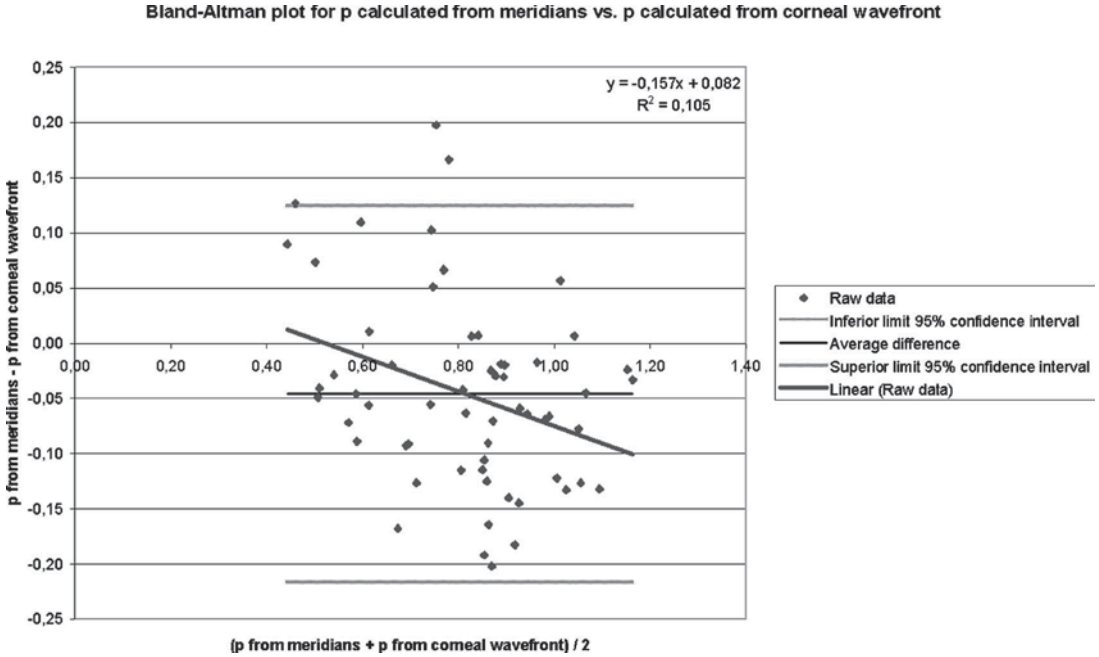

Fig. 6 Bland-Altman plot for *p* value calculated from the meridians versus *p* value calculated from the corneal wavefront.

do not necessarily represent the highest and lowest meridional asphericities of that cornea.

In the groups in this study, the postoperative asphericity deviated more from the preoperative asphericity than predicted by aberration-neutral assumptions calculated from the principal meridians as well as the corneal wavefront. Also, the postoperative asphericity showed a stronger correlation with the asphericity predicted from aberration-neutral assumptions when calculated from corneal wavefront than from the meridians (Fig. 5).

The preoperative mean corneal asphericity in myopic eyes calculated with the two methods showed a similar result, which, however, was not as consistent as the result found in the hyperopic group. The fact that both the amount of corneal astigmatism, which was larger in the hyperopic group (Table 1), and the offset between the corneal vertex and the pupil center, which was also larger in the hyperopic group,[25] may play a role here.

Note also that the Zernike decomposition predicted only 37% of the variance of asphericity change, i.e., there is high scatter (Fig. 5) and there is a tendency toward higher asphericity, which is also reflected by the induction of spherical aberrations.

A possible cause of measured differences in induced asphericity between calculated and real postoperative corneas could be the fact that changes in radius and changes in asphericity were analyzed separately. This is strictly valid only if both parameters are independent, however, there is a very strong correlation between changes in asphericity and changes in radius. This correlation may have two origins: (1) artifacts of the measurement or the fitting procedure or (2) a real correlation in changes of radius and asphericity in the cornea, possibly due to biomechanical constraints. Similarly to Pérez-Escudero et al.[26] and to the findings of a paper presented earlier by the authors,[27] a topography describing a perfect rotationally symmetric ellipsoid with radius $R=7.87$ mm and asphericity $p=0.75$, which are typical values for the anterior corneal surface, was created. Subsequently, random noise was added to the elevation. Normally distributed random noise with a standard deviation of 3 μm was employed, which is the same order of magnitude observed in measurements with the Scout videokeratoscope. This results in a data set similar to the experimental data sets, however, without the particularities that may be specific to our setup. One hundred such surfaces were created using the same base ellipsoid and changing only the noise. Subsequently, this surface was fitted. The results show that the parameters of the base ellipsoid are well recovered by the mean, but that there is a strong correlation between changes in R and changes in p. The same applies to correlations between changes in $1/R$ and changes in p/R^3. These correlations are not particular to our specific fitting procedure, rather are they a general characteristic of fits to surfaces that derive from ellipses. These correlations are an artifact caused by the fit's sensitivity to measurement noise and are probably common to all fits of ellipse-based surfaces. Both the biomechanical response of the stroma and wound healing could also contribute to this phenomenon.

Navarro et al.[28] proposed a relatively simple general model to represent the corneal surface in its canonical form with respect to the axes of corneal symmetry. One limitation of the Navarro et al. model is that it assumes that the orientations of the principal curvatures, i.e., the steepest and flattest radii, related to corneal toricity, correspond to the orientations of the principal asphericities. Kiely et al.[3] investigated this problem in 1982, using a model more general than an ellipsoid, which was oriented according to the instrument axes.

The mean asphericity is a convenient parameter for the comparison of different eyes and characterization of spherical aberration of a conicoid, but it cannot be a substitute for corneal topography. There are circumstances when knowledge of the asphericity in the two principle meridians might be more useful for vision correction than the mean asphericity. However, as already mentioned, the asphericity of the two principle meridians might not be the minimum and maximum meridional asphericities for that cornea. In this respect, Navarro's corneal model presents a good basis for corneal topography, representing a realistic anatomic situation and employing additional terms of Zernike expansion to describe extra surface deformation of real corneas. Zernike terms would resolve the issue, with the strongest asphericity not being along the principal meridians. On the other hand, the quadratic surface basis for the corneal surface will provide only an aberration-free basis with the instrument on axis and will not be as realistic as the Navarro et al. ellipsoid. As a consequence, the quadratic surface will require larger additional Zernike terms to represent the real corneal topography.

Corneal description should not be limited to the mean asphericity, related to spherical aberration, when corneal topography in Zernike terms gives much more general information on corneal aberrations. However, if a simple corneal model based on asphericity is of interest for reasons of simplicity, we advocate for calculating the mean asphericity from the corneal wavefront rather than from the asphericity of the two principle meridians. This simplification is less complicated but essentially similar to a reduction of the wavefront aberration map to a generic description based on n weight coefficients of the Zernike expansion. This approach is no attempt to discredit the full details of corneal topography or the optical description provided by Zernike polynomials. Rather the aim is to reduce the complexity of the description to an appropriate minimal set of parameters.[29,30]

In particular cases, spherical aberration could be described by way of comparison of the Zernike terms with radial symmetry, such as $C[4,0]$ and $C[6,0]$; to be more accurate, the contribution from the power terms with pure ρ^4 and ρ^6 in the corneal topography expansion (ρ is the normalized pupil radius). In this way, a higher order aspheric surface could be characterized rather than limiting analysis to the mean asphericity that corresponds to a conicoid surface, which in some cases is a poor approximation for high-order aspheric corneas.

Another possible model, which is also direct and simple and combines the advantages of other different models is that of a quadric surface free on the space, i.e., oriented according to the natural corneal axes, however, with a fixed constant asphericity corresponding to the Cartesian oval for the refractive index (p value of +0.472 with a corneal refractive index of 1.376), without astigmatism, to determine the apical curvature and the corneal axis. The modeled surface would always be a surface free of on-axis aberrations for any particular apical curvature. The residual component would be adjusted to a

Zernike polynomial expansion, because it would directly represent the surface aberration of the corneal wavefront.

This paper suggests that the corneal wavefront alone is a useful metric to evaluate the optical quality of an ablation in refractive surgery, and a useful metric to evaluate corneal asphericity. The corneal wavefront can be used effectively to analyze laser refractive surgery, avoiding complicated nonlinear effects in the analysis. On these grounds, this method has the potential to replace or perhaps supplement currently used methods of asphericity analysis based on simple averaging of asphericity values.

Acknowledgments

The authors thank Alfonso Pérez Escudero for fruitful discussions and his time and expertise to critically review this manuscript. Samuel Arba-Mosquera is an employee of SCHWIND eye-tech-solutions. Diego de Ortueta is a consultant for SCHWIND eye-tech-solutions.

References

1. D. Gatinel, M. Haouat, and T. Hoang-Xuan, "A review of mathematical descriptors of corneal asphericity," *J. Fr. Ophtalmol* **25**, 81–90 (2002).
2. A. Calossi, "Corneal asphericity and spherical aberration," *J. Refract. Surg.* **23**, 505–514 (2007).
3. P. M. Kiely, G. Smith, and L. G. Carney, "The mean shape of the human cornea," *Opt. Acta* **29**, 1027–1040 (1982).
4. M. Sheridan and W. A. Douthwaite, "Corneal asphericity and refractive error," *Ophthalmic Physiol. Opt.* **9**, 235–238 (1989).
5. A. Stojanovic, L. Wang, M. R. Jankov, T. A. Nitter, and Q. Wang, "Wavefront optimized versus custom-Q treatments in surface ablation for myopic astigmatism with the WaveLight ALLEGRETTO laser," *J. Refract. Surg.* **24**, 779–789 (2008).
6. J. R. Jimenez, R. G. Anera, J. A. Díaz, and F. Pérez-Ocón, "Corneal asphericity after refractive surgery when the Munnerlyn formula is applied," *J. Opt. Soc. Am. A Opt. Image Sci. Vis* **21**, 98–103 (2004).
7. P. Vinciguerra and F. I. Camesasca, "Treatment of hyperopia: a new ablation profile to reduce corneal eccentricity," *J. Refract. Surg.* **18**, S315–317 (2002).
8. D. Gatinel, T. Hoang-Xuan, and D. T. Azar, "Determination of corneal asphericity after myopia surgery with the excimer laser: a mathematical model," *Invest. Ophthalmol. Visual Sci.* **42**, 1736–1742 (2001).
9. R. G. Anera, J. R. Jiménez, L. Jiménez del Barco, J. Bermúdez, and E. Hita, "Changes in corneal asphericity after LASER in situ keratomileusis," *J. Cataract Refractive Surg.* **29**, 762–768 (2003).
10. J. L. Alio, J. I. Belda, A. A. Osman, and A. M. Shalaby, "Topography-guided laser in situ keratomileusis (TOPOLINK) to correct irregular astigmatism after previous refractive surgery," *J. Refract. Surg.* **19**, 516–527 (2003).
11. M. Mrochen, M. Kaemmerer, and T. Seiler, "Clinical results of wavefront-guided laser in situ keratomileusis 3 months after surgery," *J. Cataract Refractive Surg.* **27**, 201–207 (2001).
12. M. Mrochen, C. Donetzky, C. Wüllner, and J. Löffler, "Wavefront-optimized ablation profiles: theoretical background," *J. Cataract Refractive Surg.* **30**, 775–785 (2004).
13. D. Z. Reinstein, D. R. Neal, H. Vogelsang, E. Schroeder, Z. Z. Nagy, M. Bergt, J. Copland, and D. Topa, "Optimized and wavefront guided corneal refractive surgery using the Carl Zeiss Meditec platform: the WASCA aberrometer, CRS-Master, and MEL80 excimer laser," *Ophthalmol. Clin. North. Am.* **17**, 191–210 (2004).
14. T. Koller, H. P. Iseli, F. Hafezi, M. Mrochen, and T. Seiler, "Q-factor customized ablation profile for the correction of myopic astigmatism," *J. Cataract Refractive Surg.* **32**, 584–589 (2006).
15. D. de Ortueta, "Planar flaps with the Carriazo-Pendular microkeratome," *J. Refract. Surg.* **24**, 322 (2008).
16. M. C. Arbelaez, C. Vidal, B. A. Jabri, and S. Arba Mosquera, "LASIK for myopia with aspheric 'aberration neutral' ablations using the ESIRIS laser system," *J. Refract. Surg.* **25**, 991–999 (2009).
17. D. de Ortueta, S. Arba Mosquera, and H. Baatz, "Comparison of standard and aberration-neutral profiles for myopic LASIK with the SCHWIND ESIRIS platform," *J. Refract. Surg.* **25**, 339–349 (2009).
18. R. Mattioli and N. K. Tripoli, "Corneal geometry reconstruction with the Keratron videokeratographer," *Optom. Vision Sci.* **74**, 881–894 (1997).
19. ISO "Ophthalmic instruments—corneal topographers," ISO Standard 19980:2005.
20. D. De Ortueta and S. Arba-Mosquera, "Mathematical properties of asphericity: a method to calculate with asphericities," *J. Refract. Surg.* **24**, 119–121 (2008).
21. D. Gatinel, J. Malet, T. Hoang-Xuan, and D. T. Azar, "Corneal asphericity change after excimer laser hyperopic surgery: theoretical effects on corneal profiles and corresponding Zernike expansions," *Invest. Ophthalmol. Visual Sci.* **45**, 1349–1359 (2004).
22. F. Zernike, "Diffraction theory of the knife-edge test and its improved form, the phase-contrast method," *Mon. Not. R. Astron. Soc.* **94**, 377–384 (1934).
23. L. N. Thibos, R. A. Applegate, J. T. Schwiegerling, R. Webb, and VSIA Standards Taskforce Members, "Standards for reporting the optical aberrations of eyes," *J. Refract. Surg.* **18**, S652–S660 (2002).
24. D. G. Altman and J. M. Bland, "Measurement in medicine: the analysis of method comparison studies," *Statistician* **32**, 307–317 (1983).
25. M. C. Arbelaez, C. Vidal, and S. Arba-Mosquera, "Clinical outcomes of corneal vertex versus central pupil references with aberration-free ablation strategies and LASIK," *Invest. Ophthalmol. Visual Sci.* **49**, 5287–5294 (2008).
26. A. Pérez-Escudero, C. Dorronsoro, and S. Marcos, "An artifact in fits to conic-based surfaces," E-pub only: arXiv:0905.0814v1 (2009).
27. S. Arba-Mosquera and D. de Ortueta, "Analysis of optimized profiles for 'aberration-free' refractive surgery," *Ophthalmic Physiol. Opt.* **29**, 535–548 (2009).
28. R. Navarro, L. González, and J. L. Hernández, "Optics of the average normal cornea from general and canonical representations of its surface topography," *J. Opt. Soc. Am. A* **23**, 219–232 (2006).
29. P. R. Preussner and J. Wahl, "Simplified mathematics for customized refractive surgery," *J. Cataract Refractive Surg.* **29**, 462–470 (2003).
30. P. R. Preussner, J. Wahl, and C. Kramann, "Corneal model," *J. Cataract Refractive Surg.* **29**, 471–477 (2003).

Topic B MODEL OF AN ABERRATION-FREE PROFILE
(Modelo de un perfil libre de aberraciones)

3. Arbelaez MC, Vidal C, Arba Mosquera S. Clinical outcomes of corneal vertex versus central pupil references with aberration-free ablation strategies and LASIK. Invest Ophthalmol Vis Sci; 2008; 49: 5287-94

4. Arbelaez MC, Vidal C and Arba-Mosquera S. Bilateral Symmetry before and Six Months after Aberration-Free™ Correction with the SCHWIND AMARIS TotalTech Laser: Clinical Outcomes. J Optom 2010;3:20-28

5. Arba-Mosquera S, Arbelaez MC, de Ortueta D. Laser corneal refractive surgery in the twenty-first century: a review of the impact of refractive surgery on high-order aberrations (and vice versa). Journal of Modern Optics, Volume 57 Issue 12, 1041-1074

6. Arbelaez MC, Vidal C and Arba-Mosquera S. Six-month clinical outcomes in LASIK for high myopia with aspheric «aberration neutral» ablations using the AMARIS laser system. J Emmetropia 2010; 1: 111-116

7. Arbelaez MC, Vidal C and Arba-Mosquera S. Six-month experience Hyperopic correction with the SCHWIND AMARIS Total-Tech Laser: Clinical Outcomes. J Optom 2010;3:198-205

AUTHOR CONTRIBUTIONS

Study concept and design (S.A.M.); data collection (D.P., C.V., D.O., J.G.); analysis and interpretation of data (S.A.M.); drafting (D.O., S.A.M.); critical revision (J.L.A., M.C.A., H.B., T.M., J.G.); statistical expertise (S.A.M.).

Clinical Outcomes of Corneal Vertex Versus Central Pupil References with Aberration-Free Ablation Strategies and LASIK

Maria Clara Arbelaez,[1] *Camila Vidal,*[1] *and Samuel Arba-Mosquera*[2]

Purpose. To compare the clinical outcomes of aberration-free ablation profiles based on the normal corneal vertex (CV) and the pupil center (PC) in relation to laser in situ keratomileusis. Aberration-free aspheric ablation treatments were performed in all cases.

Methods. Two myopic astigmatism groups (CV centered using the offset between pupil center and normal corneal vertex and PC centered using the pupil center) comprising 24 and 29 eyes (16 and 19 patients), respectively, with a 6-month follow-up, were included. All enrolled eyes had <0.65 μm RMS-higher order aberration (HOA) for 6.00 mm analysis diameter and pupillary offset >200 μm. In all cases, standard examinations, and preoperative and postoperative wavefront analysis were performed. Custom ablation software was used to plan aberration-free aspheric treatments and a flying spot excimer laser system was used to perform ablations. The clinical outcomes were evaluated for predictability, refractive outcome, safety, ocular wavefront aberration, and asphericity.

Results. Of the CV eyes, 38% had improved best spectacle-corrected visual acuity (BSCVA) compared with 24% of the PC eyes (comparison CV/PC $P = 0.38$). Induced ocular coma was on average 0.17 μm in the CV group and 0.26 μm in the PC group (comparison CV/PC $P = 0.01$ favoring CV). Induced ocular spherical aberration was on average $+0.01$ μm in the CV group and $+0.07$ μm in the PC group (comparison CV/PC $P = 0.05$ favoring CV). Change in asphericity was on average $+0.56$ in the CV group and $+0.76$ in the PC group (comparison CV/PC $P = 0.05$ favoring CV). No significant shift was observed in the pupillary offset after treatments.

Conclusions. In myopic eyes with moderate to large pupillary offset, CV-centered treatments performed better in terms of induced ocular aberrations and asphericity, but both centrations were identical in photopic visual acuity. (*Invest Ophthalmol Vis Sci.* 2008;49:5287–5294) DOI:10.1167/iovs.08-2176

Controversy remains regarding where to center corneal refractive procedures to maximize visual outcomes. A misplaced refractive ablation may result in undercorrection and other undesirable side effects. Pande and Hillman[1] postulated that the coaxial light reflex lies nearer to the corneal intercept of the visual axis than the pupil center (PC) and recommended that the corneal coaxial light reflex be centered during refractive surgery. Boxer Wachler et al.[2] identified the coaxial light reflex and used it as the center of the ablation. de Ortueta and Arba Mosquera[3] used the corneal vertex (CV) measured by videokeratoscopy as the morphologic reference to center corneal refractive procedures. However, Uozato and Guyton[4] recommended the pupil center as the reference for refractive surgery. Mandell[5] proposed the line of sight as the reference, because it minimizes the required optical zone.

An excimer laser is typically used to alter the corneal curvature and compensate for ocular refractive errors in corneal refractive surgery.[6] This is currently the most successful technique, mainly due to its submicrometer precision and capacity to achieve highly repeatable corneal ablations with minimal side effects. Although standard ablation profiles to correct myopic astigmatism based on removing convex–concave tissue lenticules with spherocylindrical surfaces effectively compensate for primary refractive errors, the quality of vision deteriorates substantially, especially under mesopic and low-contrast conditions.[7] Preoperative wavefront analyses (either corneal or ocular) have created individualized ablation patterns to compensate for preexisting HOAs.[8] Topographic-guided,[9] wavefront-driven,[10] wavefront-optimized,[11] asphericity preserving, and Q-factor profiles[12] have all been proposed as solutions. Parallel to the improvements in more detailed ablation patterns and more capable laser systems, a highly precise and optimal definition of a centration reference is necessary.

In the present study, we compared the postoperative outcomes among eyes treated with laser in situ keratomileusis (LASIK), by using CV or PC as a reference for aberration-free profiles. We evaluated the efficacy, predictability, stability, refractive outcome, and safety of each of the references implemented in the Custom Ablation Manager (CAM; Schwind Eye-Tech-Solutions, Kleinostheim, Germany) software platform and evaluated the impact on HOAs and asphericity.

Materials and Methods

Thirty-five patients (53 eyes) seeking laser correction at the Muscat Eye Laser Center, Sultanate of Oman, were enrolled. Informed consent was obtained from each patient in adherence to the tenets of the Declaration of Helsinki. The patients were divided into two myopic astigmatism groups. In the CV group (24 eyes, 16 patients, 8 patients with both eyes enrolled in the study and 8 patients with one eye enrolled), the ablation was centered by using the pupillary offset (i.e., the distance between the pupil center and the normal CV measured by videokeratoscopy (Keratron Scout topographer; Optikon 2000, SPA, Rome, Italy). The measurement was performed under photopic conditions of 1500 lux, similar to the conditions under the operating microscope according to a method was suggested and described by de Ortueta and Arba Mosquera.[3] The excimer laser allows for modification of the ablation centration from the pupillary center with an offset by entering either X and Y cartesian values or R and θ polar values in a regular treatment. The measurement of the pupillary offset was translated into the treatment planning as polar coordinates to be manually entered in the excimer laser computer.

From the [1]Muscat Eye Laser Center, Muscat, Sultanate of Oman; and [2]Schwind Eye-Tech-Solutions, Kleinostheim, Germany.

Submitted for publication April 16, 2008; revised May 30 and June 23, 2008; accepted September 22, 2008.

Disclosure: **M.C. Arbelaez**, Schwind Eye-Tech-Solutions (R); **C. Vidal**, None; **S. Arba-Mosquera**, Schwind Eye-Tech-Solutions (E)

The publication costs of this article were defrayed in part by page charge payment. This article must therefore be marked "*advertisement*" in accordance with 18 U.S.C. §1734 solely to indicate this fact.

Corresponding author: Maria Clara Arbelaez, Muscat Eye Laser Center, P.O. Box 938; P.C. 117, Muscat, Sultanate of Oman; drmaria@omantel.net.om.

TABLE 1. Preoperative Refractive Data from the Treatment Groups

	CV Group		PC Group	
	Mean ± SD	Range	Mean ± SD	Range
Defocus (D)	−3.14 ± 1.71	−6.88 to −0.38	−3.79 ± 2.36	−8.50 to −0.38
Astigmatism (D)	0.68 ± 0.73	0.00 to 2.25	1.00 ± 0.94	0.00 to 4.00
BSCVA	1.18 ± 0.23	0.7 to 1.3	1.16 ± 0.20	0.7 to 1.3
Ocular coma (μm) (6.0 mm)	0.20 ± 0.09	0.07 to 0.43	0.23 ± 0.10	0.08 to 0.46
Ocular trefoil (μm) (6.0 mm)	0.15 ± 0.12	0.03 to 0.52	0.17 ± 0.08	0.03 to 0.33
Spherical ocular aberration (μm) (6.0 mm)	+0.08 ± 0.12	−0.21 to +0.32	+0.07 ± 0.18	−0.31 to +0.42
RMS HOA (μm) (6.0 mm)	0.37 ± 0.10	0.21 to 0.58	0.40 ± 0.11	0.24 to 0.66
Pupillary offset (mm)	0.27 ± 0.08	0.20 to 0.52	0.32 ± 0.15	0.20 to 0.85

RMS, root mean square.

In the PC group (29 eyes, 19 patients, 10 patients with both eyes enrolled in the study and 9 patients with one eye enrolled), the ablation was centered by using the pupil center as observed by the eye-tracking module.

Treatment Selection Criteria

The aberration-free aspherical treatments[11] were used for all treatments. The CAM aspherical profiles were developed to achieve profiles "neutral for aberration" that induce no change in wavefront aberration within the optical zone other than the sphere and cylinder components, leaving all existing HOAs unchanged whenever the BCVA was unaffected by the preexisting aberrations.[13,14] Thus, to compensate for the aberrations induced with other types of profile definitions,[15] some of the sources of aberrations are related to the loss of efficiency of the laser ablation for non-normal incidence.[16,17]

The CAM aberration-free profiles include aspheric profiles to balance the induction of spherical aberration (prolateness optimization) by controlling the postoperative corneal asphericity. The software provides K-reading compensation, which considers the change in spot geometry and reflection losses of ablation efficiency. Real ablative spot shape (volume) is considered through a self-constructing algorithm. In addition, there is a randomized flying-spot ablation pattern that eliminates the risk of thermal damage.

Eyes were enrolled in the study groups only if they had no symptomatic aberrations (<0.65 μm root mean square (RMS)-HOA (measured by the Schwind Ocular Wavefront Analyzer and the Optikon Keratron Scout for 6.00 mm analysis diameter; <0.50 DEq[18]) and moderate-to-large pupillary offset (>200 μm). Patients were randomly assigned to the CV or PC centration groups based on a coin toss. In the patients with only one eye fulfilling the enrolling criteria, both eyes were treated with the randomly assigned centration method, but only eye was included for analysis.

The exclusion criteria included unstable refraction during the previous 6 months; signs of keratoconus or abnormal corneal topography; collagen vascular, autoimmune, or immunodeficiency diseases; severe local infective or allergic conditions; severe dry eye disease; monocularity or severe amblyopia; or cataracts.

To determine the ablation profile of the CAM, the manifest refraction was measured in each eye and cross checked with the objective refraction from the Schwind Ocular Wavefront Analyzer.[19] Preoperative topography and aberrometry measurements were taken, and the VA and mesopic pupil size (Schwind Ocular Wavefront Analyzer) were measured. The ablation for each eye was planned based on the manifest refraction using the CAM aberration-free treatments. In both groups, we used an optical zone of 6.50 mm with a variable transition zone provided automatically by the software in relation to the planned refraction.

In all cases, one surgeon (MCA) performed all standard LASIK procedures at the Muscat Eye Laser Center. Immediately before the ablation, the laser was calibrated according to the manufacturer's instructions and the calibration settings were recorded. Each eye underwent LASIK, each flap was cut with a superior hinge made by a Carriazo-Pendular microkeratome[20] with a 130-μm head, and each ablation was performed the ESIRIS laser (Schwind).[21] The ESIRIS laser system has a repetition rate of 200 Hz, produces a spot size of 0.8 mm[22,23] (full width at half maximum) with a para-Gaussian ablative spot profile, and controls the local repetition rates to minimize the thermal load.[24] High-speed eye tracking with a 330-Hz acquisition rate is accomplished with a 5-ms latency period.[25]

The manifest refraction, VA, topography, and aberrometry measurements were recorded for each eye at 1, 3, and 6 months and 1 year after surgery.

At the preoperative stage, as well as, at any of the follow-ups after the treatments, the pupillary offset was measured directly at the topographical map displayed by the videokeratoscope, and corresponds to the distance between the pupil center under photopic conditions of 1500 lux and the normal CV.

Optical errors centered on the line of sight, representing the ocular wavefront aberration, were described by the Zernike polynomials[26] and the coefficients of the Optical Society of America (OSA) standard[27] and analyzed for a standardized diameter of 6 mm.

In particular, we analyzed the possible correlations between induced ocular aberrations with defocus correction and with pupillary offset.

As the used profiles are aspherically based aiming for effects neutral for aberration, correlations between induced ocular spherical aberration and defocus assess how close (or how far) the profiles are from the targeted neutral effect when centered according to the different references, whereas correlations between induced ocular coma aberration and defocus assess whether the profiles have a systematic decentration (a spherical aberration analyzed off-axis results in coma aberration) when referred according to different points.

We performed 53 treatments without adverse events using ESIRIS aberration-free aspheric profiles and a 6.5-mm optical zone. Each eye was evaluated at a 6-month follow-up session. Table 1 shows the mean refractive data of the groups.

For statistical analysis, paired *t*-tests were used to compare postoperative versus preoperative results within each group, and unpaired *t*-tests were used to compare results between groups. For correlation tests, the coefficient of determination (r^2) was used, and the significance of the correlations was evaluated using probabilities calculated considering a metric distributed approximately as t with $n - 2$ degrees of freedom where n is the size of the sample. For all tests, $P < 0.05$ was considered statistically significant.

RESULTS

Regarding efficacy, 88% of the eyes in which the treatment was centered on the CV achieved better than 20/20 uncorrected visual acuity 6 months after surgery, compared with 97% of the

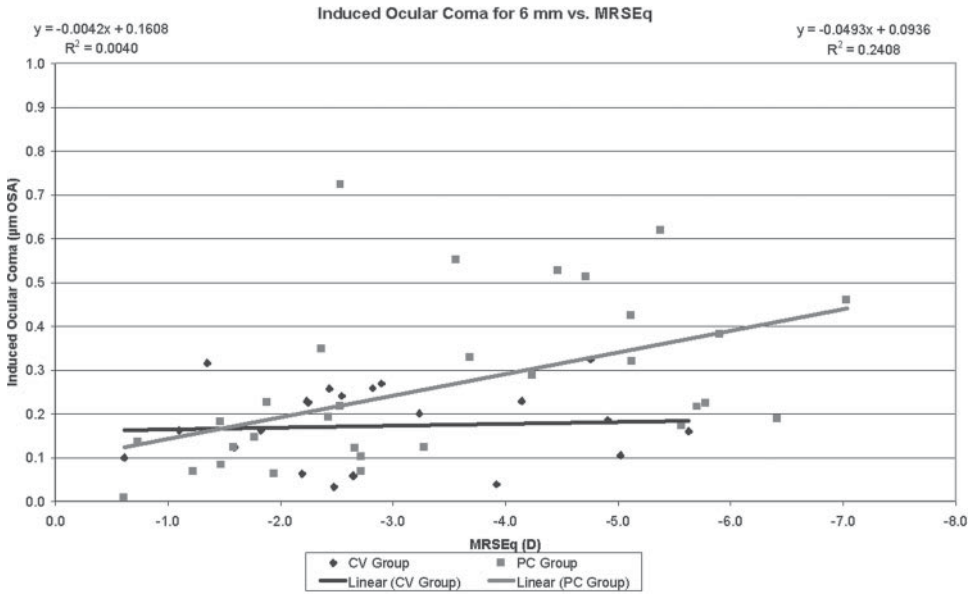

FIGURE 1. Induced ocular coma/diopter focus diopter ratio in the CV and the PC groups.

eyes centered on the PC. However, the difference in efficacy between groups did not reach significance (unpaired *t*-test $P = 0.25$).

Based on the refractive power change (in terms of achieved correction), the sphere and cylinder corrections were accurate, predictable, and stable from the 1-month follow-up.

Regarding refractive outcome, 58% of the eyes centered on the CV were within ±0.25 D and 88% were within ±0.50 D of the intended corrections 6 months after surgery, whereas 48% of the eyes centered on the PC were within ±0.25 D and 83% were within ±0.50 D of the intended correction. However, the difference in refractive outcome between the groups was not significant (unpaired *t*-test $P = 0.10$).

Regarding safety, 38% of the eyes centered on the CV had improved BSCVA compared with 24% of the eyes centered on the PC. The improvement in safety was significant in the CV group (paired *t*-test $P = 0.02$) but not in the PC group (paired *t*-test $P = 0.07$). However, the difference in safety between the groups favoring the CV strategy was not significant (unpaired *t*-test $P = 0.38$).

The amount of induced ocular coma was small with both centration strategies: an average 0.17 μm (range, 0.03–0.32 μm) in the CV group and 0.26 μm (range, 0.01–0.72 μm) in the PC group. The difference in induced ocular coma between groups favoring CV was significant (unpaired *t*-test $P = 0.01$). Furthermore, the induced ocular coma did not correlate with achieved defocus correction of the eyes treated with the CV strategy ($r^2 = 0.004$, $P = 0.78$ in the CV group), but it did correlate with achieved defocus correction of the eyes treated with the PC strategy ($r^2 = 0.24$, $P = 0.01$ in the PC group). The induced ocular coma/diopters of the achieved defocus correction ratio (the slope of the regression) was −0.004 μm of induced ocular coma/diopters in the CV group and −0.049 μm of induced ocular coma/diopters in the PC group (Fig. 1).

Theoretically, ocular coma induction is correlated directly with the amount of diopters corrected and the amount of decentration.[28] We analyzed the correlation between the induced ocular coma/diopter focus with the pupillary offset in both groups. No correlation was found for any eyes treated with either centration strategy ($r^2 = 0.07$, $P = 0.62$ in the CV group; $r^2 = 0.01$, $P = 0.87$ in the PC group). The difference between groups was not significant (unpaired *t*-test $P = 0.43$).

The induced ocular trefoil was small with both centration strategies (i.e., an average 0.09 μm; range, 0.01–0.34 μm) in the CV group and 0.13 μm (range, 0.01–0.49 μm) in the PC group. The difference in induced ocular trefoil between groups favoring the CV strategy was not significant (unpaired *t*-test $P = 0.07$). Further, the induced ocular trefoil was not correlated with the achieved defocus correction in the eyes treated with either centration strategy ($r^2 = 0.01$, $P = 0.69$ for CV group, $r^2 = 0.11$, $P = 0.07$ in the PC group). The induced ocular trefoil/diopters of achieved defocus correction ratio (the slope of the regression) was −0.005 induced ocular trefoil/diopters in the CV group, and −0.019 induced ocular trefoil/diopters in the PC group (Fig. 2).

The induced ocular spherical aberration was minute with both centration strategies: an average +0.01 μm (range, −0.25 to +0.34 μm) in the CV group and +0.07 μm (range, −0.01 to +0.46 μm) in the PC group. The difference in induced ocular coma between groups favoring the CV strategy was significant (unpaired *t*-test $P = 0.05$). Further, the induced ocular spherical aberration did not correlate with achieved defocus correction in the eyes treated with the CV strategy ($r^2 = 0.13$, $P = 0.09$ in the CV group), but it did correlate with the achieved defocus correction in the eyes treated with the PC strategy ($r^2 = 0.17$, $P = 0.02$ in the PC group). The induced ocular spherical aberration/diopters of the achieved defocus correction ratio (the slope of the regression) was −0.028 μm of induced ocular spherical aberration/diopters in the CV group and −0.035 μm of induced ocular spherical aberration/diopters in the PC group (Fig. 3).

The change in asphericity was moderate with both centration strategies (i.e., an average +0.56 [range, +0.07 to +1.31] in the CV group and +0.76 [range, −0.12 to +1.79]) in the PC group. The difference in change in asphericity between groups favoring the CV strategy was significant (unpaired *t*-test $P = 0.05$). Further, the change in asphericity correlated with the achieved defocus correction in the eyes treated with both centration strategies ($r^2 = 0.62$, $P = 0.02$ in the CV group; $r^2 = 0.18$, $P = 0.04$ in the PC group). The change in asphericity/diopters of achieved defocus correction ratio (the slope of the regression) was −0.31 change in Q-factor (DQ)/D in the CV group and −0.47 DQ/D in the PC group (Fig. 4).

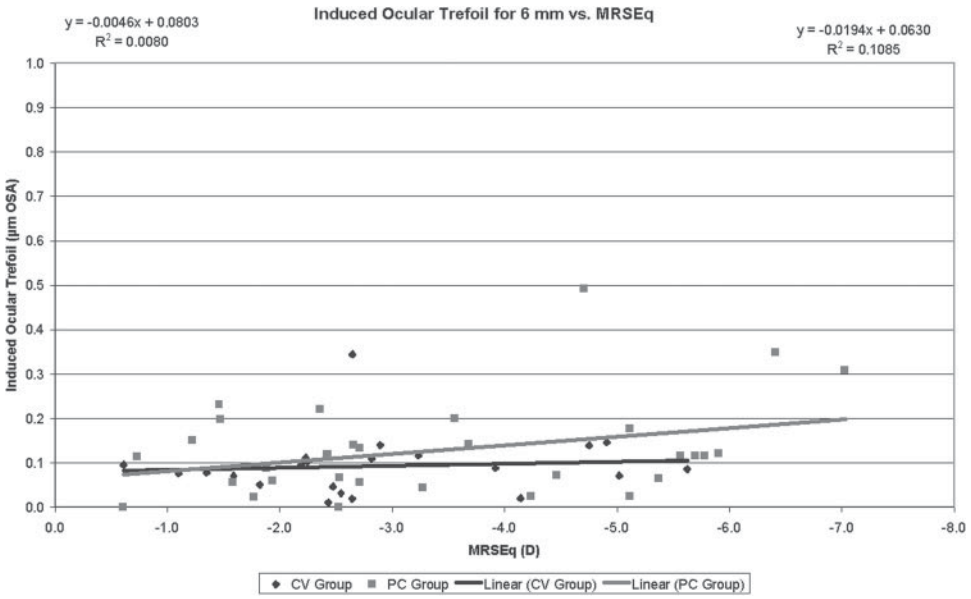

FIGURE 2. Induced ocular trefoil/diopter defocus ratio in the CV and the PC groups.

The results of the postoperative evaluation at the 6-month follow-up in both groups are shown in Table 2.

DISCUSSION

We designed our centration strategies in two different centration references that can be detected easily and measured with currently available technologies. PC may be the most extensively used centration method for several reasons. First, the pupil boundaries are the standard references observed by the eye-tracking devices. Moreover, the entrance pupil can be well represented by a circular or oval aperture, and these are the most common ablation areas. Centering on the pupil offers the opportunity to minimize the optical zone size. Because in LASIK there is a limited ablation area of approximately 9.25 mm (flap cap), the maximum allowable optical zone will be approximately 7.75 mm. Because laser ablation is a destructive tissue technique, and the amount of tissue removed is directly related to the ablation area diameter,[29] the ablation diameter, maximum ablation depth, and ablation volume should be minimized. The planned optical zone should be the same size or slightly larger than the functional entrance pupil for the patients' requirements.

The pupil center considered for a patient who fixates properly defines the line-of-sight, which is the reference axis recommended by the OSA[20] for representing the wavefront aberration.

The main HOA effects (main parts of coma and spherical aberrations) arise from edge effects—that is, strong local curvature changes from the optical zone to the transition zone and from the transition zone to the untreated cornea.[30] It then is necessary to emphasize the use of a large optical zone (6.50 mm or more) to cover the scotopic pupil size and a large and smooth transition zone.

Nevertheless, because the pupil center is unstable, a morphologic reference is more advisable. It is well known, more-

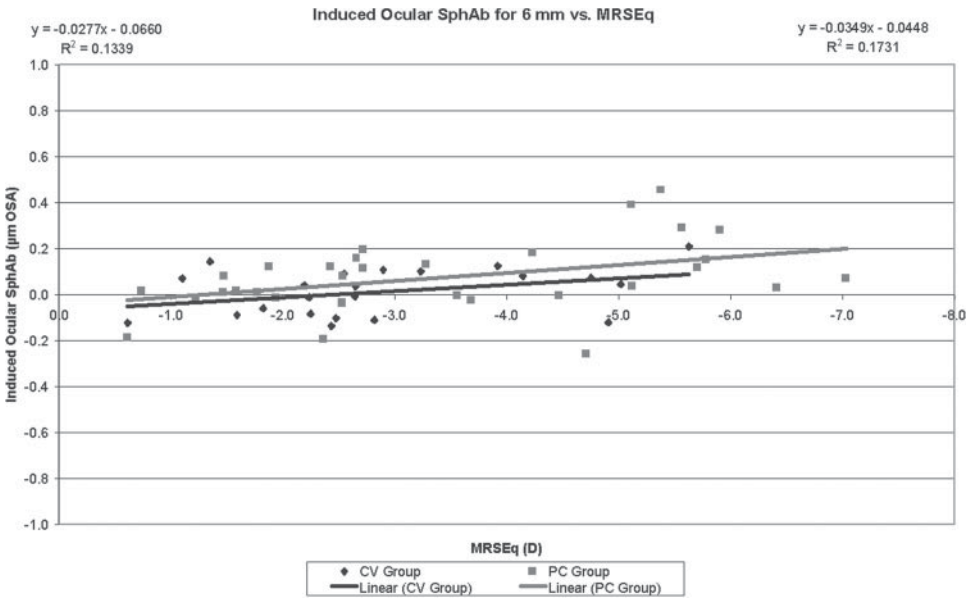

FIGURE 3. Induced spherical ocular aberration/diopter defocus ratio in the CV and the PC groups.

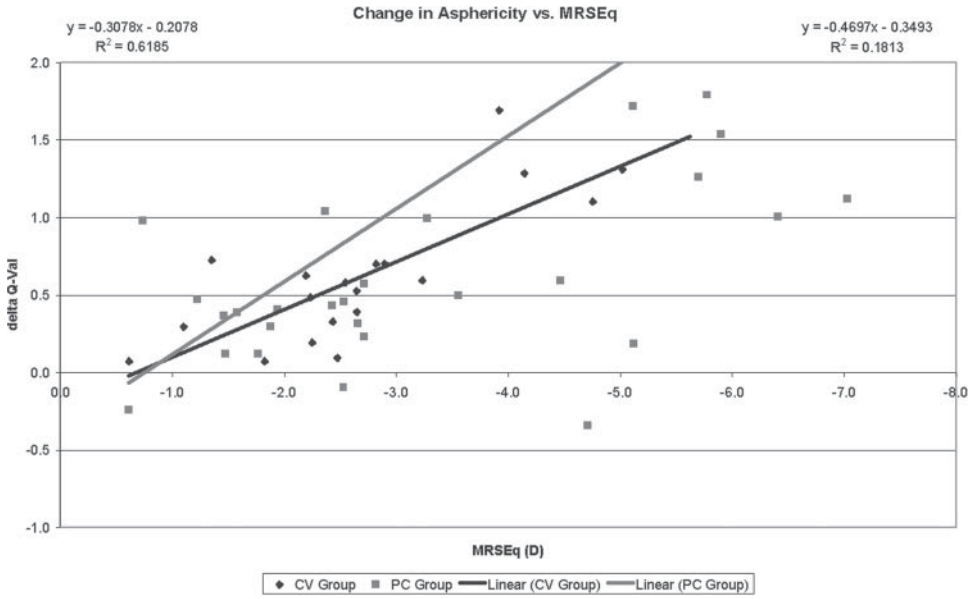

FIGURE 4. Change in asphericity (Q-Value)/defocus diopter ratio in the CV and the PC groups.

over, that the pupil center shifts with changes in pupil size,[31] since the entrance pupil we see is a virtual image of the real one.[32]

The CV in different modalities is the other major choice as the centration reference. In perfectly acquired topography, the CV represents the corneal vertex. In addition, if the human optical system were truly coaxial, the corneal vertex would represent the corneal intercept of the optical axis. Despite the fact that the human optical system is not truly coaxial, the cornea is the main refractive surface. Thus, the corneal vertex represents a stable preferable morphologic reference. However, there are several ways to determine the corneal vertex: the most extensively used one is to determine the coaxial corneal light reflex (first Purkinje image). Nevertheless, as de Ortueta and Arba Mosquera[3] have pointed out, there is a problem in using the coaxial light reflex, because surgeons differ; for instance, the coaxial light reflex is seen differently, depending on the surgeon's eye dominance, the surgeon's eye balance, or the stereopsis angle of the microscope. For example, the LadarVision platform (Alcon) uses a coaxial photograph as reference to determine the coaxial light reflex, which is independent of the surgeon's focus. For that reason, in the present study, ablations were centered using the pupillary offset, the distance between the pupil center and the normal CV, which corresponds to the angle between the line of sight and the optical axis. Thus, the three-dimensional combination of angle κ minus α minus λ. The angle κ represents the angle between the pupillary and visual axes, and the angle α represents the angle between optical and visual axes, angle λ represents the angle between the pupillary axis and the line of sight. Therefore, (visual axis − pupillary axis) − (visual axis − optical axis) − (line-of-sight − pupillary axis) = (optical axis − line of sight; Fig. 5).

In the Figure 5, for practical purposes, the foveola appears too far from the posterior pole and does not correspond to a realistic representation of the eye morphology However, it helps in understanding the key concept used in our vertex centration approach.

Considering this, for an aberration-free profile, aspherical, or, in general, noncustomized treatments, we use minimal patient data (sphere, cylinder, and axis values) from the diagnosis. Therefore, we assume that the patient's optical system is aberration-free or that those aberrations are not clinically relevant (otherwise, we would have planned a customized treatment). For those reasons, the most appropriate centering reference is the corneal vertex; we then modify the corneal asphericity with an aberration-free ablation profile, including loss of efficiency compensations. For customized wavefront treatments—that is, change in aberrations according to diagnosis measurements—we use a more comprehensive data set from the patient's diagnosis, including the aberrations, because the aberration maps are described for a reference system in the

TABLE 2. Results of Postoperative Evaluations at the 6-Month Follow-up for Both Groups

	CV Group		PC Group	
	Mean ± SD	**Range**	**Mean ± SD**	**Range**
Defocus (D)	−0.26 ± 0.49	−1.25 to +0.75	−0.29 ± 0.40	−1.00 to +0.50
Astigmatism (D)	0.15 ± 0.18	0.00 to 0.50	0.19 ± 0.21	0.00 to 0.50
BSCVA	1.24 ± 0.47	0.8 to 1.4	1.20 ± 0.45	0.7 to 1.4
Ocular coma (μm) (6.0 mm)	0.23 ± 0.11	0.02 to 0.52	0.27 ± 0.17	0.01 to 0.73
Ocular trefoil (μm) (6.0 mm)	0.15 ± 0.09	0.02 to 0.42	0.15 ± 0.08	0.02 to 0.40
Spherical ocular aberration (μm) (6.0 mm)	+0.09 ± 0.29	−0.35 to +0.59	+0.14 ± 0.30	−0.41 to +0.66
RMS HOA (μm) (6.0 mm)	0.48 ± 0.12	0.30 to 0.79	0.51 ± 0.17	0.25 to 0.93
Pupillary offset (mm)	0.28 ± 0.11	0.20 to 0.56	0.30 ± 0.19	0.20 to 0.87

Abbreviation is as in Table 1.

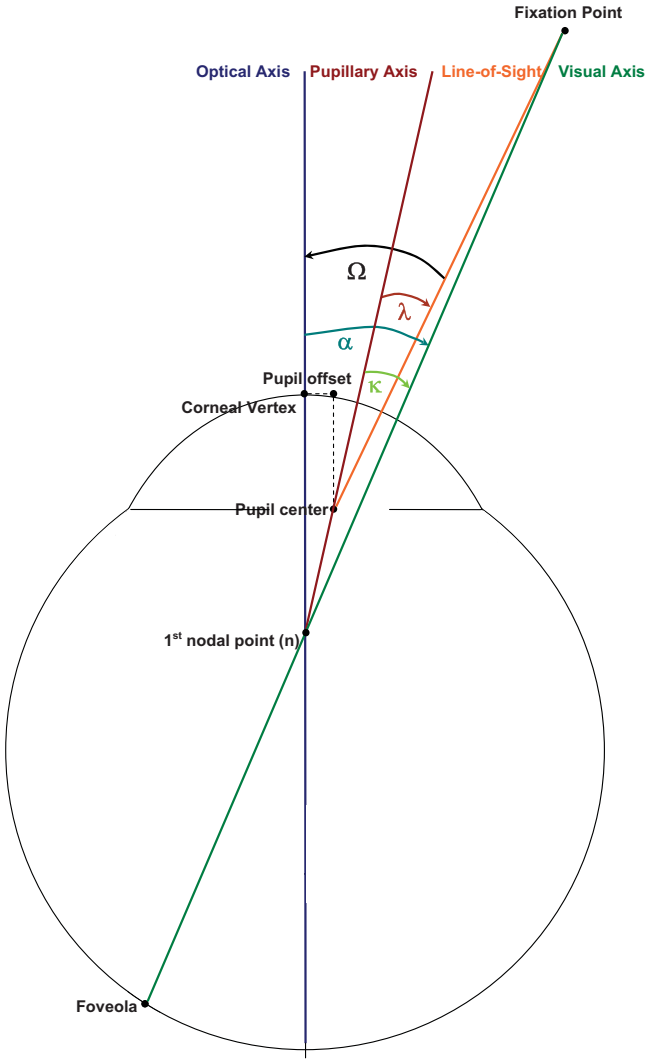

FIGURE 5. Diagram showing the key concept of alignment according to the pupillary offset and the relative orientation κ minus α minus λ angle, which represents the angle between the line of sight and the optical axis.

center of the entrance pupil. The most appropriate centering reference is the entrance pupil, as measured in the diagnosis.[26]

Providing different centering references for different types of treatments is not ideal, because it is difficult to standardize the procedures. Nevertheless, ray tracing indicates that the optical axis is the ideal centering reference. Because this is difficult to standardize and considering that the anterior corneal surface is the main refractive element of the human eye, the CV, defined as the point of maximum elevation, will be the closest reference as proposed here. It shall be, however, noticed that on the less-prevalent oblate corneas the point of maximum curvature (corneal apex) may be off center and not represented by the corneal vertex.

However, it would be interesting to refer the corneal and/or ocular wavefront measurements to the optical axis or the CV. This can be done easily for corneal wavefront analysis, because there is no limitation imposed by the pupil boundaries.[33] However, it is not as easy for ocular wavefront analysis, because the portion of the cornea above the entrance pupil alone is responsible for the foveal vision.[4] Moreover, in patients with corneal problems such as keratoconus/keratectasia, post-LASIK (pupil-centered), corneal warpage induced by contact lens wearing and other diseases causing irregularity on the anterior corneal surface, the corneal vertex and the corneal apex may shift. In those cases, the pupil center is probably more stable. Moreover, since most laser systems are designed to perform multiple procedures besides LASIK, it is more beneficial that excimer laser systems have the flexibility to choose different centration strategies.

The standard parameters to assess refractive surgery results—that is, efficacy, predictability, refractive outcome, stability, and safety, are inadequate for evaluating the optimal centration reference, at least in patients with myopic astigmatism.

With this analysis, no significant differences have been found that favor any of the centration strategies; however, trends have been found favoring CV treatments for refractive outcome and safety, and PC treatments for efficacy.

Concerning safety, 9% of the eyes lost one line of BSCVA; however, no single eye lost more than one line. The repeatability of the BSCVA within individuals from day to day is approximately one line of BSCVA. Moreover, there was a higher percentage of eyes that gained lines (38% and 24%) than that lost one line (8% and 10%).

A comparison of data in Tables 1 and 2 shows that no evaluated ocular aberration metrics increased in a clinically relevant way with either centration strategy. Further, because the ablation procedures are performed in a physical world, they are always affected by different sources of unavoidable inherent errors[34] that are sources of aberrations,[35] such as biomechanical reactions due to the flap cut,[36,37] blending zones, and cyclotorsion[38] and centration errors, spot size limitations, active eye-tracking[39] capabilities, and biomechanical reactions due to the ablation process.[40]

Although this may indicate that both centration strategies are virtually equivalent, the enrollment was limited to eyes with moderate-to-large pupil offset (>200 μm).

A deeper analysis of the induced ocular aberrations and the changes in asphericity showed significant differences favoring CV centration for the induction of coma and spherical ocular aberration and the changes in asphericity and no significant differences for the induced ocular trefoil.

Because of the smaller κ angle associated with myopes compared with hyperopes,[41,42] centration problems are less apparent. However, we wanted to test whether the κ angle in myopes was sufficiently large to show differences in results, because it is always desirable to achieve as much standardization as possible and not to treat the myopes by using one reference, while using another in the hyperopes.

Moreover, no significant differences were found in the pupillary offset before and after the treatments with any centration strategy.

With this analysis, no significant differences in visual outcomes were found that favored either centration strategy, with significant differences occurring only with the ocular aberration and asphericity measurements. The large optical zones used in the present study may be responsible for the lack of difference in postoperative visual outcomes in the two groups. Hyperopic LASIK provides smaller functional optical zones and, for this reason, these results should not be extrapolated to hyperopic LASIK.[11,43]

Previous studies[44] have reported that based on theoretical calculations with 7.0-mm pupils even for customized refractive surgery, that are much more sensitive to centration errors, it appears unlikely that optical quality would be degraded if the lateral alignment error did not exceed 0.45 mm. In 90% of eyes, even an accuracy of 0.8 mm or better would have been sufficient to achieve the goal.[43]

In our case, the pupillary offset averaged 0.29 mm and this moderate value seems to be sufficiently large to be responsible for differences in ocular aberrations, however, not large enough to correlate this difference in ocular aberrations with functional vision.

The accuracy, predictability, and stability of the refractive power change, together with the minimum external impact of the CAM ablation profiles on the HOAs led to superior VAs compared to the preoperative ones in both groups.

A limitation of this study is that we used a comparison based on two different groups of patients, with different centrations used as the reference. A direct comparison on a lateral/contralateral eye basis for the assignment of the centration reference may reduce the variability of external uncontrollable effects (such as flap cut, corneal response to the ablation, repeatability of the instruments, and cooperation of the patients). However, such a direct comparison may reduce patients' satisfaction, as patients may after surgery observe differences among eyes due to the different centrations.

In summary, the present study showed that morphologic centering references such as the CV, which are not standard in refractive surgery, yielded visual, optical, and refractive results comparable to those of pupil centration techniques for correction of myopia and myopic astigmatism in eyes with moderate to large pupillary offset. No significant differences in the comparative outcomes of both centration strategies were observed in visual results, but they were found in high order aberration results. Despite this, an absolute optimum centration reference could not be determined. Centering on the pupil offers the opportunity to minimize the optical zone size, whereas centering in the CV offers the opportunity to use a stable morphologic axis and to maintain the corneal morphology after treatment. Therefore, centration on the CV has the potential to replace the currently used standard pupil centration to correct noncustomized myopic astigmatism on normal corneas. Further studies are needed to determine stable appropriate centration references.

References

1. Pande M, Hillmann JS. Optical zone centration in keratorefractive surgery: entrance pupil center, visual axis, coaxially sighted corneal reflex, or geometric corneal center? *Ophthalmology.* 1993; 100:1230–1237.
2. Boxer Wachler BS, Korn TS, Chandra NS, Michel FK. Decentration of the optical zone: centering on the pupil versus the coaxially sighted corneal light reflex in LASIK for hyperopia. *J Refract Surg.* 2003;19:464–465.
3. de Ortueta D, Arba Mosquera S. Centration during hyperopic LASIK using the coaxial light reflex. *J Refract Surg.* 2007;23:11.
4. Uozato H, Guyton DL. Centering corneal surgical procedures. *Am J Ophthalmol.* 1987;103:264–275.
5. Mandell RB. Apparent pupil displacement in videokeratography. *CLAO J.* 1994;20:123–127.
6. Munnerlyn CR, Koons SJ, Marshall J. Photorefractive keratectomy: a technique for laser refractive surgery. *J Cataract Refract Surg.* 1988;14:46–52.
7. Mastropasqua L, Toto L, Zuppardi E, et al. Photorefractive keratectomy with aspheric profile of ablation versus conventional photorefractive keratectomy for myopia correction: six-month controlled clinical trial. *J Cataract Refract Surg.* 2006;32:109–116.
8. Mrochen M, Jankov M, Bueeler M, Seiler T. Correlation between corneal and total wavefront aberrations in myopic eyes. *J Refract Surg.* 2003;19:104–112.
9. Alio JL, Belda JI, Osman AA, Shalaby AM. Topography-guided laser in situ keratomileusis (TOPOLINK) to correct irregular astigmatism after previous refractive surgery. *J Refract Surg.* 2003;19:516–527.
10. Mrochen M, Kaemmerer M, Seiler T. Clinical results of wavefront-guided laser in situ keratomileusis 3 months after surgery. *J Cataract Refract Surg.* 2001;27:201–207.
11. Mrochen M, Donetzky C, Wüllner C, Löffler J. Wavefront-optimized ablation profiles: theoretical background. *J Cataract Refract Surg.* 2004;30:775–785.
12. Koller T, Iseli HP, Hafezi F, et al. Q-factor customized ablation profile for the correction of myopic astigmatism. *J Cataract Refract Surg.* 2006;32:584–589.
13. Levy Y, Segal O, Avni I, Zadok D. Ocular higher-order aberrations in eyes with supernormal vision. *Am J Ophthalmol.* 2005;139: 225–228.
14. Pablo Artal. *What Aberration Pattern (If Any) Produces the Best Vision?* Presented at the Sixth International Wavefront Congress, Athens, Greece; February 2005.
15. Marcos S, Cano D, Barbero S. Increase in corneal asphericity after standard laser in situ keratomileusis for myopia is not inherent to the Munnerlyn algorithm. *J Refract Surg* 2003;19:S592–S596.
16. Dorronsoro C, Cano D, Merayo-Lloves J, Marcos S. Experiments on PMMA models to predict the impact of corneal refractive surgery on corneal shape. *Opt Express.* 2006;14:6142–6156.
17. Arba Mosquera S, de Ortueta D. Geometrical analysis of the loss of ablation efficiency at non-normal incidence. *Opt Express*. 2008;16: 3877–3895.
18. Thibos LN. *Wavefront Data Reporting and Terminology.* Presented at the Second International Wavefront Congress, Monterey, CA, February 2001.
19. Thibos L, Bradley A, Applegate R. Accuracy and precision of objective refraction from wavefront aberrations. *Invest Ophthalmol Vis Sci*. 2004;4(4):329–351.
20. de Ortueta D. Planar flaps with the Carriazo-Pendular microkeratome. *J Refract Surg.* 2008;24(4):322; author reply 322–323.
21. de Ortueta D, Arba-Mosquera S. Topographical changes after hyperopic LASIK with the ESIRIS laser platform. *J Refract Surg*. 2008;24:137–144.
22. Huang D, Arif M. Spot size and quality of scanning laser correction of higher-order wavefront aberrations. *J Cataract Refract Surg*. 2002;28:407–416.
23. Guirao A, Williams D, MacRae S. Effect of beam size on the expected benefit of customized laser refractive surgery. *J Refract Surg*. 2003;19:15–23.
24. Bende T, Seiler T, Wollensak J. Side effects in excimer corneal surgery. Corneal thermal gradients. *Graefes Arch Clin Exp Ophthalmol*. 1988;226:277–280.
25. Bueeler M, Mrochen M. Simulation of eye-tracker latency, spot size, and ablation pulse depth on the correction of higher order wavefront aberrations with scanning spot laser systems. *J Refract Surg*. 2005;21:28–36.
26. Zernike F. Diffraction theory of the knife-edge test and its improved form, the phase-contrast method. *Monthly Notices of the Royal Astronomical Society.* 1934;94:377–384.
27. Thibos LN, Applegate RA, Schwiegerling JT, Webb R; VSIA Standards Taskforce Members. Standards for reporting the optical aberrations of eyes. *J Refract Surg* 2002;18:S652–S660.
28. Guirao A, Williams D, Cox I. Effect of rotation and translation on the expected benefit of an ideal method to correct the eyes higher-order aberrations. *J Opt Soc Am A.* 2001;18:1003–1015.
29. Gatinel D, Hoang-Xuan T, Azar DT. Determination of corneal asphericity after myopia surgery with the excimer laser: a mathematical model. *Invest Ophthalmol Vis Sci.* 2001;42:1736–1742.
30. Marcos S, Barbero S, Llorente L, Merayo-Lloves J. Optical response to LASIK surgery for myopia from total and corneal aberration measurements. *Invest Ophthalmol Vis Sci* 2001;42:3349–3356.
31. Yang Y, Thompson K, Burns S. Pupil location under mesopic, photopic and pharmacologically dilated conditions. *Invest Ophthalmol Vis Sci.* 2002;43:2508–2512.
32. Schruender S, Fuchs H, Spasovski S, Dankert A. Intraoperative corneal topography for image registration. *J Refract Surg.* 2002; 18:S624–S629.

33. Salmon TO. *Corneal Contribution to the Wavefront Aberration of the Eye.* PhD Thesis. Bloomington, IN: Indiana University; 1999: 70.
34. Lipshitz I. Thirty-four challenges to meet before excimer laser technology can achieve super vision. *J Refract Surg.* 2002;18:740–743.
35. Marcos S. Aberrations and visual performance following standard laser vision correction. *J Refract Surg.* 2001;17:S596–S601.
36. Tran DB, Sarayba MA, Bor Z, et al. Randomized prospective clinical study comparing induced aberrations with IntraLase and Hansatome flap creation in fellow eyes. *J Cataract Refract Surg.* 2005;31:97–105.
37. Durrie DS, Kezirian GM. Femtosecond laser versus mechanical keratome flaps in wavefront-guided laser in situ keratomileusis. *J Cataract Refract Surg.* 2005;31:120–126.
38. Smith EM Jr, Talamo JH. Cyclotorsion in the seated and the supine patient. *J Cataract Refract Surg.* 1995;21:402–403.
39. Tsai YY, Lin JM. Ablation centration after active eye-tracker-assisted photorefractive keratectomy and laser in situ keratomileusis. *J Cataract Refract Surg.* 2000;26:28–34.
40. Yoon G, MacRae S, Williams DR, Cox IG. Causes of spherical aberration induced by laser refractive surgery. *J Cataract Refract Surg.* 2005;31:127–135.
41. Artal P, Benito A, Tabernero J. The human eye is an example of robust optical design. *J Vision.* 2006;6:1–7.
42. Tabernero J, Benito A, Alcón E, Artal P. Mechanism of compensation of aberrations in the human eye. *J Opt Soc Am A.* 2007;24: 3274–3283.
43. Llorente L, Barbero S, Merayo J, Marcos S. Changes in corneal and total aberrations induced by LASIK surgery for hyperopia. *J Refract Surg*. 2004;20:203–216.
44. Bueeler M, Mrochen M, Seiler T. Maximum permissible lateral decentration in aberration-sensing and wavefront-guided corneal ablations. *J Cataract Refract Surg.* 2003;29:257–263.

Bilateral Symmetry before and Six Months after Aberration-Free™ Correction with the SCHWIND AMARIS TotalTech Laser: Clinical Outcomes

Maria Clara Arbelaez[1], Camila Vidal[1] and Samuel Arba-Mosquera[2,3]

ABSTRACT

Purpose: To compare the preoperative and postoperative bilateral symmetry between OD and OS eyes that have undergone femto-LASIK using the Ziemer LDV femtosecond laser system, the SCHWIND AMARIS Excimer Laser and the Aberration-free™ profiles implemented in the SCHWIND Custom Ablation Manager software.

Methods: A total of 25 LASIK patients were bilaterally evaluated at the six-month follow-up visit. In all cases standard examinations, pre- and postoperative analysis with corneal wavefront topography (OPTIKON Scout) were performed. Aberration-free™ aspheric treatments were devised using the Custom Ablation Manager software and ablations were performed by means of the SCHWIND AMARIS flying-spot excimer laser system (both SCHWIND eye-tech-solutions). In all cases LASIK flaps were created using an LDV femtosecond laser (Ziemer Group).

The OD/OS bilateral symmetry was evaluated in terms of corneal wavefront aberration.

Results: Preoperatively, 11 Zernike terms showed significant bilateral (OS-vs.-OD) symmetry, and only 6 Zernike terms were significantly different. Overall, 23 out of the 25 patients showed significant bilateral symmetry, and only 2 out of 25 patients showed significant differences. None of the aberration metrics changed from pre- to postoperative values by a clinically relevant amount. At the 6-month postoperative visit, 12 Zernike terms showed significant symmetry, and 8 terms were significantly different. Overall, 22 out of 25 patients showed significant bilateral symmetry (OS vs. OD), and only 3 out of 25 patients showed significant differences. Also, this postoperative examination revealed that 6 Zernike terms lost significant OS-vs.-OD symmetry, but 4 Zernike terms gained significant symmetry. Finally, 4 patients lost significant bilaterality, and 2 patients gained significant bilaterality: bilateral symmetry between eyes was better maintained in those patients with a clear preoperative bilateral symmetry.

Conclusions: Aberration-Free Treatments with the SCHWIND AMARIS did not induce clinically significant aberrations, maintained the global OD-vs.-OS bilateral symmetry, as well as the bilateral symmetry between corresponding Zernike terms (which influences binocular summation).

(J Optom 2010;3:20-28 ©2010 Spanish Council of Optometry)

Key Words: LASIK; corneal wavefront aberration; aberration-free treatment; bilateral; symmetry.

RESUMEN

Objetivo: Comparar la simetría bilateral (OD-OS) preoperativa y postoperativa, en ojos sometidos a una operación de femto-LASIK donde se empleó el sistema láser de femtosegundos Ziemer LDV, el láser de excímero SCHWIND AMARIS y donde se implementaron perfiles de ablación Aberration-free™ (sin aberraciones) en el software de control del láser (SCHWIND Custom Ablation Manager).

Métodos: Se evaluaron bilateralmente un total de 25 pacientes de LASIK transcurridos 6 meses de la operación. En todos los casos se llevó a cabo una revisión estándar, y se realizaron medidas pre- y postoperativas de topografía corneal (OPTIKON Scout). Se diseñaron tratamientos asféricos de tipo Aberration-free™ utilizando el software de control del láser, denominado Custom Ablation Manager. La ablación se realizó mediante el sistema láser de excímero SCHWIND AMARIS, con tecnología de barrido de punto flotante (flying-spot). Tanto el software como el sistema láser son de SCHWIND eye-tech-solutions. En todos los casos el "lentículo" del LASIK (también conocido como "colgajo" o "flap") se creó mediante un láser de femtosegundos LDV (Grupo Ziemer).

Se evaluó la simetría bilateral OD/OS comparando la aberración de onda asociada a la superficie anterior de la córnea en uno y otro ojo.

Resultados: Antes de la operación, existía simetría bilateral OD-OS para 11 términos de Zernike, mientras que sólo 6 de ellos eran significativamente diferentes. Globalmente, 23 de los 25 pacientes exhibían simetría bilateral, mientras que sólo para 2 de los 25 pacientes se observaron diferencias significativas. Ninguno de los parámetros utilizados para cuantificar las aberraciones varió de manera significativa (es decir, en una cantidad clínicamente relevante) debido a la operación. En la revisión postoperativa de los 6 meses, se observó una simetría significativa para 12 términos de Zernike, mientras que 8 términos resultaron ser significativamente distintos. Globalmente, 22 de los 25 pacientes presentaban simetria bilateralidad OD-OS significativa, mientras que sólo para 3 de los 25 pacientes se observaron diferencias significativas entre los dos ojos. En esta revisión postoperativa también se observó que para 6 términos de Zernike se había perdido una fracción significativa de la simetría OS-OD, mientras que para 4 términos la simetría aumentó de manera significativa. Para terminar, 4 pacientes perdieron una fracción significativa de la bilateralidad, mientras que en 2 pacientes la bilateralidad aumentó de manera significativa: la simetría bilateral entre los dos ojos se logró mantener mejor en aquellos pacientes que ya antes de la operación presentaban una clara simetría bilateral.

Conclusiones: Los tratamientos Aberration-FreeTM realizados con el sistema láser SCHWIND AMARIS no indujeron una cantidad clínicamente significativa de aberraciones y lograron mantener globalmente tanto la simetría bilateral OD-OS como la simetría bilateral entre términos de Zernike equivalentes (aspecto que influye sobre la sumación binocular).

(J Optom 2010;3:20-28 ©2010 Consejo General de Colegios de Ópticos-Optometristas de España)

Palabras Clave: LASIK; aberración de onda corneal; tratamiento libre de aberraciones; simetría bilateral.

From [1]Muscat Eye Laser Center. Muscat -Sultanate of Oman. [2]Grupo de Investigación de Cirugía Refractiva y Calidad de Visión, Instituto de Oftalmobiología Aplicada, University of Valladolid, Valladolid, Spain. [3]From SCHWIND eye-tech-solutions. Kleinostheim, Germany

Financial disclosure: Authors Arbelaez and Vidal have no proprietary interest in the materials presented herein

Received: 2 April 2009
Revised: 4 June 2009
Accepted: 23 June 2009

Corresponding author: Maria Clara Arbelaez. Muscat Eye Laser Center
P.O. Box 938; P.C. 117; Muscat; Sultanate of Oman
e-mail: drmaria@omantel.net.om

Introduction

Human vision is a binocular process. Having two eyes gives binocular summation, with which the ability to detect faint objects is enhanced.[1] It can make stereopsis possible, in which the parallax provided by the two eyes' different positions on the head gives precise depth perception.[2] Such binocular vision is usually accompanied by binocular fusion, in which a single image is seen despite each eye's having its own image of any object.[2]

Literature suggests that marked anisometropia is uncommon, in terms of either the magnitude of sphere or the amount of astigmatism,[3] with few notable exceptions[4] concluding that the axis of astigmatism does not follow any particular rule (mirror or direct symmetry) between right and left eyes.

Howland and Howland, employing the cross-cylinder aberroscope method they invented,[5] found that the optical aberrations of the eye differ greatly from subject to subject and are seldom symmetrical. Liang and Williams, using a Shack-Hartmann wave-front sensor,[6] found that although the pattern of aberrations varies from subject to subject, the aberrations (including irregular ones) of the left eye and those of the right eye of the same subject are correlated, indicating that they are not just random defects. Porter et al.[7] confirmed this observation in a large population.

The Indiana Aberration Study by Thibos et al.[8] characterized the aberration structure and the effects of these aberrations on vision, for a reasonably large population of normal, healthy eyes in young adults, and verified the hypothesis of bilateral symmetry.

Marcos and Burns[9] found that not only aberrations but also cone directionality varies across subjects, and that these two functions show a left-right eye symmetry.

Wang et al.[10] found that event though the anterior corneal surface's wave aberration varied greatly across subjects, a moderate-to-high degree of mirror symmetry existed between right and left eyes.

To our knowledge, very few studies in the literature have addressed the issue of symmetry of aberrations between eyes after corneal laser refractive surgery.[11] Jiménez et al.[11] found that binocular function deteriorates more than monocular function after LASIK, and that this deterioration increases as the interocular differences in terms of aberrations and corneal shape increase. They found that interocular differences above 0.4 μm of the Root-Mean-Square (RMS) for a 5-mm analysis diameter, lead to a decrease of more than 20% in binocular summation.

If binocular symmetry is manifested on virgin human eyes and it is an important factor for binocular vision, it shall be interesting to assess whether or not the existing symmetry is maintained after treating the cornea for ametropia correction using corneal laser refractive surgery.

Taking into account that corneal ablation in standard refractive-surgery treatments induces aberrations (one of the most significant side-effects in myopic LASIK is the induction of spherical aberration,[12] which causes halos and reduced contrast sensitivity[13]), special ablation patterns were designed to preserve the preoperative level of high-order aberrations (HOAs).[14-16]

In the current study we present measurements of the corneal wavefront aberration in 50 eyes (right and left eyes of 25 subjects), both preoperatively and 6 months after non-customised treatment. We analyzed the correlation of individual aberrations across the population, as well as the correlation of aberrations between the right and left eyes of the same subjects.

In this study, we used non-customised "Aberration-neutral" profiles, i.e., ablations were optimized to induce no change in wavefront aberration within the Optical Zone (OZ) other than sphere and cylinder components, leaving all existing HOAs unchanged because the best-corrected visual acuity (BCVA), in this patient, has been unaffected by the pre-existing aberrations (Artal P, What aberration pattern (if any) produces the best vision?, 6th International Wavefront Congress, Athens, Greece; February 2005). Thus, to compensate for the aberrations induction observed with other types of profile definitions,[17] several sources of aberration might be considered. For example, some of those sources of aberration are related to the loss of efficiency of the laser ablation for non-normal incidence.[18-20]

Patients and Methods

50 eyes (25 patients) that had been treated with the AMARIS "aberration neutral" (Aberration-Free™) aspheric ablation profiles were retrospectively analysed.

Inclusion criteria for review were bilateral surgery on the same day targeted for emmetropia, preoperative best spectacle corrected visual acuity (BCVA) ≥ 20/25 (logMAR ≤ 0.1) in both eyes, no signs of amblyopia, and successful completion of the 6-month follow-up.

Six-months follow-up data were available for all 50 eyes (100%), and their preoperative data were as follows: mean manifest defocus refraction: -2.47±2.51 D (range, -8.13 to +5.63 D) and mean manifest astigmatism magnitude: 2.02±0.91 D (range, 0.00 to 4.75 D). For all eyes we measured corneal topography[21] and derived corneal wavefront aberrations,[22,23] up to the 7th Zernike order (35 terms) (Keratron-Scout, OPTIKON2000, Rome, Italy), manifest refraction, uncorrected visual acuity[24] (UCVA) and BCVA. Measurements were performed preoperatively and also 1, 3, and 6 months after surgery.

All ablations were non-wavefront-guided but were based on aspheric[25] aberration-neutral (Aberration-Free™) profiles (and not on the profiles proposed by Munnerlyn[26]) to balance the induction of spherical aberration[27,28] (prolateness optimization[29,30]). This approach included a multidynamic aspherical transition zone, aberration and focus shift compensation due to tissue removal, pseudo-matrix-based spot positioning, enhanced compensation for the loss of efficiency;[31] all based on theoretical equations validated with ablation models and clinical evaluations.

A 6.5 mm central and fully corrected ablation zone was used in all eyes, together with a variable transition size that was automatically provided by the laser depending on the planned refractive correction (6.7 mm to 8.9 mm). The ablation was performed using the AMARIS excimer laser (SCHWIND eye-tech-solutions, Kleinostheim, Germany), which is a flying-spot laser system that uses real ablative spot volume locally considered through a self-constructing

algorithm and that controls for the local repetition rates to minimize the thermal load of the treatment.[32] Therefore, the ablated surface with the aspheric aberration-neutral (Aberration-Free™) profiles should be very smooth, possibly leading also to some benefits in terms of HOAs. Finally, all these optimizations theoretically diminish the induced wavefront aberration after myopic LASIK.

The AMARIS laser system works at a true repetition rate of 500 Hz and produces a beam with a size of 0.54 mm (Full-Width-at-Half-Maximum, FWHM) and a super-Gaussian spot profile.[33,34] High-speed eye tracking (pupil and limbus tracker with cyclotorsional tracking) with a 1050 Hz acquisition rate is accomplished with a 3-ms latency time.[35]

All flaps were created using a LDV femtosecond laser (Ziemer Group) with a 100 µm nominal flap thickness.

Optical errors centred on the line-of-sight,[36] representing the wavefront aberration, are described by means of Zernike polynomials[37] and their corresponding coefficients using OSA standard,[38] and analysed for a standardised diameter of 6 mm in order to derive corneal wavefront aberrations.

Correlations for Bilateral Symmetry of Zernike Terms Across Subjects

To test this hypothesis, we plotted left-vs.-right-eye scatter graphs for each Zernike term to analyse the predicted correlations between the two eyes. These plots reveal, for our sample, which Zernike modes show symmetry and which type of symmetry they show (pre- and postoperatively). What is expected is that 0 modes show even symmetry; -odd modes show even symmetry; -even modes show odd symmetry; +odd modes show odd symmetry and +even modes show even symmetry. The slope and intercept of the linear regression (least-square fitting) were calculated for each Zernike term up to the seventh radial order (36 coefficients). We assessed the statistical significance of the correlations using Student's T-test; the Coefficient of Determination (r^2) was also employed and the significance of the correlations has been evaluated assuming a metric that is distributed approximately as t with N—2 degrees of freedom, where N is the size of the sample.

Correlations for Symmetry of Aberrations in Right and Left Eye of the Same Subjects

Taking symmetry into account, we plotted for each subject left-vs.-right eye scatter graphs of the Zernike coefficients. These plots reveal which patients in our sample show symmetry (pre- and postoperatively). The slope and intercept of the linear regression (least-square fitting) were calculated for each subject (25 patients). We assessed the statistical significance of the correlations using Student's T-tests; the Coefficient of Determination (r^2) was also employed and the significance of the correlations has been evaluated assuming a metric that is distributed approximately as t with N—2 degrees of freedom, where N is the size of the sample.

Differences for Symmetry of Aberrations in Right and Left eye of the Same Subjects

Taking symmetry into account, we compared the Zernike coefficients obtained for the left and right eyes of the same subjects. We assessed the statistical significance using paired Student's T-tests.

Dioptrical Differences in Corneal Wavefront Aberration Between the Right and Left Eyes of the Same Subjects

For our analysis, the concept of equivalent defocus (DEQ) has been used as metric to be able to associate a dioptric power with the RMS of the Zernike coefficients.

DEQ is defined as the amount of defocus required to produce the same wavefront variance produced by one or more HOAs. A simple formula allows us to compute the DEQ in diopters if we know the total RMS wavefront error of the Zernike modes in question:

$$M_e = \frac{16\sqrt{3}RMS}{PD^2} \quad (1)$$

where M_e is the DEQ in diopters, RMS is the RMS wavefront error of the Zernike modes in question, and PD is the pupil diameter considered for the wavefront-aberration analysis.

On virgin eyes, DEQ as proposed by Thibos et al.[8] seems to be relatively insensitive to a change of analysis diameter.

Taking Symmetry into Account and Analysing the RMS of the Differential Corneal Wavefront Aberrations (RMS(ΔHOAb)) in DEQ

This theoretical difference, expressed in terms of DEQ, does not directly provide important answer to the binocular analysis. From experimental results[11] on binocular performance it was found that interocular differences above 0.4 µm of RMS for a 5 mm analysis diameter (0.4 D), lead to a decrease of more than 20% in binocular summation, whereas 0.2 µm of RMS (0.25 D), lead to a decrease of about 10%.

We have set a threshold value of 0.25 D to establish whether or not the differential corneal wavefront aberration between the left and the right eye was clinically relevant.

Changes in Bilateral Symmetryof Zernike Terms as a Result of Refractive Surgery

We analysed the number of Zernike terms that postoperatively lost, gained or preserved symmetry, compared to the preoperative baseline.

Changes in Bilateral Symmetryof Wavefront Aberration as a Result of Refractive Surgery

We analysed the number of patients that postoperatively lost, gained or preserved symmetry, compared to the preoperative baseline.

Statistical Analysis

The level of statistical significance was taken to be $P<0.05$.

Results

Adverse Events

Neither adverse events nor complications were observed intra- or postoperatively. No patient needed or demanded a retreatment of either eye.

TABLE 1
Comparison of refractive outcomes 6 months after surgery for all 50 eyes

	Pre-op (Mean ± SD)	Post-op (Mean ± SD)	*P*-value
Spherical Equivalent (D)	-2.47±2.51	-0.09±0.34	<0.0001*
Cylinder (D)	2.02±0.91	0.36±0.40	<0.001*
Predictability within ± 0.50 D (%)	---	84%	---
Predictability within ± 1.00 D (%)	---	98%	---
Spherical Aberration for 6.00 mm (µm)	0.25±0.08	0.27±0.23	.1
High-Order Aberrations for 6.00 mm (µm RMS)	0.47±0.16	0.57±0.22	<0.0005*

TABLE 2
Comparison of induced corneal aberrations after refractive surgery for all 50 eyes

Zernike term at 6-mm diameter	Preoperative (µm)	Postoperative (µm)	*P*-value
C[3,-3]	-0.14±0.15	-0.02±0.14	<0.0001
C[4,+2]	-0.08±0.09	-0.14±0.18	<0.005
C[4,+4]	+0.03±0.06	+0.01±0.06	<0.05
C[5,-3]	+0.01±0.03	-0.01±0.04	<0.0001
C[6,0]	0.00±0.02	+0.03±0.04	<0.0001

TABLE 3
Preoperative correlations for bilateral symmetry of Zernike terms across subjects for all 25 subjects (terms in bold face means these coefficients also correlated postoperatively, whereas regular face means these coefficients no longer correlated postoperatively)

Zernike term at 6-mm diameter	Slope	Intercept (µm)	*P*-value
C[2,-2]	-0.84	+0.07	<0.0005
C[2,0]	+0.90	+0.37	<0.0001
C[2,+2]	+0.77	-0.38	<0.0001
C[3,-3]	+0.74	-0.08	<0.005
C[3,-1]	+0.51	+0.05	<0.01
C[3,+1]	-0.56	+0.05	<0.01
C[4,-2]	-0.34	-0.01	<0.05
C[4,0]	+0.81	+0.02	<0.0001
C[4,+2]	+0.53	-0.02	<0.005
C[4,+4]	+0.80	+0.01	<0.01
C[5,-5]	+0.47	0.00	<0.01

TABLE 4
6-month postoperative correlations for bilateral symmetry of Zernike terms across subjects for all 25 subjects (terms in bold face means these coefficients also correlated preoperatively, whereas regular face means these coefficients did not correlate preoperatively)

Zernike term at 6-mm diameter	Slope	Intercept (µm)	*P*-value
C[2,0]	+0.80	+0.23	<0.0001
C[2,+2]	+0.84	-0.21	<0.0001
C[3,-3]	+0.81	-0.01	<0.0001
C[3,-1]	+0.65	+0.01	<0.005
C[3,+1]	-0.43	+0.07	<0.005
C[4,-4]	-0.55	-0.02	<0.05
C[4,-2]	-0.55	0.00	<0.01
C[4,0]	+0.73	+0.08	<0.0001
C[4,+2]	+0.58	-0.03	<0.0001
C[5,-3]	+0.60	-0.01	<0.01
C[6,0]	+0.73	+0.01	<0.0001
C[7,-1]	+0.67	0.00	<0.01

Refractive Outcomes

Concerning refractive outcomes, we merely want to outline the fact that at 6 months postoperatively both the spherical equivalent and the cylinder were significantly reduced to subclinical values: mean residual defocus refraction was -0.09±0.34 D (range: -1.00 to +0.75 D; *P*<.0001) and mean residual astigmatism magnitude 0.36±0.40 D (range: 0.00 to 1.50 D; *P*<.001). Also, 84% of eyes (n=42) were within ±0.50 D of the attempted correction *(Table 1)*. Despite the fact that the distribution of the corrections was bimodal (i.e., split between myopic and hyperopic corrections), and that single analysis across both groups probably isn't justified from a rigorous point of view, the analysis showed only a small difference when compared within each group individually.

Changes in Corneal Wavefront Aberration

Only 5 high-order Zernike terms (out of 30) changed significantly after treatment *(Table 2)*, whereas 25 high-order Zernike terms (out of 30) did not change after treatment. For all of them, the variation was well below the clinical relevance.

Correlations for Bilateral Symmetry of Zernike Terms Across Subjects

Preoperatively 11 Zernike terms showed significant OS-vs.-OD bilateral symmetry *(Table 3)*, whereas 6 months

TABLE 5
Preoperative correlations for symmetry of right- vs. left-eye aberrations of same subjects for 36 Zernike terms (0th-7th radial order)

	N-correl	Mean Slope	Range Slopes	Mean Intercept (µm)	Range Intercepts (µm)	*P*-value
Only horizontal terms	16	+0.526±0.524	-0.668 to +1.444	-0.004±0.011	-0.027 to +0.014	<0.05
Only vectorial terms	18	+0.704±0.401	-0.077 to +1.443	-0.003±0.008	-0.027 to +0.006	<0.05
Only HOA	23	+0.764±0.286	+0.185 to +1.294	-0.001±0.009	-0.027 to +0.014	<0.005
Ast + HOA	24	+0.841±0.265	+0.336 to +1.375	-0.003±0.018	-0.039 to +0.034	<0.005
Def + Ast + HOA	25	+0.921±0.245	+0.531 to +1.507	-0.005±0.031	-0.053 to +0.062	<0.0001

HOA =high-order aberrations; Ast = astigmatism; Def = defocus.

postoperatively 12 Zernike terms showed significant OS-vs.-OD symmetry *(Table 4)*. For the sake of simplicity, *tables 3* and *4* report only the coefficients for which a significant correlation in bilateral symmetry was observed.

Lack of Bilateral Symmetry of Individual Zernike Terms across Subjects

Preoperatively only 6 (C[4,-4], C[4,-2], C[5,+3], C[6,+6], C[7,-7], C[7,+3]) out of 33 Zernike terms were significantly different when comparing OS vs. OD for the same subject, whereas 6 months postoperatively 8 terms (C[4,-2], C[4,+4], C[5,+1], C[6,-6], C[6,-4], C[6,+2], C[7,-5], C[7,+3]) were significantly different when comparing OS vs. OD. For all of them, the difference was well below the clinical relevance.

Correlations for Symmetry of Aberrations in Right and Left Eye of the Same Subjects

Preoperatively 23 of 25 patients showed significant OS-vs.-OD bilateral symmetry (*Table 5*, the example of one patient is shown in *figure 1* for corneal aberrations and in *figure 2* for ocular aberrations), whereas 6 months postoperatively 22 of 25 patients showed significant OS-vs.-OD bilateral symmetry (*Table 6*, the postoperative example of the same patient is shown in *figure 1* for corneal aberrations and in *figure 2* for ocular aberrations). For the sake of simplicity, *tables 5* and *6* report the number of subjects for which a significant correlation in bilateral symmetry was observed, as well as mean values, standard deviation and ranges of the slopes and intercepts for different sets of Zernike terms.

Lack of Symmetry of Between the Right and Left Eye Aberrations of the Same Subjects

Preoperatively, only 2 out of 25 patients showed significant OS-vs.-OD differences, whereas 6 months postoperatively only 3 out of 25 patients showed significant OS-vs.-OD differences.

Dioptrical Differences of Corneal Wavefront Between the Right and Left Eyes of the Same Subjects

Preoperatively, only 4 out of 25 patients showed clinically relevant OS-vs.-OD differences (i.e., larger than 0.25 D), whereas 6 months postoperatively only 2 out of 25 patients showed clinically relevant OS-vs.-OD differences (i.e., larger than 0.25 D).

Changes in Bilateral Symmetry of Zernike Terms as a Result of Refractive Surgery

Six months postoperatively, 3 Zernike terms (C[2,-2], C[4,+4], C[5,-5]) had lost significant OS-vs.-OD correlation symmetry, 4 Zernike terms (C[4,-4], C[5,-3], C[6,0], C[7,-1]) had gained significant correlation symmetry, and 29 Zernike terms preserved correlation symmetry OS vs. OD compared to the preoperative baseline.

Six months postoperatively, for 6 Zernike terms (C[4,+4], C[5,+1], C[6,-6], C[6,-4], C[6,+2], C[7,-5]) the differences in OS-vs.-OD symmetry increased significantly, for 4 Zernike terms (C[4,-4], C[5,+3], C[6,+6], C[7,-7]) the differences in symmetry decreased significantly, and for 26 Zernike terms the OS-vs.-OD symmetry was preserved, compared to the preoperative baseline.

Changes in Bilateral Symmetry of Wavefront Aberration as a Result of Refractive Surgery

Six months postoperatively, 3 patients (#2, #15, #22) lost significant OS-vs.-OD correlation symmetry, 1 patient (18) gained significant correlation symmetry, and 21 patients preserved OS-vs.-OD correlation symmetry, compared to the preoperative baseline.

6 months postoperatively, for 2 patients (#6, #15) the differences in OS-vs.-OD symmetry increased significantly, for 1 patient (#7) the differences in symmetry decreased significantly, and for 22 patients the OS-vs.-OD symmetry was preserved, compared to the preoperative baseline.

An example of a patient well maintaining bilateral symmetry is shown in Figure 1 for corneal aberrations and in *figure 2* for ocular aberrations.

Discussion

The aim of this study was to evaluate the effects of laser corneal refractive surgery on the bilateral symmetry of the corneal wavefront aberration; in particular, following a treatment performed with the AMARIS system, which is

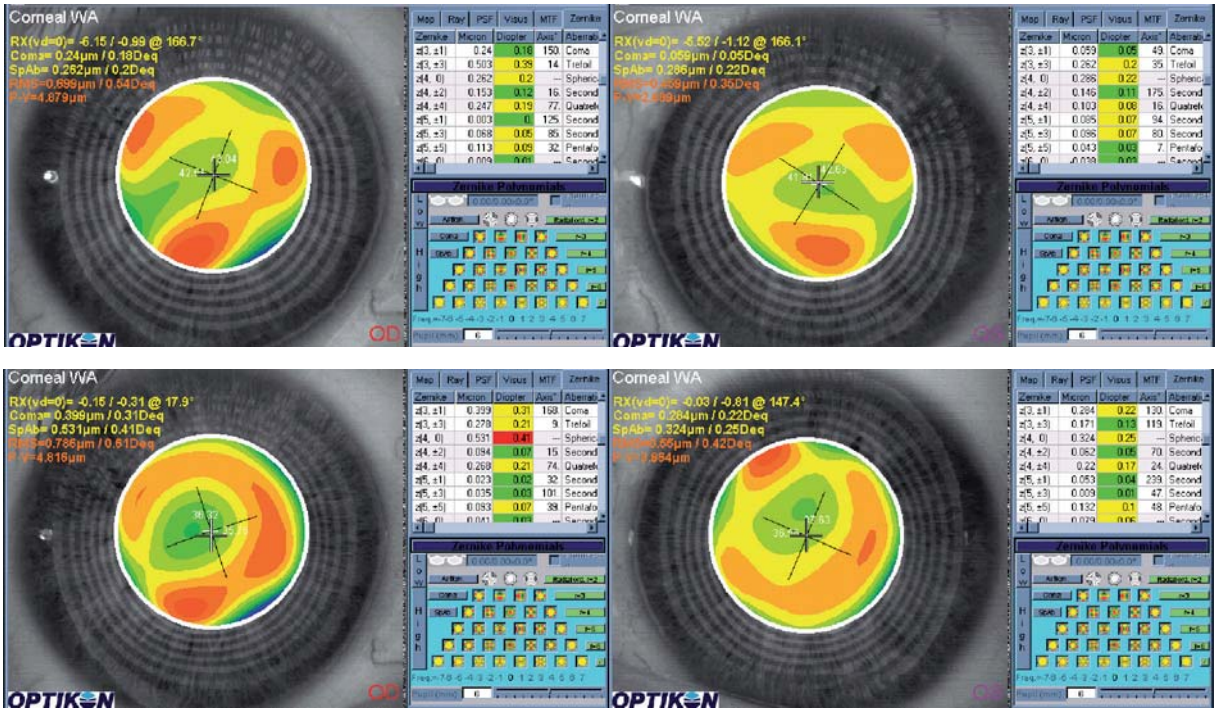

FIGURE 1
Bilateral symmetry in terms of corneal wavefront aberration, preoperatively and at the 6-month follow-up.

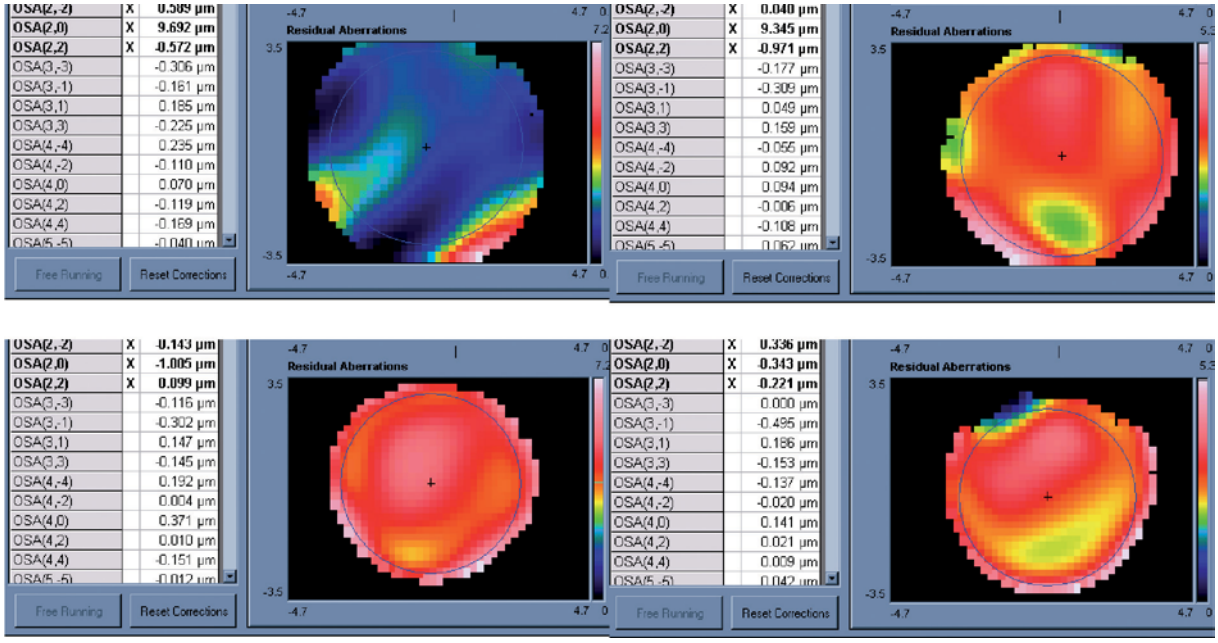

FIGURE 2
Bilateral symmetry of the ocular wavefront aberration for the same patient, preoperatively and at the 6-month follow-up.

based on an Aberration-Free™ ablation profile. The advantage of the Aberration-Free™ ablation profile is that it aims to be neutral for HOA, leaving the visual print of the patient as it was preoperatively with the best spectacle correction. If the aimed Aberration-Free concept would have been rigorously achieved, the bilateral symmetry between eyes would have been automatically obtained. In our group of patients, the aimed Aberration-Free concept does not hold rigorously true, but we had a very minor increase in corneal aberrations for a 6 mm pupil.

Our follow-up included 100% of the cases at 6 months and, although no nomogram adjustments were applied, in

TABLE 6
6-month postoperative correlations for symmetry of aberrations in the right and left eyes of the same subjects for 36 Zernike terms (0th-7th radial order)

	N-correl	Mean Slope	Range Slopes	Mean Intercept (µm)	Range Intercepts (µm)	*P*-value
Only horizontal terms	16	+0.495±0.451	-0.569 to +1.491	-0.004±0.014	-0.036 to +0.023	<0.05
Only vectorial terms	17	+0.507±0.394	-0.586 to +1.096	-0.004±0.011	-0.033 to +0.011	<0.05
Only HOAb	22	+0.651±0.248	+0.175 to +1.131	+0.002±0.012	-0.030 to +0.017	<0.005
Ast + HOAb	23	+0.804±0.298	+0.320 to +1.469	+0.004±0.017	-0.035 to +0.028	<0.005
Def + Ast + HOAb	25	+0.974±0.353	+0.509 to +1.851	+0.006±0.023	-0.040 to +0.043	<0.0001

HOA =high-order aberrations; Ast = astigmatism; Def = defocus

none of the cases retreatment was necessary. As a proof of stability, longer follow-ups and larger number of eyes would be more convincing, even though refractive spherical and astigmatic results are stable after 3 months.

Residual defocus averaged about -0.1 D, and residual cylinder about 0.4 D, with 84% of the eyes being within 0.50 D and 98% within 1.0 D of the target correction.

In our study, at the 6-month follow-up the percentage of eyes with an UCVA of 20/32 or better was 100% and 84% had an UCVA of 20/20 or better. No single eye had a loss of more than 1 line of BCVA, and 5 eyes had gained 2 or more lines of BCVA (P<.01).

As can be seen from the data presented herein, non-customised femtosecond LASIK performed with the combination LDV and AMARIS platforms is safe, effective, and it preserves reasonably well the bilateral symmetry of the corneal wavefront aberration between eyes. This may be related to the advantages of profiles aiming to be neutral for HOAs or to the fact that the high-speed AMARIS system reduces variability from stromal hydration effects, which increase with the duration of treatment.[39,40] Recognizing the high levels of defocus and astigmatism in this study, analysis of pre- and postoperative binocular vision[41] would be of interest and is a partial limitation of this study.[42] Further analysis of bilateral symmetry as a function of the analysis diameter is also of interest. Long-term follow-up on these eyes will help determine the stability of these accurate results. Comparing similar outcomes from other lasers to see if any of the parameters we measured are really different for other lasers or microkeratomes and analyses to determine if these parameters are clinically relevant will help to determine the impact of this work.

Cuesta et al.[43] found that even differences in corneal asphericity may affect the binocular visual function by diminishing the binocular contrast-sensitivity function. Jiménez et al.[11] found that following LASIK, binocular function deteriorates more than monocular function, and that this deterioration increases as the interocular differences in terms of aberrations and corneal shape increase. They also found that interocular differences above 0.4 µm of RMS for a 5 mm analysis diameter (0.4 D) lead to a drop in binocular summation of more than 20%.

In our study, only 4 out of 25 patients showed preoperative clinically relevant OS-vs.-OD differences (i.e., larger than 0.25 D), whereas 6 months postoperatively only 2 out of 25 patients showed clinically relevant OS-vs.-OD differences (i.e., larger than 0.25 D).

RMS(ΔHOAb) analysis for interocular differences accounts for the RMS of the differential corneal wavefront aberration and not for the difference of the corneal RMS(HOAb). RMS(ΔHOAb) is a rigorous analysis metric, because it accounts for any deviation (i.e. both inductions and reductions of the wavefront aberration, since both contribute positively to increase the RMS value). Furthermore, it can be mathematically demonstrated that:

$$RMS(\Delta HOAb) \geq \Delta RMS(HOAb) \qquad (2)$$

Six months postoperatively 3 Zernike terms lost significant OS-vs.-OD correlation symmetry and 4 Zernike terms gained significant correlation symmetry. However, two of them showed borderline correlations. 6 months postoperatively, for 6 Zernike terms the differences in OS-vs.-OD symmetry increased significantly whereas for 4 Zernike terms the differences in symmetry decreased significantly. However, 6 of them showed borderline significances of the difference. Also 6 months postoperatively, 3 patients lost significant OS-vs.-OD correlation symmetry, whereas 1 patient gained significant correlation symmetry. However, two of them showed borderline significances of the difference. All these borderline situations, actually shall be seen as "almost preserved" bilateral symmetry.

Despite large defocus and astigmatism magnitudes, our study shows that HOAs are either minimally increased or unchanged after surgery with the LDV and AMARIS systems (*Tables 1* and *2*). The main post-op HOAs effects (coma and spherical aberration) are caused by decentration and "edge" effects: i.e., to the strong local curvature change between the OZ and the Transition Zone (TZ) and from the TZ to the non-treated cornea. As a result, it is necessary to emphasize the use of huge OZs, covering the scotopic pupil size plus tolerance for possible decentrations, as well as well-defined TZ. In our study this was approached by the use of a 6.5-mm-diameter fully-corrected ablation zone with a mul-

tidynamic aspherical transition zone automatically calculated by the laser depending on the planned refractive correction (6.7 mm to 8.9 mm diameter).

Although this small series of treated eyes does not allow for definitive conclusions or evidence-based statements, our preliminary results are promising.

Limitations of our study include the moderate number of eyes, limited follow-up and the lack of a control group. The method to determine whether or not symmetry is maintained consist of comparing individual terms in a variety of ad hoc ways both before and after refractive surgery, ignoring the fact that retinal image quality for any given individual is based on the sum of all terms. However, similar methodologies have been already used before.[9] At this stage, we did not perform any specific visual tests on binocular vision; for example, stereotests. Some patients may not have good stereopsis but they may show good aberration symmetry. The analysis of bilateral symmetry should be related to the patients' binocular vision status. Despite these limitations, we were able to demonstrate that "aberration neutral" ablation profiles reasonably preserve the bilateral symmetry between eyes in terms of corneal wavefront aberration. The presented results cannot be extrapolated to patients with symptoms of amblyopia,[44] anisometropia, nystagmus, or aniseikonia[45] without further studies.

This does not mean any "good or bad" point for binocular vision. Taking into account that we cannot precisely evaluate the role of aberrations monocularly (patients with a high level of aberrations can have an excellent visual acuity and vice versa), it is even more difficult to do it binocularly. The important question in binocular vision is "the role of interocular-differences", and if they can influence significantly binocular performance. Interocular-differences can be minor but significant for visual performance. Further studies shall help to determine the impact of this on binocular visual performance.

In summary, this study demonstrated that "aberration neutral" profile definitions (as implemented at the SCHWIND AMARIS system), which are not standard in refractive surgery, yield very good visual, optical and refractive results, and reasonably preserve the bilateral symmetry between eyes (which influence binocular summation[44]) of the corneal wavefront aberration with no clinically relevant induction of HOAs (which influence contrast sensitivity[46]). In this sense, "Aberration neutral" ablation profiles, as demonstrated here, have therefore the potential to replace current standard algorithms for the non-customised correction of refractive ametropias in laser corneal refractive surgery.

References

1. Blake R, Fox R. The psychophysical inquiry into binocular summation. Perception & psychophysics. 1973;14:161-185.
2. Wheatstone C. Contributions to the physiology of vision.-Part the First. On some remarkable, and hitherto unobserved, phænomena of binocular vision. Philosophical Transactions of the Royal Society of London. 1838;128:371-394.
3. Almeder LM, Peck LB, Howland HC. Prevalence of anisometropia in volunteer laboratory and school screening populations. Invest Ophthalmol Vis Sci. 1990;31:2448-2455.
4. McKendrick AM, Brennan NA. The axis of astigmatism in right and left eye pairs. Optom Vis Sci. 1997;74:668-675.
5. Howland HC, Howland B. A subjective method for the measurement of monochromatic aberrations of the eye. J Opt Soc Am. 1977;67: 1508-1518.
6. Liang J, Williams DR. Aberrations and retinal image quality of the normal human eye. J Opt Soc Am A. 1997;14:2873-2883.
7. Porter J, Guirao A, Cox IG, Williams DR. Monochromatic aberrations of the human eye in a large population. J Opt Soc Am A. 2001;18: 1793-1803.
8. Thibos LN, Hong X, Bradley A, Cheng X. Statistical variation of aberration structure and image quality in a normal population of healthy eyes. J Opt Soc Am A Opt Image Sci Vis. 2002;19:2329-2348.
9. Marcos S, Burns SA. On the symmetry between eyes of wavefront aberration and cone directionality. Vision Res. 2000;40:2437-2447.
10. Wang L, Dai E, Koch DD, Nathoo A. Optical aberrations of the human anterior cornea. J Cataract Refract Surg. 2003;29:1514-1521.
11. Jiménez JR, Villa C, Anera RG, Gutiérrez R, del Barco LJ. Binocular visual performance after LASIK. J Refract Surg. 2006;22:679-688.
12. Moreno-Barriuso E, Lloves JM, Marcos S. Ocular Aberrations before and after myopic corneal refractive surgery: LASIK-induced changes measured with LASER ray tracing. Invest Ophthalmol Vis Sci. 2001; 42:1396-1403.
13. Mastropasqua L, Toto L, Zuppardi E, et al. Photorefractive keratectomy with aspheric profile of ablation versus conventional photorefractive keratectomy for myopia correction: six-month controlled clinical trial. J Cataract Refract Surg. 2006;32:109-116.
14. Mrochen M, Donetzky C, Wüllner C, Löffler J. Wavefront-optimized ablation profiles: Theoretical background. J Cataract Refract Surg. 2004;30:775-785.
15. Koller T, Iseli HP, Hafezi F, Mrochen M, Seiler T. Q-factor customized ablation profile for the correction of myopic astigmatism. J Cataract Refract Surg. 2006;32:584-589.
16. Mastropasqua L, Nubile M, Ciancaglini M, Toto L, Ballone E. Prospective randomized comparison of wavefront-guided and conventional photorefractive keratectomy for myopia with the meditec MEL 70 laser. J Refract Surg. 2004;20:422-431.
17. Marcos S, Cano D, Barbero S. Increase in corneal asphericity after standard LASIK for myopia is not inherent to the Munnerlyn algorithm. J Refract Surg. 2003;19:S592-S596.
18. Mrochen M, Seiler T. Influence of Corneal Curvature on Calculation of Ablation Patterns used in photorefractive Laser Surgery. J Refract Surg; 2001;17:584-587.
19. Jiménez JR, Anera RG, Jiménez del Barco L, Hita E. Effect on laser-ablation algorithms of reflection losses and nonnormal incidence on the anterior cornea. Applied Physics Letters. 2002;81:1521-1523.
20. Jiménez JR, Anera RG, Jiménez del Barco L, Hita E, Pérez-Ocón F. Correlation factor for ablation algorithms used in corneal refractive surgery with Gaussian-profile beams. Opt Express. 2005;13:336-343.
21. Mattioli R, Tripoli NK. Corneal geometry reconstruction with the Keratron videokeratographer. Optom Vis Sci. 1997;74:881-894.
22. Salmon TO. Corneal contribution to the wavefront aberration of the eye. PhD Dissertation, 1999:70.
23. Mrochen M, Jankov M, Bueeler M, Seiler T. Correlation between corneal and total wavefront aberrations in myopic eyes. J Refract Surg. 2003;19:104-112.
24. Letterproeven tot Bepaling der Gezichtsscherpte, Snellen H. Utrecht, Weyers, 1862.
25. Mrochen M, Büeler M. [Aspheric optics: physical fundamentals] Ophthalmologe. 2008;105:224-233.
26. Munnerlyn CR, Koons SJ, Marshall J. Photorefractive keratectomy: a technique for laser refractive surgery. J Cataract Refract Surg. 1988; 14:46-52.
27. Yoon G, MacRae S, Williams DR, Cox IG. Causes of spherical aberration induced by laser refractive surgery. J Cataract Refract Surg. 2005; 31:127-135.
28. Hersh PS, Fry K, Blaker JW. Spherical aberration after laser in situ keratomileusis and photorefractive keratectomy. Clinical results and theoretical models of etiology. J Cataract Refract Surg. 2003;29:2096-2104.
29. Gatinel D, Malet J, Hoang-Xuan T, Azar DT. Analysis of customized corneal ablations: theoretical limitations of increasing negative asphericity. Invest Ophthalmol Vis Sci. 2002;43:941-948.
30. Calossi A. Corneal asphericity and spherical aberration. J Refract Surg. 2007;23:505-514.
31. Arba Mosquera S, de Ortueta D. Geometrical analysis of the loss of ablation efficiency at non-normal incidence. Opt Express. 2008;16: 3877-3895.
32. Bende T, Seiler T, Wollensak J. Corneal thermal gradients, Graefes Arch Clin Exp Ophthalmol. 1988;226:277-280.

33. Huang D, Arif M. Spot size and quality of scanning laser correction of higher-order wavefront aberrations. J Cataract Refract Surg. 2002; 28:407-416.
34. Guirao A, Williams D, MacRae S. Effect of beam size on the Expected benefit of customized laser refractive surgery. J Refract Surg. 2003;19: 15-23.
35. Bueeler M, Mrochen M. Simulation of eye-tracker latency, spot size, and ablation pulse depth on the correction of higher order wavefront aberrations with scanning spot laser systems. J Refract Surg. 2005;21: 28-36.
36. Applegate RA, Thibos LN, Twa MD, Sarver EJ. Importance of fixation, pupil center, and reference axis in ocular wavefront sensing, videokeratography, and retinal image quality. J Cataract Refract Surg. 2009;35: 139-152.
37. Zernike F. Diffraction theory of the knife-edge test and its improved form, the phase-contrast method. Monthly Notices of the Royal Astronomical Society. 1934;94:377-384.
38. Thibos LN, Applegate RA, Schwiegerling JT, Webb R. VSIA Standards Taskforce Members. Standards for reporting the optical aberrations of eyes. J Refract Surg. 2002;18:S652-S660.
39. Kim WS, Jo JM. Corneal hydration affects ablation during laser in situ keratomileusis surgery. Cornea. 2001;20:394-397.
40. Dougherty PJ, Wellish KL, Maloney RK. Excimer laser ablation rate and corneal hydration. Am J Ophthalmol. 1994;118:169-176.
41. Fam HB, Lim KL. Effect of higher-order wavefront aberrations on binocular summation. J Refract Surg. 2004;20:S570-S575.
42. Nelson-Quigg JM, Cello K, Johnson CA. Predicting binocular visual field sensitivity from monocular visual field results. Invest Ophthalmol Vis Sci. 2000;41:2212-2221.
43. Cuesta JR, Anera RG, Jiménez R, Salas C. Impact of interocular differences in corneal asphericity on binocular summation. Am J Ophthalmol. 2003;135:279-284.
44. Mansouri B, Thompson B, Hess RF. Measurement of suprathreshold binocular interactions in amblyopia. Vision Res. 2008;48:2775-2784.
45. Jiménez JR, Ponce A, Anera RG. Induced aniseikonia diminishes binocular contrast sensitivity and binocular summation. Optom Vis Sci. 2004;81:559-562.
46. Jiménez JR, Castro JJ, Jiménez R, Hita E. Interocular differences in higher-order aberrations on binocular visual performance. Optom Vis Sci. 2008;85:174-179.

Journal of Modern Optics
Vol. 57, No. 12, 10 July 2010, 1041–1074

Taylor & Francis
Taylor & Francis Group

TOPICAL REVIEW

Laser corneal refractive surgery in the twenty-first century: a review of the impact of refractive surgery on high-order aberrations (and vice versa)

Samuel Arba-Mosquera[a,b]*, Maria C. Arbelaez[c] and Diego de Ortueta[d]

[a]*Grupo de Investigación de Cirugía Refractiva y Calidad de Visión, Instituto de Oftalmobiología Aplicada, University of Valladolid, Valladolid, Spain;* [b]*SCHWIND eye-tech-solutions, Kleinostheim, Germany;* [c]*Muscat Eye Laser Center, Sultanate of Oman;* [d]*Augenzentrum Recklinghausen, Recklinghausen, Germany*

(*Received 23 November 2009; final version received 27 April 2010*)

Here we review the situation of laser corneal refractive surgery in the twenty-first century. We pay special attention to the change in aberrations, covering the compensation of the loss of ablation efficiency at non-normal incidence, the effects of cyclotorsional errors, aspheric, wavefront optimized and aberration neutral concepts, and centration of refractive profiles. A review of the clinical outcomes is provided including myopic, hyperopic, and astigmatic, as well as wavefront customized or presbyopic outcomes.

Keywords: refractive surgery; aberrations; wavefront; cornea; ablation; excimer

1. Introduction

Since the introduction of laser technologies [1,2] for refractive surgery [3,4], the change of the corneal curvature to compensate in a controlled manner for refractive errors of the eye [5,6] is more accurate than ever [7–9]. Late in the 1980s photo-refractive keratectomy (PRK) [10] was performed with broad beam lasers, mechanical debridement, small optical zones 5 mm, without transition zones, and the surgery used to be unilateral; at the same time, excimer laser keratomileusis [11] was performed with thick free caps (240 μm), ablated on the underside of the flap and then sutured in place.

In the early 1990s [12], laser-assisted *in situ* keratomileusis (LASIK) [13] was developed, by creating a hinged flap (180 μm); ablating on the stromal surface, and no suture was needed. In the mid-1990s the first scanning lasers were used [14], and the ablation zones were increased up to 7 mm, moreover, alcohol debridement was slowly replacing mechanical debridement in surface treatments [15]. Late in the 1990s, laser systems were enhanced by adapting eye-tracking technologies [16]. In the early 2000s, laser-assisted sub-epithelial keratectomy (LASEK) [17] was introduced by creating epithelial flaps, and the laser technology improved on introducing flying spot patterns [18].

Recently, epithelial laser *in situ* keratomileusis (Epi-LASIK) [19], and epithelial laser-assisted sub-epithelial keratectomy (Epi-LASEK) [20] were introduced by creating a truly epithelial flap at the Bowman's layer level, and femtosecond-laser-assisted laser *in situ* keratomileusis (Femto-LASIK) [21,22], thin-flap laser *in situ* keratomileusis (Thin-Flap-LASIK) [23,24], and ultra-thin-flap laser *in situ* keratomileusis (Ultra-Thin-Flap-LASIK) [23] were introduced by creating a flap slightly beneath Bowman's layer level (sub-Bowman's keratomileusis [25]) [26].

Nowadays, technology has evolved significantly and uses sophisticated algorithms, optimized tools in the planning, and proposes the challenge of improving surgery outcomes in terms of visual acuity and night vision [27–29]. At the same time, patients have a better understanding and are better informed with regard to the potential of laser refractive surgery, raising quality requirements demanded of clinical staff and equipment [30].

There is now a wide variety of excimer lasers on the market for use in corneal refractive surgery. Although there are numerous studies showing good results for individual laser platforms, there are few comparative studies between lasers [31–34]. There are even fewer studies looking at outcomes in the ideal study situation where two lasers are used on the same patient, i.e. one laser for one eye and the other laser for the contralateral eye [35,36]. This in theory minimizes inter-patient differences with regards to corneal wound healing and biomechanics and allows for a more accurate assessment of outcomes, allowing a direct comparison by the same doctor on the same patients.

*Corresponding author. Email: samuel.arba.mosquera@eye-tech.net

ISSN 0950–0340 print/ISSN 1362–3044 online

DOI: 10.1080/09500340.2010.493243
http://www.informaworld.com

2. Induction of aberrations

2.1. Loss of ablation efficiency

The currently available methods allow for the correction of refractive defects such as myopia, hyperopia [37], or astigmatism [38]. One of the unintended effects induced by laser surgery is the induction of spherical aberration [39], which causes halos and reduced contrast sensitivity [40]. The loss of ablation efficiency at non-normal incidence can explain, in part, many of these unwanted effects, such as induction of spherical aberrations or high order astigmatism and consequently the extreme oblateness of postoperative corneas after myopic surgery [41].

Considering a loss of efficiency model applied to a simple myopic profile in order to get the achieved profile etched into the cornea, the profile 'shrinks', steepening the average slope and then slightly increasing the myopic power of the profile as well as inducing spherical aberrations. The net effect can be expressed as an unintended positive spherical aberration and a small overcorrection of the spherical component. Applied to a simple hyperopic profile, the profile 'softens', flattening the average slope and then decreasing the hyperopic power of the profile as well as inducing spherical aberrations. The net effect can be expressed as an undercorrection of the spherical component and a small amount of induced negative spherical aberration. Applied to a simple myopic astigmatism profile, the neutral axis becomes refractive, being less ablated in the periphery as compared to the center, whereas the refractive axis 'shrinks', steepening the curvature and then slightly increasing the myopic power of the axis as well as inducing aberrations. The net effect can be expressed as an unintended myopic ablation (hyperopic shift), and a small undercorrection of the astigmatic component. Applied to a PTK profile, the flat profile becomes myopic due to the loss of efficiency, resulting in an unintended myopic ablation (hyperopic shift) [42].

Several models have been proposed to compensate for those effects.

The simple model of ablation efficiency due to non-normal incidence [43] is based on several assumptions, including that the cornea can be shaped spherically, that the energy profile of the beam is flat, or that reflection losses are negligible. In addition, the spot overlap is not considered. The efficiency is defined as the ratio between the depth of impact on each point and the nominal impact depth (at normal incidence),

$$\mathrm{Eff}(r) = \frac{d(r)}{d(0)}, \tag{1}$$

where Eff is the ablation efficiency at a radial distance r of the optical axis of the ablation center, and d is the depth of the impact at a radial distance r of the optical axis of the ablation.

The simple model of ablation efficiency at non-normal incidence bases its success on its simplicity, which forms the reason why it is still used by some trading houses. The problems arising from the simple model directly derive from its simplicity, and consequently the limitations of application as required by their implicit assumptions. The simple model does not consider the calculation or the asphericity of the cornea, or the energy profile of the beam, or the overlap of impacts, overestimating the ablation efficiency, underestimating its compensation.

The model by Jiménez et al. [44,45] provides an analytical expression for an adjustment factor to be used in photorefractive treatments that includes both compensation for reflection and for geometric distortion. Later on, the authors refined the model by incorporation of non-linear deviations with regard to the Lambert–Beer law [46,47].

The Jiménez et al. model eliminates some problems of the simple model, by considering the energy profile of the beam, overlapping, and losses by reflection. However, it does not consider the calculation nor asphericity of the cornea, it assumes that the energy profile is a Gaussian beam, assumes unpolarized light, it does not address the size or shape of the impact, it does not consider that the radius of curvature changes locally throughout the treatment, and accordingly the angle of incidence. Therefore, it often slightly overestimates the ablation efficiency, partially underestimating its compensation.

The model by Dorronsoro et al. [48,49] provides a new approach to the problem. Flat and spherical polymethylmethacrylate (PMMA) substrates were ablated with a commercial excimer laser system. The relationship between the profiles obtained in spherical and flat sheets of PMMA was used for estimating the ablation efficiency depending on the distance from the optical axis of the lens. The predicted changes in efficiency were reasonably well correlated with the changes in asphericity and spherical aberration observed clinically using the same laser system, so that a correction factor valid for a given algorithm and a laser in particular could be derived.

The Dorronsoro et al. model provides a completely new approach to the problem. It eliminates many of the problems of both the simple model and the model by Jiménez et al., reducing the number of assumptions and using an empirical approach. Even so, it assumes that the reflection losses on the cornea and PMMA are identical, it does not consider the local radius of corneal curvature, its asphericity or applied correction, it does not consider that the radius of curvature changes locally throughout the treatment,

and accordingly the angle of incidence, and it does not consider the effects for different values of fluence.

The model by Arba-Mosquera and de Ortueta [50] provides a general method to analyze the loss of ablation efficiency at non-normal incidence in a geometrical way. The model is comprehensive and directly considers curvature, system geometry, applied correction, and astigmatism as model parameters, and indirectly laser beam characteristics and ablative spot properties. The model replaces the direct dependency on the fluence by a direct dependence on the nominal spot volume and on considerations about the area illuminated by the beam, reducing the analysis to pure geometry of impact. Compensation of the loss of ablation efficiency at non-normal incidence can be made at relatively low cost and would directly improve the quality of results.

The model by Arba-Mosquera and de Ortueta eliminates the direct dependence on fluence and replaces it by direct considerations on the nominal spot volume and on the area illuminated by the beam, reducing the analysis to pure geometry of impact. The proposed model provides results essentially identical to those obtained with the model by Dorronsoro et al. Additionally, it offers an analytical expression including some parameters that were ignored (or at least not directly addressed) in previous analytical approaches. The good agreement of the proposed model with results reported in Dorronsoro's paper – to our knowledge the first study using an empirical approach to actually measure the ablation efficiency – may indicate that the used approach including the discussed simplifications is a reasonable description of the loss of efficiency effects. In so far, this model may complement previous analytical approaches to the efficiency problem and may sustain the observations reported by Dorronsoro et al. Finally, the model by Kwon et al. [51,52] develops a rigorous simulation model to evaluate ablation algorithms and surgery outcomes in laser refractive surgery. The Corneal Ablation SIMulator (CASIM) simulates an entire surgical process, which includes calculating an ablation profile from measured wavefront errors, generating a shot pattern for a flying spot laser beam, simulation of the shot-by-shot ablation process [53] based on a measured or modeled beam profile, and healing of the cornea after surgery. Without considering the effect of corneal healing, they found that ablation efficiency reduction in the periphery depends on the peak fluence of the laser beam, corneal asphericity increases even in the surgery using an ablation profile based on the exact Munnerlyn formula, contrary to previous reports, and post-surgery corneal asphericity increases by a smaller amount in high fluence small Gaussian beam surgery than in low fluence truncated Gaussian beam. To explain the origin of changes in corneal asphericity and induced spherical aberration after laser refractive surgery, a rigorous model, including the corneal remodeling that occurs through healing was refined. When the exact Munnerlyn formula is used, the CASIM modeling and the clinical data exhibit a high degree of correlation. The modeling predicts that the postoperative cornea will be oblate, with substantial induced spherical aberration. A 6-month post-surgery asphericity is predicted by CASIM with a correlation of $R^2 = 0.94$. The corneal remodeling included in CASIM accounts, on the average, for 45% and 69% of the increase in asphericity and spherical aberration, respectively, with the remainder due to the ablation efficiency. The modeling shows that clinically observed increases in corneal asphericity and induction of spherical aberration can be explained by the effects of corneal remodeling due to healing and by the ablation efficiency reduction due to laser angle of incidence. The model is capable of predicting clinical outcomes for procedures performed with flying spot laser systems and could be used to design compensated ablation profiles to improve the clinical outcomes for custom as well as conventional laser refractive procedures [54].

A comparison of the results by applying the different models can be found in Figure 1.

Different effects interact; the beam is compressed due to the loss of efficiency, but at the same time expands due to the angular 'projection'. Losses of ablation efficiency at non-normal incidence in refractive surgery, may explain up to 45% of the reported increase in spherical aberrations. The loss of efficiency is an effect that should be offset in commercial laser systems using sophisticated algorithms that cover most of the possible variables. Parallel to the clinical developments, increasingly capable, reliable, and safer laser systems with better resolution and accuracy are required.

Corneal curvature and applied correction play an important role in the determination of the ablation efficiency and are taken into account for accurate results. However, corneal toricity and applied astigmatism do not have a relevant impact as long as their values correspond to those of normal corneas. Only when toricity or astigmatism exceeds 3 D, their effects on ablation efficiency start to be significant. The ablation efficiency is very poor close to the ablation threshold [55] and steadily increases with increasing radiant exposure. In addition, differences between the efficiencies for the cornea and PMMA increase with lowering radiant exposure.

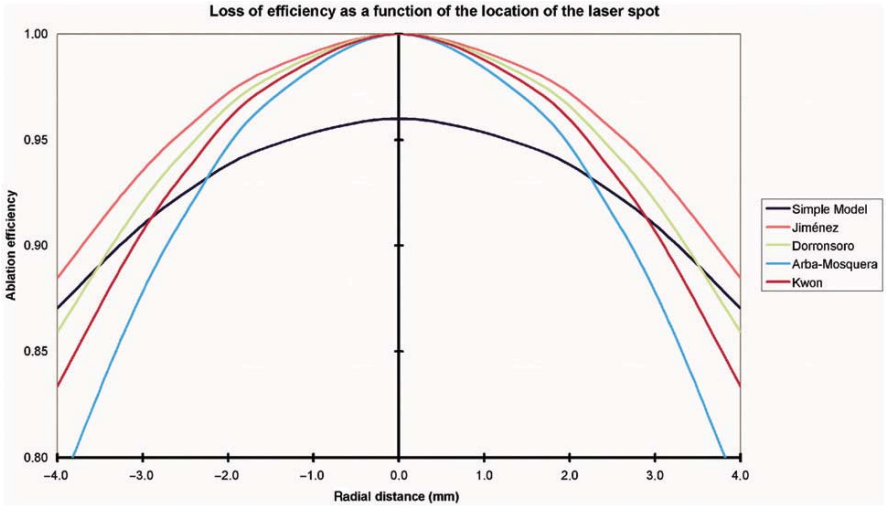

Figure 1. Loss of ablation efficiency due to non-normal incidence. While in the central 4 mm in diameter, efficiency losses account for less than 5% of ablation difference, for peripheral diameters (beyond 7 mm diameter) account for more than 15% of ablation difference. This is one of the reasons of the higher induction of spherical aberration in hyperopia (where pulse density is highest at the periphery) as compared to myopia (where highest pulse density occurs in the center). (The color version of this figure is included in the online version of the journal.)

2.2. *Surface asphericity showed minor effects*

The loss of efficiency in the ablation and non-normal incidence are responsible for much of the induction of spherical aberrations observed in the treatments as well as the excessive oblateness of postoperative corneas observed after myopic corrections (also part of some overcorrections observed in high myopias and many undercorrections observed in hyperopia) with major implications for treatment and optical outcome of the procedure. Compensation can be made at relatively low cost and directly affects the quality of results (after a correction of the profiles to avoid over-corrections or undercorrections in defocus and marginally in the cylinder).

Today, several approaches to import, visualize, and analyze high detailed diagnostic data of the eye (corneal or ocular wavefront data) are offered. At the same time, several systems are available to link diagnostic systems for measurement of corneal and ocular aberrations [56] of the eye to refractive laser platforms. These systems are state of the art with flying spot technology, high repetition rates, fast active eye trackers, and narrow beam profiles. Consequently, these systems offer new and more advanced ablation capabilities, which may potentially suffer from new sources of 'coupling' (different Zernike orders [57] affecting each other with impact on the result). The improper use of a model that overestimates or underestimates the loss of efficiency will overestimate or underestimate its compensation and will only mask the induction of aberrations under the appearance of other sources of error.

In coming years, the research and development of algorithms will continue on several fronts in the quest for zero aberration. This includes identification of sources for induction of aberrations, development and refinement of models describing the pre-, peri- and postoperative biomechanics of the cornea, development of aberration-free profiles leaving pre-existing aberrations of the eye unchanged, redevelopment of ablation profiles to compensate for symptomatic aberrated eyes in order to achieve an overall postoperative zero level of aberration (corneal or ocular) [58]. Finally, the optimal surgical technique (LASIK (laser assisted *in situ* keratomileusis), LASEK (laser epithelial keratomileusis), PRK (photorefractive keratectomy), Epi-LASIK ...) to minimize the induction of aberrations to a noise level has not yet been determined [59].

2.3. *Thermal effects*

Achieving accurate clinical outcomes and reducing the likelihood of a retreatment procedure are major goals of refractive surgery. For that, accurately calibrated lasers are required. These calibrations, of course, cannot take place on human corneas, and different materials (mainly polymers) have been proposed and used for that aim [60–65]. Models also have been proposed to compare ablation at reference materials with equivalent corneal ablations with different degrees

of success [48,66]. Incubation effects [67–69] or thermal effects [70,71] among others differ much between polymers and corneal tissue. Spot size and, thus, overlapping of closely placed spots may differ as well [50], making difficult the comparison of roughness measurements between materials, as well as the comparison between laser systems in materials other than the human cornea [72–74].

It is well known that a successful surgery depends on the correct design of an ablation profile, precise delivery of laser energy to the corneal position, and reliable understanding of the corneal tissue response.

When refractive surgery is used, an increase of corneal temperature during surgery has been observed clinically [70,75–79] as well as in the laboratory [71,80]. The rise in corneal temperature and associated consequences are not yet fully understood.

A large number of factors influence the laser ablation and outcome. Among them, laser energy delivery technique [81,82], ablation decentration and registration [83,84], eye tracking [85,86], flap [87], physical characteristics of ablation [43,44,48,88–91] wound-healing and biomechanics of the cornea [92–95] have been explored to predict or explain the clinically observed discrepancy between intended and actual outcomes. The quantification of influence of these factors is important for providing the optimal outcome with refractive surgeries.

The thermal load of a LASER pulse (the temperature rise at the end of a laser pulse) is governed by [80,96]:

$$\Delta T = \frac{\alpha}{\rho c} I(1 - R), \tag{2}$$

where I is the radiant exposure; R is the reflectivity; α is the absorption coefficient; r is the density; and c is the specific heat.

From the blow-off model (derived from the Beer–Lambert law), we know that the real energy density absorbed at that point determines the ablation depth:

$$d_{ij} = \frac{\ln\left([I_{ij}(1 - R_{ij})]/I_{\mathrm{Th}}\right)}{\alpha_{\mathrm{Cornea}}}, \tag{3}$$

where d_{ij} is the actual depth per pulse at the location i, j; I_{ij} is the radiant exposure of the pulse at location i, j; R_{ij} is the reflectivity at location i, j; I_{Th} is the corneal threshold; and α_{Cornea} is the corneal absorption coefficient. In general:

$$d(r) = \frac{\ln([I(r)(1 - R(r))]/I_{\mathrm{Th}})}{\alpha_{\mathrm{Cornea}}}. \tag{4}$$

Reversing this equation, we get:

$$I(r)(1 - R(r)) = I_{\mathrm{Th}} \exp[d(r)\alpha_{\mathrm{Cornea}}]. \tag{5}$$

Replacing in the thermal load equation:

$$\Delta T(r) = \frac{\alpha_{\mathrm{Cornea}}}{\rho c} I_{\mathrm{Th}} \exp[d(r)\alpha_{\mathrm{Cornea}}]. \tag{6}$$

The problem of the thermal load of a refractive surgery treatment relies on the sequential delivery of a multiplicity of laser pulses each one ablating and heating up locally a small amount of corneal tissue, the global process being an integral effect.

If the corneal tissue is heated up beyond a certain limit, the collagen proteins denaturize altering their normal function. Denaturising of the corneal collagen proteins seems to occur at temperatures higher than about 40°C inducing a risk of thermal damage [78]. The repetition rate with which a laser pulse with a given radiant exposure can be continuously delivered onto the same corneal tissue location without denaturising the proteins is defined as the maximum allowed local frequency.

With this given radiant exposure, firing at higher local frequencies will result in proteins denaturising and finally suboptimal ablation results. There are several ways to avoid this problem:

- reducing the radiant exposure allowing higher repetition rates;
- limiting the repetition rate of the system below the maximum allowed local frequency.

The problem of both alternatives is that they need extra time for the ablation procedure, which may produce other inconveniences.

Another possibility used in the prior art is to use defined sorting patterns (linear scanning, spiral scanning, randomization), but they do not address the problem of the local frequency directly, only on a statistical basis.

The gained ablation volume has to be applied onto the cornea by thousands of single laser shots at different but partly repeated corneal positions, because the ablated volume of a single spot is much smaller than the total ablation volume, generating the sequence of laser shot coordinates in a way that:

- guarantees a high fidelity reproduction of the given ablation volume line shape;
- avoids vacancies and roughness of the cornea;
- reduces as much as possible the thermal impact of the ablation by arranging laser shot energy in spatial and temporal distribution;
- controls pulse recreation time versus interspot distance to minimise the heat propagation [97] during the ablation procedure by dynamically limiting the allowed local frequency. This should result in a minimized thermal load on

the cornea, less induced aberrations, less need for nomograms and finally better visual quality post-op.

Laser refractive surgery is based upon the sequential delivery of a multiplicity of laser pulses each one removing (ablating) a small amount of corneal tissue. Despite UV radiation being considered 'cold' radiation, it is only because the thermal relaxation time of the molecules used is shorter than the thermal denaturasing time. However, this does not imply that the laser UV radiation does not increase the temperature locally. The thermal load of a single pulse describes the variation of temperature in the cornea at a given position after receiving a laser spot. The thermal load model is characterized by an immediate effect on the initial temperature in the cornea at a given position, proportional to the beam energy density at that point.

Literature has suggested that cornea ablation is a dynamic process [47]. Fisher and Hahn described a global ablation model that incorporates a dynamically changing tissue absorption [98] coefficient and that substantially deviates from a static Beer–Lambert model. The dynamic model predicts an enhancement in the tissue absorption coefficient of about 25%–50% as compared with the initial, static value. In addition, the model predicts an increase in the tissue ablation rate as corneal hydration increases [99].

Kim et al. [100] studied the expression patterns of heat shock proteins, after eyeball heating or cooling related to corneal wound healing and intraocular complications after excimer laser treatment. The study showed that heat shock proteins were induced by the heating or cooling preconditioning, and appeared to be a major factor in protecting the cornea against serious thermal damage.

Ishihara et al. [75] measured the temperature of the corneal surface during photorefractive keratectomy using a mercury-cadmium-telluride detector with a 1 μs time constant. They observed corneal surface temperature up to 70°C. In another study, Ishihara et al. [76] developed a temperature measurement system with nanosecond time response to monitor the transient temperature of the corneal surface during laser refractive surgery. Thermal radiation from the surface of porcine corneas during ArF excimer laser irradiation was measured using a photovoltaic HgCdTe detector with a response bandwidth of 150 MHz. The temperature derived from the detected signal reached over 100°C at a fluence of 80 mJ cm^{-2}, which was the ablation threshold, and reached 240°C at a fluence of 180 mJ cm^{-2}. They showed that the transient surface temperature of the cornea during ablation is much higher than that previously reported.

Vetrugno et al. [70] evaluated the thermal variations during photorefractive keratectomy induced by a Laserscan 2000 flying spot excimer laser using a non-contact infrared thermometer on 58 eyes with an attempted correction ranging from −1.25 to −9.00 D. The eyes were randomly divided into two groups to test the thermal effects of two different ablation scan techniques: sequential and randomized modes. Thermal measurements were also performed during myopic ablations on polymethylmethacrylate (PMMA) test plates. On PMMA plates, a significant relationship between the amount of attempted myopic correction and thermal changes was established, but not for human eyes. With the sequential mode, an unexpected cooling effect after PRK was reported for each myopia subgroup.

Maldonado-Codina et al. [101] investigated the temperature changes occurring during PRK when performed at different ablation depths using noncontact, color-coded ocular thermography with an infrared detector apparatus during PRK ablation on 19 ovine corneas. They observed a temperature rise at the corneal surface of 8°C on average with a maximum rise in temperature of 9°C. A positive correlation was found between the refractive correction and the peak rise in temperature.

Clinical systems currently operate with rather high repetition rates and more conventional treatment algorithms (i.e. fixed overall rep rate), yet they do not produce damage to the tissue. Shanyfelt et al. [102] investigated bovine corneal ablations generated at laser repetition rates of up to 400 Hz and found no statistical difference between corneal ablation profiles created at 60 and 400 Hz, with an average rate of 0.94 μm/pulse at 60 Hz versus 0.9294 μm/pulse at 400 Hz. In addition, based on plume imaging and transmission studies, the bulk ablation plume was found to dissipate on a time-scale less than the pulse-to-pulse separation for a laser repetition rate up to about 400 Hz. A persistent, diffuse gas-phase component of the ablation products was observed and concluded to be comparable at both repetition rates. Finally, SEM and TEM analysis revealed no signs of differential thermal tissue damage, including collagen fibril analysis, for laser repetition rates up to 400 Hz.

2.4. Ocular cyclotorsion

Human eyes have six degrees of freedom to move: X/Y lateral shifts, Z leveling, horizontal/vertical rotations, and cyclotorsion (rotations around the optical axis). The analysis of these cyclotorsion movements have been made since the middle of the twentieth century. Several papers demonstrate some dynamic

compensatory movement to keep the image at the retina aligned to a natural orientation, whereas some suggestions have been made on significant cyclotorsion occurring under monocular viewing conditions [103]. Laser technology for refractive surgery allows corneal alterations to correct refractive errors more accurately than ever. Ablation profiles are based on the removal of tissue lenticules in the form of sequential laser pulses that ablate a small amount of corneal tissue to compensate for refractive errors. However, the quality of vision can deteriorate significantly especially under mesopic and low-contrast conditions [40].

Induction of aberrations, such as spherical aberrations and coma, is related to loss of visual acuity (VA) and quality. Some aberrations, however, may be subject to neural adaptation. A study by Artal et al. [104] on the effects of neural compensation on vision indicated that visual quality in humans is superior to the optical quality provided by the human eye. To balance already existing aberrations, customized treatments were developed that use either wavefront measurements of the whole eye [105,106] (obtained, e.g. by Scheiner aberroscopes [107], Tscherning aberroscopes [108,109], Hartmann screens [110,111], Slit skiascopic refractometer [112], Hartmann–Shack [113] or other types of wavefront sensors [114–120]) or by using corneal topography-derived wavefront analyses [121,122]. Topographic-guided [123], wavefront-driven [124], wavefront-optimized [125], asphericity preserving [126], and Q-factor profiles [127] have been forwarded as solutions. Measuring rotation when the patient is upright [128] to when the refractive treatments are performed with the patient supine may lead to ocular cyclotorsion, resulting in mismatching of the applied versus the intended profiles [129,130]. Recently, some equipment can facilitate measurement of and potential compensation for static cyclotorsion occurring when the patient moves from upright to the supine position during the procedure [131], quantifying the cyclorotation occurring between wavefront measurement and laser refractive surgery [132] and compensating for it [133–135]. Further measuring and compensating ocular cyclotorsion during refractive treatments with the patient supine may reduce optical noise of the applied versus the intended profiles [136–138].

It usually happens that the pupil size and center differ for the treatment compared to that during diagnosis [139]. Then, excluding cyclotorsion, there is already a lateral displacement that mismatches the ablation profile. Further, cyclotorsion occurring around any position other than the ablation centre results in additional lateral displacement combined with cyclotorsion [140].

Many studies, in recent times have worked out in an excellent way, the methodologies and implications of ocular cyclotorsion, but due to inherent technical problems, not many papers pay attention to the repeatability and reproducibility of the measurements.

Arba Mosquera et al. [130] obtained an average cyclotorsional error of 4.39°, which agrees with the observations of Ciccio et al. [141], who reported 4°. However, a non-negligible percentage of eyes may suffer cyclotorsions exceeding 10°. These patients would be expected to have at least 35% residual cylinder, 52% residual trefoil, and higher residual errors of tetrafoil, pentafoil, and hexafoil. In addition, octafoil would be induced beginning at 7.5° of cyclotorsion. A comparison of the results among recent studies on ocular cyclotorsion can be found in Figure 2.

Due to the cyclic nature, the residual aberration error emanating from cyclotorsional error ranges from 0% to 200% of the original aberration. However, the induced aberrations emanating from lateral displacements always increase with decentration [129]. If we also consider that in human eyes with normal aberrations the weight $C(n, m)$ of the Zernike terms $Z(n, m)$ [142] decreases with increasing Zernike order (n) [143], then the theoretical impact of cyclotorted ablations is smaller than decentered ablations or edge effects [144] (coma and spherical aberration [145]). The results of Bará et al. [146] confirm the independent nature of the cyclotorsional effect with the radial order. Without eye registration technologies [147,148], considering that maximum cyclotorsion measured from the shift from the upright to the supine position does not exceed ±14° [141], explains why 'classical' spherocylindrical corrections in refractive surgery succeed without major cyclotorsional considerations. The limited amount of astigmatism especially that can be corrected effectively for this cyclotorsional error may explain partly some unsuccessful results reported in refractive surgery. Considering that the average cyclotorsion resulting from the shift from the upright to the supine position is about ±4° [141], without an aid other than manual orientation, confirms why spherocylindrical corrections in laser refractive surgery have succeeded.

Currently available eye registration technologies, which provide an accuracy of about ±1.5°, open up a new era in corneal laser refractive surgery, because patients may be treated for a wider range of refractive problems with enhanced success ratios. However, this requires a higher resolution than technically achievable with currently available systems [149,150].

To the best of our knowledge, currently available laser platforms for customized corneal refractive surgery include not more than the eighth Zernike order, which covers most cyclotorsion occurring when

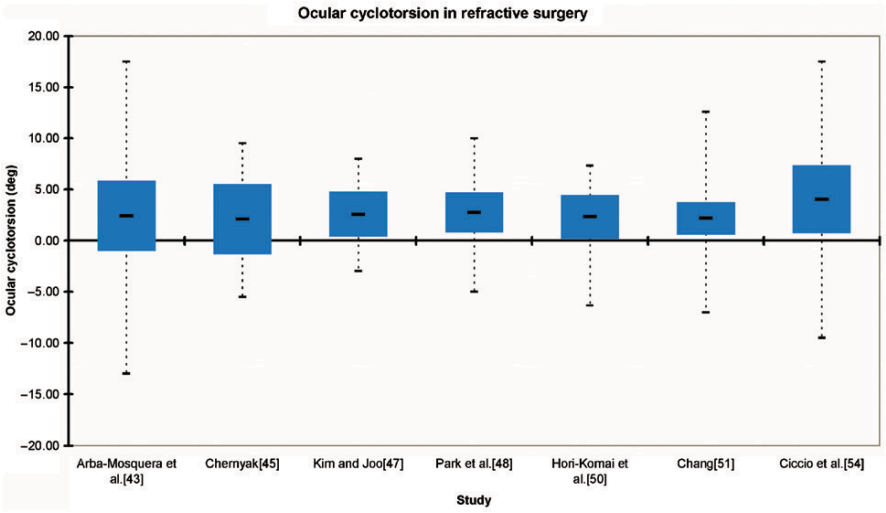

Figure 2. Box and whisker diagram summarizing the ocular cyclotorsion in refractive surgery as measured in recent studies. The box represents the first and third quartiles, with the line depicting the mean value, and the whiskers represent the minima and maxima of the data. While mean values are very similar among studies (~+3°), the ranges for cyclotorsion widely vary and large cyclotorsion values (~±7°) are not uncommon. (The color version of this figure is included in the online version of the journal.)

shifting from the upright to the supine position. Thus, the aberration status and the visual performance of the patients are expected to improve. Bueeler and co-authors [151] determined conditions and tolerances for cyclotorsional accuracy. Their OT criterion represents an optical benefit condition, and their results for the tolerance limits (29° for 3 mm pupils and 21° for 7 mm pupils) did not differ greatly from the optical benefit result for astigmatism by Arba Mosquera et al. [130], confirming that astigmatism is the major component to be considered.

In discussing visual benefit, although VA data are helpful, there may be patients with 20/20 vision who are unhappy with their visual outcomes due to poor mesopic and low-contrast VA. Cyclotorsional errors result in residual aberrations and with increasing cyclotorsional error there is a greater potential for inducing aberrations. Eyes having over 10° of calculated cyclotorsion, predict approximately a 35% residual astigmatic error. Because astigmatic error is generally the highest magnitude vectorial aberration, patients with higher levels of astigmatism are at higher risk of problems due to cyclotorsional error.

3. Baseline for refractive profiles

Refractive surgery with excimer laser is an evidence-based therapy to treat refractive errors. Nowadays the search for the best profile is wide open, as it is still unknown whether and when an 'optically-perfect eye' after surgery is better than preserving the aberrations that the eye had before surgery. Although the optical quality of the eye can be described in terms of the aberration of its wavefront, healthy individuals with more than 20/20 of high-contrast visual acuity presented a measurable degree of aberration in their wavefront. Still more, it was observed that the individuals with smaller wavefront aberration were not always those scoring the best visual qualities [152].

Controversy remains over the proper definition of an optimal ablation profile for corneal refractive surgery [153]. Nevertheless, considerations such as treatment duration, tissue removal [154], tissue remodeling [155], and overall postoperative outcomes have made it difficult to establish a universal optimal profile.

Corneal refractive treatments typically induce a change in corneal asphericity [41]. Recently, it has been argued that preserving the preoperative corneal asphericity after corneal refractive treatments might be positive, therefore, asphericity-based profiles have been developed [40,127]. However, there is no clear evidence that asphericity is the variable that alone plays the major role in the visual process [156].

One problem using Q-factor customized ablation profiles [127] are the severe difficulties to determine the Q-factor to be targeted. The average asphericity of the human cornea is about −0.28 [157]. Nevertheless, there are persons with Q-factor −0.25 and poor vision, and others with Q-factor +0.25 and supervision. Despite some remarkable theoretical works [158,159], there is no proof that more negative quotients of asphericity provide better visual quality, or that an absolute

optimum exists. When a patient is selected for non-customized aspherical treatment, the global aim of the surgeon should be to leave all existing high-order aberrations (HOA) unchanged because the best-corrected visual acuity, in this patient, has been unaffected by the pre-existing aberrations [152]. Hence, all factors that may induce HOAs, such as biomechanics, need to be taken into account prior to the treatment to ensure that the pre-operative HOAs are unchanged after treatment [125,130].

Statistical analysis of a population of human corneas showed as an average result that the best-fit aspherical surface had a Q-factor around -0.25. As a result, in general, healthy human corneas show a 'positive spherical aberration', which is balanced by the 'negative spherical aberration' of the internal lens [122]. As an average, human corneas manifest a corneal spherical aberration around 0.23 μm at 6 mm analysis diameter. One can say that the corneal-wavefront values are 'overestimated' in the topographic systems compared to the ocular wavefront values. As individuals are aging, the asphericity of the crystalline lens changes, reducing the amount of spherical aberration that can be balanced or even showing a certain amount of positive spherical aberration, whereas the corneal asphericity, thus corneal spherical aberration, remains relatively stable over time, disrupting the equilibrium between both. However, in recent times there is a clear tendency of targeting a prolate postoperative anterior corneal surface as the global optimum in refractive surgery [40,127]. The intended meaning of the terms prolate and oblate is sometimes unclear. The confusion comes from the false usage of curvature and refractive power: since the average human cornea is prolate (Q-factor -0.25), the central part of the cornea has a stronger curvature than the periphery. However, refractive power is given by Snell's law. As the corresponding Cartesian oval is the aberration-free surface (i.e. the only truly monofocal surface), and can be described by an aspherical surface with quotient of asphericity $-1/n^2$ (approx. -0.528 for human cornea), the average human cornea (Q-factor -0.25) is less prolate (so more oblate) than the corresponding Cartesian oval, thus the refractive power of the outer corneal surface increases from central towards peripheral. In this way, the multifocality towards peripheral just answers the question whether the corneal spherical aberration is positive (refractive power increases towards peripheral) or negative (refractive power decreases towards peripheral) but not the question about the geometrical concept of prolate versus oblate. The first thing to be clarified is that even the amount of corneal spherical aberration and the asphericity are intrinsically related; the goal is always described in terms of change in spherical aberration [145], because this is the factor related to the quality and sharpness of the retinal image. Then, in the treatments, the goals should be:

(a) For aspherical treatments: no induced aberrations; a change in asphericity depending on the corrected defocus.
(b) For wavefront-guided treatments: change in aberrations according to diagnosis; change in asphericity depending on the corrected defocus and on the $C(n, 0)$ coefficients applied.

Please note that only a starting surface of a Cartesian oval would lead to no corneal aberration, but the anterior cornea definitely is not a Cartesian oval and possesses corneal aberrations. However, the proposed concept is to maintain the known aberrations of every individual cornea.

Even though the condition of stigmatism, that origins 'free of aberration' verified for two points (object and image) and for a conicoid under limited conditions, is very sensitive to small deviations and decentrations (a question that usually arises in refractive surgery), the goal of these profiles is not to achieve a stigmatism condition postoperatively, but rather to maintain the original HO wavefront-aberration.

The optical quality in an individual can be maximized for a given wavelength and a given distance by canceling the aberration of his wavefront and optimizing his defocus (for a single distance), but this has direct implications dramatically negative for the optical quality for the rest of the wavelengths (greater negative effect the more extreme is the wavelength). However, the optical quality of a person showing a certain degree of aberration of his wavefront decreases compared to the maximum obtainable in the absence of aberration, but it has direct positive implications on the 'stability' of the optical quality for a wide range of wavelengths (which covers the spectral sensitivity of the human eye) [160] and in the depth of focus, i.e. for a range of distances that can be considered 'in-focus' simultaneously. Lastly, moderate levels of wavefront aberration favor the stability of the image quality for wider visual fields [161]. In such a way, there are, at least, three criteria (chromatic blur, depth of focus, wide field vision) favoring the target of leaving minor amounts of not clinically relevant aberrations (the proposed 'aberration-free' concept).

A study by Arba Mosquera and de Ortueta [162] evaluates refractive outcomes, visual outcomes, corneal-wavefront and asphericity changes in an aberration-free myopic LASIK group (100 eyes) with good visual acuity outcomes and minor amounts of coma and spherical aberration. In this study, the induced corneal spherical aberration was clearly lower than other published results [40,127,144]. The average

induced primary corneal spherical aberration changed by $-0.031\,\mu m\,D^{-1}$ for a 6 mm pupil, close to the target of preserving the preoperative aberrations when balancing the manifest refractions.

With simple spherical error, degradation of resolution begins for most people with errors of 0.25 D. A similar measure can be placed on the error due to cylinder axis error. A simple approach for classifying the clinical relevance of single aberration terms was proposed by Thibos et al. [143] who introduced the concept of equivalent defocus (DEQ) as a metric to minimize the differences in the Zernike coefficients due to different pupil sizes. DEQ is defined as the amount of defocus that produces the same wavefront variance as found in one or more higher order aberrations. The clinical relevance can be considered when postoperative magnitudes were changed by an amount higher than 0.25 DEQ (i.e. the magnitude for subjective degradation of resolution) for the magnitude of each Zernike mode (i.e. a ± 0.125 DEQ maximum deviation in one or several meridians). Induced corneal aberrations at 6 mm were below clinically relevant levels: 0.09 ± 0.10 DEQ for HO-RMS (88% in 0.25 DEQ), 0.05 ± 0.10 DEQ for spherical aberration (94% in 0.25 DEQ) and 0.04 ± 0.10 DEQ for coma (94% in 0.25 DEQ), whereas the rate of induced aberrations per achieved D of correction were -0.03 DEQ/D, -0.02 DEQ D^{-1}, and -0.02 DEQ D^{-1} for HO-RMS, SphAb, and coma.

Papers, in which direct comparison of induced corneal and ocular wavefront aberrations over the same sample was studied, showed that the induction of anterior corneal aberrations was always, at least, as high as the induction of ocular wavefront aberrations for the entire eye. Marcos et al. [144] found that ocular and corneal aberrations increased statistically significantly after LASIK myopia surgery, by a factor of 1.92 (ocular) and 3.72 (corneal), on average. They found a good correlation ($P < 0.0001$) between the aberrations induced in the entire optical system and those induced in the anterior corneal surface. However, anterior corneal aberrations increased more than ocular aberrations, suggesting also changes in the posterior corneal surface. Lee et al. [163] found that after laser refractive surgery, anterior corneal aberration and ocular aberration increased equally and showed statistically significant correlations. They found no statistically significant differences of internal optics aberration values in coma, spherical aberration, and RMS for HOA. Arbelaez et al. [164] found that on comparing corneal and ocular aberrations, the amount of induced aberrations was very similar for spherical aberration and coma. For the RMS for HOA corneal induced aberrations were moderately higher, despite not being statistically significant, than ocular induced aberrations.

One of the most affecting aberrations after myopic LASIK is the spherical aberration [88,95]. It is important to remark that preserving preoperative aberrations is not equivalent to intend preserving preoperative asphericity. Tuan and Chernyak [165] analyzed the impact of corneal asphericity on wavefront-guided LASIK at six clinical sites and found no significant correlation between corneal shape and VA or contrast sensitivity. Pop and Payette [166] studied the relationship between contrast sensitivity, Zernike wavefront-aberrations, and asphericity after LASIK to correct myopia. Contrast sensitivity was not correlated with asphericity but was correlated with wavefront-aberrations as expected. The change in asphericity was correlated with the refractive change and was predicted by the parabolic Munnerlyn equation.

Anera et al. [167] analyzed the origin of the changes in the p-factor after LASIK and the effect of post-surgical asphericity on contrast sensitivity function. An increase in the p-factor after LASIK was higher than the predictions using the paraxial formula of Munnerlyn and coauthors.

Holladay and Janes [168] determined the relationship between the spherical refractive change after myopic excimer laser surgery and the effective optical zone and corneal asphericity determined by corneal topography, which changed nonlinearly with the amount of treatment.

Figure 3 compares induced spherical aberration per diopter of correction among different recent studies.

In the Arba-Mosquera and de Ortueta study [162], BSCVA was measured under photopic conditions and no differences were observed that might be attributable to HOA induction. Apparently, increased aberrations were not strongly related to most significant visual losses and conversely, the eyes that gained visual acuity lines were not only those that experienced the least increase of corneal aberrations.

This lack of correlation between aberration induction and visual loss may be surprising, as previous studies suggested this kind of correlation in terms of contrast sensitivity [145].

Most of the non-customized profiles currently used by the LASER systems are still based on the Munnerlyn original profiles [5] or its parabolic approximations. Reserving the state-of-the-art treatments for their respective customization approaches, however, some remarkably simple 'non-customized' but sophisticated aspherical, wavefront-optimized, or aberration-free approaches are nowadays available.

ZEiSS Meditec MEL80 aspheric profiles [40] are based on the difference of two conocoids. Based on the pre-op K-reading, an assumed normal pre-op Q-value

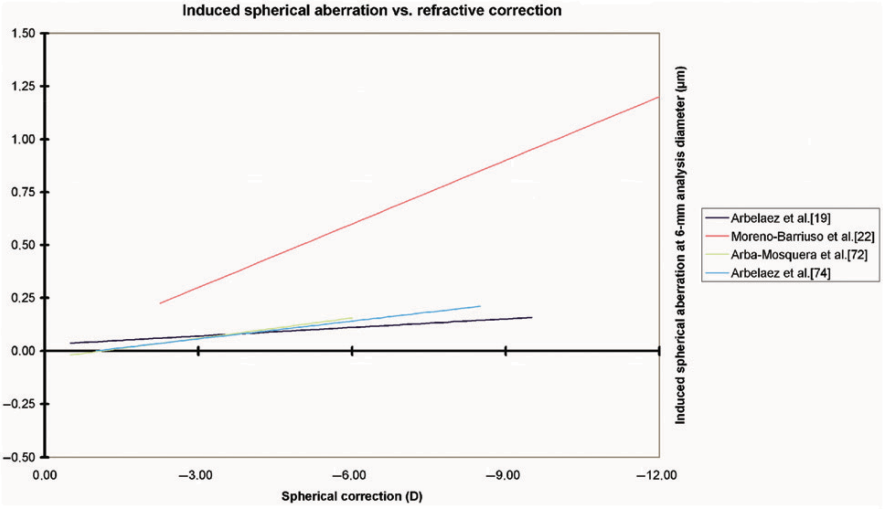

Figure 3. Scattergram summarizing the induced spherical aberration in refractive surgery as measured in recent studies. Except the results by Moreno-Barriuso et al. [39], for all other studies induced spherical aberration was very similar after myopic refractive surgery and well below +0.25 µm at 6 mm analysis diameter. (The color version of this figure is included in the online version of the journal.)

(about Q of −0.1), the SCA values and another assumed global target post-op Q-value (about Q of −0.35), it builds up the ablation profile from the difference between the pre-op and post-op ideal corneal surfaces. Therefore, the goal is not an aberration-free profile, nor is it an aberration-free cornea, nor is it an aberration-free eye, but a global target Q-factor cornea. WaveLight Q-factor profiles [127] are also based on the difference of two conocoids. Based on the pre-op K-reading and Q-factor, and on the SCA values and target Q-factor, it builds up the ablation profile from the difference between the pre-op and post-op selected corneal surfaces. Therefore, the goal is not an aberration-free profile, nor is it an aberration-free cornea, nor is it an aberration-free eye, but a customized target Q-factor cornea. SCHWIND CAM aspheric profiles [162] and WaveLight wavefront-optimized profiles [125] are based on an aberration-free profile concept where the wavefront aberration (within optical zone, OZ) after surgery equals the wavefront aberration (within optical zone, OZ) prior to surgery after balancing sphere and cylinder components. In other words, there is no induced change in wavefront aberration (within optical zone, OZ) other than sphere and cylinder components. Thus, balancing the effects on the wavefront aberration, and providing normal eyes with the best quality of vision, without affecting their perception of the world. So the goal is either an aberration-free profile, or an aberration-free cornea, or an aberration-free eye, all concepts wavefront derived and clearly related to the quality and sharpness of the retinal image, and not any target Q-factor cornea, which is elevation derived.

In summary, optimized patterns for refractive surgery aiming to be neutral for aberrations together with the consideration of other sources of aberrations such as blending zones, eye-tracking, and corneal biomechanics yielded results comparable to those of some customization approaches. Having close-to-ideal ablation profiles should improve the clinical results decreasing the need for nomograms, and reducing the induced aberrations after surgery.

4. Centration of refractive profiles

Controversy remains regarding where to centre corneal refractive procedures to maximize the visual outcomes. A misplaced refractive ablation might result in undercorrection and other undesirable side effects. The coaxial light reflex seems to lie nearer to the corneal intercept of the visual axis than the pupil centre (PC) and is, thus, recommended that the corneal coaxial light reflex be centered during refractive surgery. Boxer Wachler et al. [169] identified the coaxial light reflex and used it as the centre of the ablation. De Ortueta and Arba Mosquera [170] used the corneal vertex (CV) measured by videokeratoscopy [171] as the morphologic reference to centre corneal refractive procedures.

Mainly, there are two different centration references that can be detected easily and measured with currently available technologies. PC may be the most extensively used centration method for several reasons.

First, the pupil boundaries are the standard references observed by the eye-tracking devices. Moreover, the entrance pupil can be well represented by a circular or oval aperture, and these are the most common ablation areas. Centering on the pupil offers the opportunity to minimize the optical zone size. Because in LASIK there is a limited ablation area of about 9.25 mm (flap cap), the maximum allowable optical zone will be about 7.75 mm. Because laser ablation is a destructive tissue technique, and the amount of tissue removed is directly related to the ablation area diameter [172], the ablation diameter, maximum ablation depth, and ablation volume should be minimized. The planned optical zone should be the same size or slightly larger as the functional entrance pupil for the patients' requirements.

The pupil center considered for a patient who fixates properly defines the line-of-sight, which is the reference axis recommended by the OSA for representing the wavefront aberration [173]. The main HOA effects (main parts of coma and spherical aberrations) arise from edge effects, i.e. strong local curvature changes from the optical zone to the transition zone and from the transition zone to the untreated cornea. It then is necessary to emphasize the use of a large optical zone (6.50 mm or more) to cover the scotopic pupil size, and a large and smooth transition zone.

Nevertheless, because the pupil center is unstable, a morphologic reference is more advisable [174–176]. It is well known that the pupil centre shifts with changes in the pupil size [139], moreover, because the entrance pupil we see is a virtual image of the real one. The CV in different modalities is the other major choice as the centration reference. In perfectly acquired topography, if the human optical system were truly coaxial, the corneal vertex would represent the corneal intercept of the optical axis. Despite the fact that the human optical system is not truly coaxial, the cornea is the main refractive surface. Thus, the corneal vertex represents a stable preferable morphologic reference. However, there are several ways to determine the corneal vertex: the most extensively used one is to determine the coaxial corneal light reflex (1st Purkinje image). Nevertheless, as de Ortueta and Arba Mosquera [170] pointed out, there is a problem using the coaxial light reflex because surgeons differ; for instance, the coaxial light reflex will be seen differently depending on surgeon eye dominance, surgeon eye balance, or the stereopsis angle of the microscope. For example, the LadarVision platform (Alcon) uses a coaxial photograph as reference to determine the coaxial light reflex [177], which is independent of the surgeons' focus. Ablations can be centered using the pupillary offset, the distance between the pupil center and the normal CV, which corresponds to the angle between the line of sight and the optical axis. Thus, the three-dimensional combination of angle kappa minus alpha minus lambda. The angle kappa represents the angle between the pupillary and visual axes, and the angle alpha represents the angle between optical and visual axes, angle lambda represents the angle between the pupillary axis and the line of sight. Therefore, (visual axis – pupillary axis) – (visual axis – optical axis) – (line-of-sight – pupillary axis) = (optical axis – line-of-sight).

In Figure 4 the black cross indicates the pupil centre and the black circle the maximum pupil boundaries, whereas the orange cross represents the corneal apex. If an optical zone equivalent to the maximum pupil size (scotopic pupil size or dim mesopic) (blue circle) is applied on the corneal apex, due to the offset, the ablation will not cover the full pupil area and it will be cut across it. As the pupil aperture represents the only area capable of collecting light, then the full pupil should be cover and an 'oversized' OZ centered on the apex shall be selected (green circle) as:

$$OZ > \text{Pupil}_{\text{Sco}} + 2(\|\text{OffSet}\| + \|\text{AETAcc}\|). \quad (7)$$

However, centering in the pupil with a right selected OZ is not an easy task. We know that the pupil center shifts versus pupil size changes; moreover, the pupil we see (entrance pupil) is a virtual image of the real one. In Figure 5 the black cross indicates the laser pupil center (photopic) and the black circle the laser pupil boundaries (photopic), whereas black circle indicates the maximum pupil boundaries and the black cross its pupil center. If an optical zone equivalent to the maximum pupil size (scotopic pupil size or dim mesopic) (blue circle) is applied on the laser pupil center, due to the pupil center offset, the ablation will not cover the full maximum pupil area and it will be cut across it. As the pupil aperture represents the only area capable of collecting light, then the full pupil should be cover and an 'oversized' OZ centered on the apex shall be selected (green circle) using the same formula.

Only centering in the scotopic pupil (orange circle and cross) offers the opportunity to minimize the optical zone (OZ) size, but under the laser, pupil size is likely in a photopic state rather than a dim mesopic one. Therefore, centering on the laser pupil an optical zone equivalent to the maximum pupil size (scotopic pupil size or dim mesopic) will induce edge effects.

Considering this, for aspherical, or, in general, non-wavefront-guided treatments, in which the minimum patient data set (sphere, cylinder, and axis values) from the diagnosis is used, it is assumed that the patient's optical system is aberration-free or that those aberrations are not clinically relevant (otherwise

a wavefront-guided treatment would have been planned). For those reasons, the most appropriate centering reference is the corneal vertex; modifying the corneal asphericity with an ablation profile neutral for aberrations, including loss of efficiency compensations. For wavefront-guided treatments, change in aberrations according to diagnosis measurements, a more comprehensive data set from the patient diagnosis is used, including the aberrations, because the aberration maps are described for a reference system in the center of the entrance pupil. The most appropriate centering reference is the entrance pupil as measured in the diagnosis [173].

Providing different centering references for different types of treatments is not ideal, because it is difficult to standardize the procedures. Nevertheless, ray tracing indicates that the optical axis is the ideal centering reference. Because this is difficult to standardize and considering that, the anterior corneal surface is the main refractive element of the human eye, the CV, defined as the point of maximum elevation, will be the closest reference. It shall be, however, noticed that on the less prevalent oblate corneas the point of maximum curvature (corneal apex) might be off centre and not represented by the corneal vertex. However, it would be interesting to refer the corneal and/or ocular wavefront measurements to the optical axis or the CV. This can be done easily for corneal wavefront analysis, because there is no limitation imposed by the pupil boundaries. However, it is not as easy for ocular wavefront analysis, because the portion of the cornea above the entrance pupil alone is responsible for the foveal vision. Moreover, in patients with corneal problems such as keratoconus/keratectasia, post-LASIK (pupil-centered), corneal warpage induced by contact lens wearing and other diseases causing irregularity on the anterior corneal surface, the corneal vertex and the corneal apex may shift. In those cases, pupil center is probably more stable. Moreover, since most laser systems are designed to perform multiple procedures besides LASIK, it is more beneficial that excimer laser systems have the flexibility to choose different centration strategies.

The standard parameters to assess refractive surgery results, i.e. efficacy, predictability, refractive outcome, stability, and safety, are inadequate for evaluating the optimal centration reference. Further, because the ablation procedures are performed in a physical world, they are always affected by different sources of unavoidable inherent errors [178] that are sources of aberrations, such as biomechanical reactions due to the flap cut [21,179], blending zones, cyclotorsion [130], and centration errors, spot size limitations [149,150], active eye-tracking capabilities [129,151,180,181], and biomechanical reactions due to the ablation process. While this may indicate that both centration strategies are virtually equivalent, the difference starts being significant for eyes with moderate-to-large pupil offset ($>200\,\mu m$) [174]. A deeper analysis of the induced ocular aberrations and the changes in asphericity showed significant differences favoring CV centration for the induction of coma and spherical ocular aberration and the changes in asphericity, and no significant differences for the induced ocular trefoil.

Due to the smaller angle kappa associated with myopes compared with hyperopes [182,183], centration issues are less apparent. However, angle kappa in myopes may be sufficiently large to show differences in results, because it is always desirable to achieve as much standardization as possible and not to treat the myopes using one reference, whereas the hyperopes use a different one. The use of large optical zones may be responsible for the lack of difference in postoperative visual outcomes using two different centrations. However, hyperopic LASIK provides smaller functional optical zones and, for this reason, special caution shall be paid to these patients [184].

Previous studies have reported that based on theoretical calculations with 7.0 mm pupils even for customized refractive surgery, that are much more sensitive to centration errors, it appears unlikely that optical quality would be degraded if the lateral alignment error did not exceed 0.45 mm [129]. In 90% of eyes, even accuracy of 0.8 mm or better would have been sufficient to achieve the goal [129].

A pupillary offset of 0.25 mm seems to be sufficiently large to be responsible for differences in ocular aberrations [174], however, not large enough to correlate this difference in ocular aberrations with functional vision.

A limitation of most of the reviewed studies is that they use a comparison based upon two different groups of patients with different centrations used as reference. A direct comparison in a lateral/contralateral eye basis for the assignment of the centration reference maybe would reduce the variability of external uncontrollable effects (like flap cut, corneal response to the ablation, repeatability of the instruments, cooperation of the patients, etc.). However, such direct comparison may reduce patients' satisfaction, as patients may postoperatively observe differences among eyes due to the different centrations. In summary, morphologic centering references such as the CV, which are not standard in refractive surgery, yielded visual, optical, and refractive results better to those of pupil centration techniques in eyes with moderate to large pupillary offset. No significant differences in the comparative outcomes of both centration strategies were observed

in visual results but they were found in high order aberration results. Despite this, an absolute optimum centration reference could not be determined. Centering on the pupil offers the opportunity to minimize the optical zone size, whereas centering in the CV offers the opportunity to use a stable morphologic axis and to maintain the corneal morphology after treatment.

5. Myopic outcomes

The optical quality of the human eye does not necessarily determine its visual quality [185]. Previous studies have shown that spherical aberration show a consistent increase after excimer laser ablation directly proportional to the achieved refractive correction [186]. It has been suggested that almost half of the induced spherical aberration is due to the lower delivery of excimer laser energy in the peripheral cornea due to corneal curvature [50,186].

The recent advances in excimer laser technology, such has the use of aspheric ablation profiles, incorporation of higher order aberration (HOA) treatment and eye trackers have presumably led to better refractive outcomes and reduced HOA induction postoperatively which have been recently reported [187,188].

Ocular wavefront-guided and wavefront-optimized treatments can increase HOAs by 100% postoperatively [187]. A significant number of refractive surgery patients may not benefit from ocular wavefront guided treatment as the induction of HOAs is related to baseline levels of HOAs [187,189]. For example, HOAs tend to be induced in patients with less than 0.30 μm at 6 mm analysis diameter and reduced in patients with greater than 0.30 μm at 6 mm analysis diameter of HOAs [187,189]. Furthermore, physiologic optical aberrations may be warranted to maintain the optical quality of the eye. Based on these studies [104,160,187,189] it seems the custom ablation algorithm may not be appropriate for the entire refractive surgery population. McLellan and colleagues have reported a beneficial effect on the visual quality of pre-existing higher order aberrations [160]. There is evidence of neural adaptation to the baseline wavefront profile [104]. The interaction between higher order aberrations can be beneficial to visual quality regardless of the magnitude HOAs [190,191].

Furthermore, higher order aberrations seem to be induced in patients with 0.30 μm at 6 mm analysis diameter or less of preoperative HOAs [187,189]. Approximately half the patients that present for refractive surgery have HOAs of 0.30 μm at 6 mm analysis diameter or less [187]. To date the induction of wavefront aberrations postoperatively is random and the wavefront profile postoperatively cannot be predicted. Based on the random nature of the HOA induction and current research, it may be beneficial to maintain the preoperative wavefront profile for a significant number of refractive surgery candidates.

A contralateral study of 35 patients under LASIK with custom ablation and aspheric algorithm, reported an increase of HOAs of 0.20 μm at 6 mm analysis diameter after aspheric LASIK and an increase of 0.14 μm at 6 mm analysis diameter after custom ablation [127]. A larger retrospective study reported an increase in spherical aberration of 0.03 μm at 6 mm analysis diameter for custom ablation treatments and 0.11 μm at 6 mm analysis diameter for aspheric treatments [187].

We know that induction of aberrations such as spherical aberrations or coma results in a loss of visual acuity [192], accommodative lag [193] or, in general, visual quality. It has also been suggested that some aberrations are compensated by the neural system. Artal et al. [182] performed an interesting study on the role of aberrations demonstrating that the human eye is an example of robust optical design. The average magnitude of the high order aberrations is similar in groups of eyes with different refractive errors, even though individual eyes are comparatively different in shape. Internal ocular optics (mainly the crystalline lens) play a significant role in the compensation for the corneal aberrations, and this compensation is larger in the less optically centered eyes. In a study by de Ortueta et al. [194] comparing refractive outcomes, visual outcomes and topographical changes in a standard myopic LASIK group and an aberration neutral (Aberration-Free^{TM}) myopic LASIK group (70 eyes each), better visual acuity outcomes and lower amounts of corneal coma and corneal spherical aberration in the aberration neutral (Aberration-Free^{TM}) LASIK group were found.

The goal of a laser refractive treatment is to obtain the best possible visual function without spectacle correction. Attempting to correct low order aberrations, sphere and cylinder, good results can be achieved in the majority of the cases [195], however, in some cases the patients complain about halos or other impairing visual effects [196]. In general, scanning-spot algorithms use a matrix of movement (i.e. there is a latent matrix representing locations in the ablation map, and a spot matrix, smaller in size representing locations in the spot profile, the spot matrix moves all across the latent matrix in a predetermined manner until ablation is completed). As spot overlapping is a major parameter, and the spot spacing is small compared to the spot width and multiple spots overlap, all contributing to the ablation at each corneal

location, the characteristics and symmetry of the latent matrix may induce different kinds of aberrations due to differences in spot overlapping in different directions (hexagonal symmetry: trefoil + hexafoil, square symmetry: astigmatism + tetrafoil, polar symmetry: spherical aberration, spiral symmetry: spherical aberration). Moreover, scanning spot algorithms may suffer from problems of thermal effects [76] and plume shielding [197] due to adjacent spot positioning. Different theoretical models are available [125,127, 158–162]. In wavefront guided ablation the objective is not only to reduce the induction, but moreover to reduce the aberration of the eye, although, if we analyze the studies of wavefront guided ablation [198,199] the result in some laser platforms is that they induce less aberration than standard profiles [200] but cannot reduce the postoperative HO aberrations below the preoperative levels [201,202].

Jiménez et al. [203] deduced a mathematical equation for corneal asphericity after refractive surgery, when the Munnerlyn formula is used. Equations for corneal asphericity may be of clinical relevance in quantitatively studying the role of different factors (decentration, type of laser, optical role of the flap, wound healing, biomechanical effects, technical procedures) during corneal ablation.

As published in previous studies [90,144], the induced spherical aberration is of positive sign in the case of myopia and of negative sign in the case of hyperopia [184,204]. The refractive patient who is myopic before surgery has a 'natural' focal point for the near distance. After refractive surgery and having induced positive spherical aberrations, two scenarios are possible: either the patient is centrally overcorrected and emmetropized at the periphery, which means that under mesopic conditions the visual acuity is good but under photopic conditions or when the pupil is miotic there will be difficulties when reading (miotic hyperopia), the other scenario is that the center is emmetropized and the periphery is undercorrected, once the pupil dilates, the patient will have difficulties in distance vision (mydriatic myopia). The problem becomes more obvious with an increase in multifocality. In this way, the surgeon can optimize the correction of a classical standard profile by using a nomogram, but an application of the nomogram results in an overcorrection of the center. We want to clarify the use of the term 'multifocality' in this context. Here 'spherical aberration' and 'multifocality'

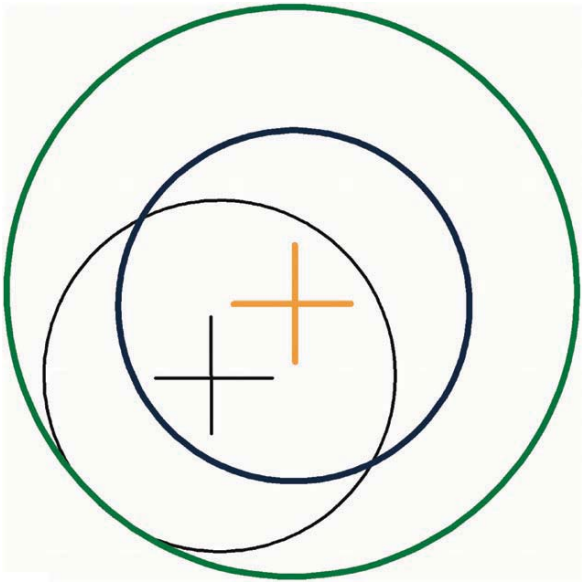

Figure 4. In the graph, the black cross indicates the pupil center and the black circle the maximum pupil boundaries, whereas the orange cross represents the corneal apex. Note that if an optical zone equivalent to the maximum pupil size (scotopic pupil size or dim mesopic) (blue circle) is applied on the corneal apex, due to the offset, the ablation will not cover the full pupil area and it will be cut across it. As the pupil aperture represents the only area capable of collecting light, then the full pupil should be cover and an 'oversized' OZ centered on the apex shall be selected (green circle). (The color version of this figure is included in the online version of the journal.)

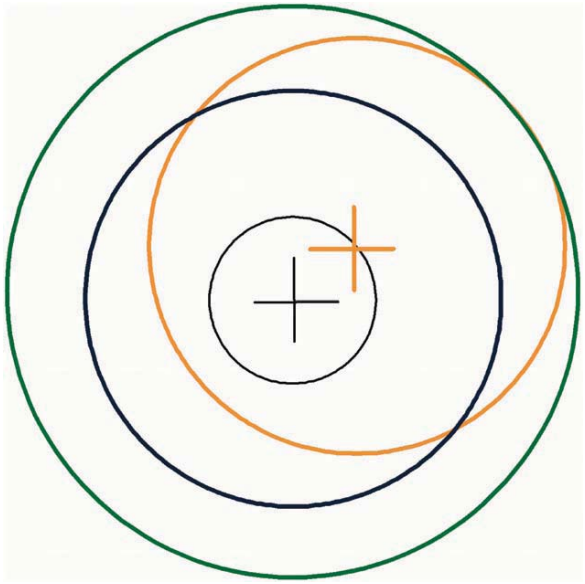

Figure 5. Only centering in the scotopic pupil (orange circle and cross) offers the opportunity to minimize the optical zone (OZ) size, but under the laser, pupil size is likely in a photopic state rather than dim mesopic one. Therefore, centering in the laser pupil an optical zone equivalent to the maximum pupil size (scotopic pupil size or dim mesopic) will induce edge effects. (The color version of this figure is included in the online version of the journal.)

are considered as 'unwanted effects' and should not be mixed up with a multifocality generally sought as a compensation for presbyopia.

The ideal treatment shall preserve the corneal natural multifocality and shall only bring the best focus closer to the retinal plane. For several reasons, such as loss of efficiency in the periphery, biomechanical response of the cornea, etc., the natural multifocality of the cornea results are modified.

In a study by Arbelaez et al. [164], for 6 mm analysis diameter, on average an induction high-order aberration of $0.04 \pm 0.14\,\mu m$ ocular wavefront and $0.06 \pm 0.16\,\mu m$ corneal wavefront was found. Spherical aberration changed, on average, $0.07 \pm 0.12\,\mu m$ ocular wavefront and $0.08 \pm 0.12\,\mu m$ corneal wavefront. Induced spherical aberration was correlated to achieved defocus correction ($P < 0.0001$) and increased on average by $0.028\,\mu m$ per diopter of achieved defocus correction for a 6 mm pupil in ocular wavefront and $0.030\,\mu m$ per diopter of achieved defocus correction for corneal wavefront. That compares to $0.09\,\mu m$ per diopter reported by Marcos et al. [144] and by Llorente et al. [184] for ocular spherical aberrations, and to $0.17\,\mu m$ per diopter reported for corneal spherical aberrations [184]. This compares as well to $0.04\,\mu m$ at 6 mm analysis diameter per diopter reported by Kohnen et al. [205].

Regarding coma, in the study by Arbelaez et al. [164], aberration changed, on average, $0.06 \pm 0.13\,\mu m$ at 6 mm analysis diameter ocular wavefront and $0.01 \pm 0.18\,\mu m$ corneal wavefront. The induced amount of coma at 3-month follow-up was small ($0.016\,\mu m$ per diopter for 6.0 mm pupil) and can be explained by small decentrations of the ablation as no iris registration was used [139] (a systematic decentration of $150\,\mu m$ will already induce $0.016\,\mu m$ per diopter for 6.0 mm pupil [140]).

Farooqui and Al-Muammar [206] found after conventional LASIK treatments a postoperative ocular spherical aberration of $+0.24\,\mu m$ at 6 mm analysis diameter and a postoperative ocular coma of $0.24\,\mu m$.

Kohnen et al. [205] found after non-customized LASIK a change in corneal RMSho of $0.17 \pm 0.18\,\mu m$ at 6 mm analysis diameter, a mean induction of corneal coma of $0.09 \pm 0.20\,\mu m$ and for corneal spherical aberration a significant increase $0.13 \pm 0.12\,\mu m$.

A comparison of the results among recent studies on myopia and myopic astigmatism can be found in Figure 6.

The ocular high order aberrations are customarily measured at a 6 mm pupil diameter, but most spherical aberration induction occurs at the junction between the central treatment zone/transition zone/untreated zone, and since some patients may have a mesopic/scotopic pupil diameter greater than 6 mm, the values within a 6 mm zone may not correspond with the real-life visual function of the patient in terms of glare and halos. In order not to limit the analysis to 6 mm, and this way, to omit the transition zone and junction zone from the entire analysis, and although the information is most interesting and useful from a '6 mm point of

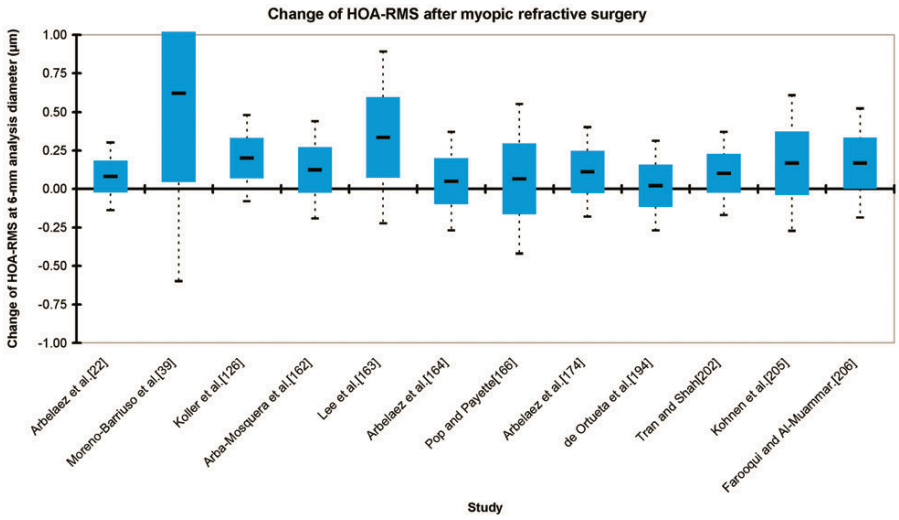

Figure 6. Box and whisker diagram summarizing the change of HO-RMS after myopic refractive surgery as measured in recent studies. The box represents the first and third quartiles, with the line depicting the mean value, and the whiskers represent the minima and maxima of the data. While mean values are small (~+0.15 µm at 6 mm analysis diameter) and similar among studies, the ranges for induction widely vary and large values (~+0.5 µm at 6 mm analysis diameter) are not uncommon. (The color version of this figure is included in the online version of the journal.)

view', it may miss the practical clinical point of the effect of changes in aberrations outside the 6 mm zone. Therefore, Arbelaez et al. [164] analyzed the available topographic information independently, reporting the corneal wavefront findings for a larger diameter zone, in this case 7 and 8 mm, to include the total treatment zone and transition zone and junction zone, as well. To check whether the increase in aberration magnitude was only due to the larger analysis diameter, analysis has been performed in defocus equivalent (DEQ). On virgin eyes, defocus equivalent as proposed by Thibos et al. [143] seems to be relatively insensitive to different analysis diameters. They observed that the change in aberration magnitudes increased with the analysis diameter. The change in corneal spherical aberration DEQ was, on average, $+0.06 \pm 0.10$ D at 6 mm analysis diameter, $+0.10 \pm 0.12$ D for 7 mm diameter, and $+0.17 \pm 0.16$ D for 8 mm. For corneal coma the change in DEQ was, on average, 0.01 ± 0.13 D at 6 mm analysis diameter, 0.03 ± 0.15 D for 7 mm diameter, and 0.05 ± 0.17 D for 8 mm, whereas for corneal RMSho it was, on average, 0.05 ± 0.12 D at 6 mm analysis diameter, 0.13 ± 0.14 D for 7 mm diameter, and 0.23 ± 0.17 D for 8 mm.

This fact confirms that actually the change in aberration magnitudes increased with the analysis diameter. This could be expected as the tested profile attempts to be neutral for aberrations within the disc limited by the optical zone size (6.5 mm diameter for that study) which was closely achieved, and increases when analysis diameters beyond the optical zone are included.

6. Hyperopic outcomes

The introduction of the excimer laser for refractive surgery has opened up the possibility to change the corneal curvature to compensate for refractive errors of the eye. In the case of small spot hyperopic laser *in situ* keratomileusis (H-LASIK), excimer laser systems produce a steepness of the cornea by ablating mainly at the periphery of the cornea. By comparison of the intended and achieved topographical changes after H-LASIK surgery, de Ortueta et al. [207] obtained information as to whether the corneal power was changed as calculated, thus providing help in optimizing the ablation profiles (either in terms of nomogram adjustments or more sophisticated optimization algorithms like multifocal algorithms). Additionally, actual under- or overcorrection can be differentiated from under- or overcorrection due to wrong intended correction in this way.

In this study [207], H-LASIK with the ESIRIS [211] system showed a good predictability, with 92% of the eyes (61) having a postoperative refraction within ± 0.50 D of the attempted correction. Moreover, as expected, the achieved refractive change was significantly correlated with intended refractive correction ($r^2 = 0.91$), and was very close to the ideal correction.

By analyzing the corneal topographical changes, a highly significant correlation between the resulting Maloney change and the intended refractive correction ($r^2 = 0.81$), which was very close to the ideal correction, could be observed.

Based on the good agreement between refractive and topographical changes, topographical indices could be used instead of the manifest refraction to compare the results of different surgeons or for nomogram optimization. In this way, any undesired accommodative effects can be directly avoided in the analysis, such as different methods to determine the subjective refraction, and the influence of the technician or patient can be minimized, since topography is a highly reproducible method. This is very important, as the majority of hyperopic patients have the ability of a certain degree of accommodation, thus masking their hyperopia. In cases of young patients manifesting hyperopia, the refraction used to be underestimated, as accommodative response helps those patients to achieve good visual acuities without full hyperopic correction. In this way, the topographic method of analysis allows surgeons to assess whether an under- or overcorrection is real or due to a wrong refraction or intended correction.

The topographic changes were analyzed using other indices.

The achieved sim-K change was significantly correlated with the intended refractive correction ($r^2 = 0.36$), and was still quite close to the ideal correction, and only slightly undercorrected.

Maloney analysis was chosen as a better descriptor compared to sim-K analysis because it showed lower scatter ($r^2 = 0.81$ for Maloney versus $r^2 = 0.36$ for sim-K). Moreover, by definition, sim-K represents the flattest meridian at 3 mm analysis and takes the other principal meridian 90° away, independent from its curvature, so that it is not necessarily the steepest meridian. Alternative representations could have been taking the steepest meridian at 3 mm analysis and the meridian 90° away independently from its curvature, but again not necessarily the flattest meridian, or the two meridians 90° away at 3 mm analysis that maximize the astigmatism and therefore are not necessarily the flattest and steepest meridians. In 'normal' corneas, without irregular astigmatism, these three methods of analysis provide very similar results. Sim-K analysis is just a two-dimensional cross-sectional analysis. Maloney indices additionally use the inner 3 mm zone, to fit this disk area best to a spherocylindrical

surface in three-dimensions. Cylinder orientation defines the two principal meridians, and sphere and cylinder provide the curvatures of the principal meridians. Again, in 'normal' corneas (without irregular astigmatism) sim-K and Maloney analyses provide very similar results.

Rosa et al. [209] analyzed the topographic changes after photorefractive keratectomy in myopia and found, as well, a better correlation with the Maloney index compared to sim-K. The achieved power changes at 5 and 7 mm were not correlated with the intended refractive correction, and they showed a decreasing correction factor indicating a progressive severe undercorrection, and at 7 mm a myopic-like effect even for intended hyperopic corrections.

The myopic-like behavior can be explained by the fact that the treatments were planned at 6.25 mm optical zone, and the analysis addressed the 7 mm zone, meaning that analysis already included the transition zone (TZ) area, where the hyperopic profiles show a myopic-like shape.

The good agreement between refractive and topographical changes at 3 mm (with both Maloney and sim-K) can be explained by 3 mm being a common pupil size during manifest refraction diagnosis.

The reason for the progressive undercorrection of the profiles towards the periphery is that the used profiles were non-customized, non-optimized, parabolic profiles, and suffered from effects related to loss of efficiency of the laser ablation for non-normal incidence [43,44,48,50]. This is predominantly caused by the loss of efficiency at the periphery and the biomechanics of the cornea, and has been described previously by other authors [186,210]. The change in mean corneal asphericity (Q) at 6 mm was statistically significant ($P < 0.001$), with -0.19 preoperatively compared to -0.72 at three months postoperatively, and slightly correlated to achieved defocus correction ($r^2 = 0.30$) with an impact of -0.16 dQ-Val/D, lower than other values reported for hyperopia [211,212].

In the study by de Ortueta et al. [207], they found an average induction of higher-order aberrations resulting in changes from 0.45 and 0.14 μm in root-mean-square preoperatively for 6 and 4 mm, respectively, to 0.57 and 0.18 μm postoperatively (1.25-fold for 6 and 4 mm).

The average corneal spherical aberration changed from 0.21 and 0.05 μm preoperatively for 6 and 4 mm, respectively, to -0.09 and -0.01 μm postoperatively. The average induced corneal spherical aberration decreased by -0.09 μm per diopter for a 6 mm pupil and by -0.01 μm per diopter for a 4 mm pupil. Spherical aberration was induced, which could be expected, since hyperopic corrections, especially higher ones, always induce some negative spherical aberration. Earlier studies on hyperopic treatments with excimer lasers also suggested an increase in negative spherical aberration [213,214].

Spherical aberration is also directly related to multifocality, and confirms the topographical findings of multifocality, with a progressive undercorrection of the profiles towards the periphery. The central part of the cornea is slightly overcorrected (inducing a postoperative central myopia), and there is an extended depth-of-focus of about 1 D (probably helping the patients who approach presbyopia). This may explain why the patients, although presbyopic, in some cases report improved near vision after the procedure, confirmed by reduced need of or less addition for reading. The knowledge of the resulting positive effect in presbyopic-hyperopic laser treatments may allow us to optimize the amount of spherical aberration to be induced.

With respect to coma, the induced amount of coma at three-month follow-up was small (0.04 μm per diopter for 6 mm pupil, 0.01 μm per diopter for 4 mm pupil) and can be explained by small decentrations of the ablation [215].

Topographic changes of the Maloney indices can be effectively used in analyzing laser corneal refractive surgeries for hyperopia, avoiding undesired accommodative effects in the analysis. In this way, the topographic method of analysis is objective and allows surgeons to assess whether an undercorrection or an overcorrection is real or due to a wrong refraction or intended correction. On these grounds, this method has the potential to replace, or, at least, supplement currently used methods of analysis based on subjective manifest refractions for presentation of refractive surgery results or for optimization of nomograms. Hyperopic laser *in situ* keratomileusis (H-LASIK) treatments induce aberrations [184]. The conventionally accepted limits for H-LASIK (about 5 diopters SEQ, spherical equivalent) are lower than the ones accepted for myopic LASIK (up to about 10 diopters if the residual stromal bed is thicker than 250–300 μm). One of the causes is that the induction of aberrations per achieved diopter is higher in hyperopic treatments [186]. The centration of refractive surgery remains also controversial. The offset between the corneal vertex and pupil centre is higher in hyperopic eyes, with a nasal fixation in most of the cases [216]. This is also a problem to take into account [169,170]. Hyperopic eyes are usually short in axial length, showing higher values for the angles alpha, kappa, and lambda. This also causes an offset between the corneal vertex and the pupil center of higher magnitude than in myopic eyes, making it difficult to decide where to center the refractive procedure.

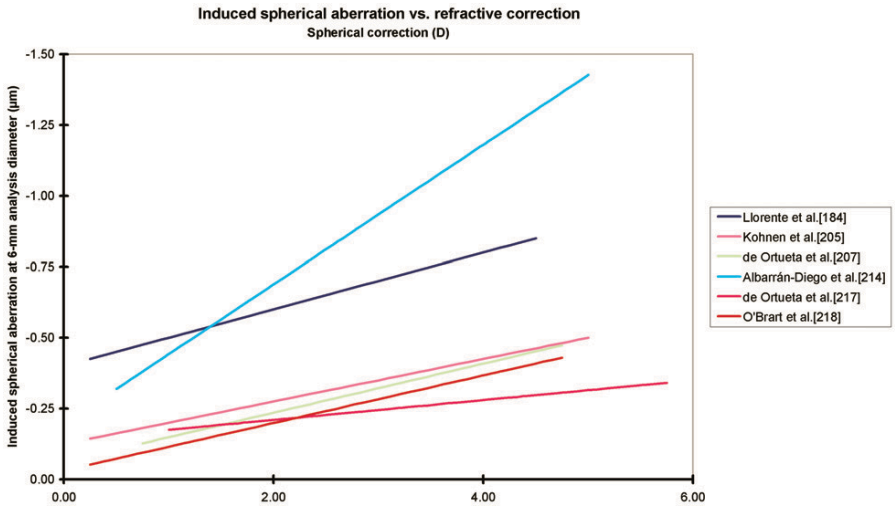

Figure 7. Scattergram summarizing the induced spherical aberration in refractive surgery as measured in recent studies. Except the results by Llorente et al. [184] and by Albarrán-Diego et al. [214], for all other studies induced spherical aberration was very similar after hyperopic refractive surgery and well below −0.50 µm at 6 mm analysis diameter. (The color version of this figure is included in the online version of the journal.)

New ablation patterns, which minimize the induction of aberrations, will allow us to perform H-LASIK more predictably and safely and may allow us in the future to treat higher hyperopia.

In another study by de Ortueta et al. [217], the induced aberrations as shown are less than in previous publications. A study by O'Brart et al. [218] analyzing hyperopic LASEK with the same laser platform using a Munnerlyn based classical profile used a 7 mm optical zone with a total treated zone of 9 mm. O'Brart et al. also analyzed the created aberrations at 6 mm with the LASEK technique and found that they induced a RMS of the HO which was 0.07 µm, and the spherical aberrations −0.19 µm and a coma of 0.04 µm. Therefore, the induced aberrations were lower than with the Munnerlyn profile in LASIK but higher than the aberration-free LASIK.

Reducing the corneal aberrations after H-LASIK will possibly allow us to treat higher hyperopia, however, further studies are necessary to confirm this hypothesis. Figure 7 compares induced spherical aberration per diopter of correction among different recent studies.

A comparison of the results among recent studies on hyperopia and hyperopic astigmatism is given in Figure 8.

7. Astigmatic outcomes

For the correction of astigmatism, many different approaches have been tested, with different degrees of success, through the years [219]. However, while for quasi-spherical corrections the focus has been moved from primary refractive outcomes to effects of the ablation in postoperative high order aberrations (HOA) [50,130,162,164,174,194,217], for astigmatism the focus mainly remained at the primary refractive outcomes, principally due to the encountered problems as 'coupling factors' [50] or cyclotorsion errors [130], which result in residual astigmatism. Not to forget the fact that astigmatism (especially high ones) has its main origin in the anterior corneal surface, and topographically is usually found located two-fold symmetrically from the normal corneal vertex (CV) and not at the pupil center. Patient satisfaction in any refractive surgery, wavefront-guided or not, is primarily dependent on successful treatment of the lower order aberrations (LOA) of the eye (sphere and cylinder). Achieving accurate clinical outcomes and reducing the likelihood of a retreatment procedure are major goals of refractive surgery. LASIK has been successfully used for low to moderate myopic astigmatism, whether LASIK is acceptably efficacious, predictable, and safe in correcting higher myopic astigmatism is less documented, especially with regard to the effects of astigmatic corrections in HOAs.

The correction of astigmatism has been approached using several techniques and ablation profiles. There are several reports showing good results for compound myopic astigmatism using photorefractive keratectomy (PRK) and LASIK, but ablation profiles usually cause a hyperopic shift because of a coupling effect in the flattest corneal meridian. A likely mechanism of this coupling effect is probably due to epithelial remodeling and other effects such as smoothing by the LASIK

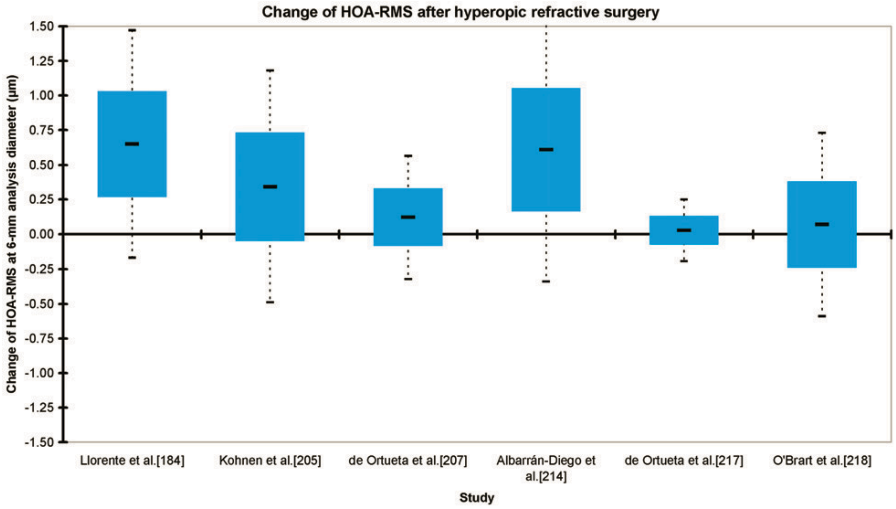

Figure 8. Box and whisker diagram summarizing the change of HO-RMS after hyperopic refractive surgery as measured in recent studies. The box represents the first and third quartiles, with the line depicting the mean value, and the whiskers represent the minima and maxima of the data. Both mean values (median $\sim +0.3\,\mu m$ at 6 mm analysis diameter) and ranges for induction widely vary among studies and large values ($\sim +0.8\,\mu m$ at 6 mm analysis diameter) are not uncommon. (The color version of this figure is included in the online version of the journal.)

flap. In cases of large preoperative amounts of astigmatism, deviations from the target refractive outcome are usually attributed to 'coupling factors'. Nevertheless, the investigation of the coupling factor remains a rather difficult task, because it seems to be dependent on various factors. Individual excimer laser systems may have different coupling factors, cutting the flap could alter the initial prescription and different preoperative corneal curvatures (K-reading) may have influence on coupling factor. Arbelaez et al. [220] found a residual defocus averaged about −0.1 D, and residual cylinder about 0.5 D, with > 72 within 0.50 D, and > 92% within 1.0 D of the target correction in defocus and astigmatism simultaneously. The mean decrease in astigmatism magnitude was 93%, representing a slight undercorrection of astigmatism. Analyzing the mean postoperative defocus component, no hyperopic shift was observed despite the fact that no nomogram adjustments or coupling effects were accounted for.

Multivariate correlation analysis of the achieved defocus correction versus the attempted defocus correction and the magnitude of the attempted astigmatism correction showed that the contribution of the magnitude of the attempted astigmatism correction was not statistically significant ($r^2 = 0.01$, $p = 0.6$ for the whole study group; $r^2 = 0.11$, $p = 0.3$ for a subgroup ($n = 14$) with astigmatism of 3.50 D or higher), so no coupling effects from the correction of the astigmatism in the correction of the defocus were observed. Even if the lack of statistical significance were due to the limited number of analyzed eyes (50, $n = 14$ for astigmatism of 3.50 D or higher), the magnitude of the potential coupling factor would be less than 5% (12% for astigmatism of 3.50 D or higher), well below other reported values [219,221].

In the study by Arbelaez et al. [220], at six months follow-up, the percentage of eyes with an UCVA of 20/32 or better was 100% and 84% had an UCVA of 20/20 or better. No single eye had a loss of more than one line of BSCVA, and five eyes had gained two or more lines of BSCVA ($p < 0.01$). The mean decrease in astigmatism magnitude of 93% favorably compares to other reports (which range from 36% to 91% mean decrease in astigmatism magnitude).

Payvar and Hashemi [222] studied the efficacy, predictability, and safety of LASIK for moderate to high simple and compound myopic astigmatism among 92 eyes. At six months after LASIK, mean astigmatism was 0.32 D at 7° at six months. 80% of the eyes had UCVA of 20/40 or better.

Despite large defocus and astigmatism magnitudes, the study by Arbelaez et al. [220] shows high order aberrations are either minimally increased or unchanged after surgery with the LDV and AMARIS systems. The most dominant correlations of induced HOAb occurred for $C[4,0]$, and $C[6,0]$ versus defocus correction, for $C[4,+2]$ versus cardinal astigmatism correction, and $C[4,-2]$ versus oblique astigmatism correction. The refractive results in this clinical setting show a trend toward slight undercorrection in astigmatism. On the other hand, the low standard deviation and the tight dispersion of the cluster of data demonstrate the consistency of

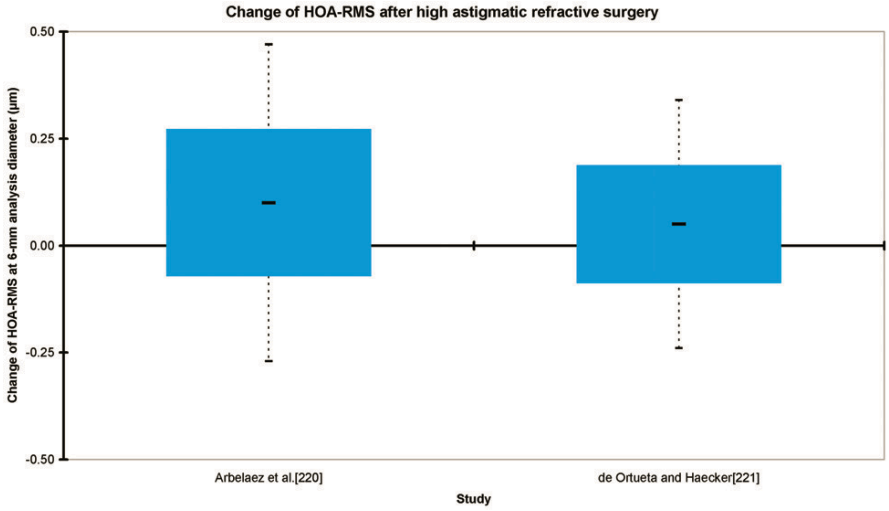

Figure 9. Box and whisker diagram summarizing the change of HO-RMS after high astigmatic refractive surgery as measured in two recent studies. The box represents the first and third quartiles, with the line depicting the mean value, and the whiskers represent the minima and maxima of the data. Both low mean values ($\sim+0.1\,\mu$m at 6 mm analysis diameter) and the ranges for induction of aberrations ($\sim\pm0.2\,\mu$m at 6 mm analysis diameter) are similar among studies. (The color version of this figure is included in the online version of the journal.)

the achieved results. Given the small deviation of the refractive results, we believe that with some slight adjustment for astigmatic correction, the percentage of eyes within ±0.50 D of intended correction will increase significantly. The same applies for the difference observed between the rate of aberration induction related to defocus and astigmatic corrections, resulting in the latter being about twice as large as the former. Induced corneal spherical aberration was correlated to achieved defocus correction ($p < 0.0001$) and increased on average by 0.05 µm per diopter of achieved defocus correction for a 6 mm analysis diameter, whereas induced corneal secondary astigmatism aberrations (terms $C[4, \pm2]$) were correlated to astigmatism correction (cardinal and oblique) ($p < 0.0001$) and increased on average by 0.09 µm per diopter of achieved astigmatism correction. The astigmatic correction was highly satisfactory, with no difference between lower and higher corrections. Although this small series of treated eyes does not allow for definitive conclusions or evidence-based statements, preliminary results are promising. A comparison of the results between two recent studies on high astigmatism can be found at Figure 9.

8. Wavefront customized outcomes

The proper definition of an optimal ablation profile for corneal refractive surgery is still controversially discussed and it remains unknown.

In a study [223], ablations customized based on Hartmann–Shack [113] measurements of the wavefront aberration of the entire eye optimized to reduce the wavefront aberration of the entire eye (within OZ) close to a zero level, compensating, as well, for the aberration induction observed with other types of profiles, the improvement in safety was statistically significant ($P = 0.04$) with 33% of the eyes treated improving BSCVA. 7% of the eyes 'have lost' one line of BSCVA in the OW group, however, no single eye has lost more than one line of BSCVA.

Coma aberration of the patients did not increase significantly ($P = 0.22$). Notably, the achieved coma correction was only marginally correlated with the attempted coma correction. This might have been due to small decentrations of the ablation pattern that also induce coma aberration and because ocular coma is a coupling of corneal and internal coma.

The correction of trefoil terms was successful both in magnitude ($P = 0.002$) and correlation attempted versus achieved ($P < 0.0001$), whereas the decrease in spherical aberration was not statistically significant ($P = 0.45$), but correlation attempted versus achieved was successful ($P < 0.0001$).

It should be noted that opposing the preoperative wavefront aberration in laser refractive surgery constituted only a first approximation of a perfect refractive correction, as tissue removal occurs.

Data suggest that ocular wavefront customized treatments can only be successful, if the pre-existing aberrations are greater than the repeatability and the

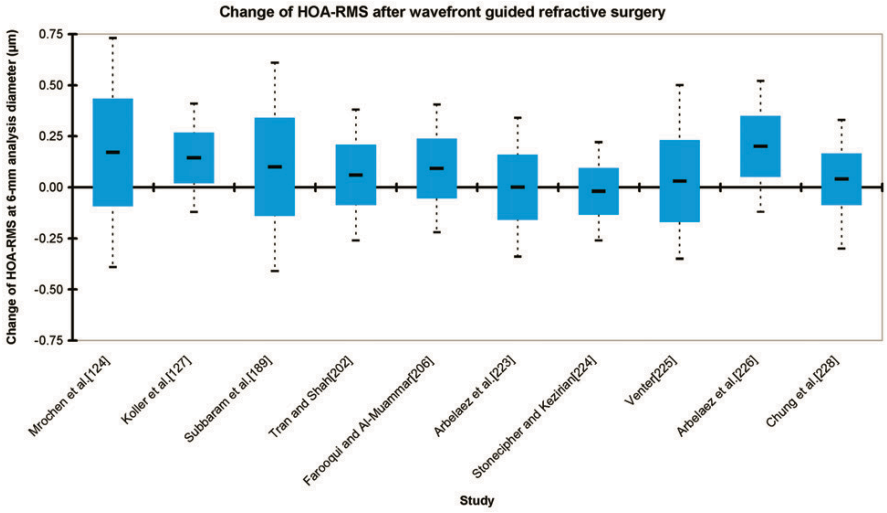

Figure 10. Box and whisker diagram summarizing the change of HO-RMS after wavefront customized refractive surgery as measured in recent studies. The box represents the first and third quartiles, with the line depicting the mean value, and the whiskers represent the minima and maxima of the data. Reports demonstrate no consistent reduction in HOA-RMS. While mean values are small (~+0.1 µm at 6 mm analysis diameter) and similar among studies, the ranges for induction widely vary and large values (~+0.4 µm at 6 mm analysis diameter) are not uncommon. (The color version of this figure is included in the online version of the journal.)

biological noise. The fact that in order to appropriately treat patients with profiles such as these described, the patients need to have a significant level of preoperative aberrations [224,225].

Aspheric OW ablation profiles, are highly efficient in eyes with greater than 0.25 µm RMS ocular HOA at 6 mm analysis diameter, or where individual components of the OW such as coma, trefoil or spherical aberration are greater than 0.2 µm RMS. Corneal wavefront guided treatments showed promising results in a study [226]. When evaluating the outcomes of wavefront customization strategies, wavefront aberration analysis is mandatory to be able to determine whether the customization aims could be achieved.

In this study [226], the average coma, trefoil and spherical aberrations changed by +23%, −51%, and +105%, respectively. This might indicate that the ablation strategies were partly unsuccessful, however, the small amount of aberration found in this group, similar to the repeatability/accuracy (~0.2 µm at 6 mm analysis diameter) of the devices when measuring living tissue, introduced some scatter. This value of 0.2 µm comes from experience, and a similar value can be found with aberrometers as well when measuring living tissue and not test lenses or static objects; similar values can be found at the literature [227]. It has been suggested, as well, that the surface ablation procedures are better suited for the wavefront guided ablation as they would avoid the induction of aberrations due to flap and interface [228,229]. When only low aberration subjects were analyzed, an average change in coma from 0.12 µm at 6 mm analysis diameter to 0.33 µm (+165%) ($P = 0.008$), in trefoil from 0.13 to 0.14 µm (+3%) ($P = 0.48$), and in spherical aberration from −0.49 to +0.12 µm (−123%) ($P = 0.001$) was observed, whereas for moderately aberrated subjects, an average change in coma from 0.38 to 0.31 µm (−19%) ($P = 0.04$), in trefoil from 0.35 to 0.12 µm (−66%) ($P = 0.0005$), and in spherical aberration from +0.14 to +0.08 µm (−48%) ($P = 0.02$) was noted. Corneal wavefront [230] customized treatments can only be successful, if the pre-existing aberrations are greater than the repeatability and the biological noise, which is also demonstrated by selective group split on the basis of preoperative aberration values (intended aberration corrections).

Furthermore, coupling effects between different high order aberration terms and between HOAs and manifest refraction is still one of the major sources of residual aberrations after refractive surgery. This topic has been discussed from a theoretical perspective by Guirao et al. [140] or by Bará et al. [146]. They all found mutually affecting interactions, for example, between defocus and spherical aberration, or between third order aberrations and low order terms, between spherical aberration and coma, or between secondary and primary astigmatisms.

A comparison of the results among recent studies on wavefront guided refractive surgery can be found in Figure 10.

9. Other concerns

9.1. Binocular effects

Human vision is a binocular process. Having two eyes gives binocular summation in which the ability to detect faint objects is enhanced. It can give stereopsis in which parallax provided by the two eyes' different positions on the head give precise depth perception. Such binocular vision is usually accompanied by binocular fusion, in which a single image is seen despite each eye having its own image of any object.

Literature suggests that marked anisometropia is uncommon, either in the magnitude of sphere or astigmatism, with few notable exceptions concluding that the axis of astigmatism does not follow any particular rule (mirror or direct symmetry) across right and left eyes. Porter et al. [231] confirmed in a large population that although the pattern of aberrations varies from subject to subject, aberrations, including irregular ones, are correlated in left and right eyes of the same subject, indicating that they are not random defects.

The Indiana Aberration Study by Thibos et al. [143] characterized the aberration structure, and the effects of these aberrations on vision, for a reasonably large population of normal, healthy eyes in young adults, and verified the hypothesis of bilateral symmetry. Wang et al. [232] found that anterior corneal wave aberrations varied greatly among subjects, but a moderate to high degree of mirror symmetry existed between right and left eyes.

To our knowledge, very few studies in the literature have addressed the issue of symmetry of aberrations between eyes after corneal laser refractive surgery [233,234]. Jiménez et al. [233] found that binocular function deteriorates more than monocular function after LASIK, and that this deterioration increases as the interocular differences in aberrations and corneal shape increase. They found that interocular differences above 0.4 μm RMS for 5 mm analysis diameter, lead to a decrease of more than 20% in binocular summation.

If binocular symmetry is manifested on virgin human eyes and it is important for binocular vision, it shall be interesting to assess whether existing symmetry is maintained after treating the cornea for correcting the ametropias using corneal laser refractive surgery. Further analysis of bilateral symmetry according to analysis diameter is also of interest. The analysis of bilateral symmetry should be related to binocular vision status of patients. Cuesta et al. [235] found that even differences in corneal asphericity might affect the binocular visual function by diminishing the binocular contrast-sensitivity function. Arbelaez et al. [234] found that only four of 25 patients showed preoperatively clinically relevant differences OS versus OD larger than 0.25 D, whereas six months postoperatively, only two of 25 patients showed clinically relevant differences OS versus OD larger than 0.25 D. Six-month postoperatively three Zernike terms lost significant correlation symmetry OS versus OD and four Zernike terms gained significant correlation symmetry. However, two of them showed borderline correlations. Six-month postoperatively six Zernike terms significantly increased differences in symmetry OS versus OD and four Zernike terms significantly decreased differences in symmetry. However, six of them showed borderline significances of the difference. Six-month postoperatively three patients lost significant correlation symmetry OS versus OD and one patient gained significant correlation symmetry. However, two of them showed borderline significances of the difference. All these borderline situations actually shall be seen as 'almost preserved' bilateral symmetry.

The presented results cannot be extrapolated to patients with symptoms of amblyopia [236], anisometropia, nystagmus, or aniseikonia [237] without further studies. Bilateral symmetry in corneal aberrations does not mean any 'good or bad' point for binocular vision. We cannot evaluate exactly the role of aberrations monocularly (patients with a high level of aberrations can have an excellent visual acuity and vice versa); therefore it is more difficult binocularly. The important question in binocular vision is 'the role of interocular differences', and if they can influence significantly binocular performance. Interocular differences can be minor but significant for visual performance. Further studies will help to determine the impact of this on binocular visual performance.

9.2. Pachymetric concerns

Corneal laser refractive surgery reshapes the cornea based on the preoperative corneal curvature in order to reduce or eliminate the refractive errors of the eye. Corneal thickness is a key factor at all stages of a refractive correction. The volume of tissue removal determines the refractive change and corneal thickness provides structural support. Ablations deeper than planned may lead to overcorrections and inadequate residual corneal thickness increases the risk of postoperative keratectasia [238].

Ultrasound is the most common method of measuring corneal thickness. Newer methods based on Scheimpflug imaging [239] and optical coherence tomography also allow the measurement of corneal pachymetry [240]. The principle of Scheimpflug imaging uses optical sectioning of the cornea with maximum depth of focus, whereas optical coherence tomography

uses low coherence interferometry to measure corneal pachymetry. In a study by Arbelaez et al. [241], preoperative pachymetry measurements correlated well for the three measurement techniques. However, optical coherence pachymetry (OCP) measurements were statistically significantly thinner compared to the both the Scheimpflug and ultrasound measurements ($p = 0.0005$ versus ultrasound pachymetry, and $p = 0.005$ versus Scheimpflug pachymetry). A similar correlation was reported by Borderie between OCP and ultrasound pachymetry [242].

In the study by Arbelaez et al. [241], there was fair correlation between ultrasound and OCP flap thickness measurements ($r^2 = 0.42$, $p < 0.0001$, slope of 0.73), however, the OCP measured statistically significantly thinner flaps ($p < 0.0001$). Thinner flap measurement using OCP compared to ultrasound pachymetry have been previously reported [242]. Based on these outcomes flap thickness measurements with OCP must be interpreted with caution.

A highly significant correlation between the corneal pachymetry changes and the planned central ablation depth were found for all three techniques. The best correlation was with OCP ($r^2 = 0.78$, $p < 0.0001$), followed by Scheimpflug ($r^2 = 0.73$, $p < 0.0001$) and ultrasound ($r^2 = 0.64$, $p < 0.0001$). Scheimpflug provided the best estimation, slightly underestimating the central ablation depth, followed by optical coherence pachymetry, which slightly overestimated the central ablation depth, and ultrasound, which underestimated the central ablation depth.

OCP estimations were statistically significantly deeper than the other two methods ($p < 0.0001$ versus ultrasound pachymetry, and $p < 0.0001$ versus Scheimpflug pachymetry), whereas Scheimpflug and ultrasonic estimates were not statistically different ($p = 0.43$). The difference in theoretical versus measured ablation depth maybe partially explained by the variability in corneal epithelial remodeling which differs from patient to patient. Theoretical calculations cannot account for this variability in corneal response whereas measurements directly incorporate this variability. This likely explains the lack of one to one correlation between theoretical and measured central ablation depth for all three techniques. Additionally, changes in corneal thickness between preoperative and intra-operative measurements using the same instrument have been previously documented [243,244].

OCP generated higher central ablation depth values compared to the other methods. This was likely due to corneal dehydration during laser ablation [244]. Unlike the other two methods, OCP provides continuous measurement during the laser ablation and likely incorporates the effect of dehydration, which increases the volume of tissue ablated. This dehydration effect may be transient and can only be detected with continuous monitoring. Similarly, Wirbelauer et al. [243] also reported good correlation with central ablation depth. However, they found the ablations were 29% deeper than planned [243]. Continuous monitoring of the effect of corneal dehydration ensures that adequate residual stromal bed thickness remains post ablation to maintain the biomechanical integrity of the cornea.

The Scheimpflug unit is not portable and ultrasound pachymetry would require numerous interruptions of the laser ablation to perform measurements. Akin to biometry, contact ultrasound pachymetry may also cause compression of the cornea. This compression may cause a divot that could accumulate fluid, masking the ablation and leading to central islands. Artefactually higher pachymetry measurements may be caused due to fluid coupling on the ultrasound probe. The advantage of non-contact measurements is that they reduce the chance of infection. From a practical perspective, OCP is the best method of the three to continually monitor corneal pachymetry.

Neither of the three measurement techniques was effective at predicting the achieved refractive outcome. This is because the major determinant of corneal refractive power is corneal curvature not change in corneal thickness. Changes from the ideal relationship between central ablation depth and residual refractive error would possibly allow the detection of residual refractive error during excimer laser treatment. Ultrasound and OCP techniques gave encouraging results with borderline correlations. The advantage of these methods over Scheimpflug is the direct measurement during or immediately after ablation. Based on the work of Wirbelauer and colleagues [243] and Arbelaez et al. [241], online OCP allowed the clinical evaluation of intra-operative ablation parameters during refractive surgery. Further studies are required to assess the active control of excimer laser ablation from continuous monitoring, which may improve laser algorithms and nomograms. Intra-operative online OCP could be an important safety feature to monitor the flap thickness during LASIK and residual stromal thickness during refractive surgery. The individual central ablation depth and possible dehydration effects are also monitored continuously. Thus, online optical coherence pachymetry if further developed and standardized could contribute to improved safety standards during refractive surgery. Changes in pachymetry can be effectively used for monitoring and analyzing corneal laser refractive surgeries, helping to circumvent biomechanical weakening of the cornea. The OCP, ultrasound, and Scheimpflug techniques are repeatable and accurate and can be used to assess both preoperative and postoperative pachymetry. However,

the Scheimpflug technique cannot be used to assess intra-operative pachymetry (e.g. flap thickness, central ablation depth during treatment).

The advantage of Scheimpflug imaging over the other two methods is that it provides pachymetry measurements over the entire cornea and is not limited to central or local pachymetry. Currently, the limitation of OCP is that it can only acquire single points of measurements. Central ablation depth can be assessed from the difference in corneal thickness, but changes in refraction are dependent on the modification of the corneal curvature. Therefore, optical coherence pachymetry is valuable for intra-operatively assessing central corneal changes, flap thickness, and residual stromal thickness.

9.3. Tissue saving concerns

The real impact of tissue saving algorithms in customized treatments is still discussed in a controversial way. The problem of minimizing the amount of tissue is that it must be done in such a way that:

(a) does not compromise the refractive correction [245–249];
(b) does not compromise the visual performance;
(c) is safe, reliable and reproducible.

In general, for the same amount of equivalent defocus, the optical blur produced by higher order aberrations increases with increasing radial order and decreases with increasing angular frequencies. With this basis, a simple approach for classification of the clinical relevance of single aberration terms (metric for dioptric equivalence) can be proposed. It is important to bear in mind that one diopter of cardinal astigmatism (at 0° for example) does not necessarily have the same effect as one diopter of oblique astigmatism (at 45° for example). Despite this, other studies have proved this assumption as reasonable [250].

According to this classification, Zernike terms can be considered not clinically relevant if their associated optical blur is lower than <0.25 D, Zernike terms that might be considered clinically relevant correspond to optical blur values between 0.25 and 0.50 D, and Zernike terms considered clinically relevant have associated optical blur values larger than 0.50 D. There are different proposed approaches for minimizing tissue ablation in refractive surgery: in the multizonal treatments [251], the minimization is based on the concept of progressive decreasing corrections in different optical zones. The problem comes from the induced aberrations (especially spherical aberration).

In the treatments planned with smaller optical zone [252] combined with bigger transition zones, the minimization is a variation of the multizone concept. The problem comes, as well, from the induced aberrations (especially spherical aberration). In the treatments planned with smaller optical zone for the cylindrical component [253] (in general for the most powerful correction axis), the minimization is based upon the concept of the maximal depth being based on the lowest meridional refraction and the selected optical zone, and the effective optical zone of the highest meridional refraction is reduced to match the same maximal depth. The problem comes from the induced aberrations (especially high order astigmatism).

In the boost slider method, minimization is produced by linear modulation of the ablated volume. The problem comes from induced changes in refraction produced by modulation. In the Z-clip method [254], minimization consists of defining a 'saturation depth' for the ablated volume, all points planned to ablate deeper than the saturation value are ablated only by an amount equal to the saturation value. The problem is that this 'saturation limit' may occur anywhere in the ablation volume, compromising the refraction when they occur close to the ablation center, and affecting the induction of aberrations in a complicated way. In the Z-shift method [254], minimization consists of defining a 'threshold value' for the ablated volume, no points planned to ablate less than the threshold value are ablated, and the rest of the points are ablated by an amount equal to the original planned ablation minus the threshold value. The problem comes from the fact that this 'threshold value' may occur anywhere in the ablation volume, compromising the refraction when they occur close to the ablation center, and the functional optical zone when occurring at the periphery. Other minimization approaches [255] consist of simplifying the profile by selecting a subset of Zernike terms that minimizes the necessary ablation depth of ablation volume but respecting the Zernike terms considered as clinically relevant.

For each combination subset of Zernike terms, the low order terms are recalculated in a way that it does not compromise the refractive correction. Considering that the Zernike terms are either planned to be corrected or left, it does not compromise the visual performance because all left (not planned to correct) terms are below clinical relevance. The proposed approaches are safe, reliable and reproducible due to the objective foundation upon which they are based. In the same way, the selected optical zone will be used for the correction. It is important to remark that the selection of the Zernike terms to be included in the correction is not trivial. Only Zernike terms considered not clinically relevant or minor clinically relevant can be excluded from the correction, but they must not be

necessarily excluded. Actually, single Zernike terms considered not clinically relevant will only be disabled when they represent an extra tissue for the ablation, and will be enabled when they help to save tissue for the ablation.

In this way, particular cases are represented by the full wavefront correction, by disabling all not clinically relevant terms, or by disabling all high order terms.

The selection process is completely automatically driven by a computer, ensuring systematic results, and minimization of the amount of tissue to be ablated, simplifying the foreseeable problems of manually selecting the adequate set of terms.

A critic to this methodology is the fact that it does not target a diffraction limited optical system. That means it reduces the ablated tissue at the cost of accepting a 'trade-off' in the optical quality. However, there are, at least, three criteria (chromatic blur, depth of focus, wide field vision) favoring the target of leaving minor amounts of not clinically relevant aberrations. There are, as well, no foreseeable risks derived from the proposed minimization functions because they propose ablation profiles simpler than the full wavefront corrections.

Some drawbacks and potential improvements may be hypothesized.

There may be a sort of 'edge' problem considering the case that a Zernike term with DEq of 0.49 D can be enabled or disabled, due to its expected minor clinical relevance, whereas a Zernike term with DEq of 0.51 D will be corrected.

It is controversial, as well, whether the clinical relevance of every Zernike term can be considered independently. The visual effect of an aberration does not only depend on it but also in the other possible aberration present; e.g. a sum of small, and previously considered clinically irrelevant aberration, could suppose a clear loss of overall optical quality. A possible improvement comes from the fact that current selection strategy is in an 'ON/OFF' fashion for each Zernike term, better corrections and higher amounts of tissue saving could be obtained by using a correcting factor $F[n, m]$ (range 0 to 1) for each Zernike correcting a wavefront of the form:

$$\mathrm{Abl}(\rho,\theta) = \sum_{n=0}^{\infty} \sum_{m=-n}^{+n} F_n^m C_n^m Z_n^m(\rho,\theta). \qquad (8)$$

However, this would correspond to a much higher computation cost.

Another possible improvement would be to consider possible aberration couplings, at least, between Zernike modes of the same angular frequency as a new evaluation parameter. New algorithms and ablation strategies for efficiently performing laser corneal refractive surgery in a customized form minimizing the amount of ablated tissue without compromising the visual quality are being developed. The availability of such profiles, potentially maximizing visual performance without increasing the factors of risk, would be of great value for the refractive surgery community and ultimately for the health and safety of the patients.

10. Presbyopic outcomes, the next frontier

Presbyopia (Greek word 'presbys' (πρέσβυς), meaning 'old man', or 'elder', with Latin root '-opia', meaning 'eye') describes the condition where the eye exhibits a progressively diminished ability to focus on near objects with age.

Although, the ability to focus on near objects declines throughout life, the first symptoms are usually first noticed between the ages of 40–50. Accommodation decays from 5 D (ability to focus at 20 cm away) to 2 D (ability to focus at 50 cm away) in only 10 years, deteriorating near vision.

Presbyopia cannot be cured, but the symptoms associated with it can be reduced. The methods most commonly used are the glasses or bifocals or multifocal lenses, and refractive surgery recently.

The use of contact lenses (or glasses) to correct one eye for near and one eye for far with a method is called 'monovision' (which can interfere with depth perception due to loss of focusing ability in the other eye).

When we are looking at a near object, the so-called near triad (convergence, miosis, and accommodation) occurs. Presbyopia is the difficulty of accommodation, however, the reflex of convergence and miosis (reduction of the pupil) are still occurring.

The main goal of a surgical procedure to correct presbyopia is to enhance not only distance but also near visual acuity and the range of relatively clear vision. The surgical techniques to correct presbyopia can be broadly categorized as follows: systems that mimic the crystalline lens and bi- or multifocal techniques that enhance depth of focus and monovision. The success of any ophthalmologic intervention can be judged by using quality of life markers. Attempts to compare the outcomes of surgical techniques using patient satisfaction scores are fraught with difficulties because of the highly subjective nature of such markers. Patients may rate an intervention highly even though essential features of normal visual perception are degraded. For example, monovision is highly rated by patients even though binocular vision is compromised [256].

Bi- and multifocal techniques are simultaneous vision techniques that enhance the depth of focus. During the average lifetime, there is a near linear reduction in accommodation up to approximately

50 years of age, a reduction in pupil size, and a shift in the general pattern of ocular spherical aberration. Pupil constriction, and in some individuals, the change in ocular spherical aberration will enhance the depth of focus of the eye and offer some relief from the deficiencies in near vision attributed to loss of accommodation. Bi- and multifocal surgical techniques tend to emulate and enhance these natural phenomena aimed at combating presbyopia.

Presbyopic patients complain of a loss in range of clear vision and inability to read at an acceptable speed. Measuring the depth of focus is a useful marker but measuring acuity at typical near vision distances may be closer related to patients' real expectations and concerns [257].

PresbyLASIK treatment uses the principles of LASIK surgery to create a multifocal corneal surface aimed at reducing near vision spectacle dependence in presbyopic patients. This treatment constitutes the next step in the correction of presbyopia after monovision LASIK [258,259].

The term presbyLASIK indicates a corneal surgical procedure based on traditional LASIK to create a multifocal surface able to correct any visual defect for distance while simultaneously reducing the near spectacle dependency in presbyopic patients [260,261]. There are two different techniques for presbyLASIK treatment. In the first technique, known as central presbyLASIK, a central area is created for near vision and a peripheral area is created for distance vision [262], whereas in the second technique, known as peripheral presbyLASIK, the central area is for distance vision and the mid-peripheral area is for near vision [263] (although some authors argue peripheral presbyLASIK is not well defined [264]). Both techniques create a multifocal pseudo-accommodative corneal surface.

More specifically, central presbyLASIK produces an increased curvature (smaller radius) in the central pupil, thus it produces more refractive power in the corneal vertex than at the periphery, improving near vision with miosis.

PresbyLASIK, as LASIK, corrects the defocus effect and astigmatism, improving UCVA, but it also improves distant corrected near visual acuity (DCNVA), and may reduce or even eliminate the need for reading aids.

The effective treatment of hyperopic astigmatism and presbyopia has proven to be a significant challenge to refractive surgeons. One of the preferred methods of treating hyperopic astigmatism in presbyopic patients is to perform monovision excimer laser surgery. Monovision LASIK has been found to produce high levels of patient satisfaction, with Goldberg [265] reporting 96% satisfaction and Miranda and Krueger [266] 92%. Contact lens monovision and LASIK-induced monovision traditionally use a nomogram for near addition, with the degree of anisometropia increasing from approximately -1.50 D for a 45-year-old patient up to -2.50 D for a 65-year-old patient [267].

The refractive correction of presbyopia is one of the most frequently discussed topics in refractive surgery today, generating curiosity and great interest throughout the world among surgeons and the ophthalmic industry.

Monovision correction (by corneal refractive surgery or refractive lens exchange) is a surgical strategy for those patients who need distance and near vision with realistic expectations, but it may show some disadvantages, such as the decrease in contrast sensitivity. Accurate patient selection is also crucial for this strategy because monovision is not well tolerated by all patients.

The performance of different types of IOLs (refractive, diffractive, pseudo-accommodating, and multifocal) is constantly being improved [268,269], but the IOLs cause a decrease in near vision contrast sensitivity [270].

Pinelli et al. [263] investigated the outcomes of the correction of presbyopic patients with hyperopia using a peripheral presbyLASIK algorithm called peripheral multifocal LASIK (PML). This treatment creates a multifocal corneal profile in a 6.5 mm diameter zone by the combination of a positive ablation performed over a 6.5 mm zone and a negative ablation performed over an optical zone no smaller than 5 mm. The hypothesis is that the ring between the 5 and 6.5 mm optical zones provides multifocality.

Using a micro-monovision protocol, Reinstein et al. [271] recently succeeded with an intended postoperative refraction that is plano for the dominant eye and in the range of -1.00 to -1.50 D for the non-dominant eye, irrespective of the patient's age, and determined that the near eye had a beneficial effect on binocular distance UCVA when compared to the monocular distance UCVA of the dominant (distance) eye.

In several reports [262,272], Alió and co-workers demonstrated the efficiency, predictability, stability, safety, and visual quality of central presbyLASIK in presbyopic patients with hyperopia.

In another study [273], they reported the correlation of the clinical results of this presbyLASIK method with a theoretical predictive model, showing the adjustment of both.

11. Outlook

We would like to close this review by briefly outlining our expectations of the future evolution of refractive

surgery for the next five years. For that, we have paid attention to four different foci:

- Presbyopic surgery
  As seen in the previous section, presbyopia is the next frontier but certainly not the last frontier. In coming years, presbyopia cannot be cured, but major advances will be made in techniques specifically addressed to restore true accommodation.

  While this is a very challenging goal, the methods based on pseudo-accommodation and extended depth of focus will continue to improve and reach a maturity in which the compromise in distance in near visions will reach a minimum in simultaneous vision (already opened up with the PresbyMAX technique by SCHWIND eye-tech-solutions). With the help of better-suited aberrometers including adaptive optics technology installed at the clinical sites, we will be able to fully understand what patients need, and to honestly determine based upon solid scientific foundations whether we can offer them a solution to cover their actual needs.

  Concerning pseudo-accommodation and multifocality, it will be possible to reduce dependency on reading-spectacles by providing controlled extended depth of focus. Treatments will be prescribed for preventing latent presbyopic symptoms, delaying reading-spectacles demands while presbyopia progresses and treatments will be repeated with minimum risk if reading-spectacles demands renew. If no cataracts are present, but refractive defects exist, presbyLASIK will correct far-distance refraction and drastically alleviate the presbyopic symptoms, offering spectacle-free vision at all distances.
- Technical capabilities of ablative systems
  The range of repetition rates of the laser systems for refractive surgery currently available in the market runs from about 10 to about 1000 Hz (median 250 Hz), with spot size diameters ranging from 6.5 to about 0.3 mm (median 1 mm), corresponding to treatment velocities from about 9 to about $1.7\,s\,D^{-1}$ (mean $5\,s\,D^{-1}$).

  If we compare these values to the situation at the beginning of the twenty-first century, a technological quantum leap is observed. In 2001, repetition rates of the laser systems for refractive surgery in the market ranged from about 10 to about 300 Hz (median 50 Hz), with spot size diameters ranging from 6.5 to about 0.8 mm (median 2–6 mm), corresponding to treatment velocities from about 9 to about $1.7\,s\,D^{-1}$ (mean $12\,s\,D^{-1}$). To foresee the future trends for these essential values when defining the technological capabilities of a system, four driving forces shall be considered:

  – The technological progress of the last 10 years indicating an exponential improvement of the technology.
  – The non-linear cost-to-benefit ratio for new developments indicating a continued improvement of the technology at a slower rate.
  – The actual clinical needs for faster or more precise systems indicating a slow-down improvement of the technology achieving maturity and stability.
  – The limitations imposed by the biological tissue response to the laser interaction (e.g. thermal issues [78], haze development [274]).

  Considering these effects, we can hypothesize a scenario with repetition rates of the laser systems for refractive surgery ranging from about 300 to about 1500 Hz, with spot size diameters ranging from 1.5 to about 0.2 mm, corresponding to treatment velocities from about 4 to about $1.3\,s\,D^{-1}$.
- Laser systems for intrastromal refractive surgery
  Coming years will show the confirmation of the intrastromal technologies (e.g. femtosecond laser systems) not only for creating corneal flaps for LASIK or SBK (already established), but for the creation of therapeutic corneal solutions. Further development in intrastromal technologies will enable them for intrastromal refractive treatments (already opened up with the FLEX and SMILE techniques by Carl-ZEiSS-Meditec).
- Additive techniques for refractive surgery
  Finally, the coming years will see the introduction of sophisticated additive technologies and techniques (maybe combined with subtractive techniques) not only for creating external or therapeutic corneal solutions. Further development in the combination additive technologies and techniques + subtractive technologies will enable them for tailor-made refractive treatments basically free of risk due to true reversibility.

Acknowledgements

S. Arba-Mosquera is an employee of SCHWIND eye-tech-solutions GmbH and M.C. Arbelaez and D. de Ortueta are consultants to SCHWIND eye-tech-solutions GmbH.

References

[1] Gould, G. Light Amplifiers Employing Collisions to Produce a Population Inversion. US Patent Appl. 5/823611, August 11, 1977.
[2] Schawlow, A.L.; Townes, C.H. *Phys. Rev.* **1958,** *112,* 1940–1949.
[3] Swinger, C.A. *Trans. Ophthalmol. Soc. U.K.* **1981,** *101,* 434–439.
[4] Moo-Young, G.A. *West J. Med.* **1985,** *143,* 745–750.
[5] Munnerlyn, C.R.; Koons, S.J.; Marshall, J. *J. Cataract Refract. Surg.* **1988,** *14,* 46–52.
[6] Seiler, T.; Genth, U.; Holschbach, A.; Derse, M. *Refract. Corneal Surg.* **1993,** *9,* 166–172.
[7] Trokel, S.L.; Srinivasan, R.; Braren, B. *Am. J. Ophthalmol.* **1983,** *96,* 710–715.
[8] Krueger, R.R.; Trokel, S.L. *Arch. Ophthalmol.* **1985,** *103,* 1741–1742.
[9] Pettit, G.H.; Ediger, M.N.; Weiblinger, R.P. *Lasers Surg. Med.* **1991,** *11,* 411–418.
[10] McDonnell, P.J.; Moreira, H.; Garbus, J. *Arch. Ophthalmol.* **1991,** *109,* 710–713.
[11] Buratto, L.; Ferrari, M.; Rama, P. *Am. J. Ophthalmol.* **1992,** *113,* 291–295.
[12] Waring, G.O. *Trans. Am. Ophthalmol. Soc.* **1989,** *87,* 854–983.
[13] Pallikaris, I.G.; Siganos, D.S. *J. Refract. Corneal Surg.* **1994,** *10,* 498–510.
[14] Ren, Q.; Simon, G.; Legeais, J.M.; Parel, J.M.; Culbertson, W.; Shen, J.; Takesue, Y.; Savoldelli, M. *Ophthalmology* **1994,** *101,* 883–889.
[15] Mearza, A.A.; Aslanides, I.M. *Expert Opin. Drug Saf.* **2007,** *6,* 27–32.
[16] Gobbi, P.G.; Carones, F.; Brancato, R.; Carena, M.; Fortini, A.; Scagliotti, F.; Morico, A.; Venturi, E. *J. Refract. Surg.* **1995,** *11,* S337–S342.
[17] Camellin, M. *J. Refract. Surg.* **2003,** *19,* 666–670.
[18] Simon, G.; Huang, C.-H. Laser Beam Ophthalmological Surgery Method and Apparatus. Patent WO9717903, 1997.
[19] Pallikaris, I.G.; Naoumidi, I.I.; Kalyvianaki, M.I.; Katsanevaki, V.J. *J. Cataract Refract. Surg.* **2003,** *29,* 1496–1501.
[20] Camellin, M.; Wyler, D. *J. Refract. Surg.* **2008,** *24,* S57–S63.
[21] Tran, D.B.; Sarayba, M.A.; Bor, Z.; Garufis, C.; Duh, Y.J.; Soltes, C.R.; Juhasz, T.; Kurtz, R.M. *J. Cataract Refract. Surg.* **2005,** *31,* 97–105.
[22] Arbelaez, M.C.; Arba Mosquera, S. *Cataract Refract. Surg. Today* **2009,** *Feb,* 37–43.
[23] Arbelaez, M.C.; Vidal, C.; Arba Mosquera, S. Comparison of LASEK and LASIK with Thin and Ultrathin Flaps After Excimer Laser Ablation with the SCHWIND Aspheric Ablation Profile. *J. Refract. Surg.* [Online early access]. DOI: 10.3928/1081597x-20100406-01 (accessed April 28, 2010).
[24] Aslanides, I.M.; Tsiklis, N.S.; Astyrakakis, N.I.; Pallikaris, I.G.; Jankov, M.R. *J. Refract. Surg.* **2007,** *23,* 45–49.
[25] Durrie, D.S.; Slade, S.G.; Marshall, J. *J. Refract. Surg.* **2008,** *24,* S77–S84.
[26] Cheng, Z.Y.; He, J.C.; Zhou, X.T.; Chu, R.Y. *J. Refract. Surg.* **2008,** *24,* 524–529.
[27] Cui, M.; Chen, X.M.; Lü, P. *Chin. Med. J. (Engl.)* **2008,** *121,* 2331–2335.
[28] Gamaly, T.O.; El Danasoury, A.; El Maghraby, A. *J. Refract. Surg.* **2007,** *23,* S1015–S1020.
[29] O'Doherty, M.; Kirwan, C.; O'Keeffe, M.; O'Doherty, J. *J. Refract. Surg.* **2007,** *23,* 133–138.
[30] Duffey, R.J.; Leaming, D. *J. Refract. Surg.* **2003,** *19,* 357–363.
[31] Awwad, S.T.; El-Kateb, M.; Bowman, R.W., et al. *J. Refract. Surg.* **2004,** *20,* S636–S643.
[32] Fraunfelder, F.W.; Rich, L.F. *J. Refract. Surg.* **2004,** *20,* 127–131.
[33] Durrie, D.; Stahl, J. *J. Refract. Surg.* **2004,** *20,* S644–S648.
[34] Seward, S.S.; Oral, D.; Bowman, W.; El-Agha, M.S.; Cavanagh, H.D.; McCulley, J.P. *J. Cataract Refract. Surg.* **2003,** *29,* 2351–2357.
[35] Slade, S. *J. Refract. Surg.* **2004,** *20,* S631–S635.
[36] Lipshitz, I.; Fisher, L.; Lazar, M.; Loewenstein, A. *J. Refract. Surg.* **1999,** *15,* 334–337.
[37] Ditzen, K.; Huschka, H.; Pieger, S. *J. Cataract Refract. Surg.* **1998,** *24,* 42–47.
[38] el Danasoury, M.A.; Waring, G.O. 3rd; el Maghraby, A.; Mehrez, K. *J. Refract. Surg.* **1997,** *13,* 511–520.
[39] Moreno-Barriuso, E.; Lloves, J.M.; Marcos, S. *Invest. Ophthalmol. Vis. Sci.* **2001,** *42,* 1396–1403.
[40] Mastropasqua, L.; Toto, L.; Zuppardi, E.; Nubile, M.; Carpineto, P.; Di Nicola, M.; Ballone, E. *J. Cataract Refract. Surg.* **2006,** *32,* 109–116.
[41] Marcos, S.; Cano, D.; Barbero, S. *J. Refract. Surg.* **2003,** *19,* S592–S596.
[42] Ginis, H.S.; Katsanevaki, V.J.; Pallikaris, I.G. *J. Refract. Surg.* **2003,** *19,* 443–448.
[43] Mrochen, M.; Seiler, T. *J. Refract. Surg.* **2001,** *17,* 584–587.
[44] Jiménez, J.R.; Anera, R.G.; Jiménez del Barco, L.; Hita, E. *Appl. Phys. Lett.* **2002,** *81,* 1521–1523.
[45] Jiménez, J.R.; Anera, R.G.; Jiménez del Barco, L.; Hita, E.; Pérez-Ocón, F. *Opt. Express* **2005,** *13,* 336–343.
[46] Fisher, B.T.; Hahn, D.W. *Appl. Opt.* **2004,** *43,* 5443–5451.
[47] Fisher, B.T.; Hahn, D.W. *J. Opt. Soc. Am. A Opt. Image Sci. Vis.* **2007,** *24,* 265–277.
[48] Dorronsoro, C.; Cano, D.; Merayo-Lloves, J; Marcos, S. *Opt. Express* **2006,** *14,* 6142–6156.

[49] Dorronsoro, C.; Marcos, S. *Opt. Express* **2007,** *15,* 7245–7246.
[50] Arba Mosquera, S.; de Ortueta, D. *Opt. Express* **2008,** *16,* 3877–3895.
[51] Kwon, Y.; Choi, M.; Bott, S. *Opt. Express* **2008,** *16,* 11808–11821.
[52] Kwon, Y.; Bott, S. *Eye* **2009,** *23,* 1845–1850.
[53] Campos, M.; Wang, X.W.; Hertzog, L.; Lee, M.; Clapham, T.; Trokel, S.L.; McDonnell, P.J. *Invest. Ophthalmol. Vis. Sci.* **1993,** *34,* 2493–2500.
[54] Seiler, T.; Kaemmerer, M.; Mierdel, P.; Krinke, H.-E. *Arch. Ophthalmol.* **2000,** *118,* 17–21.
[55] Berns, M.W.; Chao, L.; Giebel, A.W.; Liaw, L.H.; Andrews, J.; VerSteeg, B. *Invest. Ophthalmol. Vis. Sci.* **1999,** *40,* 826–830.
[56] Carvalho, L.A. *Invest. Ophthalmol. Vis. Sci.* **2005,** *46,* 1915–1926.
[57] Zernike, F. *Mon. Not. R. Astron. Soc.* **1934,** *94,* 377–384.
[58] Klein, S.A. *J. Opt. Soc. Am. A Opt. Image Sci. Vis.* **1998,** *15,* 2580–2588.
[59] Kirwan, C.; O'Keefe, M. *Am. J. Ophthalmol.* **2009,** *147,* 77–83.
[60] Gottsch, J.D.; Rencs, E.V.; Cambier, J.L.; Hall, D.; Azar, D.T.; Stark, W.J. *J. Refract. Surg.* **1996,** *12,* 401–411.
[61] Assouline, M.; Moossavi, J.; Müller-Steinwachs, M.; Cohen-Sabban, J.; Thompson, H.W.; Pouliquen, Y. *Surv. Ophthalmol.* **1997,** *42,* S35–S51.
[62] Anschütz, T.; Pieger, S. *J. Refract. Surg.* **1999,** *15,* S252–S256.
[63] Fisher, B.T.; Hahn, D.W. *Ophthalmic Surg. Lasers Imag.* **2004,** *35,* 41–51.
[64] Dorronsoro, C.; Siegel, J.; Remon, L.; Marcos, S. *Opt. Express* **2008,** *16,* 20955–20967.
[65] Dorronsoro, C.; Remon, L.; Merayo-Lloves, J.; Marcos, S. *Opt. Express* **2009,** *17,* 15292–15307.
[66] Thomas, J.W.; Mitra, S.; Chuang, A.Z.; Yee, R.W. *J. Refract. Surg.* **2003,** *19,* 623–628.
[67] Pettit, G.H.; Ediger, M.N.; Weiblinger, R.P. *Lasers Surg. Med.* **1991,** *11,* 411–418.
[68] Noack, J.; Tönnies, R.; Hohla, K.; Birngruber, R.; Vogel, A. *Ophthalmology* **1997,** *104,* 823–830.
[69] Munnerlyn, C.R.; Arnoldussen, M.E.; Munnerlyn, A.L.; Logan, B.A. *J. Biomed. Opt.* **2006,** *11,* 064032.
[70] Vetrugno, M.; Maino, A.; Valenzano, E.; Cardia, L. *J. Refract. Surg.* **2001,** *17,* 454–459.
[71] Mrochen, M.; Schelling, U.; Wuellner, C.; Donitzky, C. *J. Cataract Refract. Surg.* **2009,** *35,* 738–746.
[72] Argento, C.; Valenzuela, G.; Huck, H.; Cremona, G.; Cosentino, M.J.; Gale, M.F. *J. Refract. Surg.* **2001,** *17,* 43–45.
[73] Canals, M.; Elies, D.; Costa-Vila, J.; Coret, A. *J. Refract. Surg.* **2004,** *20,* 106–109.
[74] Doga, A.V.; Shpak, A.A.; Sugrobov, V.A. *J. Refract. Surg.* **2004,** *20,* S730–5733.
[75] Ishihara, M.; Arai, T.; Sato, S.; Morimoto, Y.; Obara, M.; Kikuchi, M. *Front. Med. Biol. Eng.* **2001,** *11,* 167–175.
[76] Ishihara, M.; Arai, T.; Sato, S.; Morimoto, Y.; Obara, M.; Kikuchi, M. *Lasers Surg. Med.* **2002,** *30,* 54–59.
[77] Ishihara, M.; Sato, M.; Sato, S.; Arai, T.; Obara, M.; Kikuchi, M. *J. Biomed. Opt.* **2004,** *9,* 187–192.
[78] Bende, T.; Seiler, T.; Wollensak, J. *Graefes Arch. Clin. Exp. Ophthalmol.* **1988,** *226,* 277–280.
[79] Betney, S.; Morgan, P.B.; Doyle, S.J.; Efron, N. *Cornea* **1997,** *16,* 158–161.
[80] Brygo, F.; Semerok, A.; Oltra, R.; Weulersse, J.M.; Fomichev, S. *Appl. Surf. Sci.* **2006,** *252,* 8314–8318.
[81] O'Donnell, C.B.; Kemner, J.; O'Donnell, F.E. Jr. *J. Cataract. Refract. Surg.* **1996,** *22,* 682–685.
[82] Muller, B.; Boeck, T.; Hartmann, C. *J. Cataract. Refract. Surg.* **2004,** *30,* 464–470.
[83] Mrochen, M.; Kaemmerer, M.; Mierdel, P.; Seiler, T. *J. Cataract. Refract. Surg.* **2001,** *27,* 362–369.
[84] Mrochen, M.; Krueger, R.R.; Bueeler, M.; Seiler, T. *J. Refract. Surg.* **2002,** *18,* 418–429.
[85] Taylor, N.M.; Eikelboom, R.H.; v. Sarloos, P.P.; Reid, P.G. *J. Refract. Surg.* **2000,** *16,* S643–S646.
[86] Bueeler, M.; Mrochen, M.; Seiler, T. Effect of Spot Size, Ablation Depth, and Eye-tracker Latency on the Optical Outcome of Corneal Laser Surgery with a Scanning Spot Laser. *Ophthalmic Technologies XIII*; SPIE: Bellingham, WA, 2003; pp 150–160.
[87] Zadok, D.; Carrillo, C.; Missiroli, F.; Litwak, S.; Robledo, N.; Chayet, A.S. *Am. J. Ophthalmol.* **2004,** *138,* 190–193.
[88] Hersh, P.S.; Fry, K.; Blaker, J.W. *J. Cataract. Refract. Surg.* **2003,** *29,* 2096–2104.
[89] Anera, R.G.; Jiménez, J.R.; del Barco, L.J.; Hita, E. *Opt. Lett.* **2003,** *28,* 417–419.
[90] Cano, D.; Barbero, S.; Marcos, S. *J. Opt. Soc. Am. A* **2004,** *21,* 926–936.
[91] Jiménez, J.R.; Rodríguez-Marín, F.; Anera, R.G.; del Barco, L.J. *Opt. Express* **2006,** *14,* 5411–5417.
[92] Roberts, C. *J. Refract. Surg.* **2002,** *18,* S589–S592.
[93] Huang, D.; Tang, M.; Shekhar, R. *Am. J. Ophthal.* **2003,** *135,* 267–278.
[94] Roberts, C. *J. Cataract. Refract. Surg.* **2005,** *31,* 2–5.
[95] Yoon, G.; MacRae, S.; Williams, D.R.; Cox, I.G. *J. Cataract. Refract. Surg.* **2005,** *31,* 127–135.
[96] Welch, A.J.; Gardne, C. Optical and Thermal Response of Tissue to Laser Radiation. In *Lasers in Medicine*: Waynant, R.W., Ed.; CRC: Boca Raton, CA, 2001; pp 27–46, Chapter 2.
[97] López-Molina, J.A.; Rivera, M.J.; Trujillo, M.; Burdío, F.; Lequerica, J.L.; Hornero, F.; Berjano, E.J. *Open Biomed. Eng. J.* **2008,** *10,* 22–27.
[98] Lembares, A.; Hu, X.H.; Kalmus, G.W. *Invest. Ophthalmol. Vis. Sci.* **1997,** *38,* 1283–1287.
[99] Patel, S.; Alió, J.L.; Pérez-Santonja, J.J. *Invest. Ophthalmol. Vis. Sci.* **2004,** *45,* 3523–3530.
[100] Kim, J.M.; Kim, J.C.; Park, W.C.; Seo, J.S.; Chang, H.R. *J. Korean Med. Sci.* **2004,** *19,* 437–446.
[101] Maldonado-Codina, C.; Morgan, P.B.; Efron, N. *Cornea* **2001,** *20,* 509–515.

[102] Shanyfelt, L.M.; Dickrell, P.L.; Edelhauser, H.F.; Hahn, D.W. *Lasers Surg. Med.* **2008,** *40,* 483–493.

[103] Tjon-Fo-Sang, M.J.; de Faber, J.T.; Kingma, C.; Beekhuis, W.H. *J. Cataract Refract. Surg.* **2002,** *28,* 599–602.

[104] Artal, P.; Chen, L.; Fernandez, E.J.; Singer, B.; Manzanera, S.; Williams, D.R. *J. Vis.* **2004,** *4,* 281–287.

[105] Smirnov, M.S. *Biofizika* **1961,** *6,* 687–703.

[106] Thibos, L.; Hong, X.; Bradley, A.; Applegate, R.A. *J. Vis.* **2004,** *4,* 329–351.

[107] Burns, S.A. *J. Refract. Surg.* **2000,** *16,* S566–S569.

[108] Tscherning, M. *Auges Z. Psychol. Physiol. Sinn.* **1894,** *6,* 456–471.

[109] Mrochen, M.; Kaemmerer, M.; Mierdel, P.; Krinke, H.E.; Seiler, T. *J. Refract. Surg.* **2000,** *16,* S570–S571.

[110] Hartmann, J. *Z. Instrumentenkunde* **1900,** *20,* 47.

[111] Shack, R.B.; Platt, B.C. *J. Opt. Soc. Am.* **1971,** *61,* 656.

[112] MacRae, S.; Fujieda, M. *J. Refract. Surg.* **2000,** *16,* S576–S580.

[113] Liang, J.; Grimm, B.; Goelz, S.; Bille, J.F. *J. Opt. Soc. Am. A Opt. Image Sci. Vis.* **1994,** *11,* 1949–1957.

[114] Babcock, H.W. *Science* **1990,** *250,* 192.

[115] Moreno-Barriuso, E.; Marcos, S.; Navarro, R.; Burns, S.A. *Optom. Vis. Sci.* **2001,** *78,* 152–156.

[116] Carvalho, L.A.; Castro, J.C. *Optom. Vis. Sci.* **2006,** *83,* 108–118.

[117] Díaz-Doutón, F.; Benito, A.; Pujol, J.; Arjona, M.; Güell, J.L.; Artal, P. *Invest. Ophthalmol. Vis. Sci.* **2006,** *47,* 1710–1716.

[118] Díaz-Doutón, F.; Pujol, J.; Arjona, M.; Luque, S.O. *Opt. Lett.* **2006,** *31,* 2245–2247.

[119] Corbett, A.D.; Wilkinson, T.D.; Zhong, J.J.; Diaz-Santana, L. *J. Opt. Soc. Am. A Opt. Image Sci. Vis.* **2007,** *24,* 1266–1275.

[120] Warden, L.; Liu, Y.; Binder, P.S.; Dreher, A.W.; Sverdrup, L. *J. Refract. Surg.* **2008,** *24,* 188–196.

[121] Salmon, T.O. Corneal Contribution to the Wavefront Aberration of the Eye. Ph.D. Dissertation, Indiana University, IN, 1999.

[122] Mrochen, M.; Jankov, M.; Bueeler, M.; Seiler, T. *J. Refract. Surg.* **2003,** *19,* 104–112.

[123] Alio, J.L.; Belda, J.I.; Osman, A.A.; Shalaby, A.M. *J. Refract. Surg.* **2003,** *19,* 516–527.

[124] Mrochen, M.; Kaemmerer, M.; Seiler, T. *J. Cataract Refract. Surg.* **2001,** *27,* 201–207.

[125] Mrochen, M.; Donetzky, C.; Wüllner, C.; Löffler, J. *J. Cataract Refract. Surg.* **2004,** *30,* 775–785.

[126] Reinstein, D.Z.; Neal, D.R.; Vogelsang, H.; Schroeder, E.; Nagy, Z.Z.; Bergt, M.; Copland, J.; Topa, D. *Ophthalmol. Clin. North Am.* **2004,** *17,* 191–210.

[127] Koller, T.; Iseli, H.P.; Hafezi, F.; Mrochen, M.; Seiler, T. *J. Cataract Refract. Surg.* **2006,** *32,* 584–589.

[128] Buehren, T.; Lee, B.J.; Collins, M.J.; Iskander, D.R. *Cornea* **2002,** *21,* 346–351.

[129] Bueeler, M.; Mrochen, M.; Seiler, T. *J. Cataract Refract. Surg.* **2003,** *29,* 257–263.

[130] Arba Mosquera, S.; Merayo-Lloves, J.; de Ortueta, D. *Invest. Ophthalmol. Vis. Sci.* **2008,** *49,* 4828–4836.

[131] Chernyak, D.A. *J. Refract. Surg.* **2005,** *21,* 463–468.

[132] Chernyak, D.A. *J. Cataract Refract. Surg.* **2004,** *30,* 633–638.

[133] Bharti, S.; Bains, H.S. *J. Refract. Surg.* **2007,** *23,* S1041–S1045.

[134] Kim, H.; Joo, C.K. *J. Cataract Refract. Surg.* **2008,** *34,* 557–561.

[135] Park, S.H.; Kim, M.; Joo, C.K. *Ophthalmologica* **2009,** *223,* 166–171.

[136] Porter, J.; Yoon, G.; MacRae, S.; Pan, G.; Twietmeyer, T.; Cox, I.G.; Williams, D.R. *J. Cataract Refract. Surg.* **2005,** *31,* 2058–2066.

[137] Hori-Komai, Y.; Sakai, C.; Toda, I.; Ito, M.; Yamamoto, T.; Tsubota, K. *J. Refract. Surg.* **2007,** *23,* 911–915.

[138] Chang, J. *J. Cataract Refract. Surg.* **2008,** *34,* 1720–1726.

[139] Yang, Y.; Thompson, K.; Burns, S. *Invest. Ophthalmol. Vis. Sci.* **2002,** *43,* 2508–2512.

[140] Guirao, A.; Williams, D.; Cox, I. *J. Opt. Soc. Am. A* **2001,** *18,* 1003–1015.

[141] Ciccio, A.E.; Durrie, D.S.; Stahl, J.E.; Schwendeman, F. *J. Refract. Surg.* **2005,** *21,* S772–S774.

[142] Thibos, L.N.; Applegate, R.A.; Schwiegerling, J.T.; Webb, R. *J. Refract. Surg.* **2002,** *18,* S652–S660.

[143] Thibos, L.N.; Hong, X.; Bradley, A.; Cheng, X. *J. Opt. Soc. Am. A Opt. Image Sci. Vis.* **2002,** *19,* 2329–2348.

[144] Marcos, S.; Barbero, S.; Llorente, L.; Merayo-Lloves, J. *Invest. Ophthalmol. Vis. Sci.* **2001,** *42,* 3349–3356.

[145] Marcos, S. *J. Refract. Surg.* **2001,** *17,* S596–S601.

[146] Bará, S.; Arines, J.; Ares, J.; Prado, P. *J. Opt. Soc. Am. A.* **2006,** *23,* 2061–2066.

[147] Chernyak, D.A. *IEEE Trans. Biomed. Eng.* **2005,** *52,* 2032–2040.

[148] Schruender, S.; Fuchs, H.; Spasovski, S.; Dankert, A. *J. Refract. Surg.* **2002,** *18,* S624–S629.

[149] Huang, D.; Arif, M. *J. Cataract Refract. Surg.* **2002,** *28,* 407–416.

[150] Guirao, A.; Williams, D.; MacRae, S. *J. Refract. Surg.* **2003,** *19,* 15–23.

[151] Bueeler, M.; Mrochen, M.; Seiler, T. *J. Cataract Refract. Surg.* **2004,** *30,* 17–25.

[152] Levy, Y.; Segal, O.; Avni, I.; Zadok, D. *Am. J. Ophthalmol.* **2005,** *139,* 225–228.

[153] Patel, S.; Marshall, J.; Fitzke, F.W. *Refract. Corneal Surg.* **1993,** *9,* 366–375.

[154] Gatinel, D.; Malet, J.; Hoang-Xuan, T.; Azar, D.T. *Invest. Ophthalmol. Vis. Sci.* **2002,** *43,* 941–948.

[155] Perez-Escudero, A.; Dorronsoro, C.; Sawides, L.; Remon, L.; Merayo-Lloves, J; Marcos, S. *Invest. Ophthalmol. Vis. Sci.* **2009,** *50,* 4146–4154.

[156] Somani, S.; Tuan, K.A.; Chernyak, D. *J. Refract. Surg.* **2004,** *20,* S581–S585.

[157] Calossi, A. *The Optical Quality of the Cornea*; Fabiano Editore: Italy, 2002.

[158] Manns, F.; Ho, H.; Parel, J.M.; Culbertson, W. *J. Cataract Refract. Surg.* **2002,** *28,* 766–774.
[159] Díaz, J.A.; Anera, R.G.; Jiménez, J.R.; Jiménez del Barco, L. *J. Mod. Opt.* **2003,** *50,* 1903–1915.
[160] McLellan, J.S.; Marcos, S.; Prieto, P.M.; Burns, S.A. *Nature* **2002,** *417,* 174–176.
[161] Bará, S.; Navarro, R. *J. Opt. Soc. Am. A* **2003,** *20,* 1–10.
[162] Arba Mosquera, S.; de Ortueta, D. *Ophthalmic Physiol. Opt.* **2009,** *29,* 535–548.
[163] Lee, J.M.; Lee, D.J.; Jung, W.J.; Park, W.C. *Korean J. Ophthalmol.* **2008,** *22,* 164–168.
[164] Arbelaez, M.C.; Vidal, C.; Al Jabri, B.; Arba Mosquera, S. *J. Refract. Surg.* **2009,** *25,* 991–999.
[165] Tuan, K.M.; Chernyak, D. *Optom. Vis. Sci.* **2006,** *83,* 605–610.
[166] Pop, M.; Payette, Y. *J. Refract. Surg.* **2004,** *20,* S678–S684.
[167] Anera, R.G.; Jiménez, J.R.; Jiménez del Barco, L.; Bermdez, J.; Hita, E. *J. Cataract Refract. Surg.* **2003,** *29,* 762–768.
[168] Holladay, J.T.; Janes, J.A. *J. Cataract Refract. Surg.* **2002,** *28,* 942–947.
[169] Boxer Wachler, B.S.; Korn, T.S.; Chandra, N.S.; Michel, F.K. *J. Refract. Surg.* **2003,** *19,* 464–465.
[170] de Ortueta, D.; Arba Mosquera, S. *J. Refract. Surg.* **2007,** *23,* 11.
[171] Mattioli, R.; Tripoli, N.K. *Optom. Vis. Sci.* **1997,** *74,* 881–894.
[172] Gatinel, D.; Hoang-Xuan, T.; Azar, D.T. *Invest. Ophthalmol. Vis. Sci.* **2001,** *42,* 1736–1742.
[173] Thibos, L.N.; Applegate, R.A.; Schwiegerling, J.T.; Webb, R.; VSIA Standards Taskforce Members. *J. Refract. Surg.* **2002,** *18,* S652–S660.
[174] Arbelaez, M.C.; Vidal, C.; Arba-Mosquera, S. *Invest. Ophthalmol. Vis. Sci.* **2008,** *49,* 5287–5294.
[175] de Ortueta, D.; Schreyger, F.D. *J. Refract. Surg.* **2007,** *23,* 198–200.
[176] Bueeler, M.; Iseli, H.P.; Jankov, M.; Mrochen, M. *J. Cataract Refract. Surg.* **2005,** *31,* 1986–1994.
[177] Chan, C.C.; Boxer Wachler, B.S. *J. Refract. Surg.* **2006,** *22,* 467–471.
[178] Lipshitz, I. *J. Refract. Surg.* **2002,** *18,* 740–743.
[179] Durrie, D.S.; Kezirian, G.M. *J. Cataract Refract. Surg.* **2005,** *31,* 120–126.
[180] Bueeler, M.; Mrochen, M. *J. Refract. Surg.* **2004,** *20,* 371–378.
[181] Bueeler, M.; Mrochen, M. *J. Refract. Surg.* **2005,** *21,* 28–36.
[182] Artal, P.; Benito, A.; Tabernero, J. *J. Vis.* **2006,** *6,* 1–7.
[183] Tabernero, J.; Benito, A.; Alcón, E.; Artal, P. *J. Opt. Soc. Am. A* **2007,** *24,* 3274–3283.
[184] Llorente, L.; Barbero, S.; Merayo, J.; Marcos, S. *J. Refract. Surg.* **2004,** *20,* 203–216.
[185] Artal, P. What aberration pattern (if any) produces the best vision? *6th International Wavefront Congress*, Athens, Greece, February 10–13, 2005.
[186] Yoon, G.; MacRae, S.; Williams, D.R.; Cox, I.G. *J. Cataract Refract. Surg.* **2005,** *31,* 127–135.
[187] Binder, P.S.; Rosenshein, J. *J. Cataract Refract. Surg.* **2007,** *33,* 1158–1176.
[188] Hori-Komai, Y.; Toda, I.; Asano-Kato, N.; Ito, M.; Yamamoto, T.; Tsubota, K. *J. Refract. Surg.* **2006,** *22,* 546–555.
[189] Subbaram, M.V.; MacRae, S.M. *J. Refract. Surg.* **2007,** *23,* 435–441.
[190] Applegate, R.A.; Sarver, E.J.; Khemsara, V. *J. Refract. Surg.* **2002,** *18,* S556–S562.
[191] Applegate, R.A.; Marsack, J.D.; Ramos, R.; Sarver, E.J. *J. Cataract Refract. Surg.* **2003,** *29,* 1487–1495.
[192] Applegate, R.A.; Howland, H.C. *J. Refract. Surg.* **1997,** *13,* 295–299.
[193] Gambra, E.; Sawides, L.; Dorronsoro, C.; Marcos, S. *J. Vis.* **2009,** *9,* 1–15.
[194] de Ortueta, D.; Arba-Mosquera, S.; Baatz, H. *J. Refract. Surg.* **2009,** *25,* 339–349.
[195] Bailey, M.D.; Zadnik, K. *Cornea* **2007,** *26,* 246–254.
[196] Bailey, M.D.; Mitchell, G.L.; Dhaliwal, D.K.; Boxer Wachler, B.S.; Zadnik, K. *Ophthalmology* **2003,** *110,* 1371–1378.
[197] Manns, F.; Milne, P.; Parel, J.M. *J. Refract. Surg.* **2002,** *18,* S610–S614.
[198] Tuan, K.M. *J. Cataract Refract. Surg.* **2006,** *32,* 577–583.
[199] Subbaram, M.V.; MacRae, S.; Slade, S.G.; Durrie, D.S. *J. Refract. Surg.* **2006,** *22,* 746–753.
[200] Sharma, M.; Wachler, B.S.; Chan, C.C. *J. Refract. Surg.* **2007,** *23,* 252–256.
[201] Buhren, J.; Kohnen, T. *J. Cataract Refract. Surg.* **2006,** *32,* 1166–1174.
[202] Tran, D.B.; Shah, V. *J. Refract. Surg.* **2006,** *22,* S961–S964.
[203] Jiménez, J.R.; Anera, R.G.; Díaz, J.A.; Pérez-Ocón, F. *J. Opt. Soc. Am. A* **2004,** *21,* 98–103.
[204] Chen, C.C. *J. Cataract Refract. Surg.* **2002,** *28,* 1539–1545.
[205] Kohnen, T.; Mahmoud, K.; Bühren, J. *Ophthalmology* **2005,** *112,* 1692.
[206] Farooqui, M.A.; Al-Muammar, A.R. *J. Refract. Surg.* **2006,** *22,* 741–745.
[207] de Ortueta, D.; Arba-Mosquera, S.; Baatz, H. *J. Refract. Surg.* **2008,** *24,* 137–144.
[208] Mearza, A.A.; Muhtaseb, M.; Aslanides, I.M. *J. Refract. Surg.* **2008,** *24,* 885–890.
[209] Rosa, N.; Furgiuele, D.; Lanza, M.; Capasso, L.; Romano, A. *J. Refract. Surg.* **2004,** *20,* 478–483.
[210] Dupps, W.J.; Roberts, C. *J. Cataract Refract. Surg.* **2002,** *18,* S589–S592.
[211] Chen, C.C.; Izadshenas, A.; Asghar Rana, M.A.; Azar, D.T. *J. Cataract Refract. Surg.* **2002,** *28,* 1539–1545.
[212] Jiménez, J.R.; Anera, R.G.; del Barco, L.J.; Hita, E. *J. Cataract Refract. Surg.* **2003,** *29,* 1468.
[213] Wang, L.; Koch, D. *J. Cataract Refract. Surg.* **2003,** *29,* 1702–1708.
[214] Albarrán-Diego, C.; Mu noz, G.; Montés-Micó, R.; Rodriguez, A.; Alió, J.L. *J. Refract. Surg.* **2006,** *22,* 34–42.

[215] de Ortueta, D.; Schreyger, F. *J. Cataract Refract. Surg.* **2006,** *32,* 906–907.

[216] Applegate, R.A.; Thibos, L.N.; Twa, M.D.; Sarver, E.J. *J. Cataract Refract. Surg.* **2009,** *35,* 139–152.

[217] de Ortueta, D.; Arba Mosquera, S.; Baatz, H. *J. Refract. Surg.* **2009,** *25,* 175–184.

[218] O'Brart, D.P.; Mellington, F.; Jones, S.; Marshall, J. *J. Refract. Surg.* **2007,** *23,* 343–354.

[219] Chayet, A.S.; Montes, M.; Gómez, L.; Rodríguez, X.; Robledo, N.; MacRae, S. *Ophthalmology* **2001,** *108,* 303–308.

[220] Arbelaez, M.C.; Vidal, C.; Arba Mosquera, S. *J. Cataract Refract. Surg.* **2009,** *35,* 1789–1798.

[221] de Ortueta, D.; Haecker, C. *Eur. J. Ophthalmol.* **2008,** *18,* 869–876.

[222] Payvar, S.; Hashemi, H. *J. Refract. Surg.* **2002,** *18,* 225–233.

[223] Arbelaez, M.C.; Vidal, C.; Arba Mosquera, S. *J. Refract. Surg.* **2009,** *25,* 1083–1090.

[224] Stonecipher, K.G.; Kezirian, G.M. *J. Refract. Surg.* **2008,** *24,* S424–S430.

[225] Venter, J. *J. Refract. Surg.* **2008,** *24,* 487–493.

[226] Arbelaez, M.C.; Vidal, C.; Arba Mosquera, S. *Ophthalmic Physiol. Opt.* **2009,** *29,* 487–496.

[227] Padmanabhan, P.; Mrochen, M.; Basuthkar, S.; Viswanathan, D.; Joseph, R. *J. Cataract Refract. Surg.* **2008,** *34,* 389–397.

[228] Chung, S.H.; Lee, I.S.; Lee, Y.G.; Lee, H.K.; Kim, E.K.; Yoon, G.; Seo, K.Y. *J. Cataract Refract. Surg.* **2006,** *32,* 779–784.

[229] Buzzonetti, L.; Iarossi, G.; Valente, P.; Volpi, M.; Petrocelli, G.; Scullica, L. *J. Cataract Refract. Surg.* **2004,** *30,* 1929–1933.

[230] Smolek, M.K.; Klyce, S.D. *Invest. Ophthalmol. Vis. Sci.* **2003,** *44,* 4676–4681.

[231] Porter, J.; Guirao, A.; Cox, I.G.; Williams, D.R. *J. Opt. Soc. Am. A* **2001,** *18,* 1793–1803.

[232] Wang, L.; Dai, E.; Koch, D.D.; Nathoo, A. *J. Cataract Refract. Surg.* **2003,** *29,* 1514–1521.

[233] Jiménez, J.R.; Villa, C.; Anera, R.G.; Gutiérrez, R.; del Barco, L.J. *J. Refract. Surg.* **2006,** *22,* 679–688.

[234] Arbelaez, M.C.; Vidal, C.; Arba Mosquera, S. *J. Optom.* **2010,** *3,* 20–28.

[235] Cuesta, J.R.; Anera, R.G.; Jiménez, R.; Salas, C. *Am. J. Ophthalmol.* **2003,** *135,* 279–284.

[236] Mansouri, B.; Thompson, B.; Hess, R.F. *Vision Res.* **2008,** *48,* 2775–2784.

[237] Jiménez, J.R.; Ponce, A.; Anera, R.G. *Optom. Vis. Sci.* **2004,** *81,* 559–562.

[238] Binder, P.S. *J. Cataract Refract. Surg.* **2007,** *33,* 1530–1538.

[239] O'Donnell, C.; Maldonado-Codina, C. *Cornea* **2005,** *24,* 920–924.

[240] Wirbelauer, C.; Pham, D.T. *J. Refract. Surg.* **2003,** *19,* 372–377.

[241] Arbelaez, M.C.; Vidal, C.; Arba Mosquera, S. *J. Cataract Refract. Surg.* **2009,** *25,* 699–708.

[242] Borderie, V. *J. Fr. Ophtalmol.* **2006,** *29,* 40–44.

[243] Wirbelauer, C.; Aurich, H.; Pham, D.T. *Graefes Arch. Clin. Exp. Ophthalmol.* **2007,** *245,* 775–781.

[244] Aurich, H.; Wirbelauer, C.; Jaroszewski, J.; Hartmann, C.; Pham, D.T. *Cornea* **2006,** *25,* 182–184.

[245] Cheng, X.; Bradley, A.; Thibos, L.N. *J. Vis.* **2004,** *4,* 310–321.

[246] Marsack, J.D.; Thibos, L.N.; Applegate, R.A. *J. Vis.* **2004,** *4,* 322–328.

[247] Thibos, L.N. *J. Refract. Surg.* **2004,** *20,* S533–S536.

[248] Watson, A.B.; Ahumada, A.J. Jr *J. Vis.* **2008,** *8,* 1–19.

[249] Marcos, S.; Sawides, L.; Gambra, E.; Dorronsoro, C. *J. Vis.* **2008,** *8,* 1–12.

[250] Remón, L.; Tornel, M.; Furlan, W.D. *Optom. Vis. Sci.* **2006,** *83,* 311–315.

[251] Kim, H.M.; Jung, H.R. *J. Refract. Surg.* **1995,** *11,* S293–S297.

[252] Kermani, O.; Schmiedt, K.; Oberheide, U.; Gerten, G. *J. Refract. Surg.* **2003,** *19,* S190–S194.

[253] Kezirian, G.M. *Rev. Ophthalmol.* **2003,** *10,* 12.

[254] Goes, F.J. Customized Topographic Repair with the New Platform: ZEiSS MEL80/New CRS Master TOSCA II. In *Mastering the Techniques of Customised LASIK*: Garg, A., Rosen, E., Eds.; Jaypee Medical International: Delhi, 2007; Chapter 18, pp 179–193.

[255] Arba Mosquera, S.; Merayo-Lloves, J; de Ortueta, D. *J. Optom.* **2009,** *2,* 182–196.

[256] Johannsdottir, K.R.; Stelmach, L.B. *Optom. Vis. Sci.* **2001,** *78,* 646–651.

[257] Patel, S.; Alió, J.L.; Feinbaum, C. *J. Refract. Surg.* **2008,** *24,* 294–299.

[258] Cheng, A.C.; Lam, D.S. *J. Refract. Surg.* **2005,** *21,* 411–412.

[259] Jain, S.; Ou, R.; Azar, D.T. *Ophthalmology* **2001,** *108,* 1430–1433.

[260] Becker, K.A.; Jaksche, A.; Holz, F.G. *Ophthalmologe* **2006,** *103,* 667–672.

[261] Telandro, A. *J. Refract. Surg.* **2004,** *20,* S714–S717.

[262] Alió, J.L.; Chaubard, J.J.; Caliz, A.; Sala, E.; Patel, S. *J. Refract. Surg.* **2006,** *22,* 453–460.

[263] Pinelli, R.; Ortiz, D.; Simonetto, A.; Bacchi, C.; Sala, E.; Alió, J.L. *J. Refract. Surg.* **2008,** *24,* 494–500.

[264] de Ortueta, D. *J. Refract. Surg.* **2008,** *24,* 561.

[265] Goldberg, D.B. *J. Cataract Refract. Surg.* **2001,** *27,* 1449–1455.

[266] Miranda, D.; Krueger, R.R. *J. Refract. Surg.* **2004,** *20,* 325–328.

[267] Goldberg, DB. *J. Cataract Refract. Surg.* **2003,** *29,* 1695–1701.

[268] Montes-Mico, R.; Espana, E.; Bueno, I.; Charman, W.N.; Menezo, J.L. *Ophthalmology* **2004,** *111,* 85–96.

[269] Alio, J.L.; Tavolato, M.; De la Hoz, F.; Claramonte, P.; Rodriguez-Prats, J.L.; Galal, A. *J. Cataract Refract. Surg.* **2004,** *30,* 2494–2503.

[270] Montes-Mico, R.; Alio, J.L. *J. Cataract Refract. Surg.* **2003,** *10,* 703–711.

[271] Reinstein, D.Z.; Couch, D.G.; Archer, T.J. *J. Refract. Surg*. **2009,** *25,* 37–58.
[272] Illueca, C.; Alió, J.L.; Mas, D.; Ortiz, D.; Pérez, J.; Espinosa, J.; Esperanza, S. *J. Refract. Surg*. **2008,** *24,* 344–349.
[273] Ortiz, D.; Alió, J.L.; Illueca, C.; Mas, D.; Sala, E.; Pérez, J.; Espinosa, J. *J. Refract. Surg*. **2007,** *23,* 39–44.
[274] Lohmann, C.P.; Gartry, D.S.; Muir, M.K.; Timberlake, G.T.; Fitzke, F.W.; Marshall, J. *Eur. J. Ophthalmol*. **1991,** *1,* 173–180.

Six-month clinical outcomes in LASIK for high myopia with aspheric «aberration neutral» ablations using the AMARIS laser system

Maria Clara Arbelaez, MD[1]; Camila Vidal, OD[1]; Samuel Arba Mosquera, MSc[2,3]

PURPOSE: To evaluate the postoperative clinical outcomes and high order aberrations among eyes with myopia higher than 5 D that have underwent LASIK treatments using the Schwind AMARIS laser system. Schwind CAM Aberration-Free Aspheric treatments have been performed in all cases.

PATIENTS AND METHODS: LASIK treatments were performed on 75 eyes (45 patients) with mean spherical equivalent -6.46±1.15 D (range, -8.50 to -5.25 D) using a SCHWIND Pendular microkeratome with a 110 µm cutting head and the SCHWIND AMARIS excimer laser. In all cases pre- and postoperative autorefractor measurements, manifest refraction, best spectacle-corrected visual acuity (BSCVA), uncorrected visual acuity (UCVA), topography and corneal wavefront analysis using the Optikon Keratron Scout, and ocular wavefront analysis using the SCHWIND Ocular Wavefront Analyzer as well as complications, were performed. Ablations were calculated using the ORK-CAM software.
Clinical outcomes were evaluated in terms of efficacy, predictability, stability, refractive outcome, safety, and wavefront aberrations.

RESULTS: At six months, mean spherical equivalent manifest refraction was -0.30±0.34 D (range, -1.12 to +0.38 D). Eighty-one percent eyes (61) were within ±0.50 D of attempted correction. Uncorrected visual acuity was 20/20 or better in 81% (61 eyes), and 20/32 or better in 97% (73 eyes). Average root-mean-square of the high order aberrations (RMSHOA) increased 0.14 µm after the treatment, mean spherical aberration increased 0.12 µm after the treatment, and mean coma increased 0.04 µm after the treatment (all for 6.0 mm analysis diameter).

CONCLUSIONS: Our results show that non-customised «aberration neutral» ablation profiles derived from wavefront analysis are able to minimize the amount of induced aberrations even for myopic refractive corrections up to -9 D.

J Emmetropia 2010; 1: 111-116

Submitted: 2/24/2010
Revised: 5/6/2010
Accepted: 7/7/2010

[1] From Muscat Eye Laser Center. Muscat-Sultanate of Oman.
[2] From Grupo de Investigación de Cirugía Refractiva y Calidad de Visión, Instituto de Oftalmobiología Aplicada, University of Valladolid, Valladolid, Spain
[3] From SCHWIND eye-tech-solutions. Kleinostheim, Germany.

The authors Arbelaez, and Vidal have no proprietary interest in the materials presented herein.

Correspondence: Maria Clara Arbelaez, MD. Muscat Eye Laser Center P.O. Box 938; P.C. 117; Muscat; Sultanate of Oman. Tel :+96824691414 Fax +96824601212. E-mail: drmaria@omantel.net.om

INTRODUCTION

Laser corneal refractive surgery is based on the use of a laser (typically an excimer one) to change the corneal curvature to compensate for refractive errors of the eye[1]. It has become the most successful technique, mainly due to the submicron precision and the high repeatability of the ablation of the cornea accompanied by minimal side effects. One of the most significant side-effects in myopic LASIK is the induction of spherical aberration[2], which causes halos and reduced contrast sensitivity[3]. To avoid the induction of spherical aberration, so-called «customized» treatments were developed. Customization of the ablation is possible either using wavefront measurements of the whole eye[4]

(obtained, e.g., by Hartman-Shack wavefront sensors) or by using corneal topography-derived wavefront analyses[5,6]. Topographic-guided[7], Wavefront-driven[8], Wavefront-optimized[9], Asphericity preserving, and Q-factor profiles[10] have been proposed as possible solutions. Nevertheless, considerations as treatment duration, tissue removal[11], and overall postoperative outcomes make more difficult to establish a universal optimal profile for postoperative visual function.

The ORK-CAM software (SCHWIND eye-tech-solutions) is able to import, visualize, and analyse diagnostic data of the eye. The software creates an aspherical ablation profile to optimize the corneal shape. As we used non-customised «Aberration neutral» profiles in our study, ablations were optimized to induce no change in Wavefront aberration (within Optical Zone, OZ) other than Sphere and Cylinder components, leaving all existing high order aberrations (HOA) unchanged because the best corrected visual acuity, in this patient, has been unaffected by the pre-existing aberrations[12]. Thus to compensate for the aberrations induction observed with other types of profile definitions[13], some of those sources of aberrations are those ones related to the loss of efficiency of the laser ablation for non-normal incidence[14-16]. Based on the existing corneal shape and the keratometric values of the cornea, the ideal ablation profile is then calculated compensating, among others, for the cosine effect.

This study was conducted to evaluate, among myopic treatments of -5 D of more of spherical equivalent, safety, predictability, and efficacy of the «Aberration neutral» Profiles implemented in the SCHWIND AMARIS, and to evaluate the impact, in terms of high order aberrations, of the ORK-CAM «Aberration neutral» Profiles.

PATIENTS AND METHODS

A total of 75 eyes (45 patients), with myopic spherical equivalent of -5 D or more, were consecutively treated the using ORK-CAM «Aberration neutral» Aspheric ablation profiles and retrospectively analysed.

Inclusion criteria comprised: preoperative myopia higher than –5 D spherical equivalent targeted for emmetropia, preoperative BSCVA ≥ 20/25 (logMAR ≤ +0.1), preoperatively <0.6 µm RMSHOA for 6 mm diameter, postoperatively successful completion of 6 months follow-up. Exclusion criteria comprised: preoperative active ocular disease, preoperative dry eye, preoperative ectatic corneal disease, preoperative monocular patients, preoperative immunocompromised disease, preoperative systemic or retinal vascular disease, preoperative pregnancy.

Visual acuity was measured using the CSO Vision Chart. CSO Vision Chart is a state-of-the-art for computerized charts for visual testing. We selected Snellen fraction US (feet), with optotypes following the standard EN ISO 8596-8597 and used 85 cd/m^2 Sloan letters optotypes in LogMAR progression automatically randomized to avoid patient's memorization.

Six-months follow up was available in 75 of these eyes (100%), and their preoperative data were as follows: mean spherical equivalent refraction -6.46±1.15 D (range, -8.50 to -5.25 D); and mean cylinder magnitude 0.80±0.70 D (range, 0 to 5.00 D). In all eyes, we measured corneal topography and derived corneal wavefront analyses (Keratron scout, Optikon 2000 S.p.A., Rome, Italy), ocular wavefront with a high resolution Hartmann-Shack sensor[17] (ORK-Wavefront Analyzer, Schwind eye-tech-solutions, Kleinostheim, Germany), manifest refraction, and uncorrected and best spectacle-corrected Snellen visual acuity. Measurements were performed preoperatively and at one, three, and six months after surgery.

All ablations were non-customised based on «aberration neutral» profiles and calculated using the ORK-CAM software. Aspheric aberration neutral (Aberration-Free^{TM}) profiles are not based on the Munnerlyn proposed profiles, and go beyond that by adding some aspheric characteristics to balance the induction of spherical aberration (prolateness optimization).

The aberration neutral (Aberration-Free^{TM}) profile is aspherical-based, including a multidynamic aspherical transition zone, aberration and focus shift compensation due to tissue removal, pseudo-matrix based spot positioning, enhanced compensation for the loss of efficiency, and intelligent thermal effect control; all based on theoretical equations validated with ablation models and clinical evaluations.

Real ablative spot shape (volume) is locally considered through a self-constructing algorithm. In addition, there are a randomized flying-spot ablation pattern and controls for the local repetition rates to minimize the thermal load of the treatment (smooth ablation, no risk of thermal damage). Therefore, the ablated surface in the aspheric aberration neutral (Aberration-Free^{TM}) profiles should be very smooth, so that there will be some benefits in high order aberrations. Finally, all these optimizations theoretically diminish the induced wavefront aberration after myopic LASIK.

A 6.3 mm central fully corrected ablation zone was used in all eyes with a variable transition size automatically provided by the laser related to the planned refractive correction (7.3 mm to 8.7 mm). The ablation was performed using the AMARIS excimer laser (SCHWIND eye-tech-solutions, Kleinostheim, Germany) which is a flying-spot laser using randomized spot distribution to minimize thermal effects[18]. The AMARIS laser system works at a repetition rate of 500 Hz and produces a beam size of 0.54 mm Full-Width-at-Half-Maximum (FWHM) with a superGaussian ablative spot profile[19,20]. High-speed eye-tracking (pupil tracker with cyclotorsional track-

ing) with a 1050-Hz acquisition rate is accomplished with a 3-ms latency time[21].

All flaps were created using a Pendular microkeratome with 110 µm cutting head (SCHWIND eye-tech-solutions).

Optical errors centred on the line-of-sight, representing the Wavefront Aberration, are described by Zernike polynomials[22] and coefficients in OSA standard[23], and analysed for diameters of 6, 7 and 8 mm diameter zones, to include the total treatment zone and transition zone and junction zone, as well.

We assessed the statistical significance of the postoperative status compared to the preoperative baseline using paired Student's T-tests. The level of statistical significance was taken as $p<.05$.

RESULTS

We have included 75 treatments for this study, all of them without adverse events. At six months, mean manifest refraction spherical equivalent was -0.30±0.34 D (range, -1.12 to +0.38 D) and mean cylinder magnitude 0.32±0.24 D (range, 0 to 1.00 D). Eighty-one percent eyes (61) were within ±0.50 D of attempted correction (Figure 1). Uncorrected visual acuity was 20/20 or better in 81% of the treatments (61 eyes) and 20/32 or better in 97% (73 eyes) (Figure 2). Results were stable between one and six months (Figure 3). Regarding safety, 23% of eyes gained one line (17 eyes), and 7% gained two lines of best spectacle-corrected visual acuity (5 eyes) (Figure 4).

Preoperatively, mean spherical aberration was +0.27±0.15 µm (range +0.14 to +0.52 µm). Postoperatively, the values were +0.39±0.15 µm (range +0.14 to +0.67) ($P < 0.0001$).

Preoperatively, mean coma magnitude was 0.26±0.27 µm (range 0.02 to 0.50). Postoperatively, the values were 0.30±0.13 µm (range 0.01 to 0.62) ($P = 0.09$).

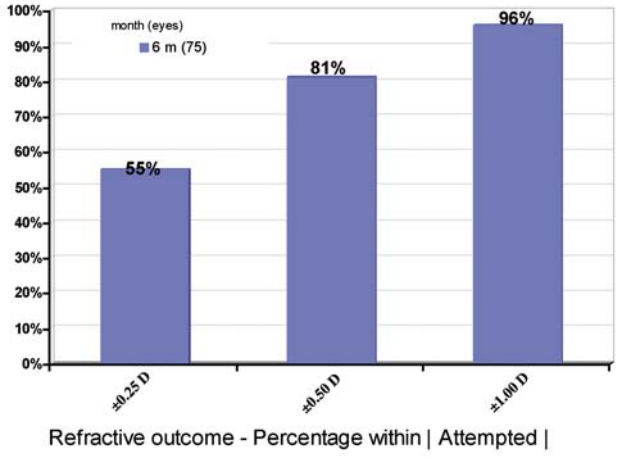

Figure 1. Achieved refractive outcome at 6 months follow-up for spherical equivalent.

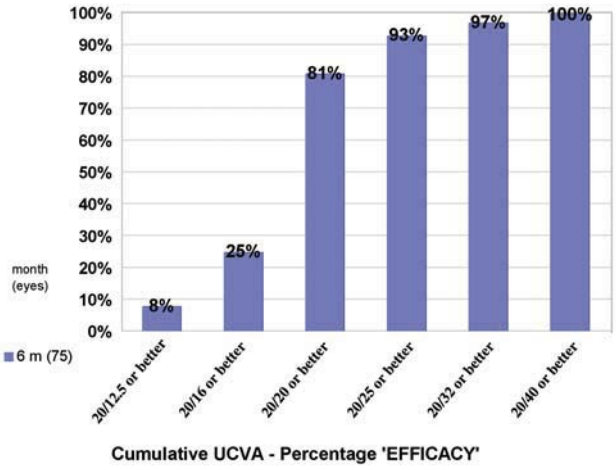

Figure 2. Efficacy plot: Uncorrected Visual Acuity at 6 months follow-up.

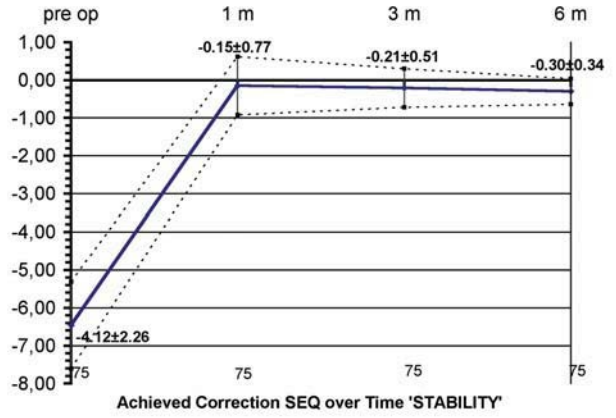

Figure 3. Achieved refractive change vs. Time at 6 months follow-up for spherical equivalent.

Preoperatively, RMSHOA was, on average, 0.44±0.09 µm (range 0.26 to 0.82). Postoperatively, the values were 0.58±0.21 µm (range 0.32 to 0.88) ($P < 0.0001$).

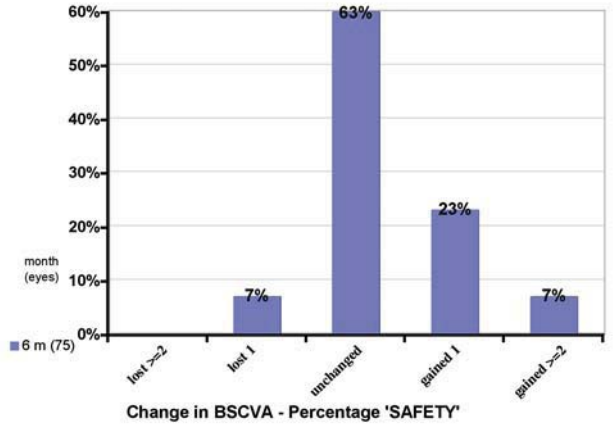

Figure 4. Safety plot: Change in BSCVA at 6 months follow-up.

At 7 mm, preoperatively, mean corneal spherical aberration was +0.42±0.15 µm (range +0.22 to +0.81). Postoperatively, the values were +0.69±0.25 µm (range +0.20 to +1.16) (P < 0.0001). Preoperatively, mean corneal coma was 0.38±0.18 µm (range 0.02 to 0.73). Postoperatively, the values were 0.48±0.25 µm (range 0.01 to 0.98) (P = 0.003). Preoperatively, corneal RMSHOA was, on average, 0.65±0.21 µm (range 0.38 to 1.22). Postoperatively, the values were 1.07±0.25 µm (range 0.54 to 1.50) (P < 0.0001).

At 8 mm, preoperatively, mean corneal spherical aberration was +0.61±0.22 µm (range +0.32 to +1.18). Postoperatively, the values were +1.18±0.41 µm (range +0.32 to +1.93) (P < 0.0001). Preoperatively, mean corneal coma was 0.53±0.25 µm (range 0.03 to 1.02). Postoperatively, the values were 0.71±0.37 µm (range 0.02 to 1.46) (P < 0.0001). Preoperatively, corneal RMSHOA was, on average, 0.93±0.31 µm (range 0.55 to 1.74). Postoperatively, the values were 1.79±0.39 µm (range 0.85 to 2.38) (P < 0.0001).

DISCUSSION

75 high-myopic treatments were analysed at 6M follow-up. Aberration-Free Treatments with the SCHWIND AMARIS are safe and very predictable (no eye lost >=2 lines BSCVA, 7% (5 eyes) gained >=2 lines BSCVA). Results were achieved without applying additional nomograms (residual sphere about -0.1 D, residual cyl about -0.3 D) (81% within 0.50 D, 96% within 1.0 D). 6-months follow-up time shows the excellent performance of the system (25% eyes 20/16 or better UCVA, 93% eyes 20/25 or better UCVA). From post-op VA, we have got 81% eyes in UCVA 20/20 or better and 29% eyes improved their pre-op BSCVA, due to the minimum aberrations induction by the AMARIS-CAM profile. From the achieved correction, both sphere and cylinder are quite accurate, predictable and stable from the first week follow-up (residual refraction increased by only -0.1 D in 6M). HOA were effectively preserved (at 6.0 mm, induced spherical aberration 0.12 µm; induced coma aberration 0.04 µm; induced HOA 0.14 µm RMS).

In our study, for 6 mm analysis diameter, we found on average an induction high-order aberrations of 0.14±0.16 µm corneal wavefront. Regarding coma, aberration changed, on average, 0.04±0.13 µm corneal wavefront. Spherical aberration changed, on average, 0.12±0.12 µm corneal wavefront. Induced spherical aberration was correlated to achieved defocus correction (P < 0.0001) and increased on average by 0.03 µm per dioptre of achieved defocus correction for a 6-mm pupil for corneal wavefront. That compares to 0.09 µm per dioptre reported by Marcos et al.[24] and by Llorente et al.[25] for ocular spherical aberrations, and to 0.17 µm per dioptre reported for corneal spherical aberrations[25]. That compares as well to 0.04 µm per dioptre reported by Kohnen et al[26]. In terms of aberrations, the induced amount of spherical aberration has been decreased when compared to literature reported values[25,26], or to previous experiences using simplified Munnerlyn profiles[1] on the same laser[27]. Nevertheless, spherical aberration was still induced even with the attempted «aberration neutral» ablation profiles, which was expected as myopic corrections, especially higher ones, always induce some spherical aberration.

Compared to other studies, Farooqui and Al-Muammar[28] found after conventional LASIK treatments a postoperative ocular spherical aberration of +0.24 µm and a postoperative ocular coma of 0.24 µm compared to our values of +0.39 µm and 0.30 µm respectively.

Kohnen et al.[26] found after non-customised LASIK a change in corneal RMSHOA of 0.17±0.18 µm, a mean induction of corneal coma of 0.09±0.20 µm and for corneal spherical aberration a significant increase 0.13±0.12 µm, this compares to our values of 0.14±0.16 µm, 0.04±0.13 µm and 0.12±0.12 µm respectively.

Induced HOA in our sample shows similar results to those found by Farooqui et al.[28] and Kohnen et al.[26] after conventional LASIK treatment, however the sample of these studies showed defocus of -3.15±1.41 D (–0.50 to -6.25D), and of -4.22±1.78 D (-1.25 to –8.00 D) respectively, compared to -6.46±1.15 D (range, -8.50 to -5.25 D) in our sample. From this, it can be inferred that our treatments induced less HOA per diopter of correction.

Remarkably, in our sample astigmatism up to 5D was treated. In fact, 12% of the treatments (9 eyes) were planned with astigmatism higher than 1.5D. In general, the correction of astigmatism induces more HOA than the correction of defocus since it induces similar amount of C[4,0] but larger amounts of C[4,+-2][29].

Until today there is no prove that the asphericity alone plays a major role in the visual process[30]. We still do not know whether an asphericity Q -0.25 is better than Q +0.50, we only know that the asphericity of the «averaged» human cornea is about -0.28[31]. As well, no absolute optimum has been found, despite of some remarkable theoretical works[32-34]. When a patient is selected for non customized aspherical treatment, the global aim of the surgeon should be to leave all existing high order aberrations (HOA) unchanged because the best corrected visual acuity, in this patient, has been unaffected by the pre-existing aberrations[35]. Hence, all factors that may induce changes in HOA's[14,36,37], such as biomechanics, need to be taken into account prior to the treatment to ensure that the preoperative HOA's are unchanged after treatment.

As the corresponding Cartesian oval[38] is the free-of-aberrations surface (i.e. the only truly monofocal sur-

face), and it can be described by an aspherical surface with Q-factor -1/n^2 (approx. -0.53 for human cornea), then the mean human cornea (Q -0.25) is less prolate (so more oblate) than the corresponding Cartesian oval, thus the refractive power of the outer corneal surface increases from central towards peripheral.

The first that we should clarify is that even the amount of corneal spherical aberration and the asphericity are intrinsically related; the goal is always described in terms of change in spherical aberration[39], because this is the factor related to the quality and sharpness of the retinal image.

Furthermore, the main high order aberration effects post-op (coma and spherical aberration) are coming from decentration and «edge» effects, the strong local curvature change from Optical Zone to Transition Zone and from Transition Zone to non-treated cornea. Then it is necessary to emphasize the use of huge Optical Zones, covering the scotopic pupil size plus some tolerance for possible decentrations, and well-defined smooth Transition Zones. In our study this was approached by the use of a 6.3 mm diameter fully corrected ablation zone with a multidynamic aspherical transition zone automatically provided by the laser related to the planned refractive correction (7.3 mm to 8.7 mm diameter).

Since we have available corneal wavefront information, we have addressed the following question. The optical high order aberrations were measured at a 6-mm pupil diameter, as is customary. The optical zone diameter was 6.3 mm. Most spherical aberration induction occurs at the junction between the central treatment zone/transition zone/untreated zone, and since some patients may have a mesopic/scotopic pupil diameter greater than 6 mm, the values within a 6-mm zone may not correspond with the real-life visual function of the patient in terms of glare and halos. In order not to limit the topographic analysis to 6 mm, and this way, to omit the transition zone and junction zone from the entire analysis, and although the information is most interesting and useful from a «6-mm point of view», it may miss the practical clinical point of the effect of changes in aberrations outside the 6-mm zone. Therefore, we have analyzed the available topographic information independently, reporting the corneal wavefront findings for a larger diameter zone, in this case 7 and 8 mm, to include the total treatment zone and transition zone and junction zone, as well.

To check whether the increasing in aberration magnitude was only due to the larger analysis diameter, analysis has been performed in defocus equivalent (DEQ). On virgin eyes, defocus equivalent as proposed by Thibos et al[40] seems to be relative insensitive to different analysis diameters.

The change in corneal spherical aberration DEQ was, on average, +0.09±0.10 D at 6 mm analysis diameter, +0.15±0.12 D for 7 mm diameter, and +0.25±0.16 D for 8 mm. For corneal coma the change in DEQ was, on average, 0.03±0.13 D at 6 mm analysis diameter, 0.06±0.15 D for 7 mm diameter, and 0.08±0.17 D for 8 mm, whereas for corneal RMSHOA was, on average, 0.11±0.12 D at 6 mm analysis diameter, 0.24±0.14 D for 7 mm diameter, and 0.37±0.17 D for 8 mm.

This fact confirms for our study, that actually the change in aberration magnitudes increased with the analysis diameter. This could be expected as the tested profile attempts to be neutral for aberrations within the disc limited by the optical zone size (6.3 mm diameter for this study) which was closely achieved, and increases when we include analysis diameters beyond optical zone.

Limitations. Limitations of our study include the short follow up and the lack of a control group. Despite these limitations, we were able to demonstrate that «aberration neutral» ablation profiles are superior to standard ablation profiles for the corrections of myopia between -5 and -9 D.

In summary, this study demonstrated that «aberration neutral» profile definitions, which are not standard in refractive surgery, yielded very good visual, optical, and refractive results for corrections of myopia and myopic astigmatism up to -9 D of spherical equivalent. «Aberration neutral» ablation profiles as demonstrated here, have, therefore, the potential to replace currently used standard algorithms for corrections of non-customised myopic astigmatism.

REFERENCES

1. Munnerlyn CR, Koons SJ, Marshall J. Photorefractive keratectomy: a technique for laser refractive surgery. J Cataract Refract Surg; 1988; 14: 46-52.
2. Moreno-Barriuso E, Lloves JM, Marcos S. Ocular Aberrations before and after myopic corneal refractive surgery: LASIK-induced changes measured with LASER ray tracing. Invest Ophthalmol Vis Sci 2001; 42: 1396-1403.
3. Mastropasqua L, Toto L, Zuppardi E, Nubile M, Carpineto P, Di Nicola M, Ballone E. Photorefractive keratectomy with aspheric profile of ablation versus conventional photorefractive keratectomy for myopia correction: six-month controlled clinical trial. J Cataract Refract Surg; 2006; 32: 109-116.
4. Thibos L, Bradley A, Applegate R. Accuracy and precision of objective refraction from wavefront aberrations. ISSN 1534-7362, 2003 ARVO.
5. Salmon TO. Corneal contribution to the Wavefront aberration of the eye. PhD Dissertation; 1999; 70.
6. Mrochen M, Jankov M, Bueeler M, Seiler T. Correlation Between Corneal and Total Wavefront Aberrations in Myopic Eyes. J Refract Surg; 2003; 19: 104-112.
7. Alio JL, Belda JI, Osman AA, Shalaby AM. Topography-guided laser in situ keratomileusis (TOPOLINK) to correct irregular astigmatism after previous refractive surgery. J Refract Surg; 2003; 19: 516-527.
8. Mrochen M, Kaemmerer M, Seiler T. Clinical results of wavefront-guided laser in situ keratomileusis 3 months after surgery. J Cataract Refract Surg. 2001; 27: 201-207.

9. Mrochen M, Donetzky C,Wüllner C, Löffler J. Wavefront-optimized ablation profiles: Theoretical background. J Cataract Refract Surg; 2004; 30: 775-785.
10. Koller T, Iseli HP, Hafezi F, Mrochen M, Seiler T. Q-factor customized ablation profile for the correction of myopic astigmatism. J Cataract Refract Surg; 2006; 32: 584-589.
11. Gatinel D, Malet J, Hoang-Xuan T, Azar DT. Analysis of customized corneal ablations: theoretical limitations of increasing negative asphericity. Invest Ophthalmol Vis Sci; 2002; 43: 941-948.
12. Artal P. et al. What aberration pattern (if any) produces the best vision?, 6th International Wavefront Congress, Athens, Greece; February 2005.
13. Marcos S, Cano D, Barbero S. Increase in corneal asphericity after standard laser in situ keratomileusis for myopia is not inherent to the Munnerlyn algorithm. J Refract Surg; 2003; 19: S592-S596.
14. Mrochen M, Seiler T. Influence of Corneal Curvature on Calculation of Ablation Patterns used in photorefractive Laser Surgery. J Refract Surg; 2001; 17: 584-587.
15. Jiménez JR, Anera RG, Jiménez del Barco L, Hita E. Effect on laser-ablation algorithms of reflection losses and nonnormal incidence on the anterior cornea. Applied Physics Letters; 2002; 81;8: 1521-1523.
16. Jiménez JR, Anera RG, Jiménez del Barco L, Hita E, Pérez-Ocón F. Correlation factor for ablation agorithms used in corneal refractive surgery with gaussian-profile beams. Optics Express; 2005; 13; 1: 336-343.
17. Salmon T. Measurement of Refractive Errors in Young Myopes using the COAS Shack-Hartmann Aberrometer. Optometry and Vision Science; 2003; Vol 80.
18. Bende T, Seiler T, Wollensak J, Corneal Thermal Gradients, Graefe's Archive Ophthalmology, 1988, 226: 277-280.
19. Huang D, Arif M. Spot size and quality of scanning laser correction of higher-order wavefront aberrations. J Cataract Refract Surg; 2002; 28: 407-416.
20. Guirao A,Williams D, MacRae S. Effect of beam size on the Expected benefit of customized laser refractive surgery. J Refract Surg; 2003; 19: 15-23.
21. Bueeler M, Mrochen M. Simulation of Eye-tracker Latency, Spot Size, and Ablation Pulse Depth on the Correction of Higher Order Wavefront Aberrations With Scanning Spot Laser Systems. J Refract Surg; 2005; 21: 28-36.
22. Zernike F. Diffraction theory of the knife-edge test and its improved form, the phase-contrast method. Physica I; 1934; 689-704.
23. Thibos LN, Applegate RA, Schwiegerling JT, Webb R, VSIA Standards Taskforce Members. Standards for Reporting the Optical Aberrations of Eyes. J Refract Surg; 2002; 18: S652-S660.
24. Marcos S, Barbero S, Llorente L, Merayo-Lloves J. Optical response to LASIK surgery for myopia from Total and Corneal Aberration Measurements. Invest Ophthalmol Vis Sci; 2001; 42: 3349-3356.
25. Llorente L, Barbero S, Merayo J, Marcos S. Changes in corneal and total aberrations induced by LASIK surgery for hyperopia. J Refract Surg; 2004; 20: 203-216.
26. Kohnen T, Mahmoud K, Bühren J. Comparison of corneal higher-order aberrations induced by myopic and hyperopic LASIK. Ophthalmology. 2005; 112: 1692.
27. de Ortueta D, Arba-Mosquera S, Baatz H. Comparison of Standard and Aberration-neutral Profiles for Myopic LASIK With the SCHWIND ESIRIS Platform. J Refract Surg. 2008 (in press).
28. Farooqui MA, Al-Muammar AR. Topography-guided CATz versus conventional LASIK for myopia with the NIDEK EC-5000: A bilateral eye study. J Refract Surg. 2006; 22: 741-745.
29. Arbelaez MC, Vidal C, Arba Mosquera S. Moderate-to-High Astigmatism correction with the SCHWIND AMARIS Total-Tech Laser: 6-month results. J Cataract Refract Surg; 2009; 35: 1789-1798.
30. Somani S, PhD; Tuan KA, OD, PhD; Chernyak D, PhD. Proceedings of the 5th International Congress of Wavefront Sensing and Optimized Refractive Corrections: Corneal Asphericity and Retinal Image Quality: A Case Study and Simulations. J Refract Surg; 2004; 20: S581-S585.
31. Calossi A. The optical quality of the cornea. Fabiano Editore 2002.
32. Patel S, Marshall J, Fitzke FW. Model for predicting the optical performance of the eye in refractive surgery. Refract Corneal Surg; 1993; 9: 366-375.
33. Manns F, Ho H, Parel JM, Culbertson W. Ablation profiles for wavefront-guided correction of myopia and primary spherical aberration. J Cataract Refract Surg; 2002; 28: 766-774.
34. Díaz JA, Anera RG, Jiménez JR, Jiménez del Barco L. Optimum corneal asphericity of myopic eyes for refractive surgery, Journal of Modern Optics; 2003; 50: 1903-1915.
35. Artal P et al. What aberration pattern (if any) produces the best vision?, 6th International Wavefront Congress, Athens, Greece; February 2005.
36. Lipshitz I. Thirty-four Challenges to Meet Before Excimer Laser Technology Can Achieve Super Vision. J Refract Surg; 2002; 18: 740-743.
37. Yoon G, MacRae S, Williams DR, Cox IG. Causes of spherical aberration induced by laser refractive surgery. J Cataract Refract Surg; 2005; 31: 127-135.
38. Clarkson ENK, Levi-Setti R. Trilobite eyes and the optics of Descartes and Huygens. Nature 1975; 254: 663-7.
39. Marcos S. Aberrations and visual performance following standard Laser vision correction. J Refract Surg; 2001; 17: S596-S601.

First author:
Maria Clara Arbelaez, MD

Muscat Eye Laser Center
Sultanate of Oman

J Optom. 2010;**3(4)**:198-205

Journal of Optometry

www.elsevier.com/locate/joptom

ORIGINAL ARTICLE

Six-month clinical outcomes after hyperopic correction with the SCHWIND AMARIS Total-Tech laser

María Clara Arbelaez[a,*], Camila Vidal[a], Samuel Arba Mosquera[b,c]

[a]*Muscat Eye Laser Centre, Muscat, Sultanate of Oman*
[b]*Grupo de Investigación de Cirugía Refractiva y Calidad de Visión, Instituto de Oftalmobiología Aplicada, University of Valladolid, Valladolid, Spain*
[c]*SCHWIND eye-tech-solutions, Kleinostheim, Germany*

Received 25 September 2010; accepted 10 November 2010

KEYWORDS
Hyperopia;
Refractive surgery;
Excimer laser;
Wavefront aberration;
Aspheric ablation

Abstract
Purpose: To evaluate postoperative clinical outcomes, and corneal High Order Aberrations, among eyes with hyperopia up to +5 D of spherical equivalent, that have undergone LASIK treatments using the SCHWIND AMARIS laser system.
Methods: At six-month follow-up, 100 eyes with preoperative hyperopia or hyperopic astigmatism up to +5 D of spherical equivalent were retrospectively analysed. Standard examinations, pre- and postoperative wavefront analysis with a corneal-wavefront-analyzer (OPTIKON Scout) were performed. Aberration-Free aspheric treatments were planned with Custom Ablation Manager software and ablations performed using the SCHWIND AMARIS flying-spot excimer laser system (both SCHWIND eye-tech-solutions). LASIK flaps were created using a LDV femtosecond laser (Ziemer Group) in all cases. Clinical outcomes were evaluated in terms of predictability, refractive outcome, safety, and wavefront aberration.
Results: At six month, 90% of eyes achieved ≥ 20/25 UCVA and 44% achieved ≥ 20/16 UCVA. Seventy-four percent of eyes were within ± 0.25D of spherical equivalent and 89% within ± 0.50D, with 94% within 0.50D of astigmatism. Mean spherical equivalent was −0.12 ± 0.51D and 0.50 ± 0.51D for the astigmatism. Fifty-two percent of eyes improved BSCVA vs. only 19% losing lines of BSCVA. Predictability slope for refraction was 1.03 and intercept +0.01 D. On average, negative corneal spherical aberrations were significantly increased by the treatments, no other aberration terms changed from pre- to postoperative values.
Conclusions: LASIK for hyperopia and hyperopic astigmatism with SCHWIND AMARIS yields very satisfactory visual outcomes. Preoperative refractions were postoperatively reduced to subclinical values with no clinically relevant induction of corneal HOA.

*Corresponding autor: M.C. Arbelaez. Postal address: P.O. Box 938, Wadi Al Kabir P.C. 117; Muscat, Sultanate of Oman. Phone: +968 24691414; Fax: +968 24601212.
E-mail address: drmaria@omantel.net.om (M.C. Arbelaez).

1888-4296/$ - see front matter

PALABRAS CLAVE
Hipermetropía;
Cirugía refractiva;
Láser excimer;
Aberración de frente de onda;
Ablación asférica

Resultados clínicos a los seis meses de una corrección de hipermetropía con el láser SCHWIND AMARIS Total-Tech

Resumen
Objetivo: Evaluar los resultados clínicos posoperatorios, aberraciones corneales de orden superior, entre ojos con una hipermetropía de hasta 5 dioptrías de equivalente esférico, previamente sometidos a tratamientos LASIK con el sistema de láser SCHWIND AMARIS.
Métodos: Tras 6 meses de seguimiento, se analizaron de manera retrospectiva 100 ojos con hipermetropía o astigmatismo hipermetrópico preoperatorio de hasta 5 dioptrías de equivalente esférico. Se llevaron a cabo exploraciones estándar, análisis de frente de onda preoperatorio y posoperatorio con un analizador de frente de onda corneal (OPTIKON Scout). Se diseñaron tratamientos asféricos sin aberraciones con el software Custom Ablation Manager y se realizaron ablaciones utilizando el sistema de láser excímero de punto flotante SCHWIND AMARIS (ambas tecnologías son de SCHWIND Eye-tech Solutions). En todos los casos, los colgajos de LASIK se crearon utilizando un láser de femtosegundo LDV (Ziemer Group). Los resultados clínicos se evaluaron a nivel de previsibilidad, resultado de refracción, seguridad y aberración de frente de onda.
Resultados: Al cabo de 6 meses, el 90% de los ojos alcanzaron agudeza visual sin corrección (AVSC) > 20/25 AVSC (UCVA) y el 44% alcanzaron > 20/16 AVSC. El 74% de los ojos se encontraban en +0,25 dioptrías de equivalente esférico y el 89% en ±0,50 dioptrías, con el 94% en 0,50 dioptrías de astigmatismo. La media del equivalente esférico fue de −0,12 ± 0,51 dioptrías y de 0,50 ± 0,51 dioptrías para astigmatismo. El 52% de los ojos vieron mejorada la mejor agudeza visual con gafa (MAVCG) (BSCVA) frente a solamente un 19% que perdieron líneas de MAVCG. La pendiente de previsibilidad de refracción fue de 1,03 y la ordenada en el origen, de +0,01 dioptrías. Como promedio, la aberración esférica negativa de la córnea fue significativamente incrementada por los tratamientos y ningún otro término de aberración cambió entre los valores preoperatorios y posoperatorios.
Conclusiones: Utilizar LASIK para la hipermetropía y el astigmatismo hipermetrópico con SCHWIND AMARIS produce unos resultados visuales muy satisfactorios. Las refracciones previas a la operación se vieron reducidas a valores subclínicos después de la operación, sin inducción clínicamente relevante de aberraciones de orden superior de la córnea.

The introduction of the excimer laser for refractive surgery has opened up the possibility to change the corneal curvature to compensate for refractive errors of the eye. In the case of small spot hyperopic laser in situ keratomileusis (H-LASIK), excimer laser systems produce a steepness of the cornea by ablating mainly at the periphery of the cornea.

H-LASIK treatments induce aberrations.[1] Studies[2,3] attempted to determine the changes in corneal asphericity after H-LASIK, and found a extreme corneal prolateness, indicating large amounts of induced negative spherical aberrations. This is predominantly caused by the loss of efficiency[4-7] at the periphery and the biomechanics of the cornea, and has been described previously by other authors.[8,9]

The pitfalls of H-LASIK are historically important and should be mentioned, as the main problems in decentrations, decreases in best corrected visual acuity, very high frequency of retreatments, frequent residual refractive error, induction of astigmatism and induction of high levels of corneal aberrations, specifically, and spherical aberration.

Later studies on hyperopic treatments with excimer lasers also suggested an increase in negative spherical aberration.[10,11]

By comparison of the intended and achieved topographical changes after H-LASIK surgery, de Ortueta et al.[12] obtained information as to whether the corneal power was changed as calculated, thus providing help in optimizing the ablation profiles (either in terms of nomogram adjustments or more sophisticated optimization algorithms like multifocal algorithms). Additionally, actual under- or overcorrection can be differentiated from under- or overcorrection due to wrong intended correction in this way.

A study by O'Brart et al.[13] analyzing hyperopic LASEK using a Munnerlyn based classical profile and a 7 mm optical zone with a total treated zone of 9 mm demonstrated that the induced aberrations were lower than with the Munnerlyn profile in LASIK. A recent study by de Ortueta et al.,[14] using aspheric aberration neutral profiles showed that induced aberrations are less than in previous publications. This study was undertaken to evaluate postoperative clinical outcomes and High Order Aberrations (HOA), among eyes with hyperopia up to +5 D of spherical equivalent, that underwent LASIK treatments using the SCHWIND AMARIS laser system.[15]

Methods

Study Design and Patient Eligibility Criteria

This is a retrospective analysis of consecutively operated eyes by a single surgeon (MCA). The first consecutive 100 eyes (50 patients) with preoperative manifest hyperopia or hyperopic astigmatism treated using the AMARIS "aberration neutral" (Aberration-Free™) aspheric ablation profiles were retrospectively analysed. In fact, there was no nomogram check before commencing the study, and there were no eyes excluded because lost to follow-up or because they required re-treatments.

This is the first series of eyes operated with this particular treatment algorithm. Due to its retrospective nature, no investigational review board or other regulatory oversight was required. The level of statistical significance was taken as $P < .05$.

Inclusion criteria for review were preoperative hyperopia or hyperopic astigmatism targeted for emmetropia, best spectacle corrected visual acuity (BSCVA) $\geq$ 20/25 (logMAR $\leq +0.1$), < 0.75 μm root mean square (RMS) of the HOA of the corneal wave aberration for 6-mm diameter, and successful completion of 6-month follow-up. All 50 patients (100 eyes) fulfilled the criteria for being taken in the retrospective analysis, and so no one was excluded.

Laser Description

All ablations were non-customised based on "aberration neutral" profiles and calculated using the ORK-CAM software module. Aspheric aberration neutral[16] (Aberration-Free™[17]) profiles are not based on the Munnerlyn proposed profiles,[18] and go beyond that by adding some aspheric characteristics to balance the induction of spherical aberration,[9,19] (prolateness optimization[20,21]).

The aberration neutral (Aberration-Free™) profile is aspherical-based,[22-24] including a multidynamic aspherical transition zone,[23] aberration and focus shift compensation due to tissue removal,[17] pseudo-matrix based spot positioning,[23] enhanced compensation for the loss of efficiency[7,25], and intelligent thermal effect control;[26-28] all based on theoretical equations validated with ablation models and clinical evaluations.

A 6.7 mm central corrected ablation zone was used in all eyes with a variable transition size automatically provided by the laser related to the planned refractive correction (6.9 mm to 9.2 mm). The ablation was performed using the AMARIS[29] excimer laser (SCHWIND eye-tech-solutions, Kleinostheim, Germany) which is a flying-spot laser using ablative spot voxels locally considered through a self-constructing algorithm. In addition, there are a randomized flying-spot ablation pattern and controls for the local repetition rates to minimize the thermal load of the treatment.[30]

Ablations were centred on the corneal vertex (CV) using the pupillary offset, i.e., the distance between the pupil centre and the normal CV measured by videokeratoscopy (Keratron Scout topographer, Optikon 2000 s.p.a., Rome, Italy). The measurement was performed under photopic conditions of 1500 lux, similar to the conditions under the operating microscope. This method was suggested and described by de Ortueta and Arba Mosquera[31] and comparatively tested by Arbelaez et al.[32] The excimer laser allows for modification of the ablation centration from the pupillary centre with an offset by entering either X and Y Cartesian values or R and θ polar values in a regular treatment. The measurement of the pupillary offset was translated into the treatment planning as polar coordinates to be manually entered into the excimer laser computer.

The AMARIS laser system works at a true repetition rate of 500 Hz and produces a beam size of 0.54 mm Full-Width-at-Half-Maximum (FWHM) with a superGaussian ablative spot profile.[33,34] High-speed eye-tracking (pupil and limbus tracker with cyclotorsional tracking[35]) with a 1050-Hz acquisition rate is accomplished with a 3-ms latency time.[36]

AMARIS technology is treating the astigmatism not by superimposing the spherical component with positive or negative cylindrical patterns, nor is it treating either positive or negative cylindrical patterns depending on the sign of the spherical component. Rather, the system analytically creates an aspherotoric volume, which is then discretised into laser pulses sorted spatially and temporally in a pseudo-random fashion. In that way, there is no sequentialization of the sphere and astigmatic components (nor the other way round), but both components are progressively and simultaneously corrected.

Further the AMARIS system has demonstrated its abilities for sparing corneal tissue[37] as well as a very even and gently ablation preserving preoperative bilateral symmetry.[38]

Preoperative Testing

Six-months follow-up was available in 100 of these eyes (100%), and their preoperative data were as follows: mean manifest spherical equivalent refraction $+3.02 \pm 2.06$ D (range, +0.13 to +5.00 D); mean manifest astigmatism magnitude 1.36 ± 1.61 D (range, 0.00 to 5.00 D). In all eyes, we measured corneal topography[39] and derived corneal wavefront[40,41] analyses (Keratron-Scout, OPTIKON2000, Rome, Italy), manifest refraction, and uncorrected and best spectacle-corrected Snellen visual acuity[42] (UCVA and BSCVA respectively). Results are reported for the measurements performed preoperatively and at three and six months after surgery.

We acquire, under non pharmacologically dilated pupils, non-cycloplegic conditions, and natural dim light conditions (to avoid pharmacologically-induced pupil shifts[43-45]), 3 aberrometries (Ocular Wavefront Analyzer, SCHWIND eye-tech-solutions GmbH & Co.KG, based on Irx3, Imagine Eyes, Orsay, France) and objective refractions for each eye of the patient.[46] In order to minimize the potential accommodative response of the patients, we ask them to "see-through-the-target" instead of "looking at the target." In this way, patients do not try to get a sharp image from the +1.5 D fogged target, since they were instructed to see-through-the-target. From those aberrometries, we calculate the mean, and select the most representative one (the aberrometry map with the highest similarity to the mean).

We assessed subjective refraction based upon non-pharmacologic and non-cycloplegic conditions, under natural photopic illumination. We use the objective refraction provided by the aberrometer analyzed for a

sub-pupil of 4 mm diameter, as starting refraction for this step. This is particularly useful for determining the magnitude and orientation of the astigmatism.[47,48] We measure manifest refraction, UCVA and BSCVA[42]. Further rules that we impose for accurately determining the manifest subjective refractions among equal levels of BSCVA are: taking the measurement with the most positive spherical equivalent (unmasking latent hyperopia), if several of them are equal in terms of spherical equivalent, we choose the measurement with the least amount of astigmatism (reducing the risk of postoperative shifts in the axis of astigmatism).

Surgical Technique and Postoperative Treatment

For corneal and conjunctival anaesthesia, two drops of proparacaine HCl 0.5% (Aurocaine®, Aurolab, Madurai, India) were instilled three times before shifting the patient to the Operation Theatre. All flaps were created using a LDV femtosecond laser (Ziemer Group) with superior hinges, 110 μm nominal flap thickness, and 9.0 mm or 9.5 mm nominal flap diameter. A 9 mm marker was used to ensure centration and to be able to objectively measure the amount of applanation. Online pachymetry[49] was performed before and after lifting flap (stromal bed thickness) with the integrated optical coherence pachymeter (Heidelberg Engineering, Heidelberg, Germany). After lifting the flap, ablation was performed preserving flap edges, hinge, and inner face of the flap disk from being ablated. Contact lens was applied at the end of surgery (Biomedics 55 evolution, Ocular Sciences, Cooper Vision, Hamble, UK) in eyes with 'achieved' flap thickness less than 110 microns to avoid flap displacements, dislocations or striae.

One eye drop Tobradex (Alcon Inc, USA) 3 times a day was used for 1 week along with Oasis soft plugs extended duration (6404 Glendora CA) and preservative free artificial tear drops during the first three months.

Outcome Measures

Safety and effectiveness metrics

Efficacy: We analysed the number of eyes with postoperative UCVA in scale from 20/16 to 20/40.

Refractive Outcome: Every dioptric power can be represented by means of a point in Euclidean three-dimensional space. The relationship between visual acuity and refractive power can be represented by closed surfaces of constant visual acuity in symmetric dioptric power space. The power of these three component lenses may be interpreted as (x,y,z) coordinates of a vector representation of the power profile (the U-vector).

The U-vector[50] can be represented as a vector in the 3-dimensional double angle astigmatism space.[51] The norm of this vector correlates to the dioptric blur and to visual acuity[52] and can be formulated as:

$$\|\vec{U}\| = \sqrt{S^2 + S \cdot C + \frac{C^2}{2}} \quad (1)$$

We analysed the mean values of spherical equivalent and astigmatism, and the number of treatments with postoperative refraction within 0.25, 0.50, 1.00 and 2.00 D, as well as, the number of treatments with norm of postoperative U-vector within 0.25, 0.50, 1.00 and 2.00 D. We assessed the statistical significance of the postoperative status compared to the preoperative baseline using paired Student's T-tests.

Safety: We analysed differences in BSCVA postoperative compared to the preoperative baseline for each eye. We assessed the statistical significance of the postoperative status compared to the preoperative baseline using paired Student's T-tests.

Predictability: We plotted scattergrams for the achieved spherical equivalent and astigmatism corrections versus the attempted ones (both at the corneal plane, where the ablation procedure occurs). We analysed slope and intercept of the correlations. We assessed the statistical significance of the correlations using Student's T-tests, the Coefficient of Determination (r^2) was used, and the significance of the correlations has been evaluated considering a metric distributed approximately as t with N−2 degrees of freedom where N is the size of the sample.

Changes in corneal wavefront aberration

Optical errors centred on the line-of-sight, representing the Wavefront Aberration, are described by Zernike polynomials[53] and coefficients in OSA standard,[54] and analysed for a standardised diameter of 6 mm for corneal wavefront.

We analysed mean values and differences, in each of the 30 HOA terms of the Zernike expansion to the seventh order, postoperative compared to the preoperative baseline for each eye. We assessed the statistical significance of the postoperative status compared to the preoperative baseline using paired Student's T-tests.

Results

Patient Demographics and Adverse events

The mean age at the time of the surgical intervention was 37 years (from 21 to 59). Forty-six percent of the patients were males and 54% females.

Neither adverse events nor complications were observed intra- or postoperatively. In the 6 months follow-up no retreatment was performed.

Efficacy and Refractive Outcome

At six-month, UCVA was 20/16 or better in 44% of the treatments (44 eyes), and 20/25 or better in 90% (90 eyes) (Figure 1). The efficacy index scored 0.89. There were no statistically significant differences between the 3 and 6 months follow-ups.

Six-month postoperatively, mean residual spherical equivalent was −0.12 ± 0.51D (range, −0.75 to + 1.75D) ($P < .0001$) and mean residual astigmatism 0.50 ± 0.51D (range, 0.00 to 1.75D) ($P < .0001$). Eighty-nine percent eyes (89) were within ± 0.50D of attempted spherical equivalent correction (Figure 2), with ninety-four percent eyes (94) within ± 0.50D of attempted astigmatic correction, ninety-seven percent eyes (97) within 1.00D, and ninety-three percent eyes (93) within 1.00D of the norm of the residual

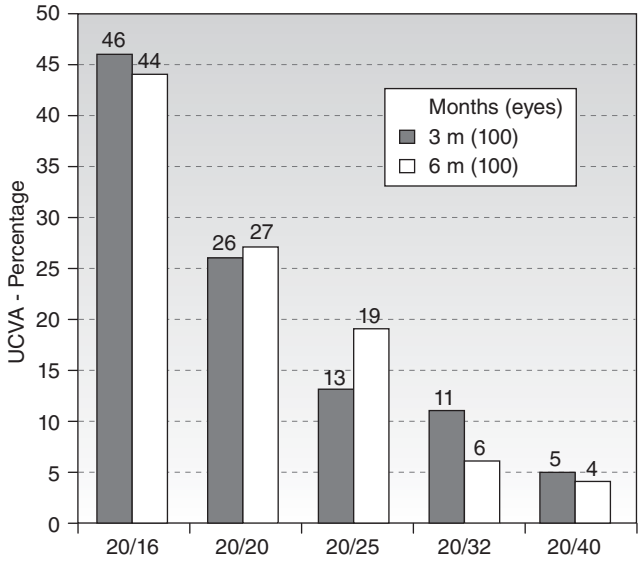

Figure 1 Efficacy plot of the UCVA at 3 and 6 months postoperative follow-up time.

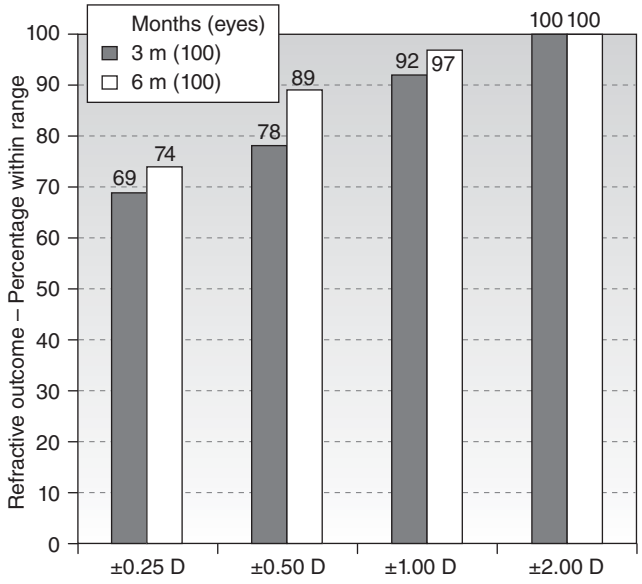

Figure 2 Refractive outcome plot of the residual refraction within range at 3 and 6 months postoperative follow-up time.

U-vector (Figure 3). There were no statistically significant differences between the 3 and 6 months follow-ups.

Safety and Predictability

Regarding safety, 14% of eyes (14 eyes) gained two lines of BSCVA (Figure 4) ($P < .01$). The safety index scored 1.10. There were no statistically significant differences between the 3 and 6 months follow-ups.

The achieved refractive change, defined as the vectorial difference in the astigmatism space of postoperative and preoperative refractions (incorporating spherical equivalent and astigmatism) at the corneal plane, was significantly correlated with the intended correction ($r^2 = .90$, $P < .0001$).

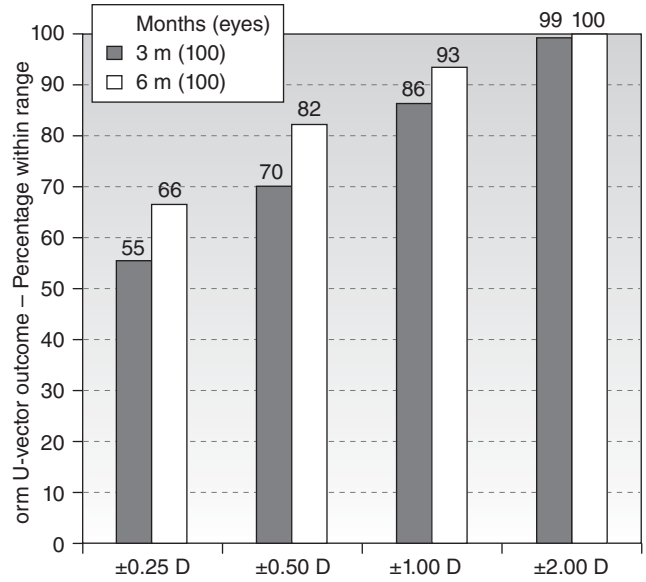

Figure 3 Plot of the residual norm of the U-vector within range at 3 and 6 months postoperative follow-up time.

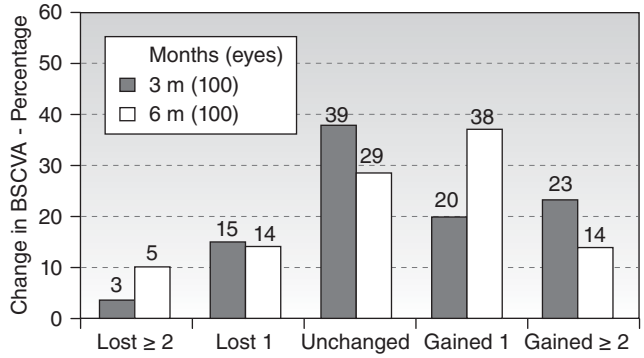

Figure 4 Safety plot of the change in BSCVA at 3 and 6 months postoperative follow-up time.

Regression slope was 1.03, very close to the ideal correction. The achieved changes in astigmatism was significantly correlated with the intended correction ($r^2 = .88$, $P < .0001$). The regression slope of 0.91 indicates slight undercorrections. There were no statistically significant differences between the 3 and 6 months follow-ups.

Changes in corneal wavefront aberration

At 6-month follow-up, corneal trefoil aberration increased by 0.03 μm ($P = .1$), corneal coma aberration increased by 0.04 μm ($P = .1$), corneal spherical aberration decreased by −0.36 μm ($P < .0001$), and corneal RMS of the HOA increased by 0.18 μm ($P < .05$) (all at 6 mm anaylsis diameter).

Discussion

In this study, results were good and promising. We can conclude that CAM Aberration-Free Hyperopic treatments

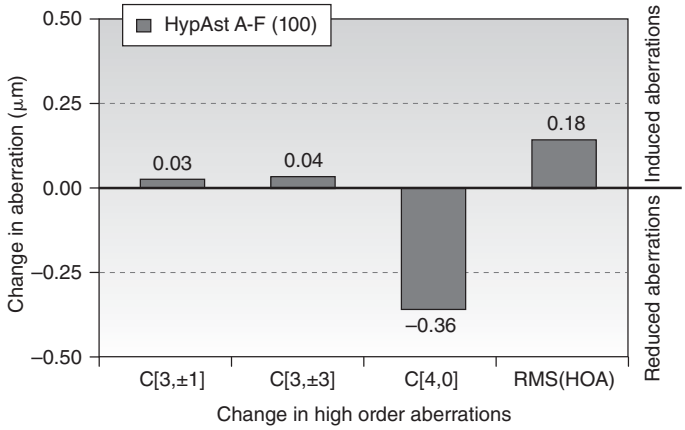

Figure 5 Plot of the change in corneal high order aberrations at 6 months postoperative follow-up time.

produce safe and predictable ablations on the cornea. From post-op VA, we have got 90% eyes in UCVA 20/25 or better and more than 50% eyes improved their pre-op BSCVA, due to the minimum aberrations induction by the ORK-CAM aspherical profile. From the refractive power change (in terms of achieved correction), we can see that both the sphere and cylinder corrections are quite accurate, predictable and stable from the first month follow-up.

Advanced H-LASIK treatments with AMARIS system yield excellent outcomes. Refractions were reduced to subclinical values. Mean spherical equivalent was -0.12 ± 0.51D and astigmatism 0.50 ± 0.51D. Seventy-four percent of eyes were within ± 0.25D of emmetropia. Fifty-two percent of eyes gained lines of BSCVA. In Aberration-Free profiles the induction of aberrations fell well below the clinical relevance (< 0.25 D). Only negative spherical aberration was significantly induced, but negative spherical aberration increases depth of focus, and thus it may help when approaching presbyopia.

In these 100 treatments no retreatments were performed in the first 6 months of follow-up, and after this timeline 5 retreatments were performed due to undercorrection or hyperopic regression. Overall, in our 30-month experience with AMARIS, of 348 simple hyperopia or compound hyperopic astigmatism treatments performed with AMARIS with more than 6 months follow up, only 15 retreatments were performed (4%). Even with today's technology, retreatments are more frequent in hyperopia. The reasons for the unexpectedly low retreatment ratio in our hyperopic series might be associated to several factors:

On the one hand we do not base our corrections on the manifest refraction or on the cycloplegic one. We use the objective refraction provided by the aberrometer analyzed for a sub-pupil of 4 mm diameter, as starting refraction, which is particularly useful for determining the magnitude and orientation of the astigmatism, and then we push the refraction under test to the the most positive spherical equivalent (unmasking latent hyperopia) consistent with the highest BSCVA scored by the patient. This does not mean, that objective refraction based on wavefront measurement is more effective compared to subjective or cicloplegic refraction, rather that it is a systematic starting refraction for the subjective refraction analysis. Further, if several refraction datasets are equal in terms of spherical equivalent, we choose the measurement with the least amount of astigmatism (reducing the risk of postoperative shifts in the axis of astigmatism).

Moreover, we centre our treatments not on the pupil or on the 1st Purkinje image, but on an objective assessment of the corneal vertex as determined by the videokeratoscopy. This offset for the treatment is actually based on the vectorial mean of 4 well acquired topographies per treated eye. The technological improvements of the AMARIS system may also help at that aim, since it incorporates a six-dimensional eye-tracking subsystem which tracks not only pupil movements, but rolling movements of the eye, as well as, torsional movements and movements along the propagation axis of the laser.

Finally, we used the objective refraction provided by the aberrometer analyzed for a sub-pupil of 4 mm diameter, as starting refraction for subjective refraction. This is particularly useful for determining the magnitude and orientation of the astigmatism. Further, we selected the measurement with the most positive spherical equivalent (unmasking latent hyperopia).

The results report an improvement of BSCVA of 2 or more lines in 14% of eyes. It is hard to understand why after the surgical correction of hyperopia, with less magnification of retinal image, compared to spectacle and without evident improvement in ocular aberration, we found an improvement in the resolving power of the eye. The minimum aberrations induction can justify no reduction of BSCVA, but not such improvement.

Although having measured HOA of the whole eye, we analyzed only the HOA of the cornea. This has several reasons: on the one hand, we used ocular aberrometry only to derive refraction, i.e. low order aberration at 4-mm diameter, so we did not have always large analysis diameters available (6-mm or more) for ocular wavefront (either pre- or postoperatively); on the other hand we were not interested on the magnitude of the aberrations, but rather on the change of aberrations.

Papers in which direct comparison of induced corneal and ocular wavefront aberrations over the same sample was studied, showed that the induction of anterior corneal aberrations was always, at least, as high as the induction of ocular wavefront aberrations for the entire eye. Marcos et al.[55] found that ocular and corneal aberrations increased statistically significant after LASIK myopia surgery, by a factor of 1.92 (ocular) and 3.72 (corneal), on average. They found a good correlation ($r = 0.97$; $P < .0001$) between the aberrations induced in the entire optical system and those induced in the anterior corneal surface. However, anterior corneal aberrations increased more than ocular aberrations, suggesting also changes in the posterior corneal surface. Lee et al.[56] found that after laser refractive surgery, anterior corneal aberration and ocular aberration increased equally and showed statistically significant correlations. They found no statistically significant differences of internal optics aberration values in coma, spherical aberration, and RMS for HOA. Arbelaez et al.[16] found that comparing corneal and ocular aberrations, the amount of induced aberrations was very similar for spherical aberration and coma. For the RMS for HOA corneal induced aberrations were moderately

higher, despite not statistically significant, than ocular induced aberrations. Arba-Mosquera and de Ortueta[57] found that induced corneal and ocular spherical aberrations were correlated in a statistically significant manner, with ocular spherical aberration being induced at a rate of half of the induced corneal spherical aberration in patients preoperative and in the same patients after LASIK for myopic astigmatism.

Hyperopic Aberration-Free Treatments with the SCHWIND AMARIS are safe and very predictable. Results were achieved without applying additional nomograms. 6-month follow-up time shows the good performance of the system. To evaluate the long-term stability further follow up is necessary. However, de Ortueta et al.[58] determined good refractive and topographic stability after H-LASIK already from the 3 month of follow-up with little to no regression occurring up to 36 months.

De Ortueta[12] found after H-LASIK with the ESIRIS system a good predictability, with 92% of the eyes (61) having a postoperative refraction within ± 0.50 D of the attempted correction. Moreover, as expected, the achieved refractive change was significantly correlated with intended refractive correction ($r^2 = 0.91$), and was very close to the ideal correction. These values are similar to the ones in this study for 1-year follow-up (95% within 0.50 D).

The conventionally accepted limits for H-LASIK (about 5D of spherical equivalent) are lower than the ones accepted for myopic LASIK (up to about 10D if the residual stromal bed is thicker than 250-300 μm). One of the causes is that the induction of aberrations per achieved diopter is higher in hyperopic treatments.[9] The centration of refractive surgery remains also controversial. The offset between the corneal vertex and pupil centre is higher in hyperopic eyes, with a nasal fixation in most of the cases. This is also a problem to take into account.[59] Hyperopic eyes are usually short in axial length, showing higher values for the angles alpha, kappa, and lambda. This also causes an offset between the corneal vertex and the pupil centre of higher magnitude than in myopic eyes, making it difficult to decide where to centre the refractive procedure.

It is possible that the 'improved' results are simply due to treatment centration, rather than to the new AMARIS technology. New ablation patterns, which minimize the induction of aberrations, will allow us to perform H-LASIK more predictably and safely and may allow us in the future to treat higher hyperopia. At this aim, the limits to the steepness of the central cornea with regards to quality of vision and tear film stability shall be carefully considered.

Reducing the induction of aberrations after H-LASIK will possibly allow us to treat higher hyperopia, however further studies are necessary to confirm this hypothesis.

Conflict of interests

Authors Arbelaez and Vidal have no proprietary interest in the materials presented herein.

Arbelaez receives travel expenses from SCHWIND eye-tech-solutions.

Arba-Mosquera is employee of SCHWIND eye-tech-solutions.

References

1. Llorente L, Barbero S, Merayo J, Marcos S. Changes in corneal and total aberrations induced by LASIK surgery for hyperopia. J Refract Surg. 2004;20:203-216.
2. Chen CC, Izadshenas A, Asghar Rana MA, Azar DT. Corneal asphericity after hyperopic laser in situ keratomileusis. J Cataract Refract Surg. 2002;28:1539-1545.
3. Jiménez JR, Anera RG, del Barco LJ, Hita E. Predicting changes in corneal asphericity after hyperopic LASIK. J Cataract Refract Surg. 2003;29:1468.
4. Mrochen M, Seiler T. Influence of corneal curvature on calculation of ablation patterns used in photorefractive laser surgery. J Refract Surg. 2001;17:584-587.
5. Jiménez JR, Anera RG, Jiménez del Barco L, Hita E. Effect on laser-ablation algorithms of reflection losses and nonnormal incidence on the anterior cornea. Applied Physics Letters. 2002;81;8:1521-1523.
6. Dorronsoro C, Cano D, Merayo-Lloves J, Marcos S. Experiments on PMMA models to predict the impact of corneal refractive surgery on corneal shape. Opt Express. 2006;14:6142-6156.
7. Arba Mosquera S, de Ortueta D. Geometrical analysis of the loss of ablation efficiency at non-normal incidence. Opt Express. 2008;16:3877-3895.
8. Dupps WJ, Roberts C. Effect of acute biomechanical changes on corneal curvature after photokeratectomy. J Cataract Refract Surg. 2002;18:S589-592.
9. Yoon G, MacRae S, Williams DR, Cox IG. Causes of spherical aberration induced by laser refractive surgery. J Cataract Refract Surg. 2005;31:127-135.
10. Wang L, Koch D. Anterior corneal optical aberrations induced by laser in situ keratomileusis for hyperopia J Cataract Refract Surg. 2003;29:1702–1708.
11. Albarrán-Diego C, Muñoz G, Montés-Micó R, Rodriguez A, Alió JL. Corneal Aberration Changes After Hyperopic LASIK: A Comparison Between the VISX Star S2 and the Asclepion-Meditec MEL 70 G Scan Excimer Lasers. J Refract Surg. 2006;22:34-42.
12. de Ortueta D, Arba-Mosquera S, Baatz H. Topographic changes after hyperopic LASIK with the SCHWIND ESIRIS laser platform. J Refract Surg. 2008;24:137-144.
13. O'Brart DP, Mellington F, Jones S, Marshall J. Laser epithelial keratomileusis for the correction of hyperopia using a 7.0-mm optical zone with the Schwind ESIRIS laser. J Refract Surg. 2007; 23:343-354.
14. de Ortueta D, Arba Mosquera S, Baatz H. Aberration-neutral ablation pattern in hyperopic LASIK with the ESIRIS laser platform. J Refract Surg. 2009;25:175-184.
15. Arba-Mosquera S, Hollerbach T. Ablation resolution in laser corneal refractive surgery: the dual fluence concept of the AMARIS Platform. Advances in Optical Technologies, vol. 2010, Article ID 538541, 13 pages, 2010. doi:10.1155/2010/538541
16. Arbelaez MC, Vidal C, Al Jabri B, Arba Mosquera S. LASIK for Myopia With Aspheric "Aberration Neutral" Ablations Using the ESIRIS Laser System. J Refract Surg. 2009;25:991-999.
17. Arba Mosquera S, de Ortueta D. Analysis of optimized profiles for 'aberration-free' refractive surgery. Ophthalmic Physiol Opt. 2009;29:535-548.
18. Munnerlyn CR, Koons SJ, Marshall J. Photorefractive keratectomy: a technique for laser refractive surgery. J Cataract Refract Surg. 1988;14:46–52.
19. Hersh PS, Fry K, Blaker JW. Spherical aberration after laser in situ keratomileusis and photorefractive keratectomy. Clinical results and theoretical models of etiology. J Cataract Refract Surg. 2003;29:2096-2104.
20. Gatinel D, Malet J, Hoang-Xuan T, Azar DT. Analysis of customized corneal ablations: theoretical limitations of increasing negative asphericity. Invest Ophthalmol Vis Sci. 2002;43:941-948.

21. Calossi A. Corneal asphericity and spherical aberration. J Refract Surg. 2007;23:505-514.
22. de Ortueta D, Arba Mosquera S. Mathematical properties of asphericity: a method to calculate with asphericities. J Refract Surg. 2008;24:119-121.
23. de Ortueta D, Arba Mosquera S, Baatz H. Comparison of Standard and Aberration neutral Profiles for Myopic LASIK With the SCHWIND ESIRIS. J Refract Surg. 2009;25:339-349.
24. Arba Mosquera S, Merayo-Lloves J, de Ortueta D. Asphericity analysis using corneal wavefront and topographic meridional fits. J Biomed Opt. 2010; 15: 028003.
25. de Ortueta D, Arba Mosquera S, Häcker C. Theoretical considerations on the hyperopic shift effect observed when treating negative cylinder in laser refractive surgery. Journal of Emmetropia 2010;1:23-28.
26. Arba Mosquera S, Shraiki M. Analysis of the PMMA and cornea temperature rise during excimer laser ablation. J Modern Opt. 2010;57:400-407.
27. Brunsmann U, Sauer U, Dressler K, Triefenbach N, Arba Mosquera S. Minimisation of the thermal load of the ablation in high-speed laser corneal refractive surgery: the 'intelligent thermal effect control' of the AMARIS platform. J Modern Opt. 2010;57:466-479.
28. Brunsmann U, Sauer U, Arba-Mosquera S, Magnago T, Triefenbach N. Evaluation of thermal load during laser corneal refractive surgery using infrared thermography. Infrared Physics & Technology. 2010;53:342–347.
29. Arbelaez MC, Vidal C, Arba Mosquera S. Excimer laser correction of moderate to high astigmatism with a non-wavefront-guided aberration-free ablation profile: Six-month results. J Cataract Refract Surg. 2009;35:1789-1798.
30. Bende T, Seiler T, Wollensak J, Corneal Thermal Gradients, Graef Arch Ophthalm. 1988;226:277-280.
31. de Ortueta D, Arba Mosquera S. Centration during hyperopic LASIK using the coaxial light reflex. J Refract Surg. 2007;23:11.
32. Arbelaez MC, Vidal C, Arba Mosquera S. Clinical outcomes of corneal vertex versus central pupil references with aberration-free strategies and LASIK. Invest Ophthalmol Vis Sci. 2008;49:5287-5294.
33. Huang D, Arif M. Spot size and quality of scanning laser correction of higher-order wavefront aberrations. J Cataract Refract Surg. 2002;28:407-416.
34. Guirao A,Williams D, MacRae S. Effect of beam size on the Expected benefit of customized laser refractive surgery. J Refract Surg. 2003;19:15-23.
35. Arba Mosquera S, Merayo-Lloves J, de Ortueta D. Clinical effects of pure cyclotorsional errors during refractive surgery. Invest Ophthalmol Vis Sci. 2008;49:4828-4836.
36. Bueeler M, Mrochen M. Simulation of Eye-tracker Latency, Spot Size, and Ablation Pulse Depth on the Correction of Higher Order Wavefront Aberrations With Scanning Spot Laser Systems. J Refract Surg. 2005;21:28-36.
37. Arba Mosquera S, de Ortueta D, Merayo-Lloves J. Tissue-Saving Zernike Terms Selection in Customized Treatments for Refractive Surgery. J Optom. 2009;2:182-196.
38. Arbelaez MC, Vidal C, Arba-Mosquera S. Bilateral Symmetry before and Six Months after Aberration-Free™ Correction with the SCHWIND AMARIS TotalTech Laser: Clinical Outcomes. J Optom. 2010;3:20-28.
39. Mattioli R, Tripoli NK. Corneal geometry reconstruction with the Keratron videokeratographer. Optom Vis Sci. 1997;74: 881-894.
40. Salmon TO. Corneal contribution to the Wavefront aberration of the eye. PhD Dissertation. 1999: 70.
41. Arbelaez MC, Vidal C, Arba Mosquera S. Clinical outcomes of corneal wavefront customized ablation strategies with SCHWIND CAM in LASIK treatments. Ophthalmic Physiol Opt. 2009;29: 487-496.
42. Snellen H. Letterproeven tot Bepaling der Gezichtsscherpte. Utrecht: Weyers; 1862.
43. Tuan KA, Somani S, Chernyak DA. Changes in wavefront aberration with pharmaceutical dilating agents. J Refract Surg. 2005;21:S530-534.
44. Yang Y, Wu F. Technical note: Comparison of the wavefront aberrations between natural and pharmacological pupil dilations. Ophthalmic Physiol Opt. 2007;27:220-223.
45. Erdem U, Muftuoglu O, Gundogan FC, Sobaci G, Bayer A. Pupil center shift relative to the coaxially sighted corneal light reflex under natural and pharmacologically dilated conditions. J Refract Surg. 2008;24:530-538.
46. Arbelaez MC, Vidal C, Arba Mosquera S. Clinical Outcomes of LASIK for Myopia Using the SCHWIND Platform With Ocular Wavefront Customized Ablation. J Refract Surg. 2009;25: 1083-1090.
47. Salmon TO, West RW, Gasser W, Kenmore T. Measurement of refractive errors in young myopes using the COAS Shack-Hartmann aberrometer. Optom Vis Sci. 2003;80:6-14.
48. Marsack JD, Thibos LN, Applegate RA. Metrics of optical quality derived from wave aberrations predict visual performance. J Vis. 2004;4:322-328.
49. Arbelaez MC, Vidal C, Arba Mosquera S. Central Ablation Depth and Postoperative Refraction in Excimer Laser Myopic Correction Measured With Ultrasound, Scheimpflug, and Optical Coherence Pachymetry. J Refract Surg. 2009;25:699-708.
50. Thibos LN, Wheeler W, Horne, D. A vector method for the analysis of astigmatic refractive errors. Vision Science and Its Applications, Washington: Optical Society of America; 1994. p. 14-17.
51. Harris WF. Representation of dioptric power in Euclidean space. Ophthal Physio Opt.1991;11:130-136.
52. Rubin A, Harris WF. Closed surfaces of constant visual acuity in symmetric dioptric power space. Optom Vis Sci. 2001;78: 744-753.
53. Zernike F. Diffraction theory of the knife-edge test and its improved form, the phase-contrast method. Monthly Notices of the Royal Astronomical Society. 1934;94:377-384.
54. Thibos LN, Applegate RA, Schwiegerling JT, Webb R, VSIA Standards Taskforce Members. Standards for Reporting the Optical Aberrations of Eyes. J Refract Surg. 2002;18:S652-660.
55. Marcos S, Barbero S, Llorente L, Merayo-Lloves J. Optical response to LASIK surgery for myopia from total and corneal aberration measurements. Invest Ophthalmol Vis Sci. 2001;42:3349-3356.
56. Lee JM, Lee DJ, Jung WJ, Park WC. Comparison between anterior corneal aberration and ocular aberration in laser refractive surgery. Korean J Ophthalmol. 2008;22:164-168.
57. Arba Mosquera S, de Ortueta D. Correlation among ocular spherical aberration, corneal spherical aberration, and corneal asphericity before and after LASIK for myopic astigmatism with the SCHWIND Amaris Platform at JRS. J Refractive Sourgery. 2010; Online Advanced Release. doi:10.3928/1081597X-20101001-01.
58. de Ortueta D, Arba Mosquera S. Topographic Stability After Hyperopic LASIK. J Refract Surg. 2010;26:547-554.
59. Boxer Wachler BS, Korn TS, Chandra NS, Michel FK. Decentration of the optical zone: Centering on the pupil versus the coaxially sighted corneal light reflex in LASIK for hyperopia. J Refract Surg. 2003;19:464-465.

Topic C **DECISION TREE ANALYSIS SYSTEM TO OPTIMISE REFRACTIVE SURGERY OUTCOMES**

(Análisis por árbol de decisión para la optimización de resultados en cirugía refractiva)

8. Arbelaez MC, Arba Mosquera S. The SCHWIND AMARIS total-tech laser as an all-rounder in refractive surgery. Middle East Afr J Ophthalmol; 2009; 16: 46-53 (Awarded "MEACO 2009 Best Paper of Session")

AUTHOR CONTRIBUTIONS

Study concept and design (S.A.M.); data collection (M.C.A., M.C., D.O., J.G., I.M.); analysis and interpretation of data (S.A.M.); drafting (S.A.M.); critical revision (T.M., M.C.A., T.E., M.C., D.O., J.G., I.M.A.); statistical expertise (S.A.M.).

Review Article

The SCHWIND AMARIS Total-Tech Laser as An All-Rounder in Refractive Surgery

Maria Clara Arbelaez, MD;[1] Samuel Arba Mosquera, MS[2,3]

Purpose: To describe and argument an overview of the main features and unique technical points of AMARIS Total-Tech Laser, coupled with patient outcomes supporting the decision to perform LASIK treatments with maximised outcomes.

Settings: Dr. M.C. Arbelaez, Muscat Eye Laser Center, Muscat, Sultanate of Oman.

Methods: The findings collected during 18-month experience using SCHWIND AMARIS Total-Tech Laser have been reviewed to provide arguments for supporting the decision to perform LASIK treatments with maximised outcomes. For updated clinical outcomes, the last 100 myopic astigmatism treatments, the last 100 hyperopic astigmatism treatments, the last 30 ocular-wavefront-guided treatments, and the last 30 corneal-wavefront-guided treatments, all with 6-month follow-up, were included. For all those, LDV femtosecond system was used to prepare the flaps, and AMARIS flying spot system was used to perform ablations. Clinical outcomes were evaluated in terms of predictability, refractive outcome, safety, wavefront aberration, and contrast sensitivity.

Results: 6-month postoperatively, mean defocus was -0.14±0.31D and astigmatism 0.25±0.37D. 70% eyes were within ±0.25D of emmetropia. 43% eyes gained lines of best spectacle-corrected visual acuity. For Aberration-Free treatments, none of the aberration metrics changed from pre- to postoperative values in a clinically relevant amount. For ocular-wavefront-guided treatments, the surgery did not change coma or spherical aberration, and reduced trefoil ($p<0.005$). For corneal-wavefront-guided treatments, the trefoil, coma, and spherical aberrations, as well as the total root-mean-square values of higher order aberration, were significantly reduced ($p<.05$) when the pre-existing aberrations were greater than the repeatability and the biological noise.

Conclusions: Although this review does not allow for evidence-based conclusions, following our strategy, LASIK results were excellent. LASIK surgery with AMARIS system yield excellent outcomes. Refractions were reduced to subclinical values with no induction of High-Order-Aberrations. Neither adverse events nor complications were observed.

Key words: LASIK, Customized Treatments, Aspheric, Aberrations, Wavefront

Aberrations are alterations of the optical surfaces of the eye that lead to deviations in the light entering the eye,[1] causing a decline in visual quality and a loss of contrast sensitivity.[2] These aberrations are essentially due to two structures, the cornea and the lens. The remaining structures can also contribute to aberrations in forms such as vitreous condensation, or even tearfilm, but to a lesser degree. Aberrations can be divided into two groups, the low order, which is best known as the spherical (myopia and hyperopia) and astigmatic defects, and a second group of high-order aberrations. Among the high-order aberrations, the spherical and comatic aberrations have the greatest importance.[3]

Aberrations change with age. A clear example of that occurs for the spherical aberration (SA). In a cornea of a young subject SA is positive, and this remains positive with age, however SA of the crystalline lens in a young subject is negative and suffers positivization with age,

The author(s) have no conflicts of interest or proprietary interest in any of the topics or products presented in this manuscript.

From [1]Muscat Eye Laser Center, Muscat, Sultanate of Oman; [2]Grupo de Investigaciün de Cirugìa Refractiva y Calidad de Visiön, Instituto de Oftalmobiologia Aplicada, University of Valladolid, Valladolid, Spain; [3]SCHWIND eye-tech-solutions, Kleinostheim, Germany.

Corresponding Author: Dr Maria Clara Arbelaez, Muscat Eye Laser Centre, PO Box 938; PC 117; Muscat, Sultanate of Oman. Telephone: +96824691414; Fax: +96824601212; E-mail: drmaria@omantel.net.om

therefore, in a young subject compensation of the SA occurs, obtaining a total SA which tends to zero, while the total SA with age tends to be positive.

As of today, it is clearly demonstrated that the treatments for the correction of the ametropias with the use of excimer laser induce corneal aberrations. Many studies have proven this.[4-10] Aberrations, whether one's own eye or induced by the treatments, are responsible for poor quality and loss of visual contrast sensitivity. It is for this reason that all manufacturers of laser devices for refractive surgery have developed commercial platforms for the non-induction of aberrations in their treatments, or even to correct the aberrations preexisting in individual eyes.

It is not yet proven that the best is the eye free of aberrations. Some hypotheses state that there are "good" aberrations and others that are to be avoided.[11-15]

For correcting aberrations we can focus on two aspects, the correction of corneal aberrations exclusively, or the correction of total eye aberrations.

Excimer laser refractive surgery has evolved from simple myopic ablations[16] to the most sophisticated topography-guided[17] and wavefront-driven,[18] either using wavefront measurements of the whole eye (obtained, e.g., by Hartman-Shack wavefront sensors) or by using corneal topography-derived wavefront analyses[19,20,] customised ablation patterns. Because the corneal ablations for refractive surgery treatments induce aberrations (one of the most significant side-effects in myopic LASIK is the induction of spherical aberration,[21] which causes halos and reduced contrast sensitivity), special ablation patterns were designed to preserve the preoperative level of high order aberrations.[22-24] Patient satisfaction in any refractive surgery, wavefront-guided or not, is primarily dependent on successful treatment of the lower order aberrations (LOA) of the eye (sphere and cylinder). Achieving accurate clinical outcomes and reducing the likelihood of a retreatment procedure are major goals of refractive surgery.

Wavefront, aspheric and conventional laser in situ keratomileusis (LASIK) for the treatment of myopia and myopic astigmatism is safe and effective.[25,26] The recent advances in excimer laser technology, such as the use of aspheric ablation profiles, incorporation of higher order aberration (HOA) treatment and eye trackers have presumably led to better refractive outcomes and reduced HOA induction postoperatively that have been recently reported.[27,28] Although most laser manufacturers incorporate the suite of products mentioned above,[25] the use of high repetition rates (500 Hz or higher) to reduce treatment times have not been widely adopted. This is likely due to technological constraints and the increased thermal effect concomitant with the use of higher repetition rates.[29,30] If left unaddressed, the thermal effect can cause tissue damage[29,30] and potentially reduce refractive outcomes.[31] The reduction of treatment times may be beneficial due to: 1. shorter treatment times that may result in less stromal dehydration; and 2. patients are less likely to lose fixation during the ablation.[32,33]

Reasonable reductions in HOAs after wavefront-guided treatments on aberrated eyes and reasonable changes in HOAs after wavefront-optimized treatments have been reported.[34,35] However, ocular wavefront-guided and conventional treatments can increase HOAs by 100% postoperatively.[27] A significant number of refractive surgery patients may not benefit from ocular wavefront guided treatment as the induction of HOAs is related to baseline levels of HOAs.[27,36] For example HOAs tend to be induced in patients with less than 0.30 μm and reduced in patients with greater than 0.30 μm of HOAs.[27,36] Physiologic optical aberrations may be required to maintain the optical quality of the eye.[37,38] Based on these studies,[27,36,37,38] it seems that customised ablation algorithms in any form (ocular wavefront guided, corneal wavefront guided, topography guided, etc.) may not be appropriate for the entire refractive surgery population (i.e. specific population groups have specific demands, and deserve specific treatment solutions. No one-size-fits-all concept can be applied).

Our definition of "Customisation" is conceptually different and can be stated as: "The planning of the most optimum ablation pattern specifically for each individual eye based on its diagnosis, and visual demands". It is often the case, that the best approach for planning an ablation is a sophisticated pattern, which can still be simply described in terms of sphere, cylinder, and orientation (axis).

PATIENTS AND METHODS

A retrospective study in which we studied 360 eyes operated using the technique of LASIK with the AMARIS laser (SCHWIND eye-tech-solutions GmbH & Co.KG, Mainparkstrasse 6-10, Kleinostheim, Germany) is presented here. 4 study groups were conformed: 100 eyes manifesting preoperative myopia with astigmatism, 100 eyes treated for hyperopia with astigmatism, 30 eyes treated by Corneal Wavefront, and 30 eyes treated by Ocular Wavefront.

In all eyes, we measured corneal topography[39] and derived corneal wavefront[19] analyses (Keratron-Scout, OPTIKON2000, Rome, Italy), ocular aberrometry and derived ocular wavefront analyses (Ocular Wavefront Analyzer, SCHWIND eye-tech-solutions GmbH & Co.KG), manifest refraction, and uncorrected and best spectacle-corrected Snellen visual acuity[40] (UCVA and BSCVA respectively).

A specific informed consent for the study was not required because of its retrospective nature and the fact that we did not perform any action on the patient other than the usual LASIK procedure.

All ablations were calculated using the ORK-CAM software module. Aspheric aberration neutral (Aberration-Free™) profiles for the baseline are not based on the

Munnerlyn proposed profiles,[16] and go beyond that by adding some aspheric characteristics to balance the induction of spherical aberration[41,42] (prolateness optimization[43,44]). The aberration neutral (Aberration-Free™) profile is aspherical-based,[45] including a multidynamic aspherical transition zone, aberration and focus shift compensation due to tissue removal, pseudo-matrix based spot positioning, enhanced compensation for the loss of efficiency,[46] and intelligent thermal effect control; all based on theoretical equations validated with ablation models and clinical evaluations.

A 6.5 mm central fully corrected ablation zone was used in all eyes with a variable transition size automatically provided by the laser related to the planned refractive correction (6.7 mm to 8.6 mm). The AMARIS excimer laser is a flying-spot laser using real ablative spot shape (volume) locally considered through a self-constructing algorithm. In addition, there are a randomized flying-spot ablation pattern and controls for the local repetition rates to minimize the thermal load of the treatment.[30] Therefore, the ablated surface in the aspheric aberration neutral (Aberration-Free™) profiles should be very smooth, so that there will be some benefits in high order aberrations. Finally, all these optimizations theoretically diminish the induced wavefront aberration after myopic LASIK. This system works at a true repetition rate of 500 Hz and produces a beam size of 0.54 mm FWHM with a superGaussian ablative spot profile.[47,48] High-speed eye-tracking (pupil and limbus tracker with cyclotorsional tracking) with a 1050-Hz acquisition rate is accomplished with a 3-ms latency time[49].

All flaps were created using a FEMTO LDV™ femtosecond laser (Ziemer Group, Port, Switzerland) with 110 μm nominal flap thickness.

Optical errors centred on the line-of-sight, representing the Wavefront Aberration, are described by Zernike polynomials[50] and coefficients in OSA standard,[51] and analysed for a standardised diameter of 6 mm for corneal wavefront.

For selecting the type of correction to be applied (Aberration-Free, Corneal Wavefront Guided or Ocular Wavefront Guided), the Decission-Tree depicted in Fig. 1 was applied.

Finally we reported, as well, the retreatment rate for each subgroup considering the total number of treatments performed since we started using the SCHWIND AMARIS.

STATISTICAL ANALYSIS

Comparative statistical analyses were conducted using Student's t-tests based on the changes in the corneal wavefront aberrations induced by refractive surgery in all subgroups of the population studied, comparing the postoperative wavefront aberrations to the preoperative baseline. We assessed whether the changes were statistically significant within the groups (Student's t-tests for paired data). The level of statistical significance was taken as $p<.05$.

RESULTS

Six-month postoperatively, mean defocus was -0.14±0.31D and astigmatism 0.25±0.37D (very similar for all subgroups).

75% eyes were within ±0.25D of emmetropia, and 100% within ±1.00D in the Myopic-Astigmatism Aberra-

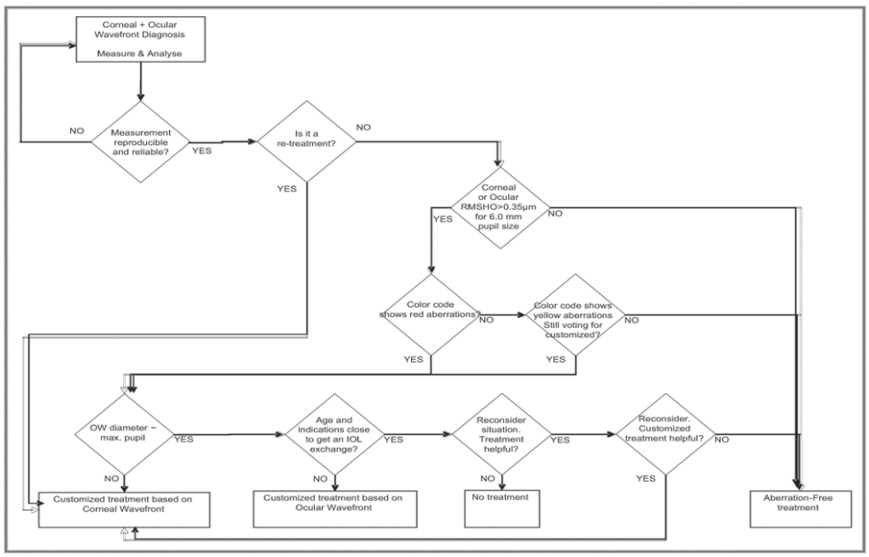

Figure 1. Decission-Tree applied for selecting the treatment mode (Aberration-Free, Corneal WavefrontGuided, or Ocular Wavefront Guided)

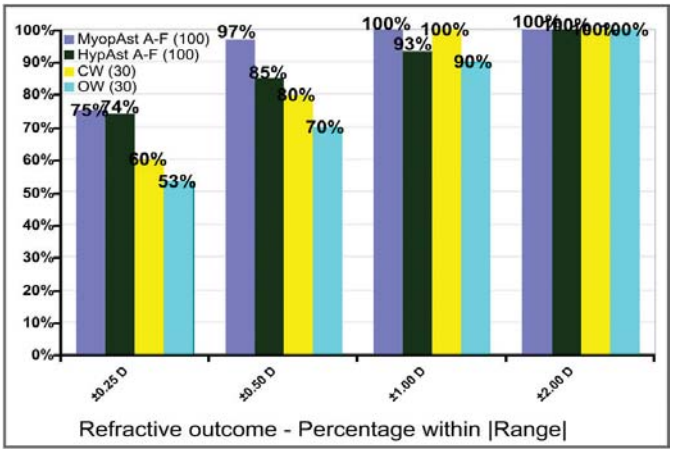

Figure 2. Refractive outcome

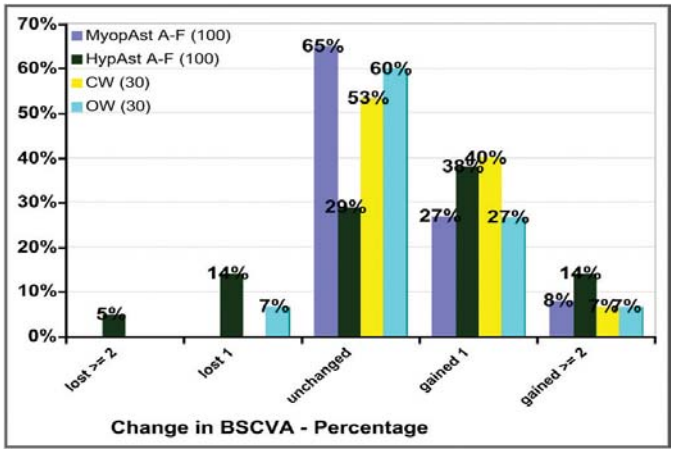

Figure 3. Safety

tion-Free subgroup; 74% eyes were within ±0.25D of emmetropia, and 93% within ±1.00D in the Hyperopic-Astigmatism Aberration-Free subgroup; 60% eyes were within ±0.25D of emmetropia, and 100% within ±1.00D in the Corneal Wavefront subgroup; and 53% eyes were within ±0.25D of emmetropia, and 90% within ±1.00D in the Ocular Wavefront subgroup (Fig. 2).

35% eyes gained 1 or more lines of best spectacle-corrected visual acuity, and no single eye lost more than 1 line of BSCVA in the Myopic-Astigmatism Aberration-Free subgroup; 52% eyes gained 1 or more lines of best spectacle-corrected visual acuity, and only 5% eyes lost more than 1 line of BSCVA in the Hyperopic-Astigmatism Aberration-Free subgroup; 47% eyes gained 1 or more lines of best spectacle-corrected visual acuity, and no single eye lost more than 1 line of BSCVA in the Corneal Wavefront subgroup; and 33% eyes gained 1 or more lines of best spectacle-corrected visual acuity, and no single eye lost more than 1 line of BSCVA in the Ocular Wavefront subgroup (Fig. 3).

For Aberration-Free treatments, none of the aberration metrics changed from pre- to postoperative values in a clinically relevant amount. For ocular-wavefront-guided treatments, the surgery did not change coma or spherical aberration, and reduced trefoil ($p<0.005$). For corneal-wavefront-guided treatments, the trefoil, coma, and spherical aberrations, as well as the total root-mean-square values of higher order aberration, were significantly reduced ($p<.05$) when the pre-existing aberrations were greater than the repeatability and the biological noise (Fig. 4).

The rate of aberration induction per dioptre of achieved defocus correction was 0.02 μm/D for the myopic baseline, and 0.05 μm/D for the hyperopic baseline.

Overall, in the 18 months we are using the SCHWIND AMARIS, we have performed 3880 LASIK treatments divided as: 3157 treatments for myopic-astigmatism using Aberration-Free profiles, 67 treatments for hyperopic-astigmatism using Aberration-Free profiles, 336 treatments using Corneal Wavefront Guided profiles, and 320 treatments using Ocular Wavefront Guided profiles. From those, we have performed 13 retreatments overall (0.3%): 10 retreatments (0.3%) after myopic-astigmatism using Aberration-Free profiles, no retreatments (0.0%) after hyperopic-astigmatism using Aberration-Free profiles, 2 retreatments (0.6%) after Corneal Wavefront Guided profiles, and 1 retreatment (0.3%) after Ocular Wavefront Guided profiles.

DISCUSSION

It was already known time ago that the treatment of ammetropias with excimer laser induced aberrations.[4-10] Since then, laser platforms have made changes in their systems to minimize the induction of these[22-24] and some have even tried to correct all the aberrations,[17,18] although there are studies showing that a certain number of aberrations, or a specific combination of them can provide better

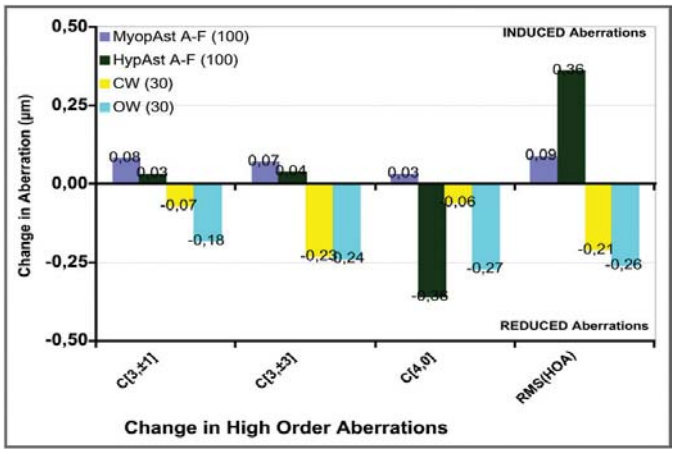

Figure 4. Comparison of induced aberrations at 6-mm analysis diameter.

vision.[11-14] There are three types of approaches. The first are those that have as their objective the elimination or reduction of the total aberrations of the eye.[18] The main critics of this approach have argued that aberrations (especially the ones of the crystalline lens) change significantly with age. In addition there are changes in the aberrations (especially the ones of the crystalline lens) during accommodation, so the goal Ñzero aberration" would be inconsistent throughout the day due to accommodation, and little lasting, since aberrations change with age.[52-54] Not to mention the changes in aberration due to the tear film. The second approach is intended to correct the corneal aberrations,[17] and we know that the corneal aberrations do not change with age.[55,56] However this concept might also be wrong considering corneal aberrations interact with internal aberrations, some of them being cancelled, and producing an aberration pattern of the total eye in general different from the aberration pattern of the cornea alone.[20] So by only removing corneal aberration we might worsen the overall aberrations, since the internal aberration in this case will not find a corneal aberration for compensation. In case that the corneal aberration is of the same sign as the internal aberration, the correction of the corneal aberration would be very useful as it would reduce the aberration of the total eye. This is why it can not be given any of the two types of treatments described previously indiscriminately to everyone. Both can be useful, but require a prior study of corneal and internal aberrations (in a non-accommodated state), to know whether and which aberrations are balanced and which ones are not, and whether a particular type of aberration is better to be removed or to leave it like it is. A third and last type of approach tries not to induce aberrations due to treatment with the excimer laser. What is intended is to leave the eye in terms of high-order aberrations as it was before the treatment. This type of treatment is not as ambitious, but much more simple to operate and can be applied to all patients in an indiscriminate way and without any prior study. The aim is by means of inducing no aberrations, to achieve an improved postoperative visual quality. The advantage of the Aberration-Free™ ablation profile is that it aims being neutral for HOA, leaving the visual print of the patient as it was preoperatively with the best spectacle correction.

Our follow-up included 100% of the cases at 6 months and, despite no nomogram adjustments were applied, the retreatment rate was below 0.3%. As a proof of stability, longer follow-up and larger number of eyes would be more convincing, even though, refractive spherical and astigmatic results are stable after 3 months.

Comparing myopic and hyperopic groups, statistical significance was observed with a less spherical aberration induction in myopia compared to hyperopia only for AMARIS in all refraction subgroups (unpaired t-tests, $p<.0005$). Similar findings were reported by Llorente et al.[57] They measured induced corneal HOA's after conventional treatments. For 6mm analysis diameter they found a rate of induced spherical aberration of 0.17 μm/D for myopia and 0.28 μm/D for hyperopia. Kohnen et al.[8] measured induced corneal HOA's after conventional treatments. For 6mm analysis diameter they found a rate of induced spherical aberration of 0.04 μm/D for myopia and 0.07 μm/D for hyperopia.

The main high order aberration effects post-op (coma and spherical aberration) are coming from decentration and "edge" effects, the strong local curvature change from Optical Zone to Transition Zone and from Transition Zone to non-treated cornea. Then it is necessary to emphasize the use of huge Optical Zones, covering the scotopic pupil size plus some tolerance for possible decentrations, and well-defined smooth Transition Zones.

Long-term follow-up on these eyes will help determine whether these accurate results also show improved stability compared to previous experiences.

The present investigation of LASIK using the SCHWIND AMARIS excimer laser with a 500 Hz repetition rate found this laser platform is safe, predictable and gives stable results. For example, 70 % of eyes were within 0.25 D of intended correction (Fig. 2). Safety was demonstrated with only 1% eyes losing more than 1 line of BSCVA 6 months after surgery (Fig. 3).

There is evidence of neural adaption to the baseline wavefront profile.[38] The interaction between higher order aberrations can be beneficial to visual quality regardless of the magnitude HOAs.[13,11] To date the induction of wavefront aberrations postoperatively is random and the wavefront profile postoperatively cannot be predicted. Based on the random nature of the HOA induction and current research,[36-38] it maybe beneficial to maintain the preoperative wavefront profile for a significant number of refractive surgery candidates.

The changes in spherical aberration can be partially explained by the biomechanical response and corneal epithelial remodeling.[58,59] The mild induction of HOAs, spherical aberration and coma may explain the maintenance of visual quality postoperatively found in the current study.

Based on the results presented here, we are however not postulating that customised ablation algorithms in any form (ocular wavefront guided, corneal wavefront guided, topography guided, etc.) are not be useful. Rather, than specific populations with specific demands deserve specific treatment solutions. Aspheric treatments aiming for preservation of the preoperative HOAs show their strengths in patients with preoperative BCVA 20/20 or better, or in patients where the visual degradation cannot be attributable to the presence of clinically relevant HOAs.

The use of a 500 Hz repetition rate did not create any postoperative complications. Thermal effects due to excimer laser ablation and associated plume debris have been previously reported.[29,30,60,61] One study reported better refractive outcomes after cooling the cornea prior to the ablation which likely reduced the thermal buildup.[31] The use a particle aspirator coupled with random place-

ment of the laser spots in this study seems to efficiently speed up the treatment without increasing the thermal load in the cornea.

The 6 month results presented in this study indicate that Aberration-Free™ treatments of myopia with and without astigmatism using the SCHWIND AMARIS is safe, gives excellent refractive and visual acuity results, and maintains preoperative contrast sensitivity.

Corneal wavefront guided treatments showed promising results in this study. Based on the findings 6 months postoperatively, it could be concluded that the

CW customized treatments AMARIS produced both safe and predictable ablation of the cornea. The CW group showed an average change in coma from 0.38 μm to 0.31 μm (-19%) (P = 0.04), in trefoil from 0.35 μm to 0.12 μm (-66%) (P = 0.0005), and in spherical aberration from +0.14 μm to +0.08 μm (-48%) (P = 0.02). The accuracy, predictability, and stability of the refractive power change, together with the minimal external impact of the AMARIS ablation profiles on the HOAs, led to very good results in terms of visual quality.

The CW customized approach shows its strength in cases where abnormal corneal surfaces are expected. Apart from the risk of minimal additional ablation of corneal tissue, systematical wavefront-customized corneal ablation can be considered as a safe and beneficial method.

In the OW group, all ablations were customised based on Hartmann-Shack measurements of the wavefront aberration of the entire eye and calculated using the ORK-CAM software module. The ORK-CAM software module is able to import, visualize, and combine diagnostic data of the eye (manifest refraction and ocular wavefront data in this case) into a customised aspherical ablation profile to optimize the corneal shape. As we used OW based profiles in this group, ablations were optimized to reduce the wavefront aberration of the entire eye (within Optical Zone, OZ) close to a zero level, compensating, as well, for the aberration induction observed with other types of profiles.

The improvement in safety was statistically significant ($P = 0.04$) with 33% of the eyes treated improving BSCVA. 7% of the eyes “have lost” 1 line of BSCVA in the OW group, however no single eye has lost more than 1 line of BSCVA. The repeatability of the BSCVA within individuals from day to day is about 1 line of BSCVA. Since only 2 eyes lost 1 line of BSCVA, we have reviewed previous follow-ups of those eyes, and observed that in one eye this loss was present at all follow-up times, whereas the other eye showed the above mentioned variability, i.e. no loss at 3-month follow-up compared to baseline.

The correction of trefoil terms was successful both in magnitude ($P = 0.002$) and correlation attempted versus achieved ($P < 0.0001$), whereas the decrease in spherical aberration was not statistically significant ($P = 0.05$), but correlation attempted versus achieved was successful ($P < 0.0001$). It should be noted that opposing the preoperative wavefront aberration in laser refractive surgery constituted only a first approximation of a perfect refractive correction, as tissue removal occurs.

Our data suggest that wavefront customized treatments can only be successful, if the pre-existing aberrations are greater than the repeatability and the biological noise. Furthermore, coupling effects between different high order aberration terms, and between HOAs and manifest refraction is still one of the major sources of residual aberrations after refractive surgery. This topic has been discussed from a theoretical perspective by Baró et al.[62] and from a clinical perspective by MacRae[63] or Buehren et al.[64] They all found mutually affecting interactions, for example, between defocus and spherical aberration, or between 3 order aberrations and low order terms, between spherical aberration and coma, or between secondary and primary astigmatisms.

Both wavefront-guided groups corroborate other findings that have been recently published. The fact that in order to appropriately treat patients with profiles such as these described the patients need to have a significant level of preoperative aberrations. Recently published independent studies by Stonecipher et al.[34] and by Venter[65] illustrated similar findings.

Our study demonstrated that aspheric ablation profiles, designed with CAM software for the AMARIS laser platform, are safe and yielded visual, optical, and refractive results comparable to those of other wavefront-guided customized techniques for correction of myopia and myopic astigmatism.[18,23,34,65] In particular, the wavefront guided approaches are highly efficient in eyes with greater than 0.35 microns RMS HOA, or where individual components of the wavefront aberration such as coma, trefoil or spherical aberration are greater than 0.25 microns RMS.

From the analysis presented here, can be concluded that the Wavefront-guided treatments are not always the Gold Standard.

Wavefront customised treatments (both Corneal or Ocular Wavefront) can only be reasonably successful when the pre-existing aberrations are huger than the repeatability, biological noise and accommodation effects. Considerations as treatment duration or tissue removal make more difficult to establish a universal optimal profile.

General optimum in non-wavefront-driven refractive surgery is to balance the effects on the Wavefront aberration, and, to provide normal eyes with the best quality of vision, without affecting their perception of the world:

Ocular Wavefront treatments have the advantage of being based on Objective Refraction of the complete human eye system; Corneal Wavefront treatments have the advantage of being independent from accommodation effects or light/pupil conditions; Aspherical treatments have the advantage of saving tissue, time and a due to their simplicity they offer a better predictability.

REFERENCES

1. Liang J, Grimm B, Goelz S, Bille JF. Objective measurement of wave aberrations of the human eye with the use of a Hartmann-Shack wave-front sensor. *J Opt Soc Am A Opt Image Sci Vis* 1994;11:1949-1957.
2. Mastropasqua L, Toto L, Zuppardi E, et al. Photorefractive keratectomy with aspheric profile of ablation versus conventional photorefractive keratectomy for myopia correction: six-month controlled clinical trial. *J Cataract Refract Surg* 2006;32:109-116.
3. Thibos LN, Hong X, Bradley A, Cheng X. Statistical variation of aberration structure and image quality in a normal population of healthy eyes. *J Opt Soc Am A Opt Image Sci Vis* 2002;19:2329-2348.
4. Oliver KM, Hemenger RP, Corbett MC, et al. Corneal optical aberrations induced by photorefractive keratectomy. *J Refract Surg* 1997;13:246-254.
5. Hong X, Thibos LN. Longitudinal evaluation of optical aberrations following laser in situ keratomileusis surgery. *J Refract Surg* 2000;16:S647-650.
6. Moreno-Barriuso E, Lloves JM, Marcos S, et al. Ocular aberrations before and after myopic corneal refractive surgery: LASIK-induced changes measured with laser ray tracing. *Invest Ophthalmol Vis Sci* 2001;42:1396-1403.
7. Porter J, MacRae S, Yoon G, et al. Separate effects of the microkeratome incision and laser ablation on the eye's wave aberration. *Am J Ophthalmol* 2003;136:327-337.
8. Kohnen T, Mahmoud K, Bühren J. Comparison of corneal higher-order aberrations induced by myopic and hyperopic LASIK. *Ophthalmology* 2005;112:1692.
9. Brint SF. Higher order aberrations after LASIK for myopia with alcon and wavelight lasers: a prospective randomized trial. *J Refract Surg* 2005;21:S799-803.
10. Benito A, Redondo M, Artal P. Laser In Situ Keratomileusis Disrupts the Aberration Compensation Mechanism of the Human Eye. *Am J Ophthalmol* 2008 [Online].
11. Applegate RA, Marsack JD, Ramos R, Sarver EJ. Interaction between aberrations to improve or reduce visual performance. *J Cataract Refract Surg* 2003;29:1487-1495.
12. Fam HB, Lim KL. Effect of higher-order wavefront aberrations on binocular summation. *J Refract Surg*. 2004;20:S570-75.
13. Applegate RA, Sarver EJ, Khemsara V. Are all aberrations equal? *J Refract Surg* 2002;18:S556-562.
14. Burns S. Is Aberration-Free Correction the Best Goal?, 4th International Wavefront Congress, San Francisco, USA; February 2003.
15. Pablo Artal et. al. What aberration pattern (if any) produces the best vision?, 6th International Wavefront Congress, Athens, Greece; February 2005.
16. Munnerlyn CR, Koons SJ, Marshall J. Photorefractive keratectomy: a technique for laser refractive surgery. *J Cataract Refract Surg*; 1988;14:46-52.
17. Alio JL, Belda JI, Osman AA, Shalaby AM. Topography-guided laser in situ keratomileusis (TOPOLINK) to correct irregular astigmatism after previous refractive surgery. *J Refract Surg* 2003;19:516-527.
18. Mrochen M, Kaemmerer M, Seiler T. Clinical results of wavefront-guided laser in situ keratomileusis 3 months after surgery. *J Cataract Refract Surg* 2001;27:201-207.
19. Salmon TO. Corneal contribution to the Wavefront aberration of the eye. *PhD Dissertation* 1999:70
20. Mrochen M, Jankov M, Bueeler M, Seiler T. Correlation Between Corneal and Total Wavefront Aberrations in Myopic Eyes. *J Refract Surg* 2003;19:104-112.
21. Moreno-Barriuso E, Lloves JM, Marcos S. Ocular Aberrations before and after myopic corneal refractive surgery: LASIK-induced changes measured with LASER ray tracing. *Invest Ophthalmol Vis Sci* 2001;42:1396-1403.
22. Mrochen M, Donetzky C,Wüllner C, Löffler J. Wavefront-optimized ablation profiles: Theoretical background. *J Cataract Refract Surg* 2004;30:775-785.
23. Koller T, Iseli HP, Hafezi F, et al. Q-factor customized ablation profile for the correction of myopic astigmatism. *J Cataract Refract Surg* 2006;32:584-589.
24. Mastropasqua L, Nubile M, Ciancaglini M, et al. Prospective randomized comparison of wavefront-guided and conventional photorefractive keratectomy for myopia with the meditec MEL 70 laser. *J Refract Surg* 2004;20:422-431.
25. Netto MV, Dupps W Jr, Wilson SE. Wavefront-guided ablation: evidence for efficacy compared to traditional ablation. Am J Ophthalmol. 2006;141:360-368.
26. Zhou C, Jin M, Wang X, Ren Q. Corneal wavefront-guided ablation with the Schwind ESIRIS laser for myopia.J Refract Surg 2007;23:573-580.
27. Binder PS, Rosenshein J. Retrospective comparison of 3 laser platforms to correct myopic spheres and spherocylinders using conventional and wavefront-guided treatments. J Cataract Refract Surg 2007;33:1158-1176.
28. Hori-Komai Y, Toda I, Asano-Kato N, et al. Comparison of LASIK using the NIDEK EC-5000 optimized aspheric transition zone (OATz) and conventional ablation profile. J Refract Surg 2006;22:546-555.
29. Ishihara M, Arai T, Sato S, et al. Temperature measurement for energy-efficient ablation by thermal radiation with a microsecond time constant from the corneal surface during ArF excimer laser ablation. Front Med Biol Eng 2001;11:167-175.
30. Bende T, Seiler T, Wollensak J. Side effects in excimer corneal surgery. Corneal thermal gradients. Graefes Arch Clin Exp Ophthalmol 1988;226:277-280.
31. Amoils SP. Using a Nidek excimer laser with a rotary epithelial brush and corneal chilling: clinical results. J Cataract Refract Surg 1999;25:1321-1326.

32. Kim WS, Jo JM. Corneal hydration affects ablation during laser in situ keratomileusis surgery. Cornea 2001;20:394-397.
33. Iseli HP, Mrochen M, Hafezi F, Seller T. Clinical photoablation with a 500-Hz scanning spot excimer laser. J Refract Surg 2004;20:831-834.
34. Stonecipher KG, Kezirian GM. Wavefront-optimized versus wavefront-guided LASIK for myopic astigmatism with the ALLEGRETTO WAVE: three-month results of a prospective FDA trial. J Refract Surg 2008; 24: S424-430.
35. Padmanabhan P, Mrochen M, Basuthkar S, et al. Wavefront-guided versus wavefront-optimized laser in situ keratomileusis: contralateral comparative study. J Cataract Refract Surg 2008;34:389-397.
36. Subbaram MV, MacRae SM. Customized LASIK treatment for myopia based on preoperative manifest refraction and higher order aberrometry: the Rochester nomogram. J Refract Surg 2007;23:435-441.
37. McLellan JS, Marcos S, Prieto PM, Burns SA. Imperfect optics may be the eye's defence against chromatic blur. *Nature* 2002;417:174-176.
38. Artal P, Chen L, Fernandez EJ, et al. Neural compensation for the eye's optical aberrations. Journal of Vision 2004;4:281-287.
39. Mattioli R, Tripoli NK. Corneal geometry reconstruction with the Keratron videokeratographer. *Optom Vis Sci* 1997;74:881-894.
40. Letterproeven tot Bepaling der Gezichtsscherpte, Snellen H. Utrecht, Weyers, 1862.
41. Yoon G, MacRae S, Williams DR, Cox IG. Causes of spherical aberration induced by laser refractive surgery. *J Cataract Refract Surg* 2005;31:127-135.
42. Hersh PS, Fry K, Blaker JW. Spherical aberration after laser in situ keratomileusis and photorefractive keratectomy. Clinical results and theoretical models of etiology. *J Cataract Refract Surg* 2003;29:2096-2104.
43. Gatinel D, Malet J, Hoang-Xuan T, Azar DT. Analysis of customized corneal ablations: theoretical limitations of increasing negative asphericity. *Invest Ophthalmol Vis Sci* 2002;43:941-948.
44. Calossi A. Corneal asphericity and spherical aberration. *J Refract Surg* 2007;23:505-514.
45. Mrochen M, Böeler M. [Aspheric optics: physical fundamentals] *Ophthalmologe* 2008;105:224-233.
46. Arba Mosquera S, de Ortueta D. Geometrical analysis of the loss of ablation efficiency at non-normal incidence. *Opt Express* 2008;16:3877-3895.
47. Huang D, Arif M. Spot size and quality of scanning laser correction of higher-order wavefront aberrations. *J Cataract Refract Surg* 2002;28:407-416.
48. Guirao A,Williams D, MacRae S.Effect of beam size on the Expected benefit of customized laser refractive surgery. *J Refract Surg* 2003;19:15-23.
49. Bueeler M, Mrochen M. Simulation of eye-tracker latency, spot size, and ablation pulse depth on the correction of higher order wavefront aberrations with scanning spot laser systems. *J Refract Surg* 2005;21:28-36.
50. Zernike F. Diffraction theory of the knife-edge test and its improved form, the phase-contrast method. *Monthly Notices of the Royal Astronomical Society* 1934;94:377-384.
51. Thibos LN, Applegate RA, Schwiegerling JT, Webb R, VSIA Standards Taskforce Members. Standards for Reporting the Optical Aberrations of Eyes. *J Refract Surg* 2002;18:S652-S660.
52. Radhakrishnan H, Charman WN. Age-related changes in ocular aberrations with accommodation. *J Vis* 2007;7:11.1-21.
53. Lüpez-Gil N, Fernández-Sánchez V, Legras R, et al. Accommodation-related changes in monochromatic aberrations of the human eye as a function of age. *Invest Ophthalmol Vis Sci* 2008;49:1736-1743.
54. Iida Y, Shimizu K, Ito M, Suzuki M. Influence of age on ocular wavefront aberration changes with accommodation. *J Refract Surg* 2008;24:696-701.
55. He JC, Gwiazda J, Thorn F, et al. Change in corneal shape and corneal wave-front aberrations with accommodation. *J Vis* 2003;3:456-463.
56. Atchison DA, Markwell EL, Kasthurirangan S, et al. Age-related changes in optical and biometric characteristics of emmetropic eyes. *J Vis* 2008;8:29.1-20.
57. Llorente L, Barbero S, Merayo J, Marcos S. Total and corneal optical aberrations induced by laser in situ keratomileusis for hyperopia. *J Refract Surg* 2004;20: 203-216.
58. Roberts C. Biomechanics of the cornea and wavefront-guided laser refractive surgery. *J Refract Surg* 2002;18:S589-592.
59. Huang D, Tang M, Shekhar R. Mathematical model of corneal surface smoothing after laser refractive surgery. *Am J Ophthalmol* 2003;135:267-278.
60. Jaycock PD, O'Brart DP, Rajan MS, Marshall J. 5-year follow-up of LASIK for hyperopia. *Ophthalmology* 2005;112:191-199.
61. Zaldivar R, Oscherow S, Bains HS. Five techniques for improving outcomes of hyperopic LASIK. J Refract Surg 2005;21:S628-632.
62. Bará S, Arines J, Ares J, Prado P. Direct transformation of Zernike eye aberration coefficients between scaled, rotated, and/or displaced pupils. J Opt Soc Am A 2006;23:2061-2066.
63. MacRae S. Aberration interaction in aberration interaction in wavefront guided custom wavefront guided custom ablation. Wavefront Congress 2007.
64 Bühren J, Yoon GY, Kenner S, et al. The effect of decentration on lower- and higher-order aberrations after myopic photorefractive keratectomy (PRK) in a cat model. Wavefront Congress 2007.
65 Venter J. Wavefront-guided custom ablation for myopia using the NIDEK NAVEX laser system. *J Refract Surg* 2008;24:487-493.

Topic D **ANALYSIS OF THE LOSS OF ABLATION EFFICIENCY AT NON-NORMAL INCIDENCE**

(Análisis de la pérdida de eficiencia de ablación para incidencia no-normal)

9. Arba Mosquera S, de Ortueta D. Geometrical analysis of the loss of ablation efficiency at non-normal incidence. Opt. Express; 2008; 16: 3877-3895

10. de Ortueta D, Arba Mosquera S, Häcker C. Theoretical considerations on the hyperopic shift effect observed when treating negative cylinder in laser refractive surgery. Journal of Emmetropia 2010; 1: 23-28

AUTHOR CONTRIBUTIONS

Study concept and design (S.A.M.); data collection (S.A.M.); analysis and interpretation of data (S.A.M.); drafting (S.A.M.); critical revision (D.O., C.H., N.T., M.S.); statistical expertise (S.A.M.).

Geometrical analysis of the loss of ablation efficiency at non-normal incidence

Samuel Arba-Mosquera, MSc[1,2,*] and Diego de Ortueta, MD[3]

1. *Grupo de Investigación de Cirugía Refractiva y Calidad de Visión, Instituto de Oftalmobiología Aplicada, University of Valladolid, Valladolid, E-47005, Spain*
2. *SCHWIND eye-tech-solutions, Kleinostheim, D-63801, Germany*
3. *Augenzentrum Recklinghausen, Recklinghausen, D-45657, Germany*

**Corresponding Author: samuel.arba.mosquera@eye-tech.net*

Abstract: A general method to analyze the loss of ablation efficiency at non-normal incidence in a geometrical way is provided. The model is comprehensive and directly considers curvature, system geometry, applied correction, and astigmatism as model parameters, and indirectly laser beam characteristics and ablative spot properties. The model replaces the direct dependency on the fluence by a direct dependence on the nominal spot volume and on considerations about the area illuminated by the beam, reducing the analysis to pure geometry of impact. Compensation of the loss of ablation efficiency at non-normal incidence can be made at relatively low cost and would directly improve the quality of results.

OCIS codes: (330.2210) Eye movements; (330.4959) Optical effects on vision; (330.7335) Visual optics; refractive surgery.

References and links

1. I. G. Pallikaris and D. S. Siganos, "Excimer laser in situ keratomileusis and photorefractive keratectomy for correction of high myopia," J. Refract. Corneal. Surg. **10**, 498-510 (1994).
2. K. Ditzen, H. Huschka, and S. Pieger, "Laser in situ keratomileusis for hyperopia," J. Cataract Refract. Surg. **24**, 42-7 (1998).
3. M. A. el Danasoury, G. O. Waring 3rd, A. el Maghraby, and K. Mehrez, "Excimer laser in situ keratomileusis to correct compound myopic astigmatism," J. Refract. Surg. **13**, 511-20 (1997).
4. E. Moreno-Barriuso, J. Merayo-Lloves, and S. Marcos, "Ocular Aberrations before and after myopic corneal refractive surgery: LASIK-induced changes measured with LASER ray tracing," Invest. Ophthalmol. Vis. Sci. **42**, 1396-1403 (2001).
5. C. Dorronsoro, D. Cano, J. Merayo-Lloves, and S. Marcos, "Experiments on PMMA models to predict the impact of corneal refractive surgery on corneal shape," Opt. Express, **14** 6142-6156 (2006).
6. A. S. Chayet, M. Montes, L. Gomez, X. Rodriguez, N. Robledo, and S. MacRae, "Bitoric laser in situ keratomileusis for the correction of simple myopic and mixed astigmatism," Ophthalmology **108**, 303-308 (2001).
7. G. Geerling and W. Sekundo, "Phototherapeutic keratectomy. Undesirable effects, complications, and preventive strategies," Ophthalmologe **103**, 576-82 (2006).
8. H. S. Ginis, V. J. Katsanevaki, and I. G. Pallikaris, "Influence of ablation parameters on refractive changes after phototherapeutic keratectomy," J. Refract. Surg. **19,** 443-448 (2003).
9. M. Mrochen and T. Seiler, "Influence of Corneal Curvature on Calculation of Ablation Patterns used in photorefractive Laser Surgery," J. Refract. Surg. **17**, 584-587 (2001).
10. J. R. Jiménez, R. G. Anera, L. Jiménez del Barco, and E. Hita, "Effect on laser-ablation algorithms of reflection losses and nonnormal incidence on the anterior cornea," Appl. Phys. Lett. **81**, 1521-1523 (2002).
11. J. R. Jiménez, R. G. Anera, L. Jiménez del Barco, E. Hita, and F. Pérez-Ocón, "Correlation factor for ablation agorithms used in corneal refractive surgery with gaussian-profile beams," Opt. Express **13**, 336-343 (2005).
12. J. R. Jiménez, F. Rodríguez-Marín, R. G. Anera, and L. Jiménez del Barco, "Deviations of Lambert-Beer's law affect corneal refractive parameters after refractive surgery," Opt. Express **14**, 5411-5417 (2006).
13. G. H. Pettit and M. N. Ediger, "Corneal-tissue absorption coefficients for 193- and 213-nm ultraviolet radiation," Appl. Opt. **35**, 3386-3391 (1996).
14. D. N. Nikogosyan and H. Goerner, "Laser-Induced Photodecomposition of Amino Acids and Peptides: Extrapolation to Corneal Collagen," IEEE J Sel. Top. Quantum Electron. **5** 1107-1115 (1999).

#91512 - $15.00 USD Received 8 Jan 2008; revised 15 Feb 2008; accepted 6 Mar 2008; published 10 Mar 2008

15. M. Hauera, D. J. Funkb, T. Lipperta, and A. Wokauna, "Time-resolved techniques as probes for the laser ablation process," Opt. Lasers Eng. **43** 545–556 (2005).
16. T. Y. Baker, "Ray tracing through non-spherical surfaces," Proceeds Of The Royal Society **55**, 361-364 (1943).
17. L. Thibos, A. Bradley, and R. Applegate, "Accuracy and precision of objective refraction from wavefront aberrations," ISSN 1534-7362 , ARVO (2003).
18. T. O. Salmon, "Corneal contribution to the Wavefront aberration of the eye," PhD Dissertation, 70 (1999).
19. M. Mrochen, M. Jankov, M. Bueeler, and T. Seiler, "Correlation Between Corneal and Total Wavefront Aberrations in Myopic Eyes," J. Refract. Surg. **19**,104-112 (2003).
20. J. L. Alio, J. I. Belda, A. A. Osman, and A. M. Shalaby, "Topography-guided laser in situ keratomileusis (TOPOLINK) to correct irregular astigmatism after previous refractive surgery," J. Refract. Surg. **19**, 516-27 (2003).
21. M. Mrochen, M. Kaemmerer, and T. Seiler, "Clinical results of wavefront-guided laser in situ keratomileusis 3 months after surgery," J. Cataract Refract. Surg **27**, 201-7 (2001).
22. M. Mrochen, C. Donetzky, C. Wüllner, and J. Löffler, "Wavefront-optimized ablation profiles: Theoretical background," J. Cataract Refract. Surg. **30**, 775-785 (2004).
23. T. Koller, H. P. Iseli, F. Hafezi, M. Mrochen, and T. Seiler, "Q-factor customized ablation profile for the correction of myopic astigmatism," J. Cataract Refract. Surg. **32**, 584-589 (2006).
24. D. Gatinel, J. Malet, T. Hoang-Xuan, and D. T. Azar, "Analysis of customized corneal ablations: theoretical limitations of increasing negative asphericity," Invest. Ophthalmol. Vis. Sci. **43**, 941–948 (2002).

1. Introduction

Since the introduction of laser refractive surgery, technology has evolved significantly. Today´s technology uses sophisticated algorithms, optimized tools in the planning, and proposes the challenge of improving surgery outcomes in terms of visual acuity and night vision. At the same time, patients have a better understanding and are better informed with regard to the potential of laser refractive surgery, raising quality requirements demanded by patients.

The available methods allow for the correction of refractive defects such as myopia [1], hyperopia [2], or astigmatism [3]. One of the unintended effects induced by laser surgery is the induction of spherical aberration [4], which causes halos and reduced contrast sensitivity. The loss of ablation efficiency at non-normal incidence can explain, in part, many of these unwanted effects, such as induction of spherical aberrations or high order astigmatism and consequently the extreme oblateness of postoperative corneas after myopic surgery [5].

Probably the earliest references related to the loss of ablation efficiency in laser refractive surgery refer to the observation of hyperopic postoperative refractions (hyperopic shifts) after negative cylinder ablation of the cornea [6]. This hyperopic postoperative refraction had not been planned and depended on various factors, such as the laser system used, the amount of negative cylinder corrected, or the presence or absence of spherical terms in the ablation profile.

For the surgeons, it was difficult to adequately compensate this effect in their nomograms in order to achieve the desired refractive correction. According to some surgeons, some manufacturers introduced the concept of coupling factor, defined as the average sphere resulting from the application of one diopter of negative cylinder. Despite its empirical nature, this coupling factor enabled surgeons to plan their treatments with a reasonable degree of success.

One clue that relates this coupling factor to the loss of efficiency is analysis of the effect in the correction of simple negative astigmatisms. As shown in Fig. 1, these cases revealed that the neutral axis became refractive, being less ablated in the periphery as compared to the center. Similar experiences [7,8] were observed using phototherapeutic keratectomy (PTK), but the results were not as conclusive, as cases where PTK is performed in large diameters are rare.

#91512 - $15.00 USD Received 8 Jan 2008; revised 15 Feb 2008; accepted 6 Mar 2008; published 10 Mar 2008

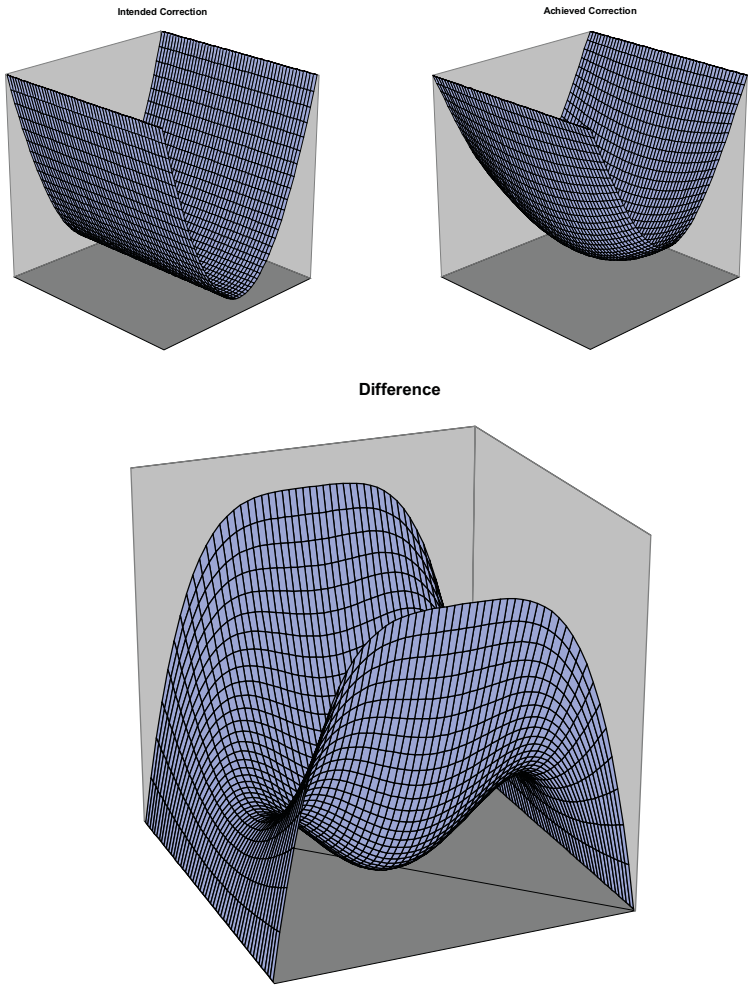

Fig. 1. Hyperopic shift and coupling factor. Ablating a simple myopic astigmatism, the neutral axis became refractive, and the ablation depth in the periphery was smaller than in the center.

1.1 The simple model [9]

The simple model of ablation efficiency due to non-normal incidence is based on several assumptions, including that the cornea can be shaped spherically, that the energy profile of the beam is flat, or that reflection losses are negligible. Also, the spot overlap is not considered. The efficiency is defined as the ratio between the depth of impact on each point and the nominal impact depth (at normal incidence),

$$Eff\left(r\right)=\frac{d\left(r\right)}{d\left(0\right)} \tag{1}$$

where Eff is the ablation efficiency at a radial distance r of the optical axis of the ablation center, and d is the depth of the impact at a radial distance r of the optical axis of the ablation.

1.2 The model by Jiménez-Anera [10,11,12]

This model provides an analytical expression for an adjustment factor to be used in photorefractive treatments that includes both compensation for reflection and for geometric

#91512 - $15.00 USD Received 8 Jan 2008; revised 15 Feb 2008; accepted 6 Mar 2008; published 10 Mar 2008

distortion. Lateron, the authors refined the model by incorporation of non-linear deviations with regard to Lambert-Beer´s law.

1.3 The model by Dorronsoro-Cano-Merayo-Marcos [5]

This model provides a new approach to the problem. Flat and spherical polymethylmetacrylate (PMMA) substrates were ablated with a commercial excimer laser system. The relationship between the profiles obtained in spherical and flat sheets of PMMA was used for estimating the ablation efficiency depending on the distance from the optical axis of the lens. The predicted changes in efficiency were reasonably well correlated with the changes in asphericity and spherical aberration observed clinically using the same laser system, so that a correction factor valid for a given algorithm and a laser in particular could be derived.

2. Materials and methods

2.1 Calculation of the depth per shot

Corneal remodeling is essentially similar to any other form of micro-machining. The lasers used in micro-machining are normally pulsed excimer lasers, where the time length of the pulses is very short compared to the time period between the pulses. Although the pulses contain little energy, given the small size of the beams, energy density can be high for this reason; and given the short pulse duration, the peak power provided can be high.

Many parameters have to be considered in designing an efficient laser ablation. One is the selection of the appropriate wavelength (193.3 ± 0.8 nm for ArF) with optimum depth of absorption in tissue, which results in a high-energy deposition in a small volume for a speedy and complete ablation. The second parameter is a short pulse duration to maximize peak power and minimize thermal conductivity to the adjacent tissue (ArF excimer based τ <20 ns).

The radiant exposure is a measure of the density of energy that governs the amount of corneal tissue removed by a single pulse. In excimer laser refractive surgery, this energy density must exceed 40-50 mJ/cm^2. The depth of a single impact relates to the fluence, and also the thermal load per pulse increases with increasing fluence. Knowing the fluence and details of the energy profile of the beam (size, profile, and symmetry), we can estimate the depth, diameter and volume of the ablation impact. Assuming a super-Gaussian beam energy profile, the following equation applies:

$$I(r) = I_0 e^{-2\left(r/R_0\right)^{2N}} \quad (2)$$

where I is the radiant exposure at a radial distance r of the axis of the laser beam, I_0 is the peak radiant exposure (at the axis of the laser beam), R_0 is the beam size when the radiant exposure falls to $1/e^2$ its peak value, and N is the super-Gaussian order of the beam profile (where N=1 represents a pure Gaussian beam profile, and N$\rightarrow\infty$ represents a flat-top beam profile).

Applying Lambert-Beer´s law (blow-off model), the footprint (diameter) of the impact is:

$$FP = 2R_0 \left(\frac{\ln\left(\frac{I_0}{I_{Th}}\right)}{2} \right)^{1/2N} \quad (3)$$

where FP is the footprint (diameter) of the ablative spot and I_{Th} is the ablation threshold for radiant exposure for the irradiated tissue or material below which no ablation occurs.

From these data (and the beam symmetry: square, hexagonal, circular), we can calculate the volume of ablation impact:

#91512 - $15.00 USD Received 8 Jan 2008; revised 15 Feb 2008; accepted 6 Mar 2008; published 10 Mar 2008

$$V_S = \int_0^{2\pi} \int_0^{\frac{FP}{2}} \frac{\ln\left(\frac{I_0}{I_{Th}}\right) - 2\left(r/R_0\right)^{2N}}{\alpha} r dr d\theta \quad (4)$$

where V_S is the volume of a single spot, and α the absorption coefficient of the irradiated tissue or material.

$$V_S = \frac{\pi}{\alpha} \frac{N}{N+1} \ln\left(\frac{I_0}{I_{Th}}\right)^{\frac{N+1}{N}} \frac{R_0^{\,2}}{2^{1/N}} \quad (5)$$

If the profile is symmetry square:

$$V_S = \frac{4}{\alpha} \frac{N}{N+1} \ln\left(\frac{I_0}{I_{Th}}\right)^{\frac{N+1}{N}} \frac{R_0^{\,2}}{2^{1/N}} \quad (6)$$

If the profile is symmetry square with rounded corners:

$$V_S = \frac{\pi+4}{\alpha} \frac{N}{N+1} \left(\frac{\ln\left(\frac{I_0}{I_{Th}}\right)}{2}\right)^{\frac{N+1}{N}} R_0^{\,2} \quad (7)$$

For human corneal tissue, the ablation threshold takes values of about 40-50 mJ/cm^2 [13,14], and the absorption coefficient is about 3.33-3.99 μm^{-1} [13,14]. We chose values of 46 mJ/cm^2 for the ablation threshold and 3.49 μm^{-1} as absorption coefficient of the human corneal tissue. For PMMA, the ablation threshold takes values of about 70-80 mJ/cm^2 [15], and the absorption coefficient is about 3.7-4.4 μm^{-1} [15]. We chose values of 76 mJ/cm^2 for the ablation threshold and 4.0 μm^{-1} as absorption coefficient for PMMA. Calculating the volume of a single spot for the cornea, and dividing it by the volume of a single impact on PMMA, we get the so-called "cornea-to-PMMA-ratio".

Another method to calculate the volume of a single impact is direct simulation. The volume of a PTK ablation corresponds to that of a truncated cone limited by the optical zone and the ablation zone (OZ and TZ) and by the depth of ablation, whereas the theoretical volume per pulse corresponds to the ablation volume divided by the number of pulses:

$$V_S = \frac{\frac{\pi}{12} \times \left[\frac{\left(TZ^3 - OZ^3\right) \times Depth}{TZ - OZ}\right]}{NumberOfShots} \quad (8)$$

The volume of a PTK ablation without transitional zone corresponds to a cylinder of the ablation depth, limited by the optical zone:

$$V_S = \frac{\pi \times OZ^2 \times Depth}{4 \times NumberOfShots} \quad (9)$$

2.2 Determination of the ablation efficiency at non-normal incidence

As shown in Fig. 2 and 3, the issue of loss of ablation efficiency is composed of reflection losses and geometrical distortions.

#91512 - $15.00 USD Received 8 Jan 2008; revised 15 Feb 2008; accepted 6 Mar 2008; published 10 Mar 2008

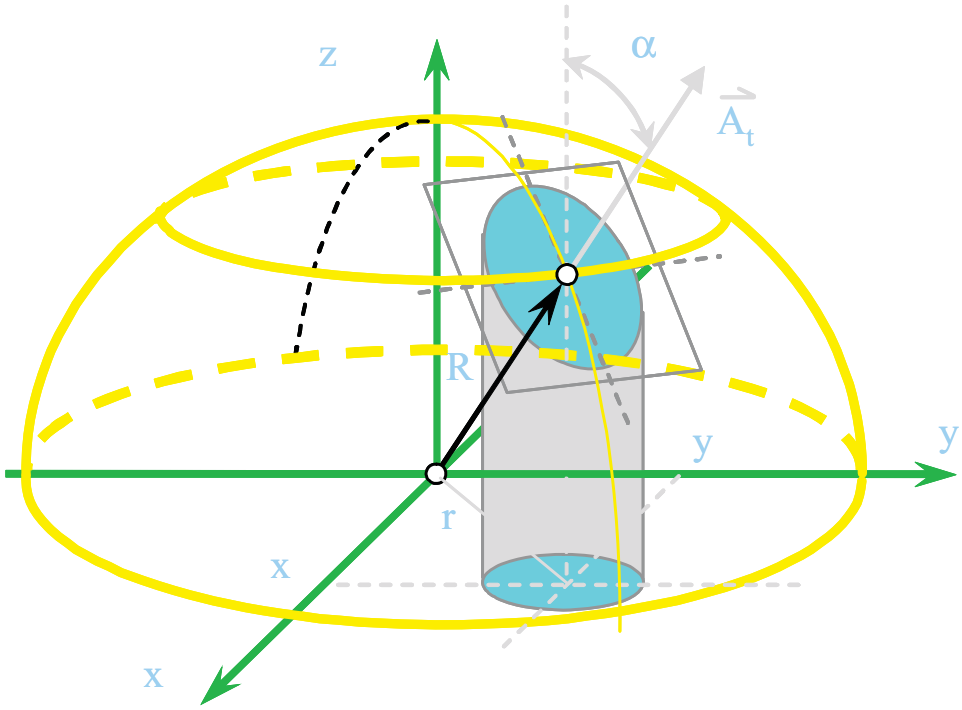

Fig. 2. Loss on reflection (Fresnel´s equations) dependent on the angle of incidence, and losses also dependent on the geometric distortion (angle of incidence).

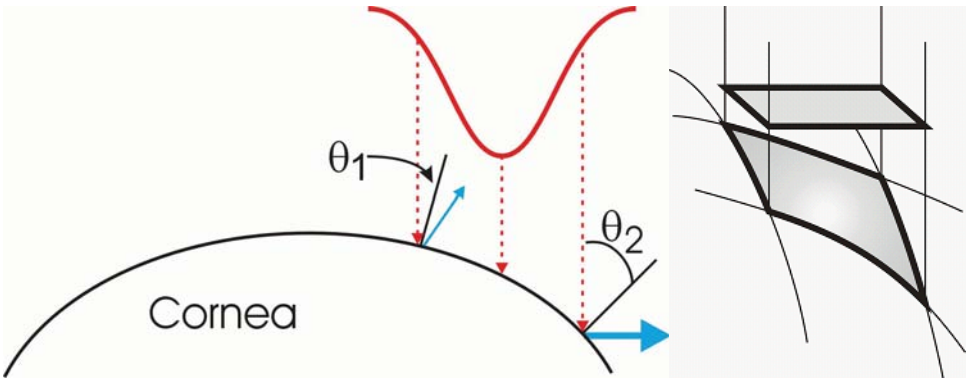

Fig. 3. Loss on reflection (Fresnel´s equations) dependent on the angle of incidence, and losses also dependent on the geometric distortion (angle of incidence).

The introduction of the concept of aberration-free profiles made it necessary to compensate for the induction of aberrations originating from deterministic and repeatable causes, thus minimizing the induction of aberrations to noise levels, so that a "new" model had to be developed. The aim in developing this model was to understand the mechanisms that govern the loss of ablation efficiency and to be able to predict their effect under different working conditions.

#91512 - $15.00 USD Received 8 Jan 2008; revised 15 Feb 2008; accepted 6 Mar 2008; published 10 Mar 2008

1 .- Considering the preoperative corneal curvature and asphericity as well as the intended refractive correction, the radius of curvature and asphericity the cornea will have after 50% of the treatment are estimated. (As the radius of corneal curvature changes during treatment, the efficiency also varies over treatment. The value at 50% of the treatment was chosen as a compromise to consider both the correction applied and the preoperative curvature).

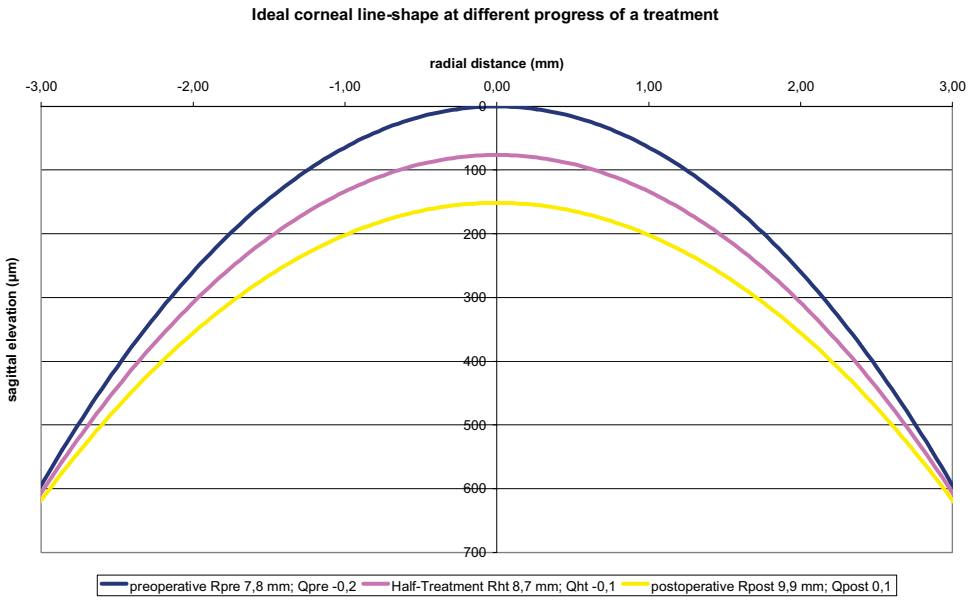

Fig. 4. The radius of corneal curvature changes during treatment, efficiency also varies over treatment, the values at 50% of the treatment represent a reasonable compromise to consider both the correction applied and the preoperative curvature.

2 .- Considering the offset of the galvoscanners´ neutral position compared to the system axis, the angle of incidence of the beam onto a flat surface perpendicular to the axis of the laser is calculated:

$$\alpha(x,y) = \arctan\left(\frac{\sqrt{(x-X_G)^2+(y-Y_G)^2}}{d_G}\right) \qquad (10)$$

where α is the angle of incidence on a "flat" surface, X_G, Y_G the position of the galvoscanners, x, y the radial positions of the incident beam, and d_G the vertical distance from the last galvoscanner to the central point of the ablation.

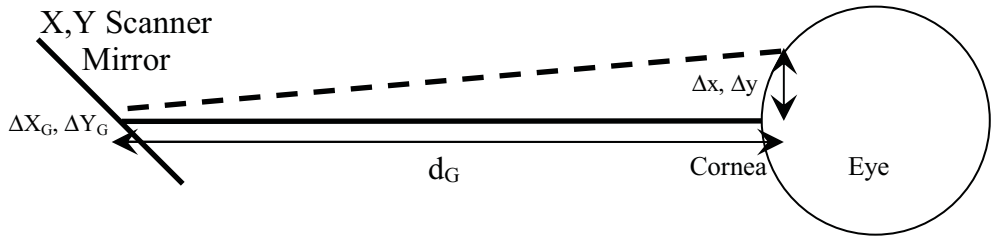

Fig. 5. The offset of the galvoscanners from the axis of the system is considered in the calculation of the angle of incidence of the beam onto a flat surface perpendicular to the axis of the laser.

#91512 - $15.00 USD Received 8 Jan 2008; revised 15 Feb 2008; accepted 6 Mar 2008; published 10 Mar 2008

3 .- Considering the calculated curvature and asphericity at 50% of the treatment, the local angle of the cornea is calculated. Assuming the cornea as an ellipsoid, which satisfies Baker's equation [13], the following equation results:

$$x^2 + y^2 + z^2\left(Q_{HT}+1\right) - 2zR_{HT} = 0 \tag{11}$$

$$\theta\left(x,y\right) = \arctan\left(\frac{\frac{\sqrt{x^2+y^2}}{R_{HT}}\left(Q_{HT}+1\right)}{Q_{HT}+\sqrt{1-\left(Q_{HT}+1\right)\times\frac{x^2+y^2}{R_{HT}{}^2}}}\right) \tag{12}$$

where θ is the angle of the local tilt of a corneal location, and R_{HT} and Q_{HT} are the predicted radius of curvature and asphericity quotient at 50% of treatment progress.

4 .- To calculate the angle of incidence for each point on the corneal surface

$$\beta = \mathrm{ang}\left(\alpha,\theta\right) \tag{13}$$

applies, where β is angle of incidence.

5 .- The ablation efficiency is calculated by consideration of geometric distortions, reflections losses, and spot overlapping:

$$\begin{aligned} I_{Eff}\left(x,y\right) &= I\left(x,y\right)\cdot \\ &\cdot\cos\left(\beta\left(x,y\right)\right)e^{2\left(\left(\frac{\left(x-x_0\right)^2+\left(y-y_0\right)^2\cos^2\left(\beta\left(x,y\right)\right)}{R_0^2}\right)^N-\left(\frac{\left(x-x_0\right)^2+\left(y-y_0\right)^2}{R_0^2}\right)^N\right)}\cdot \\ &\cdot\left(1-R\left(x,y\right)\right) \end{aligned} \tag{14}$$

where the factor $\cos\left(\beta\left(x,y\right)\right)e^{2\left(\left(\frac{\left(x-x_0\right)^2+\left(y-y_0\right)^2\cos^2\left(\beta\left(x,y\right)\right)}{R_0^2}\right)^N-\left(\frac{\left(x-x_0\right)^2+\left(y-y_0\right)^2}{R_0^2}\right)^N\right)}$ corresponds to the geometric distortions, the factor $\left(1-R\left(x,y\right)\right)$ corresponds to the reflections losses, and y is the radial direction along which angular projection occurs.

$$Eff\left(x,y\right) = \frac{\sum_{-m}^{m}\sum_{-n}^{n} d\left(x,y\right)}{\sum_{-m}^{m}\sum_{-n}^{n} d\left(0,0\right)} \tag{15}$$

The sums represent the overlap and extent along the size of the impact.

Using the efficient radiant exposure from Eq. 14 and applying Lambert-Beer´s law (blow-off model) in Eq. (15), we get:

$$Eff\left(x,y\right) = 1 + \frac{\Delta x_0 \Delta y_0 \sum_{-m}^{m}\sum_{-n}^{n} \ln\frac{\cos\left(\beta\left(x,y\right)\right)e^{2\left(\left(\frac{\left(x-x_{0,i,j}\right)^2+\left(y-y_{0,i,j}\right)^2\cos^2\left(\beta\left(x,y\right)\right)}{R_0^2}\right)^N-\left(\frac{\left(x-x_{0,i,j}\right)^2+\left(y-y_{0,i,j}\right)^2}{R_0^2}\right)^N\right)}\left(1-R\left(x,y\right)\right)}{\cos\left(\beta\left(0,0\right)\right)e^{2\left(\left(\frac{\left(-x_{0,i,j}\right)^2+\left(-y_{0,i,j}\right)^2\cos^2\left(\beta\left(0,0\right)\right)}{R_0^2}\right)^N-\left(\frac{\left(-x_{0,i,j}\right)^2+\left(-y_{0,i,j}\right)^2}{R_0^2}\right)^N\right)}\left(1-R\left(0,0\right)\right)}}{\alpha V_s} \tag{16}$$

where Δx_0 and Δy_0 are the spot overlapping distances (i.e. the distance between two adjacent pulses) and $x_{0,i,j}$ and $y_{0,i,j}$ are the respective centers of the different spots contributing to the overlap at one corneal location.

If the galvoscanners are coaxial with the laser system:

#91512 - $15.00 USD Received 8 Jan 2008; revised 15 Feb 2008; accepted 6 Mar 2008; published 10 Mar 2008

$$\beta(x,y)=\alpha(x,y)+\theta(x,y) \tag{17}$$

If the distance from the last mirror to the ablation plane is large:

$$d \gg r \tag{18}$$

$$\alpha(x,y)\to 0 \tag{19}$$

$$\beta(x,y)\simeq\theta(x,y) \tag{20}$$

$$\beta(0,0)=0 \tag{21}$$

Eq. (16) further simplifies to:

$$Eff(x,y)=1+\frac{A_S\ln\left(\cos(\beta(x,y))\frac{(1-R(x,y))(n_t+1)^2}{4n_t}\right)}{\alpha V_s}+ \\ +\frac{2\Delta x_0\Delta y_0\sum_{-m}^{m}\sum_{-n}^{n}\left(\left(\frac{(x-x_{0,i,j})^2+(y-y_{0,i,j})^2\cos^2(\beta(x,y))}{R_0^2}\right)^N-\left(\frac{(x-x_{0,i,j})^2+(y-y_{0,i,j})^2}{R_0^2}\right)^N\right)}{\alpha V_s} \tag{22}$$

If the spot overlapping is very tight and many pulses contribute to the ablation at each corneal location (i.e. $\Delta x_0,\Delta y_0 \ll FP$), Eq. 22 further simplifies to:

$$Eff(x,y)=1+\frac{A_S\ln\left(\cos(\beta(x,y))\frac{(1-R(x,y))(n_t+1)^2}{4n_t}\right)}{\alpha V_s}+ \\ +\frac{2\int_{-\frac{FP}{2}}^{+\frac{FP}{2}}\int_{-\frac{FP}{2}}^{+\frac{FP}{2}}\left(\left(\frac{(x-x_0)^2+(y-y_0)^2\cos^2(\beta(x,y))}{R_0^2}\right)^N-\left(\frac{(x-x_0)^2+(y-y_0)^2}{R_0^2}\right)^N\right)dx_0dy_0}{\alpha V_s} \tag{23}$$

In this way, we removed the direct dependency on the fluence and replaced it by a direct dependence on the nominal spot volume and on considerations about the area illuminated by the beam, reducing the analysis to pure geometry of impact.

There are two opposing effects: the beam is compressed due to reflection and at the same time expands due to its projection angle.

6.- The compensation would be the inverse of efficiency:

$$\kappa_{ij}=1/Eff_{ij} \tag{24}$$

7 .- We can develop the efficiency (or the compensation) in power series:

$$Eff=1-A\left(r/R\right)^2-B\left(r/R\right)^4+... \tag{25}$$

$$\kappa=1+C\left(r/R\right)^2+D\left(r/R\right)^4+... \tag{26}$$

Therefore, instead of using the radius at half of the treatment, we can calculate the overall effect of the variation in efficiency over treatment.

$$Eff\left(R_i,R_f,r\right)=\frac{\int_{R_i}^{R_f}\left(Eff\right)dR}{\int_{R_i}^{R_f}dR} \tag{27}$$

#91512 - $15.00 USD Received 8 Jan 2008; revised 15 Feb 2008; accepted 6 Mar 2008; published 10 Mar 2008

$$Eff\left(R_i,R_f,r\right)\approx 1-A\frac{r^2}{R_iR_f}-B\frac{r^4}{3R_i^3R_f^3}\left(R_i^2+R_iR_f+R_f^2\right) \quad (28)$$

$$\kappa\left(R_i,R_f,r\right)=\frac{\int_{R_i}^{R_f}\left(\kappa\right)dR}{\int_{R_i}^{R_f}dR} \quad (29)$$

$$\kappa\left(R_i,R_f,r\right)\approx 1+C\frac{r^2}{R_iR_f}+D\frac{r^4}{3R_i^3R_f^3}\left(R_i^2+R_iR_f+R_f^2\right) \quad (30)$$

8 .- Returning to the concept of radius and asphericity at half of the treatment, we can further simplify the model by defining an averaged spot depth as if the energy profile of the beam were flat and apply the simple model:

$$\bar{d}=\frac{\int_0^{2\pi}\int_0^{\frac{FP}{2}}\frac{\ln\left(\frac{I_0}{I_{Th}}\right)-2\left(r/R_0\right)^{2N}}{\alpha}rdrd\theta}{\int_0^{2\pi}\int_0^{\frac{FP}{2}}rdrd\theta} \quad (31)$$

$$\bar{d}=\frac{1}{\alpha}\frac{N}{N+1}\ln\left(\frac{I_0}{I_{Th}}\right) \quad (32)$$

In general:

$$\bar{d}=\frac{V_S}{A_S} \quad (33)$$

$$Eff=1+\frac{\ln\left(\frac{\cos\beta\left(1-R\right)\left(n_t+1\right)^2}{4n_t}\right)}{\alpha\bar{d}} \quad (34)$$

$$Eff=1+\frac{A_S\ln\left(\frac{\cos\beta\left(1-R\right)\left(n_t+1\right)^2}{4n_t}\right)}{\alpha V_S} \quad (35)$$

This is very similar to Eq. (22) and (23).

If this model is applied to a spherical surface (Q = 0) and the depth per layer equals the depth per pulse or the spots do not overlap, it simplifies to the simple model.

9 .- Losses due to reflection are generally negligible. This is so because the highest reflection contribution occurs for normal incidence, as well, and this component is already renormalized in Eq. (1) and (15). Therefore, we can further simplify the model as below:

$$\theta=\arcsin\left(\frac{\sqrt{X^2+Y^2}}{R_{HT}}\right) \quad (36)$$

$$Eff=1+\frac{A_S\ln\left(\cos\theta\right)}{\alpha V_S} \quad (37)$$

#91512 - $15.00 USD Received 8 Jan 2008; revised 15 Feb 2008; accepted 6 Mar 2008; published 10 Mar 2008

10 .- In the case of a strong astigmatic component, we can continue to calculate the 50% of treatment:

$$D_{Eff} = D_{\varphi} \times \cos^2(\delta - \varphi) + D_{\varphi + \pi/2} \times \sin^2(\delta - \varphi) \quad (38)$$

$$R_{Eff} = \frac{R_{\varphi} \times R_{\varphi + \pi/2}}{R_{\varphi} \times \sin^2(\delta - \varphi) + R_{\varphi + \pi/2} \times \cos^2(\delta - \varphi)} \quad (39)$$

3. Results

As the radius of corneal curvature changes during treatment, the efficiency varies over treatment, as well. This change is shown in Fig. 6 for both corneal and PMMA ablations. The graph demonstrates that the ablation efficiency decreases steadily with increasing curvature, thus resulting in improvement of ablation efficiency during myopic corrections and increasing loss of ablation efficiency during hyperopic corrections.

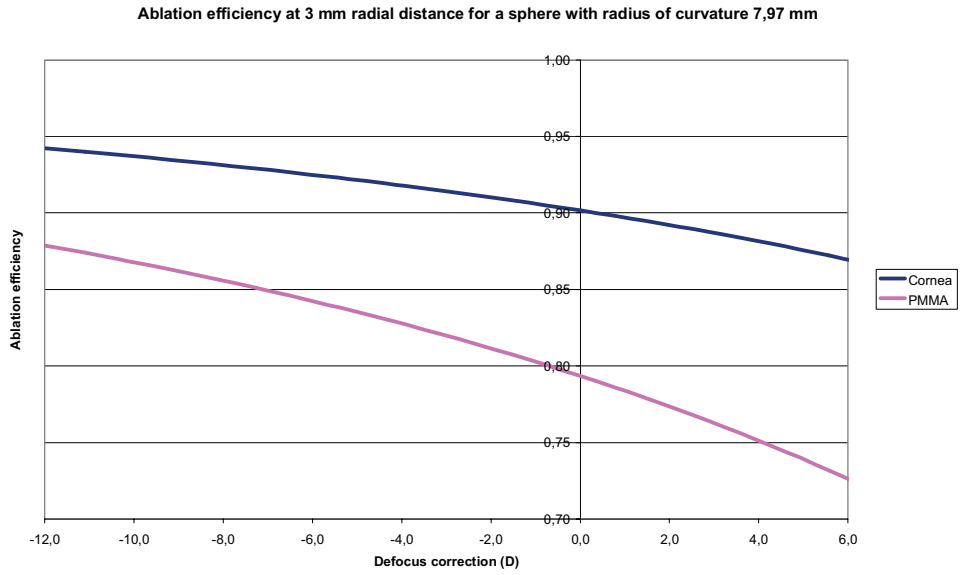

Fig. 6. Ablation efficiency at 3 mm radial distance for a sphere with 7.97 mm radius of curvature. The ablation efficiency was simulated for an excimer laser with a peak radiant exposure of 120 mJ/cm^2 and a full-width-half-maximum (FWHM) beam size of 2 mm. The radius of corneal curvature changes during treatment, accordingly also the efficiency varies over treatment. Note the improvement of ablation efficiency during myopic corrections as opposed to the increased loss of ablation efficiency during hyperopic corrections.

The model considers curvature based upon radius and asphericity, the effect of the asphericity quotient is shown in Fig. 7. As expected, a parabolic surface provides higher peripheral ablation efficiency (due to prolate peripheral flattening) compared to an oblate surface (with peripheral steepening).

#91512 - $15.00 USD Received 8 Jan 2008; revised 15 Feb 2008; accepted 6 Mar 2008; published 10 Mar 2008

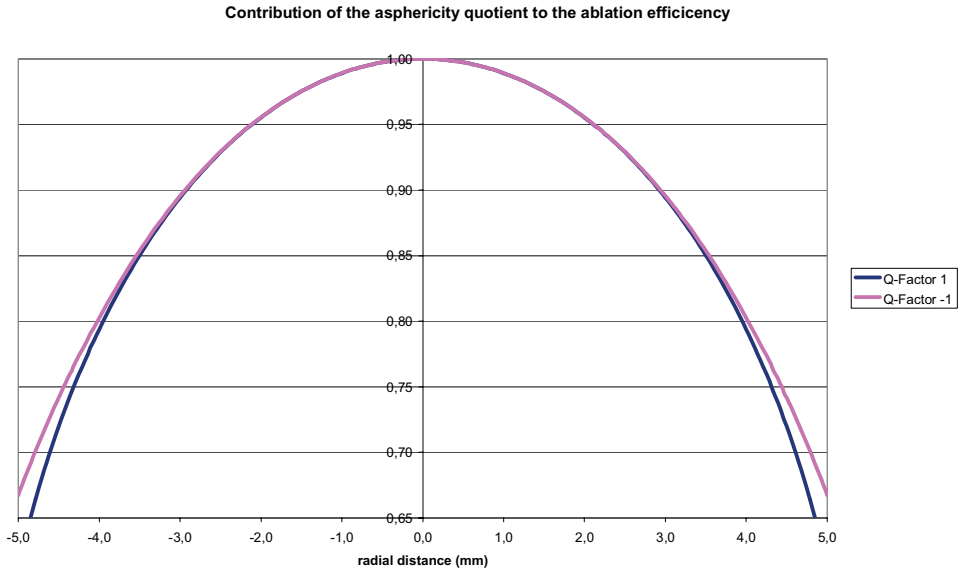

Fig. 7. Contribution of the asphericity quotient to the ablation efficiency for a radius of 7.97 mm curvature. The ablation efficiency at the cornea was simulated for an excimer laser with a peak radiant exposure of 120 mJ/cm^2 and a beam size of 2 mm (FWHM). Note the identical ablation efficiency close to the vertex as opposed to differences in ablation efficiency at the periphery. A parabolic surface provides higher peripheral ablation efficiency (due to prolate peripheral flattening) compared to an oblate surface (with peripheral steepening).

The model considers efficiency losses due to reflection losses, geometric distortions, and spot overlapping. Ablation efficiency effects due to reflection losses and geometric distortions are shown in Fig. 8. Note that the reflection losses already exist for normal incidence and decrease by a very small amounts towards the periphery. Although normal reflection losses approximately amount to 5%, they do not increase excessively for non-normal incidence. As our calculation defined ablation efficiency for a general incidence as the ratio between the spot volume for general incidence and the spot volume for normal incidence, it is evident that the so-defined efficiency equals 1 for normal incidences.

#91512 - $15.00 USD Received 8 Jan 2008; revised 15 Feb 2008; accepted 6 Mar 2008; published 10 Mar 2008

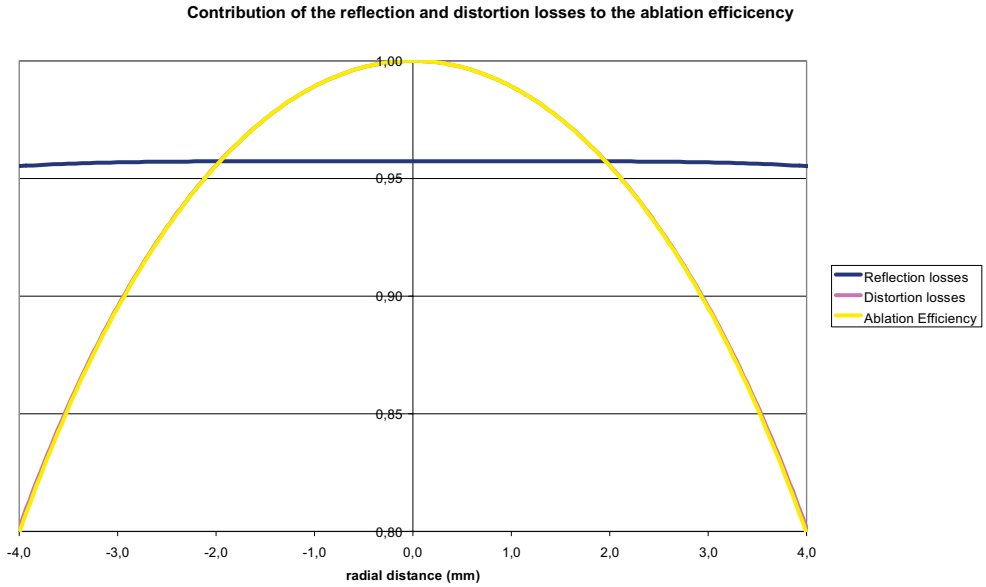

Fig. 8. Contribution of the reflection and distortion losses to ablation efficiency for a sphere with 7.97 mm radius of curvature. Note that the reflection losses already exist with normal incidence and decrease very slightly towards the periphery. Although normal reflection losses approximately amount to 5%, they do not increase excessively for non-normal incidence. As our calculation defined the ablation efficiency for a general incidence as the ratio between the spot volume for general incidence and the spot volume for normal incidence, it is evident that the so-defined efficiency equals 1 for normal incidences.

Losses due to reflection are generally negligible, since the highest reflection contribution also occurs with normal incidence and Eq. (1) and (15) already renormalize this component.

We removed the direct dependency on the fluence and replaced it by a direct dependence on the nominal spot volume and on considerations about the area illuminated by the beam, thus reducing the analysis to pure geometry of impact. However, the influence of radiant exposure can be seen in Fig. 9. Note that efficiency is very poor close to the ablation threshold and steadily increases with increasing radiant exposure approaching 100% ablation efficiency. It should also be noted that the difference between efficiencies for cornea and PMMA increases with lowering radiant exposure.

#91512 - $15.00 USD Received 8 Jan 2008; revised 15 Feb 2008; accepted 6 Mar 2008; published 10 Mar 2008

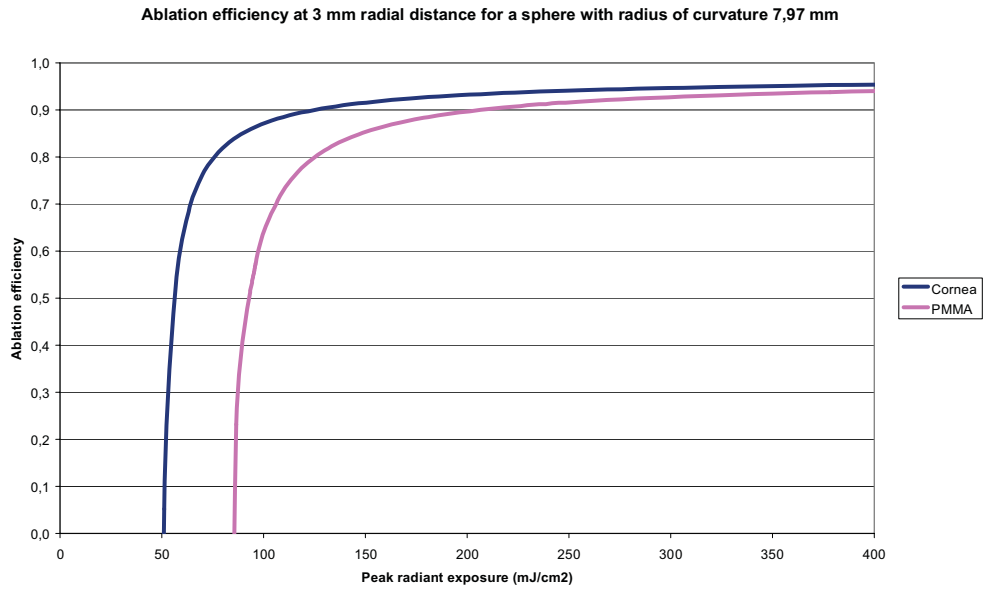

Fig. 9. Ablation efficiency at 3 mm radial distance for a sphere with 7.97 mm radius of curvature. The ablation efficiency was simulated for an excimer laser with a peak radiant exposure up to 400 mJ/cm^2 and a full-width-half-maximum (FWHM) beam size of 2 mm.

Finally, Fig. 10 to 12 compare the ablation efficiencies for cornea and PMMA obtained with the proposed model using the values reported in the study of Dorronsoro et al. In Fig. 10, the ablation efficiency for the spherical shapes prior to receiving any laser shot was evaluated, whereas Fig. 11 and 12 evaluate the average ablation efficiencies for the surfaces during a -12 D and a +6 D correction, respectively. Again, note that the ablation efficiency decreases steadily with increasing curvature, resulting in an improvement of ablation efficiency during the – 12 D correction as opposed to an increased loss of ablation efficiency during the +6 D correction.

#91512 - $15.00 USD Received 8 Jan 2008; revised 15 Feb 2008; accepted 6 Mar 2008; published 10 Mar 2008

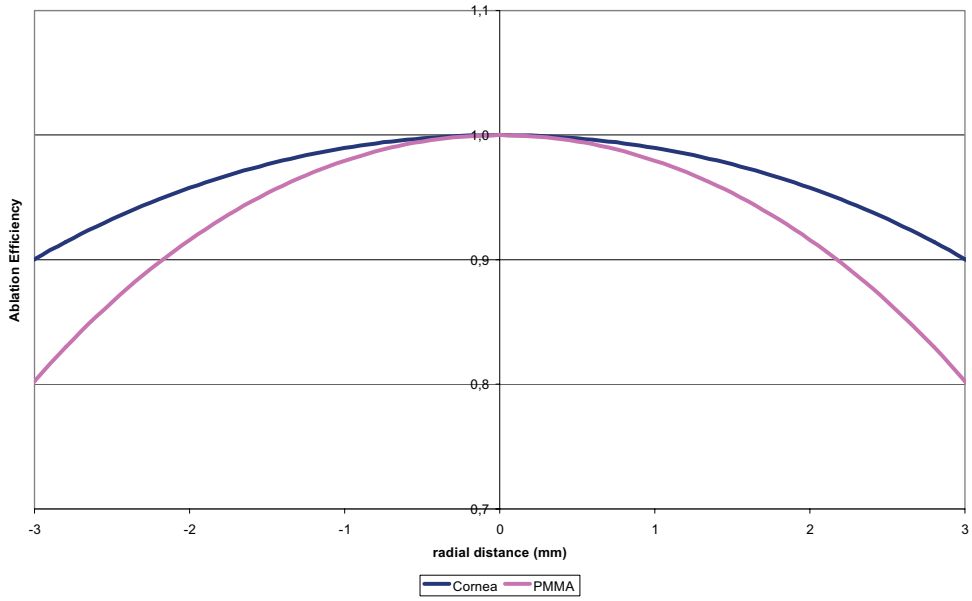

Fig. 10. Efficiency obtained with the proposed model for the conditions reported by Dorronsoro et al. Ablation efficiency for a sphere with 7.97 mm radius of curvature. The ablation efficiency was simulated for an excimer laser with a peak radiant exposure of 120 mJ/cm^2 and a full-width-half-maximum (FWHM) beam size of 2 mm.

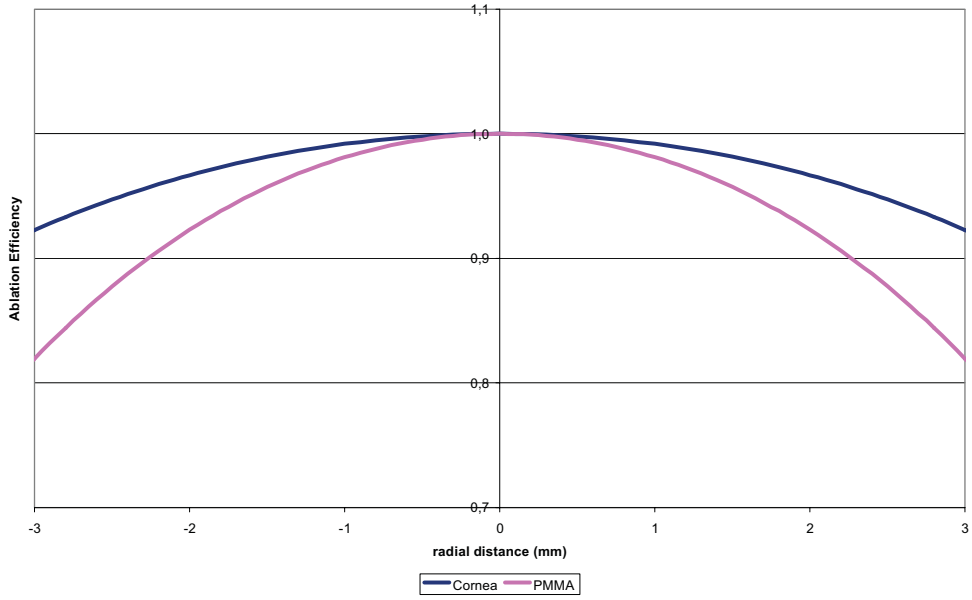

Fig. 11. Efficiency obtained with the proposed model for the conditions reported by Dorronsoro et al. Average ablation efficiency for a sphere with 7.97 mm preoperative radius of curvature and a correction of -12 D. The ablation efficiency was simulated for an excimer laser with a peak radiant exposure of 120 mJ/cm^2 and a full-width-half-maximum (FWHM) beam size of 2 mm. The radius of corneal curvature changes during treatment, consequently, also the efficiency varies over treatment. Note the improvement of ablation efficiency.

#91512 - $15.00 USD Received 8 Jan 2008; revised 15 Feb 2008; accepted 6 Mar 2008; published 10 Mar 2008

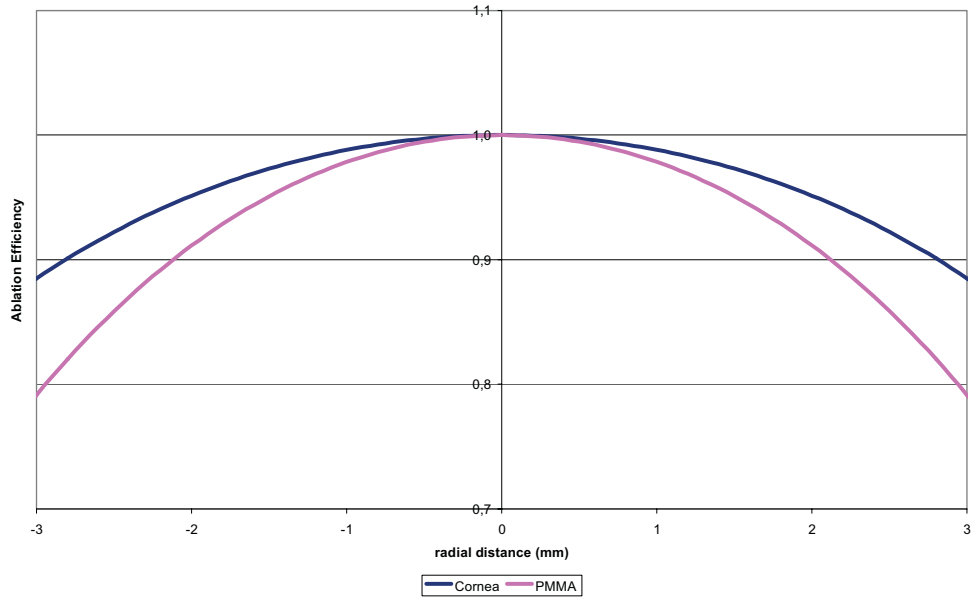

Fig. 12. Efficiency obtained with the proposed model for the conditions reported by Dorronsoro et al. Average ablation efficiency for a sphere with 7.97 mm preoperative radius of curvature and a correction of +6 D. The ablation efficiency was simulated for an excimer laser with a peak radiant exposure of 120 mJ/cm^2 and a full-width-half-maximum (FWHM) beam size of 2 mm. The radius of corneal curvature changes during treatment, consequently also the efficiency varies over treatment. Note the increased loss of ablation efficiency during hyperopic corrections.

4. Discussion

The loss of efficiency is an effect that should be offset in commercial laser systems using sophisticated algorithms that cover most of the possible variables. However, an unambiguous definition of the meaning of an optimal ablation profile for corneal refractive surgery is not available to date. To try to compensate for existing patients' aberrations, customized treatments were created. This customization can be achieved based on the wavefront aberration of the eye [17] (using Hartmann-Shack systems, for example) or by estimating the wavefront aberration of the cornea using topographic data [18,19]. Treatments guided by topography [20], guided by aberrometry [21], "wavefront-optimized" treatments [22], or treatments guided by asphericity [23] have all been proposed as solutions to the problem. However, considerations such as duration of treatment, amount of tissue removed [24], tissue remodeling, or the controversial results obtained so far difficult the selection of a unique type of profile. Parallelly to the clinical developments, increasingly capable, reliable, and safer laser systems with better resolution and accuracy are required.

This study provides an analytical expression for calculation of the ablation efficiency at non-normal incidence. The method results in a geometrical analysis of the volume per shot and of the area illuminated by the beam. The model directly considers curvature, toricity, asphericity, applied correction including astigmatism and system geometry as model parameters, and indirectly laser beam characteristics and ablative spot properties. Separate analysis of the effect of each parameter was performed.

Our approach reduces all calculations to geometrical analysis of the impact, the ablation efficiency does not primarily depend on the radiant exposure, but rather on the volume per single shot for the specific material and also on overlap and geometric considerations of the irradiated area per shot, supported by radiant exposure data. Different effects interact, the

#91512 - $15.00 USD Received 8 Jan 2008; revised 15 Feb 2008; accepted 6 Mar 2008; published 10 Mar 2008

beam is compressed due to the loss of efficiency, but at the same time expands due to the angular "projection". Using this model for ablation efficiency at non-normal incidence in refractive surgery, up to 42% of the reported increase in spherical aberrations can be explained.

Applying this comprehensive loss of efficiency model to a pure myopia profile in order to get the achieved profile etched into the cornea, we observed that the profile "shrinks", steepening the average slope and then slightly increasing the myopic power of the profile as well as inducing spherical aberrations. The net effect can be expressed as an unintended positive spherical aberration and a small overcorrection of the spherical component. Applying this model to a pure hyperopia profile, we observed that the profile "softens", flattening the average slope and then decreasing the hyperopic power of the profile as well as inducing spherical aberrations. The net effect can be expressed as an undercorrection of the spherical component and a small amount of induced negative spherical aberration. Applying this model to a PTK profile, we observed that the flat profile becomes myopic due to the loss of efficiency, resulting in an unintended myopic ablation (hyperopic shift).

Corneal curvature and applied correction play an important role in the determination of the ablation efficiency and are taken into account for accurate results. As a compromise between accuracy and simplicity, we decided to use the predicted radius of corneal curvature after 50% of the treatment as curvature metric for determination the ablation efficiency. However, corneal toricity and applied astigmatism, even though easily computed using the comprehensive model, do not have a relevant impact as long as their values correspond to those of normal corneas. Only when toricity or astigmatism exceed 3 D, their effects on ablation efficiency start to be significant.

System geometry is considered in this model using the offset of the galvoscanners´ neutral position compared to the system axis as well as the distance from the last galvoscanner to the central point of the ablation. Nevertheless, usually the galvoscanners are coaxial with (or determine the axis of) the laser system, and the distance from the last galvo-mirror to the ablation plane used to be large. Both conditions further simplify Eq. (16) to Eq. (22) explained in section 2 of this article.

We removed the direct dependency on the fluence and replaced it by a direct dependence on the nominal spot volume and on considerations about the area illuminated by the beam, reducing the analysis to pure geometry of impact in this way. The influence of the radiant exposure is shown in Fig. 9. We found that the efficiency is very poor close to the ablation threshold and steadily increases with increasing radiant exposure approaching 100% ablation efficiency. Also, differences between the efficiencies for the cornea and PMMA were observed to increase with lowering radiant exposure. Actually, the key factor is not the peak radiant exposure of the beam, but rather the average spot depth (i.e. the ratio spot volume to spot area) (Eq. (23) and (33)).

The detailed model determines ablation efficiency considering geometric distortions, reflections losses, and spot overlapping. Geometric distortions are very important, because the angular projection expands the beam, thus spreading the beam energy over a wider area and flattening its radiant exposure. At the same time, spot overlapping is a major parameter, especially in flying-spot systems, where the spot spacing is small compared to the spot width and multiple spots overlap, all contributing to the ablation at each corneal location, whereas reflection losses can be neglected, because important reflection contribution already occurs in normal incidence and does not excessively increase in non-normal incidence. Based on these facts, further simplifications are possible (Eq. (22) to Eq. (35) in section 2 of this article).

Surface asphericity before ablation, and especially after completion of 50% of the treatment, refines this comprehensive approach. Simulations, based on cornea and PMMA, for extreme asphericity values (from asphericity quotient of -1 to +1) showed minor effects with differences in ablation efficiency of 1% in the cornea and 2% in PMMA even at distances of 4 mm radially from the axis. Hence, for corneas with normal curvature and asphericity spherical geometry seems to be a reasonably simple approach for calculating the ablation efficiency at non-normal incidence (Eq. (36) and (37)).

#91512 - $15.00 USD Received 8 Jan 2008; revised 15 Feb 2008; accepted 6 Mar 2008; published 10 Mar 2008

The loss of efficiency in the ablation and non-normal incidence are responsible for much of the induction of spherical aberrations observed in the treatments as well as the excessive oblateness of postoperative corneas observed after myopic corrections [5] (also part of some overcorrections observed in high myopias and many undercorrections observed in hyperopia) with major implications for treatment and optical outcome of the procedure. Compensation can be made at relatively low cost and directly affects the quality of results (after a correction of the profiles to avoid overcorrections or undercorrections in defocus and marginally in the cylinder).

Today, several approaches to import, visualize, and analyze high detailed diagnostic data of the eye (corneal or ocular wavefront data) are offered. At the same time, several systems are available to link diagnostic systems for measurement of corneal and ocular aberrations of the eye to refractive laser platforms. These systems are state-of-the-art with flying spot technology, high repetition rates, fast active eye trackers, and narrow beam profiles. As a consequence, these systems offer new and more advanced ablation capabilities, which may potentially suffer from new sources of "coupling" (different Zernike orders affecting each other with impact on the final result). The improper use of a model that overestimates or underestimates the loss of efficiency will overestimate or underestimate its compensation and will only mask the induction of aberrations under the appearance of other sources of error.

In coming years, the research and development of algorithms will continue on several fronts in the quest for zero aberration. This includes identification of sources for induction of aberrations, development and refinement of models describing the pre-, peri- and postoperative biomechanics of the cornea, development of aberration-free profiles leaving pre-existing aberrations of the eye unchanged, redevelopment of ablation profiles to compensate for symptomatic aberrated eyes in order to achieve an overall postoperative zero level of aberration (corneal or ocular). Finally, the optimal surgical technique (LASIK (Laser assisted in-situ Keratomileusis), LASEK (Laser Epithelial Keratomileusis), PRK (Photorefractive Keratectomy), Epi-LASIK ...) to minimize the induction of aberrations to a noise level has not yet been determined.

Analyzing the different models available, the simple model of ablation efficiency at non-normal incidence bases its success on its simplicity, which forms the reason why it is still used by some trading houses. The problems arising from the simple model directly derive from its simplicity, and consequently the limitations of application as required by their implicit assumptions. The simple model does not consider the calculation nor the asphericity of the cornea, or the energy profile of the beam, or the overlap of impacts, overestimating the ablation efficiency, underestimating its compensation.

The Jiménez-Anera model provides an analytical expression for an adjustment factor to be used in photorefractive treatments, which includes both compensation for reflection and for geometric distortion, incorporating non-linear deviations with regard to Lambert-Beer´s law. It eliminates some problems of the simple model, because it considers the energy profile of the beam, overlapping, and losses by reflection. However, it does not consider the calculation nor asphericity of the cornea, it assumes that the energy profile is a Gaussian beam, assumes unpolarized light, it does not address the size or shape of the impact, it does not consider that the radius of curvature changes locally throughout the treatment, and accordingly the angle of incidence. Therefore, it often slightly overestimates the ablation efficiency, partially underestimating its compensation.

The Dorronsoro-Cano-Merayo-Marcos model provides a completely new approach to the problem. It eliminates many of the problems of both the simple model and the model by Jiménez-Anera, reducing the number of assumptions and using an empirical approach. Even so, it assumes that the reflection losses on cornea and PMMA are identical, it does not consider the local radius of corneal curvature, its asphericity or applied correction, it does not consider that the radius of curvature changes locally throughout the treatment, and accordingly the angle of incidence, and it does not consider the effects for different values of fluence.

#91512 - $15.00 USD Received 8 Jan 2008; revised 15 Feb 2008; accepted 6 Mar 2008; published 10 Mar 2008

The model described here eliminates the direct dependence on fluence and replaces it by direct considerations on the nominal spot volume and on the area illuminated by the beam, reducing the analysis to pure geometry of impact. The proposed model provides results essentially identical to those obtained with the model by Dorronsoro-Cano-Merayo-Marcos. Additionally, it offers an analytical expression including some parameters that were ignored (or at least not directly addressed) in previous analytical approaches. The good agreement of the proposed model with results reported in Dorronsoro's paper - to our knowledge the first study using an empirical approach to actually measure the ablation efficiency - may indicate that the used approach including the discussed simplifications is a reasonable description of the loss of efficiency effects. In so far, this model may complement previous analytical approaches to the efficiency problem and may sustain the observations reported by Dorronsoro et al.

Even though a large number of detailed parameters are considered, this model is still characterized by a relatively low degree of complexity. In particular, the model could be further refined by incorporating non-linear deviations according to Lambert-Beer´s law or by considering local corneal curvature directly from topographical measurements rather than modeling the best-fit surface elevation.

5. Conclusions

The loss of efficiency is an effect that should be offset in commercial laser systems using sophisticated algorithms that cover most of the possible variables. Parallelly, increasingly capable, reliable, and safer laser systems with better resolution and accuracy are required. The improper use of a model that overestimates or underestimates the loss of efficiency will overestimate or underestimate its compensation and will only mask the induction of aberrations under the appearance of other sources of error.

The model introduced in this study eliminates the direct dependence on fluence and replaces it by direct considerations on the nominal spot volume and on the area illuminated by the beam, thus reducing the analysis to pure geometry of impact and providing results essentially identical to those obtained by the model by Dorronsoro-Cano-Merayo-Marcos, however, also taking into account the influence of flying spot technology, where spot spacing is small compared to the spot width and multiple spots overlap contributing to the same target point and the correction to be applied, since the corneal curvature changes during treatment, so that also the ablation efficiency varies over the treatment.

Our model provides an analytical expression for corrections of laser efficiency losses that is in good agreement with recent experimental studies, both on PMMA and corneal tissue. The model incorporates several factors that were ignored in previous analytical models and is useful in the prediction of several clinical effects reported by other authors. Furthermore, due to its analytical approach, it is valid for different laser devices used in refractive surgery.

The development of more accurate models to improve emmetropization and the correction of ocular aberrations in an important issue. We hope that this model will be an interesting and useful contribution to refractive surgery and will take us one step closer to this goal.

Acknowledgment

We thank Dr. Jesús Merayo-Lloves for his time and expertise to criticize this work.

#91512 - $15.00 USD Received 8 Jan 2008; revised 15 Feb 2008; accepted 6 Mar 2008; published 10 Mar 2008

Theoretical considerations on the hyperopic shift effect observed when treating negative cylinder in laser refractive surgery

Diego de Ortueta, MD[1], Samuel Arba Mosquera, MSc[2], Christoph Haecker, MSc[1]

PURPOSE: To provide a theoretical background to explain the sources of «Hyperopic shift» when applying negative cylinder corrections to the cornea. The well-known effect of loss of efficiency when ablating tissue at non-normal incidence is used to get a modelling for the «Coupling Factor.»

METHODS: Microsoft™ Excel was used to calculate intended, achieved and required volumes based only on spherocylindrical refraction and loss of efficiency. The differences between each pair of ablation volumes are displayed 2D and 3D to a better understanding.

RESULTS: Theoretically, the so-called «Hyperopic shift» and «Coupling Factor» observed by applying negative cylinder correction in LASER refractive surgery can be mainly explained by the geometrical effect of the LASER applied onto an aspherical surface. Moreover, knowing some basic figures from specific LASER devices for refractive surgery the amount of this effect can be predicted.

CONCLUSIONS: The «Coupling Factor» is a nomogram-like «adjustment» introduced by surgeons to achieve the intended result. With the introduction of Wavefront guided ablation volumes and loss of efficiency compensation factors; these effects should be mainly compensated in the devices by refined algorithms instead of nomogrammed by the surgeon.

J Emmetropia 2010; 1: 23-28

INTRODUCTION

Since Laser refractive surgery was introduced[1], the technology rapidly improved. With the beginning of photoablation, the goal was to achieve predictable and stable results for myopic, hyperopic, and astigmatic corrections[2]. Today's technology is far more advanced since sophisticated diagnostic instruments such as aberrometers and topography systems offer the challenge of improving the postoperative results in terms of visual acuity and night vision[3,4]. At the same time, the better knowledge and understanding on refractive surgery by potential patients upgrades the required standard outcomes. Addressing the challenge of finding new approaches towards the close-to-zero aberrations target involves several tasks: a) finding the sources of the induced aberrations due to laser refractive surgery[5], b) developing «free-of-aberrations» ablation profiles[6], c) developing ablation profiles to compensate the natural aberrations of any single eye in order to get a close-to-zero aberrations result[7].

Although new technology was introduced, there is still the challenge of nomogram-adjusted effects such as the so-called «Hyperopic shift,» induced by applying a negative cylinder onto the cornea. This effect can be mainly explained using already published resources to generate a simple model[8-15].

The main question is to prove the validity of this model predicting the «Hyperopic shift» for a given correction for different refractive LASER systems.

Furthermore, loss of efficiency can also explain other important consequences for the clinical outcome, reported by several authors[16].

We have developed the method in two stages: first, a conceptual description of the loss of efficiency and its implications, and a second one providing samples and figures for different LASER specifications in order to get an objective comparison.

Submitted: February 24, 2010
Accepted: March 28, 2010

[1] Augenzentrum Recklinghausen, Recklinghausen Germany.
[2] SCHWIND eye-tech-solutions, Kleinostheim, Germany.

The authors have no proprietary interest in the materials presented herein.

Adress: Diego de Ortueta, MD EBOD. Augenzentrum Recklinghausen. E-mail: diego.de.ortueta@augenzentrum.org

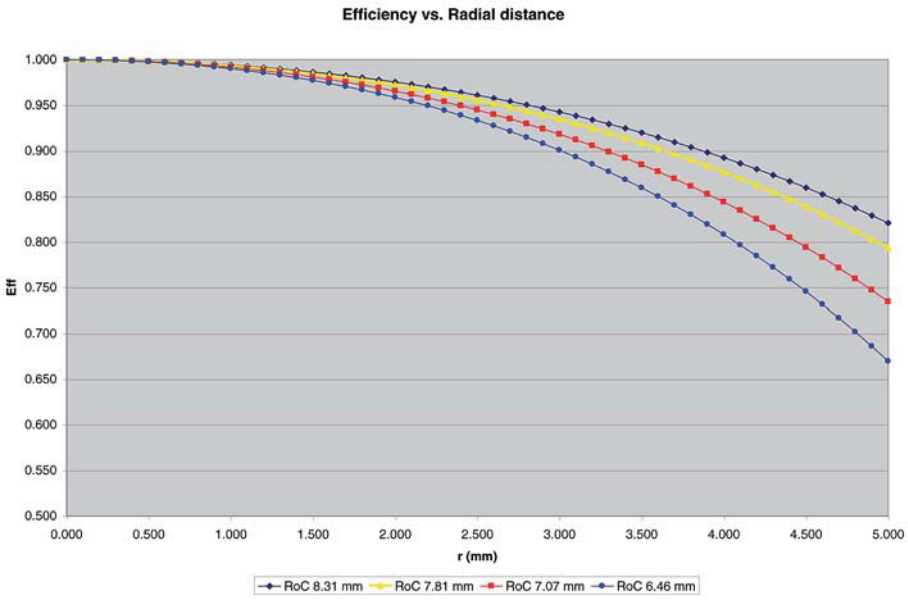

Figure 1. Efficiency plot as a function of the radial distance. Notice how the efficiency drops when the radial distance increases, also notice the steeper the paraxial radius is the faster the efficiency drops.

MATERIALS AND METHODS

Refractive surgeons have been observing post-operatively a resulting hyperopic refraction on the sphere (hyperopic shift) whenever they applied a negative cylinder onto the cornea.

This output sphere was not planned and depends on several factors:

– Variation for different refractive LASER systems.

– Dependant on the intended negative cylinder in a non-linear relation.

– Changing for sphero-cylindrical correction compared to pure cylindrical ones.

Due to all these reasons, it was an issue for the surgeons to properly include this effect in their nomograms to achieve the intended refraction.

Most of the LASER manufacturers and surgeons used the «Coupling Factor»[17] defined as the averaged output sphere per single diopter of pure negative cylinder achieved.

Despite of its empirical nature, this Coupling Factor allows the surgeon to plan the treatment with reasonable success.

The hint for one of the sources of this «coupling effect» was the analysis of a pure negative cylinder case. When a pure negative cylinder is applied, the neutral axis becomes refractive, being deeper at the centre compare to the periphery.

A simple model, which might explain this behaviour is the well-know loss of efficiency when laser ablating towards the periphery onto a curved surface[7-15] (Figure 1).

Applying this model to the negative cylinder profile in order to get the achieved profile etched in the cornea we induce two different effects in terms of main meridians (Figure 2): The neutral meridian becomes myopic, fulfilling our expectations, but also the refractive meridian is «shrinked» steepening the average slope and then increasing the myopic power of the refractive axis.

The net effect can be expressed as (Figure 3): A pure negative cylinder correction applied to the cornea, due to the loss of efficiency, with the outcome of an unintended myopia (Hyperopic shift) and a small undercorrection of the negative cylinder component.

If we intend to achieve a pure negative cylinder etched in the cornea, we should proceed as follows (Figure 4): Apply in the neutral axis certain amount of hyperopic astigmatism, enlarge the optical zone for the refractive axis reducing the amount of myopia to get the same central depth. In other words: A pure negative cylinder correction achieved in the cornea, due to the loss of efficiency, requires a hyperopia compound with negative cylinder plan (Hyperopic shift).

RESULTS

The next step is to find a mathematical expression for the effect of the loss of efficiency[13] and its compensation, and to get some values for the «Coupling Factor.»

The basic model for the loss of efficiency only considers the incidence angle, the peak fluence, and the threshold for the radiant exposure as descriptors using the blow-off model, neglecting the Fresnel reflection losses.

$$Eff = \frac{\ln\left(\frac{I_0 \cos\alpha}{I_{Th}}\right)}{\ln\left(\frac{I_0}{I_{Th}}\right)}$$

This model considers that the actual material removed at any single point only depends on the shots

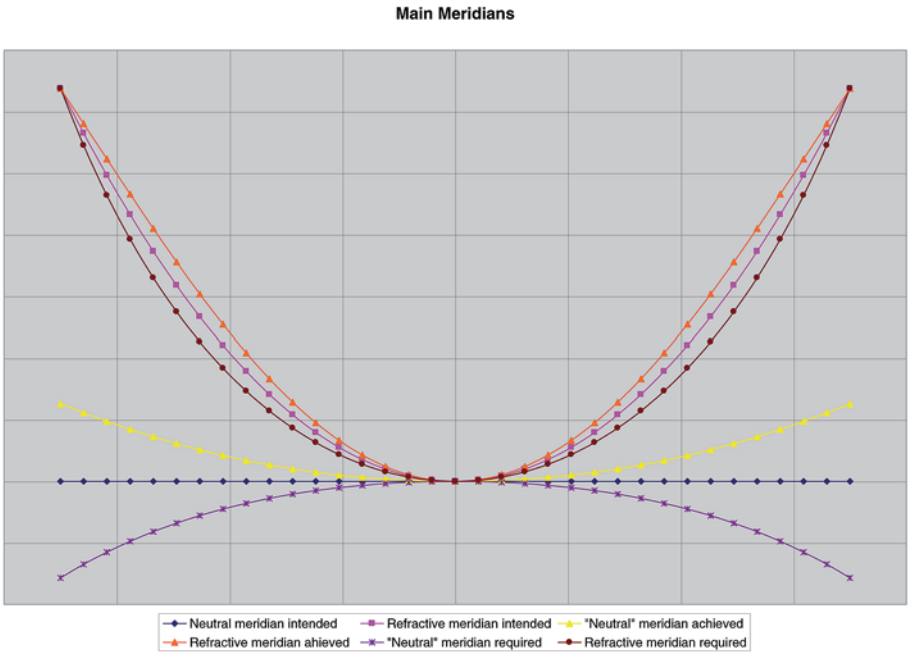

Figure 2. Cross sections of the intended, achieved, and required profiles. Notice the refractive change in the «neutral meridian» and the shrinking in the refractive meridian.

targeting this point, and we have refined the model including the influence coming from flying spot technology in which the spot spacing is small compared to the spot width and multiple spots overlap together contributing to the same target point.

$$Eff_{ij} \approx 1 + \frac{\sum_{-m}^{m}\sum_{-n}^{n}\left(\ln\left(\cos\left(\beta_{ij}\right)\right) + 2\left(\frac{y}{R_0}\right)^{2n}\left(1-\cos^{2n}\left(\beta_{ij}\right)\right)\right)\times O^2}{\alpha_{Cornea}\times V_S}$$

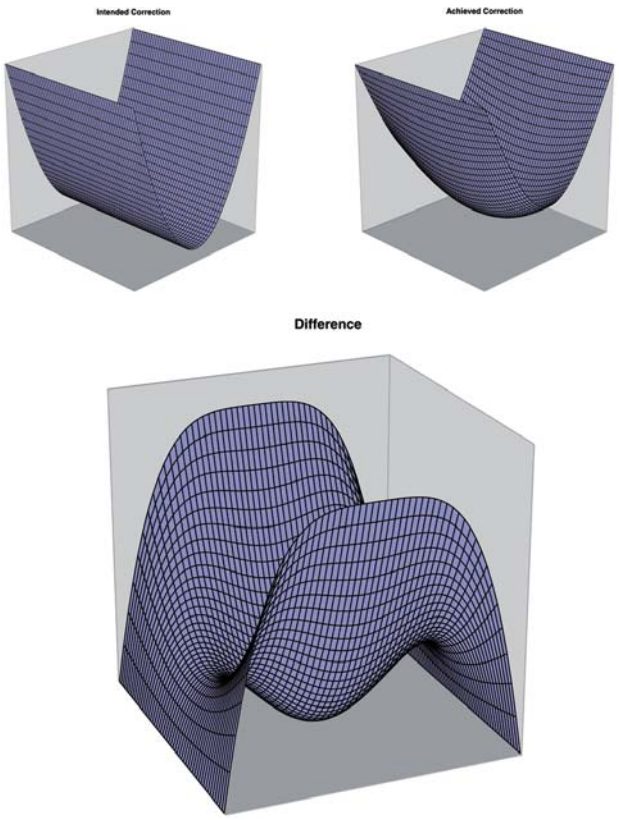

Figure 3. 3D elevation map of the intended, achieved, and differential profiles. Notice the myopia like profile in the centre of the differential map.

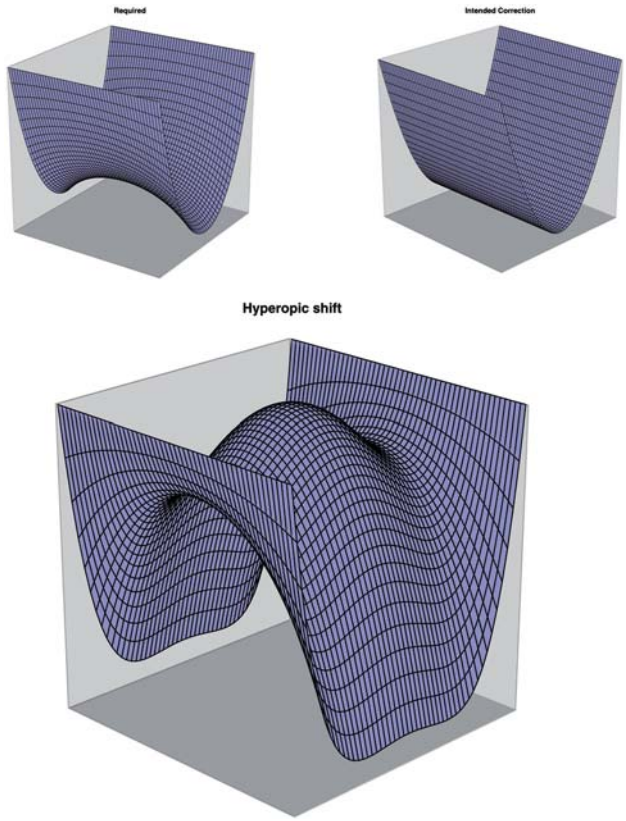

Figure 4. 3D elevation map of the required, intended, and differential profiles. Notice the hyperopia like profile in the centre of the differential map.

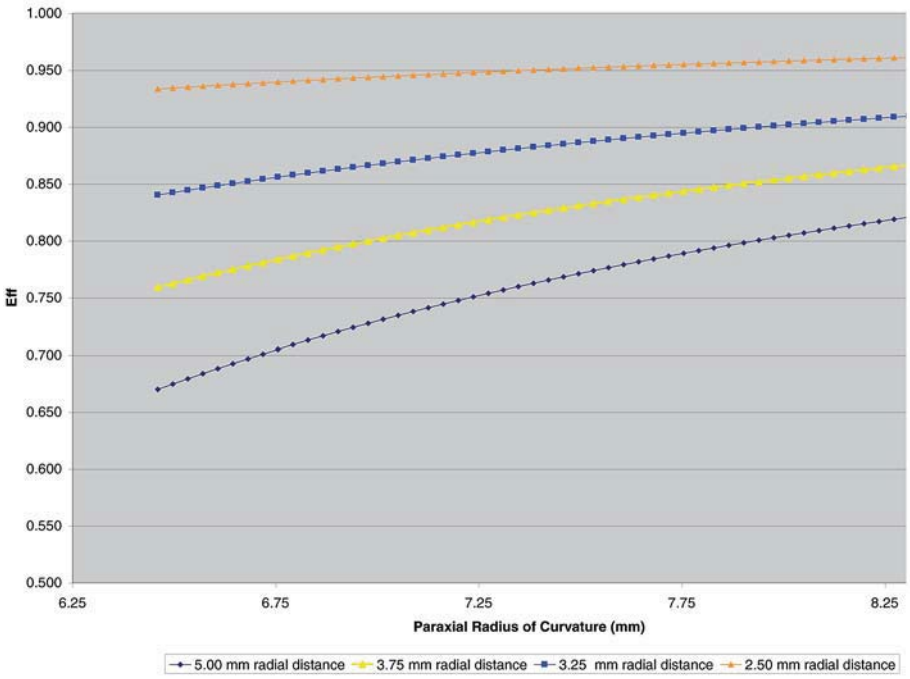

Figure 5. Efficiency plot as a function of the paraxial radius for different radial distances. Notice then that the efficiency is evolving with (myopia) or against (hyperopia) the treatment.

In addition, it is important to notice that we are modifying the corneal curvature and then the loss of efficiency effect changes across the treatment progress (Figure 5).

Considering this change is possible to get an efficiency expression in terms of radial distance and initial and final central paraxial radii of curvature.

$$Eff\left(R_i, R_f, r\right) = 1 - A\frac{r^2}{R_i R_f} - Br^4\left(\frac{R_i^2 + R_i R_f + R_f^2}{3R_i^3 R_f^3}\right)$$

Considering this model of loss of efficiency, we have applied it for different LASER peak radiant exposures (FWHM 1mm, Gaussian profile), then we have calculated the «Coupling Factor» according to the averaged output sphere per single diopter of pure negative cylinder achieved (Table 1).

We have applied this model for different intended cylinders, calculating then the «Output sphere» for a 200 mJ/cm^2 peak radiant exposure Laser system (FWHM 1mm, Gaussian profile) (Table 2).

Finally, we have also applied it for different intended sphere for the same intended negative cylinder, then we have calculated the «Output sphere» also for a 200 mJ/cm^2 peak radiant exposure Laser system (FWHM 1 mm, Gaussian profile) (Table 3).

DISCUSSION

The «Coupling Factor» is a nomogram-like «adjustment» introduced by surgeons to achieve the intended result. With the introduction of Wavefront guided ablation volumes and loss of efficiency compensation factors, these effects should be mainly compensated in the devices by refined algorithms instead of nomogrammed by the surgeon.

Table 1. Considering this comprehensive model of loss of efficiency, «Coupling Factor» for different LASER specifications, according to the averaged output sphere per single diopter of pure negative cylinder achieved

Peak Radiant Exposure (mJ/cm2)	Coupling Factor (%)
100	37
130	22
180	16
230	11
300	8
400	5

Table 2: Considering this comprehensive model of loss of efficiency, «Output Sphere» for different intended pure negative cylinders, for a 200 mJ/cm2 peak radiant exposure Laser system

Intended cylinder (D)	Output Sphere (D)
–1	–0,12
–2	–0,24
–3	–0,37
–4	–0,49
–5	–0,61
–6	–0,73

Table 3: Considering this comprehensive model of loss of efficiency, «Output Sphere» for different intended spheres for fixed negative cylinder, for a 200 mJ/cm2 peak radiant exposure Laser system.

Intended Sphere (D)	Intended Cylinder (D)	Output Sphere (D)
+3	–4	–0,46
+2	–4	–0,47
+1	–4	–0,48
0	–4	–0,50
–1	–4	–0,51
–2	–4	–0,52
–3	–4	–0,53

Nowadays there are several approaches to import, visualize, and analyse high detailed diagnostic data of the eye[18,19] (corneal or ocular wavefront data); and several systems linking diagnostics devices for measuring corneal and ocular aberrations of the eye to refractive Laser platforms[3,4,7].

These systems are nowadays state-of-the-art with their flying spot technology, high repetition rates, fast active eye-trackers, and narrow beam profile. Because of that, the systems are including new and more advanced ablation capabilities, which can potentially suffer from new sources of «coupling» (different Zernike orders affecting each other to the final result).

The ablation volumes coming from these systems should be properly adjusted throughout a comprehensive loss of efficiency model in order to get optimal results. Using a model which under- or overestimates the loss of efficiency, will lead to an under- or overestimated compensation and then will only change the figures for the «Coupling factor» but it will not remove the related nomogram adjustment.

It is important to remark that the calculi here published are only valid to calculate the «hyperopic shift» and «coupling factor» for systems without loss of efficiency compensation factors considered.

The next step will be to find the real impact and derivative effects, in terms of clinical outcome, that might be explained by this model.

Since the introduction of laser refractive surgery in the early 90's the spherocylindrical correction has been performed based on Munnerlyn's profile[20]. Although the refractive outcome was considered successful in terms of achieved change of refraction, visual acuity, and stability, the development of new diagnostic devices (wavefront sensing devices) has shown that certain amount of high order aberrations were induced by the treatment itself[21].

By briefly expanding the previous analysis of the consequences of the loss of efficiency, we can derive other important consequences for the clinical outcome, reported by several authors[22].

Applying this comprehensive loss of efficiency model to a pure myopia profile in order to get the achieved profile etched in the cornea: the profile is «shrinked» steepening the average slope and then slightly increasing the myopic power of the profile.

The net effect can be expressed as (Figure 6): A pure myopic correction applied to the cornea, due to the loss of efficiency, results in an unintended positive spherical-like aberration and a small overcorrection of the spherical component.

Applying this model to a pure hyperopia profile in order to get the achieved profile etched in the cornea: the profile is «softened» flattening the average slope and then decreasing the hyperopic power of the profile.

The net effect can be expressed as: A pure myopic correction applied to the cornea, due to the loss of effi-

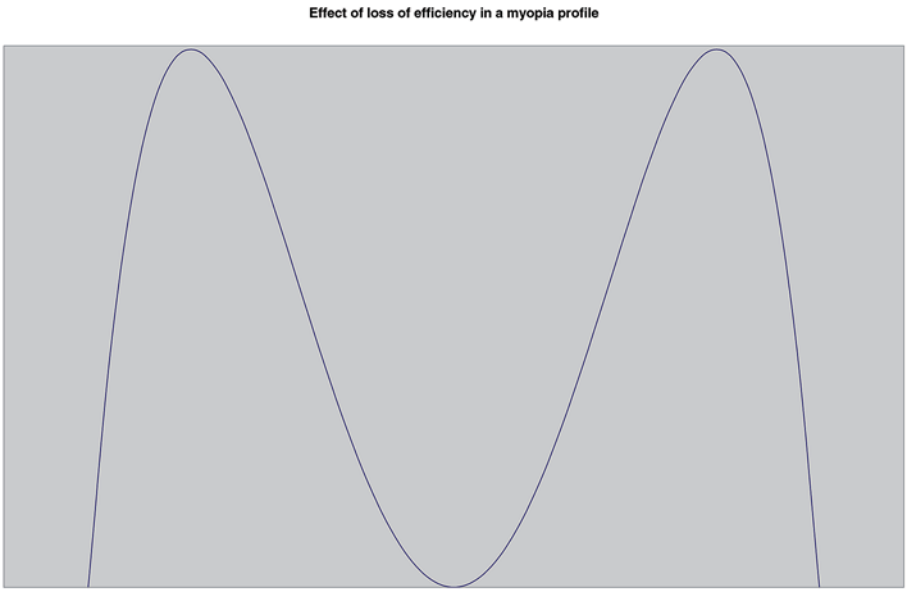

Figure 6. Effect of the loss of efficiency in a myopia profile. Notice that no transition zones were considered in the simulation. The loss of efficiency results in a spherical-like aberration (maybe combination of Z[4,0] and Z[6,0] Zernike polynomials).

ciency, results in an undercorrection of the spherical component.

Applying this model to a PTK profile in order to get the achieved profile etched in the cornea: The flat profile becomes myopic due to the loss of efficiency, resulting in an unintended myopic ablation (Hyperopic shift).

For the next years, the research should progress toward the close-to-zero aberrations target focusing on several areas:

– Finding the sources of the induced aberrations due to laser refractive surgery.

– Developing «free-of-aberrations» ablation profiles (aspherical profiles).

– Developing ablation profiles to compensate the natural aberrations of any single eye in order to get a close-to-zero aberrations result.

– Finding the best clinical approach in terms of applied technique: LASIK (Laser assisted in situ Keratomileusis), LASEK (Laser Epithelial Keratomileusis), PRK (Photorefractive Keratectomy), or Epi-LASIK.

In addition, there are still several other open questions such as remaining challenges[23], dealing with ocular changes, healing process, technical limitations, and surgeon related variables.

REFERENCES

1. Trokel SL, Srinivasan R, Braren B. Excimer laser surgery of the cornea. Am J Ophthalmol. 1983; 96: 710-715.
2. Munnerlyn CR, Koons SJ, Marshall J. Photorefractive keratectomy: a technique for laser refractive surgery. J Cataract Refract Surg; 1988; 14: 46-52.
3. Arbelaez MC, Vidal C, Arba Mosquera S. Clinical Outcomes of LASIK for Myopia Using the SCHWIND Platform With Ocular Wavefront Customized Ablation. J Refract Surg; 2009; in press.
4. Arbelaez MC, Vidal C, Arba Mosquera S. Clinical outcomes of corneal wavefront customized ablation strategies with SCHWIND CAM in LASIK treatments. Ophthalmic Physiol Opt;. 2009; 29: 487-496.
5. Kohnen T, Mahmoud K, Bühren J. Comparison of corneal higher-order aberrations induced by myopic and hyperopic LASIK. Ophthalmology. 2005; 112: 1692.
6. Arba Mosquera S, de Ortueta D. Analysis of optimized profiles for «aberration-free» refractive surgery. Ophthalmic Physiol Opt;. 2009; 29: 535-548.
7. Mrochen M, Kaemmerer M, Seiler T. Clinical results of wavefront-guided laser in situ keratomileusis 3 months after surgery. J Cataract Refract Surg 2001; 27: 201-207.
8. Mrochen M, Seiler T. Influence of Corneal Curvature on Calculation of Ablation Patterns used in photorefractive Laser Surgery. J Refract Surg; 2001; 17: 584-587.
9. Jiménez JR, Anera RG, Jiménez del Barco L, Hita E. Effect on laser-ablation algorithms of reflection losses and nonnormal incidence on the anterior cornea. Applied Physics Letters; 2002; 81; 8: 1521-1523.
10. Jiménez JR, Anera RG, Jiménez del Barco L, Hita E, Pérez-Ocón F. Correlation factor for ablation agorithms used in corneal refractive surgery with gaussian-profile beams. Optics Express; 2005; 13; 1: 336-343.
11. Dorronsoro C, Cano D, Merayo-Lloves J, Marcos S. Experiments on PMMA models to predict the impact of corneal refractive surgery on corneal shape. Opt Express. 2006; 14: 6142-56.
12. Dorronsoro C, Marcos S. Experiments on PMMA model to predict the impact of corneal refractive surgery on corneal shape: Reply. Opt Express. 2007; 15: 7245-6.
13. Arba Mosquera S, de Ortueta D. Geometrical analysis of the loss of ablation efficiency at non-normal incidence. Opt. Express; 2008; 16: 3877-3895.
14. Kwon Y, Choi M, Bott S. Impact of ablation efficiency reduction on post-surgery corneal asphericity: simulation of the laser refractive surgery with a flying spot laser beam. Opt. Express; 2008; 16:, 11808-11821.
15. Kwon Y, Bott S. Postsurgery corneal asphericity and spherical aberration due to ablation efficiency reduction and corneal remodelling in refractive surgeries. Eye; 2009; 23: 1845-1850.
16. Marcos S, Cano D, Barbero S. Increase in corneal asphericity after standard laser in situ keratomileusis for myopia is not inherent to the Munnerlyn algorithm. J Refract Surg; 2003; 19: S592-6.
17. Chayet AS, Montes M, Gómez L, Rodríguez X, Robledo N, MacRae S. Bitoric laser in situ keratomileusis for correcction of simple myopic and mixed astigmatism. Ophthalmol. 2001; 108: 303-8.
18. Moreno-Barriuso E, Lloves JM, Marcos S. Ocular Aberrations before and after myopic corneal refractive surgery: LASIK-induced changes measured with LASER ray tracing. Invest Ophthalmol Vis Sci 2001; 42: 1396-1403.
19. Mrochen M, Jankov M, Bueeler M, Seiler T. Correlation between corneal and total wavefront aberrations in myopic eyes. J Refract Surg 2003; 19: 104-112.
20. Munnerlyn CR, Koons SJ, Marshall J. Photorefractive keratectomy: a technique for laser refractive surgery. J Cataract Refract Surg; 1988; 14: 46-52.
21. Marcos S, Barbero S, Llorente L, Merayo-Lloves J. Optical response to LASIK surgery for myopia from total and corneal aberration measurements. Invest Ophthalmol Vis Sci; 2001 42: 3349-3356.
22. Anera RG, Jiménez JR, Jiménez del Barco L, Bermúdez J, Hita E. Changes in corneal asphericity after laser in situ keratomileusis. J Cataract Refract Surg. 2003; 29: 762-8.
23. Lipshitz I. Thirty-four challenges to meet before excimer laser technology can achieve super vision. J Refract Surg 2002; 18: 740-743.

First author:
Diego de Ortueta, MD

Augenzentrum Recklinghausen, Recklinghausen Germany

Topic E **CLINICAL EFFECTS OF CYCLOTORSIONAL ERRORS DURING REFRACTIVE SURGERY**

(Efectos clínicos de los errores de ciclotorsión durante cirugía refractiva)

11. Arba Mosquera S, Merayo-Lloves J, de Ortueta D. Clinical effects of pure cyclotorsional errors during refractive surgery. Invest Ophthalmol Vis Sci; 2008; 49: 4828-4836

AUTHOR CONTRIBUTIONS

Study concept and design (S.A.M.); data collection (D.O., M.C.A., I.M.A.); analysis and interpretation of data (S.A.M.); drafting (S.A.M.); critical revision (J.M., D.O., M.C.A., I.M.A.); statistical expertise (S.A.M.).

Clinical Effects of Pure Cyclotorsional Errors during Refractive Surgery

Samuel Arba-Mosquera,[1,2] *Jesús Merayo-Lloves,*[1] *and Diego de Ortueta*[3]

Purpose. To describe the theoretical effects of cyclotorted ablations on induced aberrations and determine the limits of tolerance of cyclotorsional accuracy.

Methods. A method was developed to determine the average cyclotorsion during refractive surgery without a cyclotorsion tracker. Mathematical conditions were simulated to determine the optical, visual, and absolute benefits in 76 consecutive treatments performed on right eyes. The results were evaluated as Zernike expansion of residual wavefront aberrations.

Results. Ablations based purely on Zernike decomposition but with cyclotorsion applied resulted in residual aberrations of the same Zernike modes of different magnitudes and orientations, indicating that the effect of cyclotorted compensation can be analyzed by single Zernike modes in magnitude and orientation. The effect on single Zernike modes depends on angular frequency, and not on radial order. A mean of 4.39° of cyclotorsion was obtained. A theoretical optical benefit was achieved in 95% of treatments, a theoretical visual benefit in 95%, and an absolute benefit in 93% compared with 89%, 87%, and 96% of treatments achieving actual benefits, respectively.

Conclusions. Residual aberrations resulting from cyclotorsion depend on aberrations included in the ablation and cyclotorsional error. The theoretical impact of cyclotorted ablations is smaller than that of decentered ablations or edge effects in coma and spherical aberrations. The results are valid within a single-failure condition of pure cyclotorsional errors, because no other sources of aberrations are considered. The leap from the mathematical model to the real-world outcome cannot be extrapolated without further study. (*Invest Ophthalmol Vis Sci.* 2008;49:4828–4836) DOI:10.1167/iovs.08-1766

Human eyes have 6 degrees of freedom to move: *x/y* lateral shifts, *z* leveling, horizontal/vertical rotations, and cyclotorsion (rotations around the optical axis).

Laser technology for refractive surgery allows corneal alterations that correct refractive errors[1] more accurately than ever. Ablation profiles are based on the removal of tissue lenticules in the form of sequential laser pulses that ablate a small amount of corneal tissue to compensate for refractive errors. However, the quality of vision can deteriorate significantly, especially under mesopic and low-contrast conditions.[2]

Induction of aberrations, such as spherical aberrations and coma, is related to loss of visual acuity (VA)[3] and quality. Some aberrations, however, may be subject to neural adaptation. Artal et al.,[4] in a study of the effects of neural compensation on vision, indicated that visual quality in humans is superior to the optical quality provided by the human eye.

To balance already existing aberrations, customized treatments were developed that use either wavefront measurements of the whole eye[5] (obtained, e.g., by Hartmann-Shack wavefront sensors) or corneal topography–derived wavefront analysis.[6,7] Topography-guided,[8] wavefront-driven,[9] wavefront-optimized,[10] asphericity preserving, and Q-factor profiles[11] have been proposed as solutions.

Measuring rotation when the patient is upright compared with when the refractive treatments are performed with the patient supine may lead to ocular cyclotorsion,[12] resulting in mismatching of the applied versus the intended profiles[13] (Fig. 1). Recently, some equipment has been developed that can facilitate measurement of and potential compensation for static cyclotorsion that occurs when the patient moves from the upright to the supine position during the procedure.

In the present study, we examined the effects of pure uncompensated cyclotorsional errors during refractive surgery.

Methods

Determination of Cyclotorsion during Refractive Surgery

The study was conducted in accordance with the Declaration of Helsinki.

All surgeries were performed by one surgeon (DO), flaps were created using a microkeratome (Pendular; Schwind Eye-Tech-Solutions GmbH, Kleinostheim, Germany), and ablations were performed with a system that delivers aberration-free profiles (ESIRIS; Schwind Eye-Tech-Solutions GmbH).

We analyzed the topographies using the Keratron-Scout videokeratoscope (Optikon2000 S.p.A, Rome, Italy), before surgery and 3 months after LASIK, and measured the Maloney indices in 76 consecutive right eyes with myopic astigmatism. Using only right eyes or only left eyes simplifies calculations because it directly avoids considering potential bilateral symmetry effects of cyclotorsion between eyes (i.e., cyclotorsional values in the left eye might be multiplied by −1).

As reported previously,[14] the achieved correction after refractive surgery can be calculated from the topographic changes. The vectorial differences in the astigmatic space between the postoperative and preoperative Maloney indices[14,15] were compared to the intended corrections—for example, a preoperative topography of 41.6 D at 111° and 41.2 D at 21° and a postoperative topography of 44.4 D at 114° and 43.5 D at 24° results in a spherical change of +3.0 D with a cylindrical component of −0.5 D at 117° compared with the planned +3.0 D, −0.5 D × 110° at the 12-mm vertex distance, resulting in 7° of counterclockwise cyclotorsion (Fig. 2). Maloney indices use the inner 3-mm zone, to fit this disc area best to a spherocylindrical surface in 3 dimensions. Cylinder orientation defines the two principal meridians, and sphere and cylinder provide the curvatures of the principal me-

From the [1]Grupo de Investigación de Cirugía Refractiva y Calidad de Visión, Instituto de Oftalmobiología Aplicada, University of Valladolid, Valladolid, Spain; [2]Schwind Eye-Tech-Solutions, Kleinostheim, Germany; and the [3]Augenzentrum Recklinghausen, Recklinghausen, Germany.

The current work is part of a thesis submitted by SA-M for evaluation at Instituto Universitario de Oftalmobiología Aplicada in partial fulfillment of the requirements for the academic degree of Master of Science (MSc) in Sciences of Vision Research Group "Cirugía Refractiva y Calidad de Visión."

Submitted for publication January 19, 2008; revised April 16, May 8, and June 16, 2008; accepted September 10, 2008.

Disclosure: **S. Arba-Mosquera**, Schwind Eye-Tech-Solutions (E); **J. Merayo-Lloves**, None; **D. de Ortueta**, Schwind Eye-Tech-Solutions (C)

The publication costs of this article were defrayed in part by page charge payment. This article must therefore be marked "*advertisement*" in accordance with 18 U.S.C. §1734 solely to indicate this fact.

Corresponding author: Samuel Arba-Mosquera, Schwind Eye-Tech-Solutions, Mainparkstrasse 6–10, D-63801 Kleinostheim, Germany; samuel.arba.mosquera@eye-tech.net.

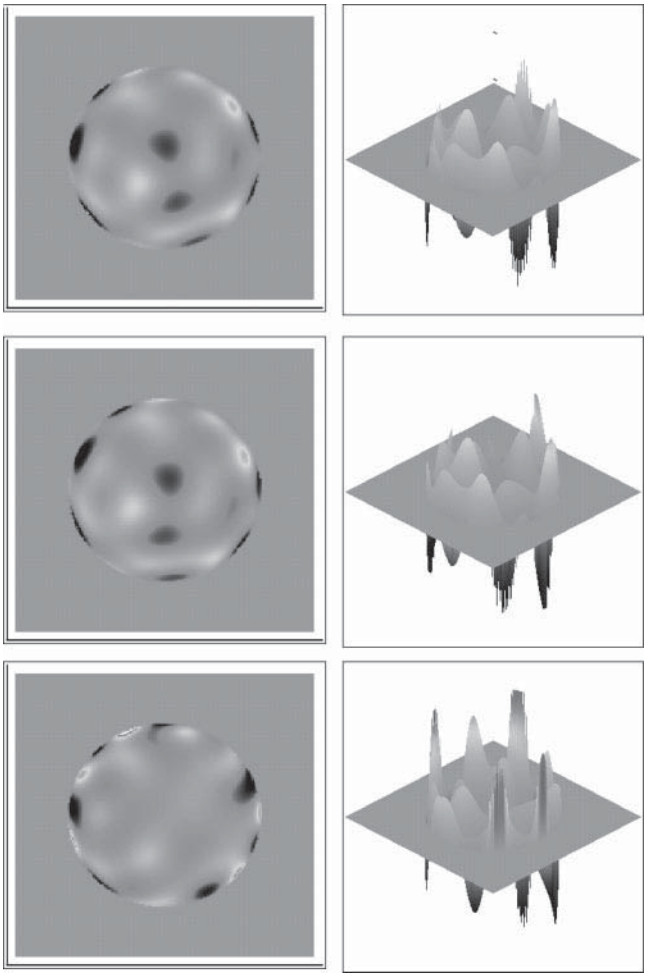

FIGURE 1. *Top*: Original wavefront error; *middle*: 15° clockwise torted wavefront error; *bottom*: residual wavefront error (all in two dimension and three dimensions).

ridians. In normal corneas (without irregular astigmatism) sim-K and Maloney analyses provide very similar results.

Residual Aberration after Cyclotorsional Errors during Refractive Surgery

When the rotation angle is 0, the aberration and compensation patterns cancel each other, resulting in no residual aberration. Based on the definition of the Zernike polynomials[16] ($Z(n,m)$, where n is a null or positive integer and m is an integer ranging from $-n$ to $+n$, representing the radial and meridional orders, respectively), it is evident that the polynomials $Z(n,0)$ are invariant under rotations around their center. The only aberrations affected by cyclotorsional errors are vectorial. For those, Zernike polynomials are structured in two complementary sets, governed by sine/cosine functions that avoid coupling of different orders of aberration for rotations around the center.

After rotation of the opposite Zernike components around their origins, the aberration mode still can be decomposed into two Zernike components:

$$C'^{m}_{n} = -[C_n^{m} \cos(m\theta) + C_n^{-m} \sin(m\theta)]. \quad (1)$$

where n is the radial order; m, the angular frequency; C'^{m}_{n}, the rotated Zernike compensation; $C_n^{\pm m}$, the original Zernike components; and θ, the cyclotorsional angle.

After compensating for the original pattern with a rotated one, the residual components are:

$$C''^{m}_{n} = C_n^{m}[1 - \cos(m\theta)] - C_n^{-m} \sin(m\theta), \quad (2)$$

where C''^{m}_{n} is the residual Zernike component.

Expressing each aberration in magnitude and orientation[17]:

$$|C''_{nm}| = |C_n^{\pm m}| 2 \sin\left(\frac{m\theta}{2}\right) \quad (3)$$

and

$$\Delta\alpha = \alpha - \alpha_0 = \frac{\theta}{2} - \frac{\pi}{2m}. \quad (4)$$

According to the previous example, a planned correction of +3.0, –0.5 D × 110° at the 12-mm vertex distance and an actual spherical change of +3.0 D with a cylindrical component of −0.5 D at 117° results in 7° of counterclockwise cyclotorsion and would lead to a postoperative refraction of +0.07, −0.13 D × 69°.

The relative amount of residual aberrations depends only on cyclotorsional error (Figs. 3, 4). Since the original aberration can be described as a linear combination of Zernike polynomials[16] and each of these Zernike terms results in a residual Zernike term after partial compensatory rotation, the residual wavefront aberration is the sum of all residual terms.

Derivation of a Mathematic Condition to Determine an Optical Benefit

A condition in which any postoperative aberration smaller than its preoperative magnitude was considered positive was referred to as an optical benefit:

$$2\left|\sin\left(\frac{m\theta}{2}\right)\right| < 1 \quad (5)$$

and

$$|m| < \frac{2 \arcsin(1/2)}{|\theta|} < \left|\frac{\pi}{3\theta}\right|. \quad (6)$$

According to this example, 7° of cyclotorsion would produce an optical benefit up to the octafoil angular frequencies.

Considering the cyclotorsional error and the preoperative astigmatism, we calculated how many treatments would theoretically achieve an optical benefit for the astigmatism component ($m = 2$). Because the treatments were planned as aberration-free profiles and therefore were based only on sphere, cylinder, and axis inputs, the astigmatism was the only vectorial aberration included. Moreover, astigmatism is in magnitude the major Zernike mode of a vectorial nature. We compared this value to the percentage of eyes that actually obtained a postoperative cylinder lower than the preoperative value.

Derivation of a Mathematic Condition to Determine a Visual Benefit

To distinguish between optical benefit (merely reducing the aberration magnitude) and visual performance (visual benefit), we adopted a model based on the findings of Artal et al.[4] In their study, equivalent human optical systems that differed only in the orientation of the aberration patterns (produced by adaptive optics) achieved different visual performances mainly due to neural compensation for the unique aberration pattern of each individual. For that reason, matching factor (MF) behavior based on single aberrations was modeled. MF is at its maximum (equal to 1) in aberrations of the same orientation and at its minimum for aberrations of the opposite orientation in the Zernike

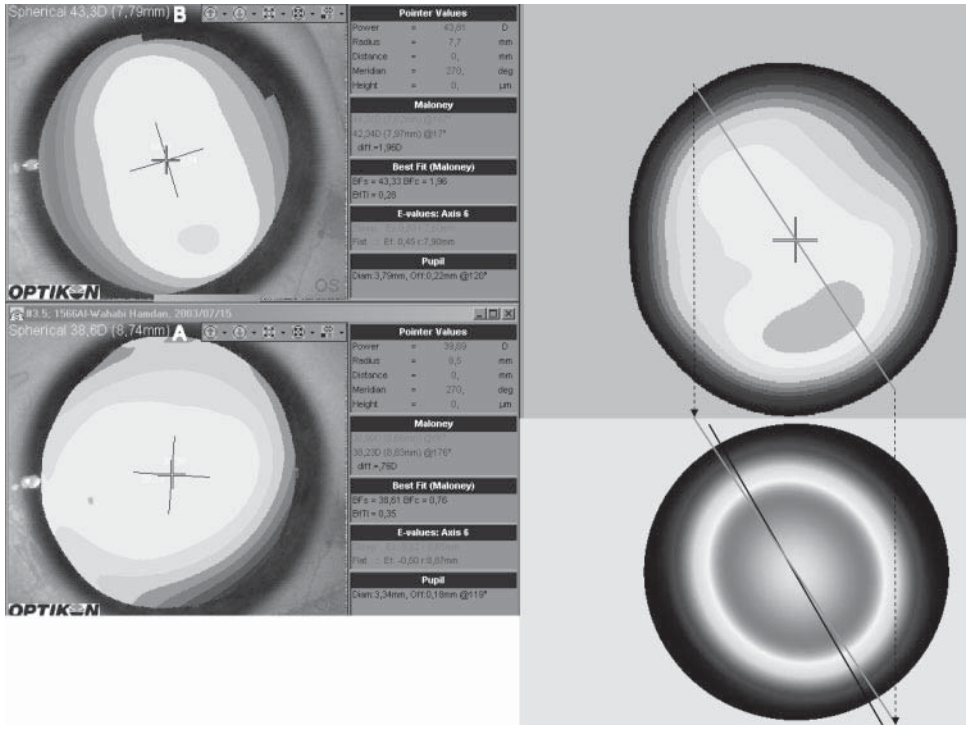

FIGURE 2. The difference between the postoperative and preoperative topographies compared to the intended correction. The difference in the orientation of the astigmatism defines the cyclotorsional error. (**A**) Preoperative topography, (**B**) postoperative topography, (*top right*) differential topography, (*bottom right*) planned correction. Counterclockwise torsion of the astigmatism can be seen.

space. The magnitude of aberration distribution was considered as a decreasing exponential with the Zernike order as described by Thibos et al.[18]

Visual benefit was defined as a condition in which the postoperative aberration was smaller than its preoperative magnitude times the MF for that relative orientation:

$$2\left|\sin\left(\frac{m\theta}{2}\right)\right| < MF + (1 - MF)\left|\cos\left(m\Delta\alpha\right)\right| \quad (7)$$

and

$$|m| < \frac{2\arcsin\left(\frac{MF}{MF+1}\right)}{|\theta|}. \quad (8)$$

The arbitrary value of 0.625 was chosen as the MF generator; this value produces a maximum equal to 1 and a minimum equal to 0.25 (Fig. 5):

$$MF = 0.625 \quad (9)$$

and

$$|m| < \frac{2\arcsin\left(\frac{5}{13}\right)}{|\theta|}. \quad (10)$$

According to this example, 7° of cyclotorsion would produce a visual benefit up to the hexafoil angular frequencies.

With the cyclotorsional error and the preoperative astigmatism and assuming that cyclotorsional errors around the ablation center were the only failure, the number of eyes was calculated that would have

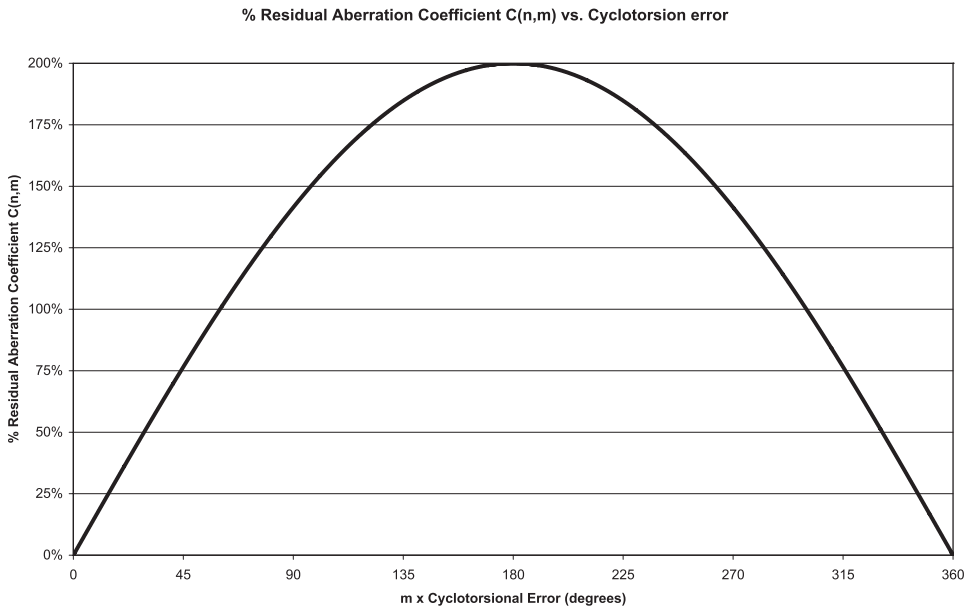

FIGURE 3. The percentage of residual aberrations versus cyclotorsional error. Modulation of the cyclotorsional error by the angular frequency (m) is shown; the higher the angular frequency, the faster the residual aberration varies. For $m = 1$ (coma), the maximum residual error is achieved for 180° torsion; for $m = 2$ (cylinder), the maximum residual error would be achieved for 90° torsion; for $m = 3$ (trefoil), the maximum residual error would be achieved for 60° torsion, and so on.

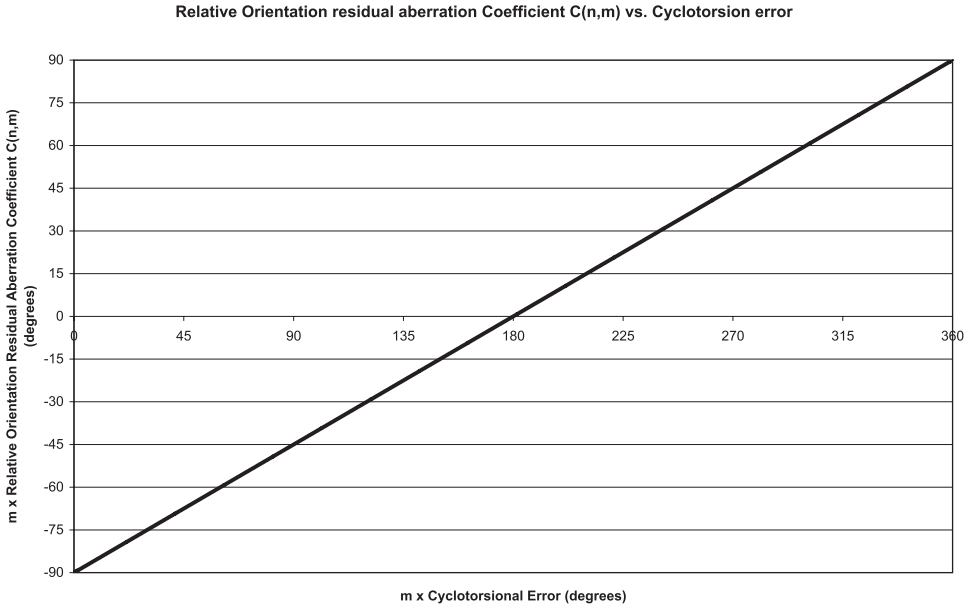

FIGURE 4. The relative orientation of residual aberrations versus cyclotorsional error. Modulation of the cyclotorsional error and the relative orientation by the angular frequency (*m*) are shown.

obtained a visual benefit for cylinder if the correction were correct but the axis was incorrect. We compared this value to the percentage of eyes in which postoperative uncorrected visual acuity (UCVA) was maintained or improved, compared with the preoperative best spectacle-corrected visual acuity (BSCVA) and with the percentage of eyes with actually maintained or improved BSCVA.

Derivation of a Mathematic Condition to Determine an Absolute Benefit

The major ocular aberrations are defocus and primary astigmatism, which is the major aberration affected by a rotational error. The amount of tolerable residual astigmatism after surgery cannot be defined as a percentage of the preoperative astigmatism, because the tolerance limit is set by the image-forming characteristics of the eye and so takes an absolute value. With simple spherical error, degradation of resolution begins, in most people, with errors of 0.25 D. A similar measure can be placed on the error due to cylinder axis error.[19]

A simple approach for classifying the clinical relevance of single aberration terms was proposed by Thibos et al.,[20] who introduced the concept of equivalent defocus[20] (DEQ) as a metric to minimize the differences in the Zernike coefficients due to different pupil sizes.

DEQ is defined as the amount of defocus that produces the same wavefront variance as that found in one or more higher order aberrations:

$$DEQ_{nm} = \frac{16\sqrt{3}|C_{nm}|}{AD^2}, \qquad (11)$$

where AD is the diameter considered for the wavefront aberration analysis

The absolute benefit considers as positive any result for which the postoperative aberration pattern was smaller than an absolute limit of 0.50 DEQ for the magnitude of each Zernike mode (i.e., a ±0.25 DEQ maximum deviation in one or several meridians).

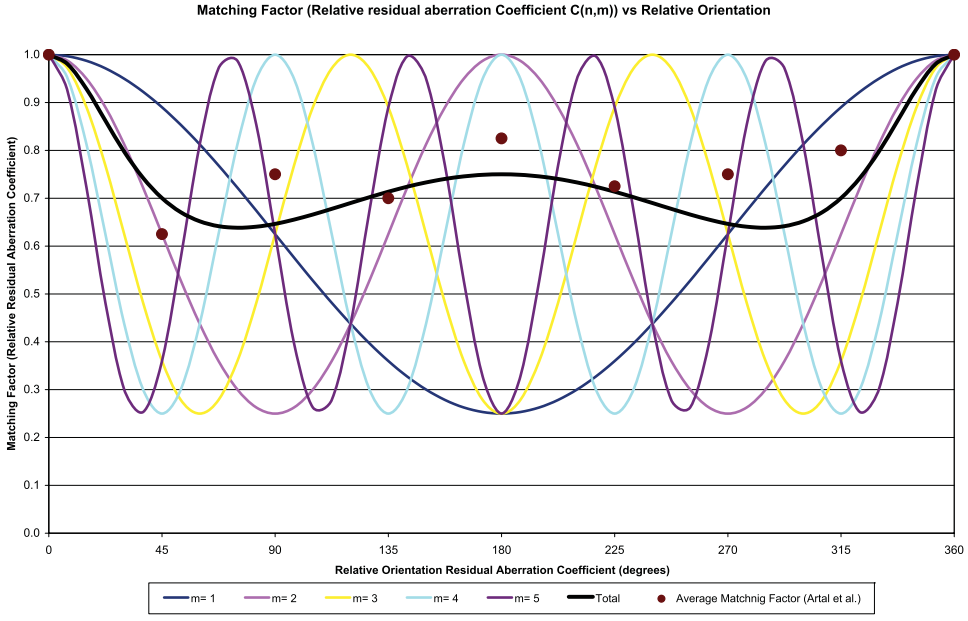

FIGURE 5. Matching factor versus relative orientation of residual aberrations. These data agree with those of Artal et al.[4]

The absolute benefit is ruled by the condition

$$\left| DEQ_{nm} 2 \sin\left(\frac{m\theta}{2}\right)\right| < 0.50 \quad (12)$$

and

$$|DEQ_{nm}| < \frac{1}{4\left|\sin\left(\frac{m\theta}{2}\right)\right|}. \quad (13)$$

According to this example, 7° of cyclotorsion, Zernike modes should not exceed 4.10 DEQ for coma, 2.05 DEQ for astigmatism, and 1.37 DEQ for trefoil, for theoretically successful results.

With the torsional error and the preoperative astigmatism and assuming that cyclotorsion around the ablation center was the only failure, the number of eyes was calculated that would have obtained an absolute benefit for cylinder (postoperative magnitude, ≤0.50 D) if the cylindrical correction were correct but the axis was wrong. We compared this value to the eyes in which postoperative astigmatism was less than 0.50 D.

Results

Static Cyclotorsion during Laser Refractive Surgery

Preoperative and postoperative topographies were compared 3 months after treatment in 76 consecutives right eyes treated without adverse events at Augenzentrum Recklinghausen.

The preoperative spherical equivalent (SE) was −3.56 D with a standard deviation (SD) of 1.51 D (range, −7.00 to −1.25 D), sphere, −3.15 ± 1.48 D (−6.50 to −0.50 D); and cylinder, −0.82 ± 0.66 D (−3.00 to −0.25 D).

The distribution of the attempted astigmatic correction is shown in Figure 6; 30% of the treatments (n = 23) had corrections of −0.25 D of astigmatism, 20% (n = 15) corrections of −0.50 D of astigmatism, 39% (n = 30) corrections between −0.75 and −1.50 D of astigmatism, and 11% (n = 8) corrections between −1.50 and −3.00 D of astigmatism.

At the 3-month follow-up, the mean SE was −0.14 ± 0.30 D (range, −1.00 to +0.25 D); sphere, −0.06 ± 0.29 D (−0.75 to +0.25 D); and cylinder, −0.17 ± 0.26 D (−1.25 to 0.00 D). Eighty-seven percent of the eyes (n = 66) were within ±0.50 D of the attempted correction, and 100% (n = 76) were within ±1.00 D.

The direct average of the cyclotorsional errors was 2.42°, whereas the absolute error averaged 4.39°. Figure 7 is a stratification of the cyclotorsional error expressed in absolute values. Seventy-one percent of the eyes (n = 54) had less than 2.5° of cyclotorsion, 78% (n = 59) less than 5.0°, and 87% (n = 66) less than 10.0°.

Theoretical Ranges for Optical, Visual, and Absolute Benefits

The maximum angular frequency and Zernike mode magnitudes that fulfill these conditions were calculated for specific cyclotorsional errors (Fig. 8, Tables 1, 2), but for the description of the magnitudes, we focused on astigmatism, coma, and trefoil because these are the major Zernike modes of a vectorial nature.

For cyclotorsional errors up to ±14°, it is possible to obtain a visual benefit for comatic, astigmatic, and trefoil angular frequencies and an optical benefit for tetrafoil angular frequencies, as well. It also is possible to control the creation of blur under an absolute limit whenever coma magnitudes do not exceed 2.05 DEQ; astigmatism, 1.03 D; and trefoil, 0.70 DEQ.

For maximum cyclotorsional errors up to ±4°, the theoretical limit for visual benefit extends up to endecafoil (11-fold) angular frequencies and for optical benefit up to 15-fold (pentadecafoil) angular frequencies. The magnitudes for the major Zernike modes should not exceed 7.16 DEQ for coma, 3.58 DEQ for astigmatism, and 2.39 DEQ for trefoil.

For cyclotorsional errors up to ±1.5°, visual benefit extends up to triacontafoil (30-fold) angular frequencies and optical benefit even beyond these frequencies. Moreover, coma magnitudes below 19.10 DEQ, astigmatism up to 9.55 D, and trefoil up to 6.37 DEQ produce a postoperative blur under 0.50 DEQ.

Table 3 summarizes the residual aberration ratios and relative orientations for different cyclotorsional errors. The percentage is the amount of postoperative residual in magnitude, and the angle is the relative orientation of the postoperative residual. For example, 1.00 μm of trefoil at 30° with a 5° clockwise torsional error results a postoperative residual error of 0.26 μm of trefoil at 58°, or 3.00 DEQ astigmatism at 75° with a 10° counterclockwise torsional error results in a postoperative residual error of 1.04 DEQ astigmatism at 35°.

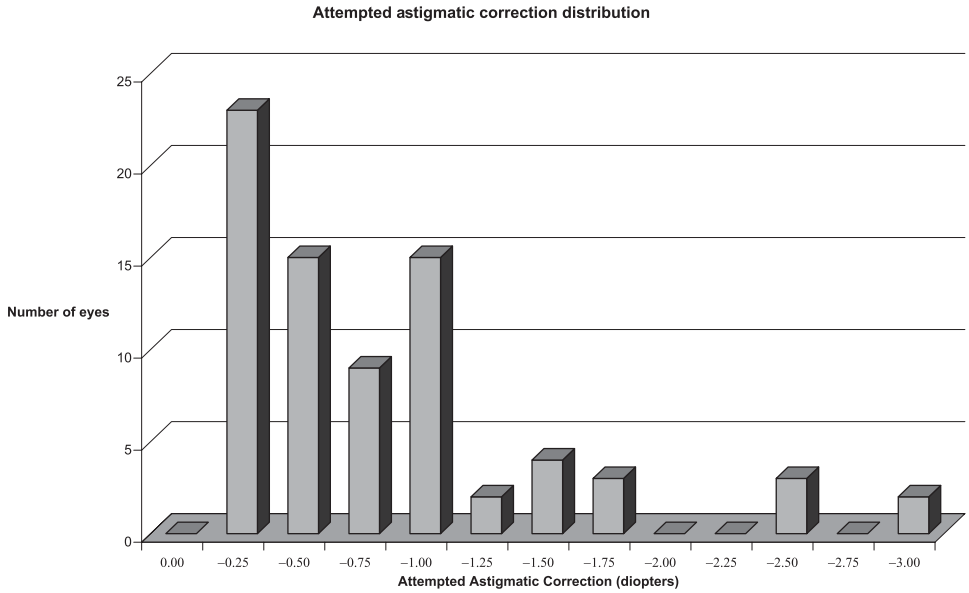

Figure 6. Distribution of the magnitudes of the attempted astigmatic correction.

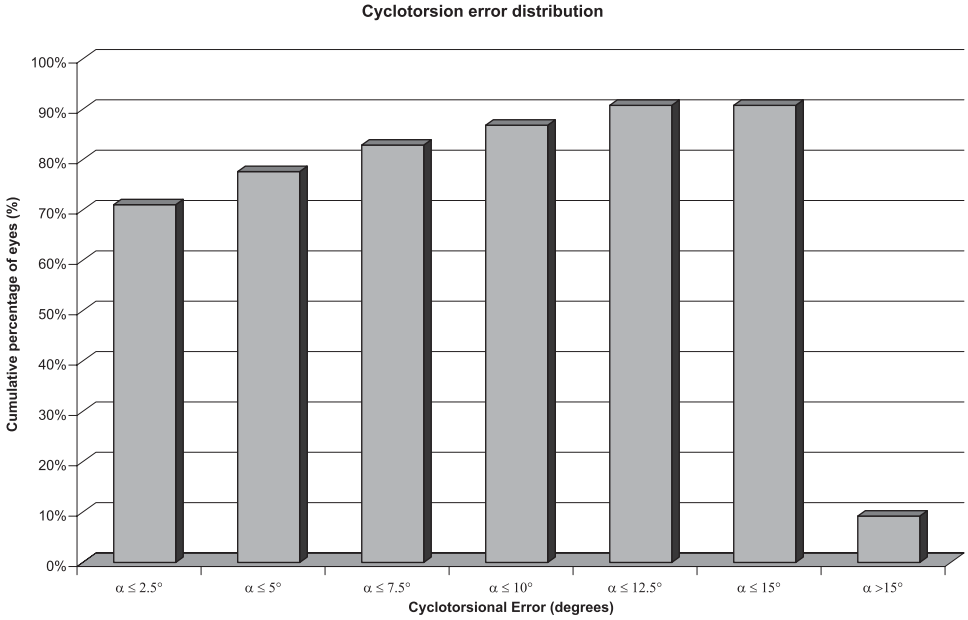

FIGURE 7. Distribution of the retrospectively calculated cyclotorsional errors.

Clinical Optical Benefit

Considering the cyclotorsional error and the preoperative astigmatism, we calculated the number of treatments that would theoretically achieve an optical benefit for the astigmatism component ($m = 2$).

With these settings, 95% of the eyes ($n = 72$) would have obtained an optical benefit for the cylinder if the cylindrical correction were correct but the axis was wrong and if cyclotorsional errors occurring around the ablation center were the only failures. This compared with 89% of the eyes ($n = 68$) that actually obtained a postoperative cylinder lower than preoperative value. The differences between the theoretical and the empiric results were marginally significant ($P = 0.05$).

Clinical Visual Benefit

With the same settings as previously, 95% of the eyes ($n = 72$) would have obtained a visual benefit for the cylinder compared with 87% of the eyes ($n = 66$) that actually had a stable or improved postoperative UCVA compared with the preoperative BSCVA ($P < 0.01$) and with 91% of the eyes ($n = 69$) with a stable or improved BSCVA ($P = 0.09$).

Clinical Absolute Benefit

With the same settings as previously, 93% of the eyes ($n = 71$) would have obtained an absolute benefit for the cylinder compared with 96% of the eyes ($n = 73$) in which the postoperative astigmatism was smaller than 0.50 D ($P = 0.21$).

Clinical Ranges for Optical, Visual, and Absolute Benefits

Combining all success ratios to calculate the number of eyes that obtained (theoretically and empirically) optical, visual, and absolute benefits simultaneously, 89% of the eyes ($n = 68$) with theoretical global success vs. 79% of the eyes ($n = 60$) obtained a postoperative cylinder lower than that before sur-

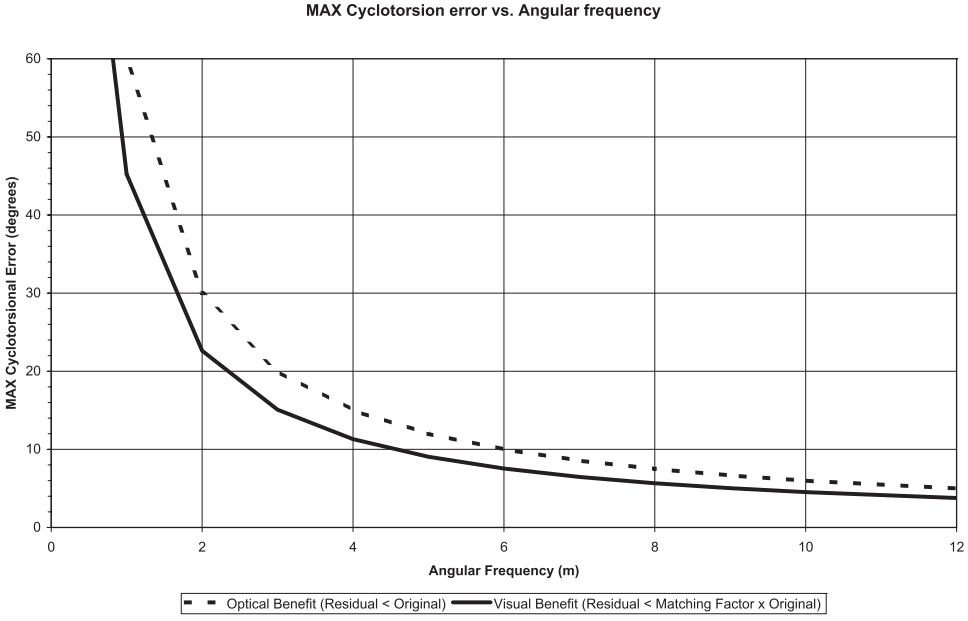

FIGURE 8. The maximum allowable cyclotorsional errors versus angular frequency for different criteria.

TABLE 1. Maximum Allowable Cyclotorsional Errors for Different Aberration Components and Different Criteria

Aberrations	*m*	Optical Benefit (Residual < Original)	Visual Benefit (Residual < Matching Factor)
Coma	1	60.0	45.2
Astigmatism	**2**	**30.0**	**22.6**
Trefoil	3	20.0	15.1
Tetrafoil	4	15.0	11.3
Pentafoil	5	12.0	9.0
Hexafoil	6	10.0	7.5
Heptafoil	7	8.6	6.5
Octafoil	8	7.5	5.7
Eneafoil	9	6.7	5.0
Decafoil	10	6.0	4.5
Dodecafoil	12	5.0	3.8
Pentadecafoil	15	4.0	3.0
Icosafoil	20	3.0	2.3
Triacontafoil	30	2.0	1.5
Hexacontafoil	60	1.0	0.8

In bold: astigmatism, as it is the major aberration mode with a vector nature.

gery, lower than 0.50 D, and a stable or improved BSCVA ($P < 0.005$).

Considering the cyclotorsional error, we calculated a hypothetical case simulating the condition in these patients, for which Zernike mode the treatments could have been planned to achieve optical and visual benefits (Table 4).

DISCUSSION

The method used in this study to determine the cyclotorsional error incurred during laser refractive surgery is indirect, because it calculates the torsional error retrospectively after the ablation procedures have been performed. However, it is easy and straightforward and does not require additional equipment or complicated algorithms. Its retrospective nature ensures that the calculated error corresponds to the average cyclotorsional error during the entire refractive surgery procedure. This way, the method could be used to validate the cyclotorsional errors obtained with other prospective methods.

The study had limitations. Because the method considers that the difference between the planned astigmatism axis and the axis of the effectively achieved cylindrical correction is due only to cyclotorsional errors, it may be affected by other sources of unavoidable errors in laser refractive surgery, such as flap cuts, pattern decentration, blending zones, and corneal biomechanics. The results are valid in the absolute single-failure condition of pure cyclotorsional errors. Moreover, we assumed for the study that the torsion always occurred around the intended ablation center. It usually happens that the pupil size and center differ for the treatment compared with that during diagnosis.[21] Then, excluding cyclotorsion, there is already a lateral displacement that mismatches the ablation profile. Further, cyclotorsion occurring around any position other than the ablation center results in additional lateral displacement combined with cyclotorsion.[22] Finally, this analysis considers the results in terms of the residual monochromatic wavefront aberration. However, the visual process is more complex than just an image-projection system and involves elements such as neural compensation and chromatic aberration, which were beyond the scope of this study. The cortical aspect of visual processing especially may affect the subjective symptoms associated with residual wavefront aberration.

With our indirect analysis of cyclotorsional error, we obtained an average error of 4.39°, which, despite the mentioned limitations of the method, agrees with the observations of Ciccio et al.,[23] who reported 4°. The distribution of the percentage of eyes versus cyclotorsional error (Fig. 7) is similar to the findings of Carones,[24] who used a prospective method in a population based on eye registration of recognizable iris structures and reported a mean torsion of 3.3° (range, 0–13°); 224 eyes (74.7%) had less than 4° of cyclotorsion, and 8 eyes (2.7%) had more than 10° of cyclotorsion. In our sample, however, 13% of eyes had cyclotorsion exceeding 10°. These patients would be expected to have at least 35% residual cylinder, 52% residual trefoil, and higher residual errors of tetrafoil, pentafoil, and hexafoil (Table 3). In addition, octafoil would be induced beginning at 7.5° of cyclotorsion.

Because of the cyclic nature, the residual aberration error emanating from cyclotorsional error ranges from 0% to 200% of the original aberration. However, the induced aberrations emanating from lateral displacements always increase with decentration.[25] If we also consider that in human eyes with normal aberrations the weight $C(n,m)$ of the Zernike terms $Z(n,m)$ decreases with increasing Zernike order (n),[18] then the theoretical impact of cyclotorted ablations is smaller than decentered ablations or edge effects[26] (coma and spherical aberration[27]). The results of the work of Guirao et al.[22] and Bará et al.,[28,29] are confirmed by those of the present study, with special emphasis on the independent nature of the cyclotorsional effect with the radial order.

We adopted three criteria based on the accuracy that can be achieved to overcome cyclotorsion: optical benefit provides the maximum angular frequency that can be included in the correction for which an objective improvement in the optical quality can be expected; visual benefit, the maximum angular frequency for which a subjective improvement in the visual

TABLE 2. Maximum Treatable Magnitude for Different Aberration Components and Different Cyclotorsional Errors for the <0.50 DEQ Criterion

Cyclotorsional Error		Optical Benefit Angular Frequency *m*	Visual Benefit Angular Frequency *m*	Treated Coma $C(n,1)$ (DEQ)	Treated Cylinder $C(n,2)$ (DEQ)	Treated Trefoil $C(n,3)$ (DEQ)	Treated Tetrafoil $C(n,4)$ (DEQ)	Treated Pentafoil $C(n,5)$ (DEQ)	Treated Hexafoil $C(n,6)$ (DEQ)	Treated Octafoil $C(n,8)$ (DEQ)
Torsion tracker	1.5	40	**30**	19.10	**9.55**	6.37	4.78	3.82	3.19	2.13
	2.5	24	**18**	11.46	**5.73**	3.82	2.87	2.30	1.92	1.28
Average torsion	4.0	15	**11**	7.16	**3.58**	2.39	1.80	1.44	1.20	0.81
	5.0	12	**9**	5.73	**2.87**	1.92	1.44	1.16	0.97	0.65
	7.5	8	**6**	3.82	**1.92**	1.28	0.97	0.78	0.65	0.45
	10.0	6	**4**	2.87	**1.44**	0.97	0.73	0.59	0.50	0.35
	12.5	4	**3**	2.30	**1.16**	0.78	0.59	0.48	0.41	0.30
Maximum torsion	14.0	4	**3**	2.05	**1.03**	0.70	0.53	0.44	0.37	0.28
	15.0	4	**3**	1.92	**0.97**	0.65	0.50	0.41	0.35	0.27

In bold: astigmatism, as it is the major aberration mode with a vector nature.

TABLE 3. Residual Aberration Ratios and Relative Orientations for Different Cyclotorsional Errors

Cyclotorsional Error		Residual Coma $C(n,1)$	Residual Cylinder $C(n,2)$	Residual Trefoil $C(n,3)$	Residual Tetrafoil $C(n,4)$	Residual Pentafoil $C(n,5)$	Residual Hexafoil $C(n,6)$	Residual Octafoil $C(n,8)$
Torsion tracker	1.5	3% @ 271°	**5% @ 136°**	8% @ 91°	10% @ 68°	13% @ 55°	16% @ 46°	24% @ 35°
	2.5	4% @ 271°	**9% @ 136°**	13% @ 91°	17% @ 69°	22% @ 55°	26% @ 46°	39% @ 35°
Average torsion	4.0	7% @ 272°	**14% @ 137°**	21% @ 92°	28% @ 70°	35% @ 56°	42% @ 47°	62% @ 36°
	5.0	9% @ 273°	**17% @ 138°**	26% @ 93°	35% @ 70°	43% @ 57°	52% @ 48°	77% @ 36°
	7.5	13% @ 274°	**26% @ 139°**	39% @ 94°	52% @ 71°	64% @ 58°	77% @ 49°	111% @ 38°
	10.0	17% @ 275°	**35% @ 140°**	52% @ 95°	68% @ 73°	85% @ 59°	100% @ 50°	141% @ 39°
	12.5	22% @ 276°	**43% @ 141°**	64% @ 96°	85% @ 74°	104% @ 60°	122% @ 51°	166% @ 40°
Maximum torsion	14.0	24% @ 277°	**48% @ 142°**	72% @ 97°	94% @ 75°	115% @ 61°	134% @ 52°	178% @ 41°
	15.0	26% @ 278°	**52% @ 143°**	77% @ 98°	100% @ 75°	122% @ 62°	141% @ 53°	185% @ 41°

The percentage is the amount of postoperative residual in magnitude, whereas the angle is the relative orientation of the postoperative residual. In bold: astigmatism, as it is the major aberration mode with a vector nature.

performance can be expected; and absolute benefit, the maximum magnitudes for each Zernike mode for which an effective result can be expected.

When all criteria are met without other sources of aberration, the result is expected to be successful. When only the terms allowed by the visual benefit condition are included, but any of their magnitudes exceed the limits imposed by the <0.50 DEQ condition, the visual performance is expected to improve, but it might not be successful. When terms beyond the limits set by the visual benefit condition are included, the risk that the patient will require time to readapt to the new aberration must be considered. When terms beyond the limits set by the optical benefit condition are included, the risk that the aberrations will worsen must be considered carefully.

Without eye registration technologies,[30,31] considering that maximum cyclotorsion measured from the shift from the upright to the supine position does not exceed ±14°,[23] it is theoretically possible to obtain a visual benefit up to the trefoil angular frequencies and an optical benefit up to the tetrafoil angular frequencies. This explains why classic spherocylindrical corrections in refractive surgery succeed without major cyclotorsional considerations. However, using our limit of absolute residual dioptric error smaller than DEQ 0.50, only up to 2.05 DEQ coma, 1.03 DEQ astigmatism, and 0.70 DEQ trefoil can be corrected successfully. The limited amount of astigmatism, especially that can be corrected effectively for this cyclotorsional error, may explain partly some of the unsuccessful results reported in refractive surgery.

TABLE 4. Percentage of Treatments That Could Have Been Planned to Achieve an Optical and a Visual Benefit as a Function of the Highest Included Zernike Mode

m	Aberration	Optical Benefit (%) (Residual < Original)	Visual Benefit (%) (Residual < Matching Factor)
1	Coma	97	96
2	**Astigmatism**	**95**	**95**
3	Trefoil	93	92
4	Tetrafoil	92	89
5	Pentafoil	89	87
6	Hexafoil	87	83
7	Heptafoil	84	78
8	Octafoil	82	75
9	Eneafoil	78	74
10	Decafoil	75	71
12	Dodecafoil	71	66
15	Pentadecafoil	66	61
20	Icosafoil	61	58
30	Triacontafoil	57	57
60	Hexacontafoil	55	55

In bold: astigmatism, as it is the major aberration mode with a vector nature.

Considering that the average cyclotorsion resulting from the shift from the upright to the supine position is about ±4°,[23] without an aid other than manual orientation, the theoretical limits for achieving a visual benefit extend up to the endecafoil (11-fold) angular frequencies and up to the pentadecafoil (15-fold) angular frequencies for optical benefit. Our limit of absolute residual dioptric error less than 0.50 DEQ increases to 7.16 DEQ for coma, 3.58 DEQ for astigmatism, and 2.39 DEQ for trefoil. The extended limits confirm why spherocylindrical corrections in laser refractive surgery have succeeded.

With currently available eye registration technologies, which provide an accuracy of about ±1.5°, it is theoretically possible to achieve a visual benefit up to the triacontafoil (30-fold) angular frequencies and an optical benefit even beyond these angular frequencies, and using our limit of absolute residual dioptric error less than 0.50 DEQ, up to 19.10 DEQ coma, 9.55 DEQ astigmatism, and 6.37 DEQ trefoil can be corrected successfully. This finding opens a new era in corneal laser refractive surgery, because patients may be treated for a wider range of refractive problems with enhanced success ratios, however, at a higher resolution than technically achievable with currently available systems.[32,33]

To the best of our knowledge, currently available laser platforms for customized corneal refractive surgery include not more than the eighth Zernike order, which theoretically corresponds to a visual benefit range for cyclotorsional tolerance of ±5.7° and an optical benefit range for cyclotorsional tolerance of ±7.5°, which covers most cyclotorsion occurring when shifting from the upright to the supine position. Thus, the aberration status and the visual performance of the patients are expected to improve. Moreover, the same ±7.5° cyclotorsional tolerance means that the magnitudes for the major Zernike modes should not exceed 3.82 DEQ for coma modes, 1.92 DEQ for astigmatic modes, and, 1.28 DEQ for trefoil modes for theoretically successful results.

Based on different criteria, Bueeler et al.[34] also determined conditions and tolerances for cyclotorsional accuracy. Their OT criterion corresponds approximately to our optical benefit condition, and their results for the tolerance limits (29° for 3-mm pupils and 21° for 7-mm pupils) do not differ greatly from the optical benefit result for astigmatism, confirming that astigmatism is the major component to be considered.

In our study, the theoretical percentage of treatments that would achieve an optical benefit was significantly higher than the percentage of treatments that actually obtained a postoperative cylinder lower than before surgery (95% vs. 89%; $P = 0.05$). The percentage of treatments that theoretically would achieve a visual benefit was significantly higher than the percentage of treatments with a stable or improved postoperative

UCVA compared with the preoperative BSCVA (95% vs. 87%; $P < 0.01$). Both indicate that other sources of aberrations have substantial impact on the final results. The percentage of treatments that theoretically would achieve a visual benefit was higher than the percentage of treatments with a stable or improved BSCVA (95% vs. 91%; $P = 0.09$). That residual cylinder can be corrected with spectacles indicates that other factors induce aberrations and affect the final results. In discussing visual benefit, although VA data are helpful, there may be patients with 20/20 vision who are unhappy with their visual outcomes due to poor mesopic and low-contrast VA, which were not addressed in the present study.

Of interest, the percentage of treatments achieving a theoretical absolute benefit was 93%, whereas the percentage of treatments that actually had postoperative astigmatism reduced to an absolute residual error smaller than 0.50 D was higher (96%; $P = 0.21$).

Finally, the percentage of treatments that theoretically would achieve global success (optical, visual, and absolute benefits simultaneously) was significantly higher than the percentage of treatments that actually obtained a postoperative cylinder lower than the preoperative value, a stable or improved BSCVA, and decreased postoperative astigmatism to an absolute residual error less than 0.50 D (89% vs. 79%; $P < 0.005$). This confirms that cyclotorsion is not the only reason for differences between theory and practice. Wound healing and surgical variation are also keys factors in the outcome.

In summary, the present study showed that cyclotorsional errors result in residual aberrations and that with increasing cyclotorsional error there is a greater potential for inducing aberrations. Thirteen percent of eyes had more than 10° of calculated cyclotorsion, which predicts approximately a 35% residual astigmatic error in these eyes. Because astigmatic error is generally the highest magnitude of vectorial aberration, patients with higher levels of astigmatism are at higher risk of problems due to cyclotorsional error.

Acknowledgments

The authors thank Lynda Charters for editing the manuscript.

References

1. Munnerlyn CR, Koons SJ, Marshall J. Photorefractive keratectomy: a technique for laser refractive surgery. *J Cataract Refract Surg*. 1988;14:46–52.
2. Mastropasqua L, Toto L, Zuppardi E, et al. Photorefractive keratectomy with aspheric profile of ablation versus conventional photorefractive keratectomy for myopia correction: six-month controlled clinical trial. *J Cataract Refract Surg*. 2006;32:109–116.
3. Applegate RA, Howland HC. Refractive surgery, optical aberrations, and visual performance. *J Refract Surg*. 1997;13:295–299.
4. Artal P, Chen L, Fernandez EJ, Singer B, Manzanera S, Williams DR. Neural compensation for the eye's optical aberrations. *J Vis*. 2004;4:281–287.
5. Thibos L, Bradley A, Applegate R. Accuracy and precision of objective refraction from wavefront aberrations. *J Vis*. 2004;4:329–351.
6. Salmon TO. Corneal contribution to the wavefront aberration of the eye. PhD dissertation. Bloomington, IN: Indiana University; 1999:70.
7. Mrochen M, Jankov M, Bueeler M, Seiler T. Correlation between corneal and total wavefront aberrations in myopic eyes. *J Refract Surg*. 2003;19:104–112.
8. Alio JL, Belda JI, Osman AA, Shalaby AM. Topography-guided laser in situ keratomileusis (TOPOLINK) to correct irregular astigmatism after previous refractive surgery. *J Refract Surg*. 2003;19:516–527.
9. Mrochen M, Kaemmerer M, Seiler T. Clinical results of wavefront-guided laser in situ keratomileusis 3 months after surgery. *J Cataract Refract Surg*. 2001;27:201–207.
10. Mrochen M, Donetzky C,Wüllner C, Löffler J. Wavefront-optimized ablation profiles: theoretical background. *J Cataract Refract Surg*. 2004;30:775–785.
11. Koller T, Iseli HP, Hafezi F, Mrochen M, Seiler T. Q-factor customized ablation profile for the correction of myopic astigmatism. *J Cataract Refract Surg*. 2006;32:584–589.
12. Smith EM Jr, Talamo JH. Cyclotorsion in the seated and the supine patient. *J Cataract Refract Surg*. 1995;21:402–403.
13. Bueeler M, Mrochen M, Seiler T. Maximum permissible lateral decentration in aberration-sensing and wavefront-guided corneal ablations. *J Cataract Refract Surg*. 2003;29:257–263.
14. de Ortueta D, Arba Mosquera S, Baatz H. Topographical changes after hyperopic LASIK with the ESIRIS laser platform. *J Refract Surg*. 2008;24:137–144.
15. Rosa N, Furgiuele D, Lanza M, Capasso L, Romano A. Correlation of changes in refraction and corneal topography after photorefractive keratectomy. *J Refract Surg*. 2004;20:478–483.
16. Zernike F. Diffraction theory of the knife-edge test and its improved form, the phase-contrast method. *Monthly Notices of the Royal Astronomical Society*. 1934;94:377–384.
17. Campbell CE. A new method for describing the aberrations of the eye using Zernike polynomials. *Optom Vis Sci*. 2003;80:79–83.
18. Thibos LN, Hong X, Bradley A, Cheng X. Statistical variation of aberration structure and image quality in a normal population of healthy eyes. *J Opt Soc Am A Opt Image Sci Vis*. 2002;19:2329–2348.
19. Campbell CE. A method to analyze cylinder axis error. *Optom Vis Sci*. 1999;76:254–255.
20. Cheng X, Bradley A, Thibos LN. Predicting subjective judgment of best focus with objective image quality metrics. *J Vis*. 2004;4:310–321.
21. Yang Y, Thompson K, Burns S. Pupil location under mesopic, photopic and pharmacologically dilated conditions. *Invest Ophthalmol Vis Sci*. 2002;43:2508–2512.
22. Guirao A, Williams D, Cox I. Effect of rotation and translation on the expected benefit of an ideal method to correct the eyes higher-order aberrations. *J Opt Soc Am A*. 2001;18:1003–1015.
23. Ciccio AE, Durrie DS, Stahl JE, Schwendeman F. Ocular cyclotorsion during customized laser ablation. *J Refract Surg*. 2005;21:S772–S774.
24. Carones F. The influence of dynamic cyclotorsion during laser surgeries. Presented at the 24th Congress of the European Society of Cataract and Refractive Surgeons (ESCRS). London, UK, September 2006.
25. Uozato H, Guyton DL. Centering corneal surgical procedures. *Am J Ophthalmol*. 1987;103:264–275.
26. Marcos S, Barbero S, Llorente L, Merayo-Lloves J. Optical response to LASIK surgery for myopia from total and corneal aberration measurements. *Invest Ophthalmol Vis Sci*. 2001;42:3349–3356.
27. Marcos S. Aberrations and visual performance following standard Laser vision correction. *J Refract Surg*. 2001;17:S596–S601.
28. Bará S, Mancebo T, Moreno-Barriuso E. Positioning tolerances for phase plates compensating aberrations of the human eye. *Appl Opt*. 2000;39:3413–3420.
29. Bará S, Arines J, Ares J, Prado P. Direct transformation of Zernike eye aberration coefficients between scaled, rotated, and/or displaced pupils. *J Opt Soc Am A*. 2006;23:2061–2066.
30. Chernyak DA. Iris-based cyclotorsional image alignment method for wavefront registration. *IEEE Trans Biomed Eng*. 2005;52:2032–2040.
31. Schruender S, Fuchs H, Spasovski S, Dankert A. Intraoperative corneal topography for image registration. *J Refract Surg*. 2002;18:S624–S629.
32. Huang D, Arif M. Spot size and quality of scanning laser correction of higher-order wavefront aberrations. *J Cataract Refract Surg*. 2002;28:407–416.
33. Guirao A,Williams D, MacRae S. Effect of beam size on the expected benefit of customized laser refractive surgery. *J Refract Surg*. 2003;19:15–23.
34. Bueeler M, Mrochen M, Seiler T. Maximum permissible torsional misalignment in aberration-sensing and wavefront-guided corneal ablation. *J Cataract Refract Surg*. 2004;30:17–25.

Topic F THE EFFECTIVE OPTICAL ZONE AFTER REFRACTIVE SURGERY
(La zona óptica efectiva tras cirugía refractiva)

12. Samuel Arba-Mosquera and Thomas Hollerbach, “Ablation Resolution in Laser Corneal Refractive Surgery: The Dual Fluence Concept of the AMARIS Platform,” Advances in Optical Technologies, vol. 2010, Article ID 538541, 13 pages, 2010. doi:10.1155/2010/538541

AUTHOR CONTRIBUTIONS

Study concept and design (S.A.M.); data collection (M.C.); analysis and interpretation of data (S.A.M.); drafting (S.A.M.); critical revision (M.C.); statistical expertise (S.A.M.).

Hindawi Publishing Corporation
Advances in Optical Technologies
Volume 2010, Article ID 538541, 13 pages
doi:10.1155/2010/538541

Research Article

Ablation Resolution in Laser Corneal Refractive Surgery: The Dual Fluence Concept of the AMARIS Platform

Samuel Arba-Mosquera[1,2] and Thomas Hollerbach[1]

[1] *Research and Development Department, SCHWIND Eye-Tech-Solutions, 63801 Kleinostheim, Germany*
[2] *Grupo de Investigación de Cirugía Refractiva y Calidad de Visión, Instituto de Oftalmobiología Aplicada, University of Valladolid, 47011 Valladolid, Spain*

Correspondence should be addressed to Samuel Arba-Mosquera, samuel.arba.mosquera@eye-tech.net

Received 15 February 2010; Revised 21 June 2010; Accepted 8 July 2010

Academic Editor: Maria Calvo

Purpose. To evaluate to which extent individual Zernike terms can be corrected. Methods. Ablation time and fidelity was analysed using different fluence levels (range 90–2000 mJ/cm^2) and aspheric ablation profiles. With optimal parameters, the extent to which individual Zernike modes can be corrected was evaluated. *Results*. The range 188–565 mJ/cm^2 resulted as optimum fluence level with an optimum proportion range 50%–90% for high fluence. With optimal parameters, it corresponds to 2.4 s/D at 6 mm OZ, with fidelity variance of 53 μm RMS, and average ablation error of 0.5 μm for each location. Ablation simulation of coma Z[3,±1] showed 98,4% accuracy and 98% fit quality; trefoil Z[3,±3], 99,9% accuracy and 98% fit quality; spherical aberration Z[4,0], 96,6% accuracy and 97% fit quality; secondary astigmatism Z[4,±2], 97,9% accuracy and 98% fit quality. Real ablation on a flat plate of PMMA of coma Z[3,±1] showed 96,7% accuracy and 96% fit quality; trefoil Z[3,±3], 97,1% accuracy and 96% fit quality; spherical aberration Z[4,0], with 93,9% accuracy and 90% fit quality; secondary astigmatism Z[4,±2], with 96,0% accuracy and 96% fit quality. *Conclusions*. Ablation of aspherical and customised shapes based upon Zernike polynomials up to the the 8th order seems accurate using the dual fluence concept implemented at the AMARIS platform.

1. Introduction

With the introduction of the laser technologies for refractive surgery, the change of the corneal curvature to compensate in a controlled manner for refractive errors of the eye [1] is more accurate than ever. The procedure is nowadays a successful technique, due to its submicrometric precision and the high predictability and repeatability of corneal ablation accompanied by minimal side effects. Standard ablation profiles based on the removal of convex-concave tissue lenticules with spherocylindrical surfaces proved to be effective in the compensation of primary refractive errors. However, the quality of vision deteriorated significantly, especially under mesopic and low-contrast conditions [2].

With the introduction of wavefront analysis, it was proved that the conventional refractive LASER techniques were far from ideal, by measuring the aberrations induced by conventional algorithms and the aberrations induced by the LASIK flap cut itself.

With the LASIK (Laser in Situ Keratomileusis [3]) treatment, we have an accepted method to correct refractive errors such myopia [4], hyperopia [5], and astigmatism [6]. One of the most significant side effects in myopic LASIK, is the induction of spherical aberration [7], which causes halos and reduced contrast sensitivity [2]. However, the different laser platforms are always introducing new concepts and optimising their ablation profiles.

Since Laser refractive surgery was introduced, the technology rapidly improved. With the beginning of photoablation, the goal was to achieve predictable and stable results for myopic, hyperopic, and astigmatic corrections. Today's technology is far more advanced since sophisticated diagnostic instruments, such as aberrometers and topography systems, offer the challenge of improving the postoperative

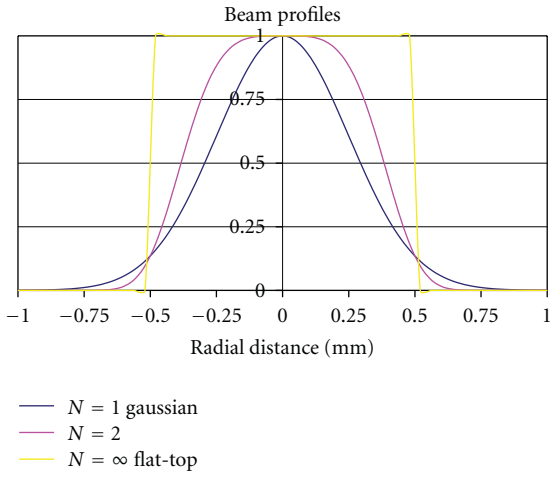

Figure 1: Beam profiles for different beam geometries. Gaussian profile in blue, supergaussian profile ($N = 2$) in pink, Flat-Top profile in yellow.

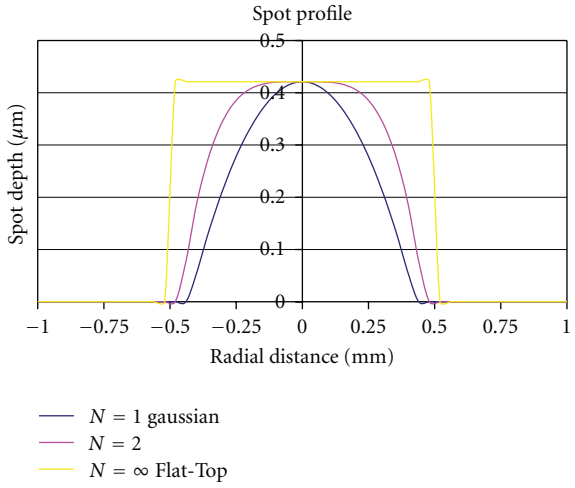

Figure 2: Spot profiles for different beam geometries. Parabolic spot profile (from Gaussian beams) in blue, quartic spot profile (from supergaussian ($N = 2$) beams) in pink, Flat-Top spot profile (from Flat-Top beams) in yellow.

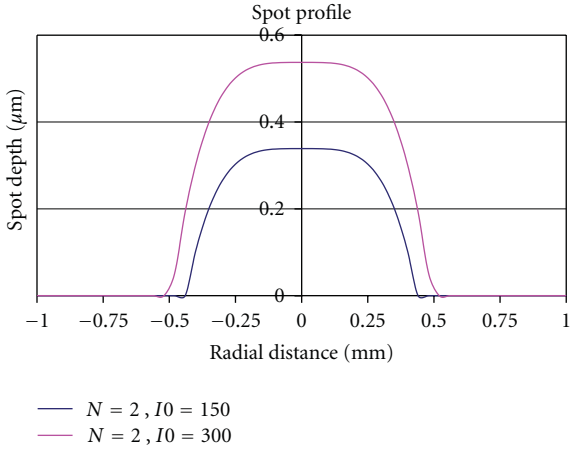

Figure 3: Spot profiles for different radiant exposures. Quartic spot profiles (from supergaussian ($N = 2$) beams) for a peak radiant exposure of 150 mJ/cm^2 in blue and for a peak radiant exposure of 300 mJ/cm^2 in pink.

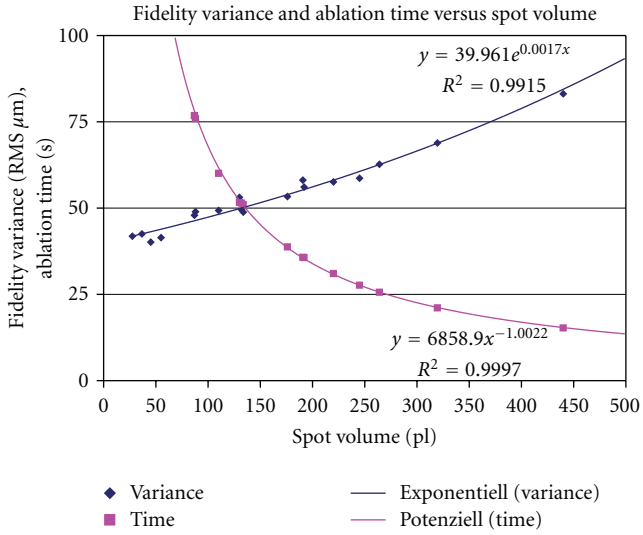

Figure 4: Fluence simulation results.

results in terms of visual acuity and night vision. At the same time, the better knowledge and understanding on refractive surgery by potential patients upgrades the required standard outcomes. Making more challenge finding new approaches towards the close-to-zero aberrations target results in several senses: (a) finding the sources of the induced aberrations due to laser refractive surgery, (b) developing "free-of-aberrations" ablation profiles, (c) developing ablation profiles to compensate the natural aberrations of any single eye in order to get a close-to-zero aberrations result.

To eliminate already existing aberrations, the so-called "customized" treatments were developed. Customisation of the ablation is possible either using wavefront measurements of the whole eye [8] (obtained, e.g., by Hartman-Shack wavefront sensors) or by using corneal topography-derived wavefront analyses [9, 10]. Topographic-guided [11], Wavefront-driven [12], Wavefront-optimized [13], Asphericity preserving, and Q-factor profiles [14] have all been put forward as solutions. Nevertheless, considerations such as treatment duration, tissue removal [15], tissue remodelling, and overall postoperative outcomes have made it difficult to establish a universal optimal profile.

Therefore, the topic "ablation resolution in laser corneal refractive surgery" is still worth to be analysed and considered, because its clinical implications are not yet deeply explored.

The real impact of ablation resolution in laser corneal refractive surgery is still discussed in a controversial way. The

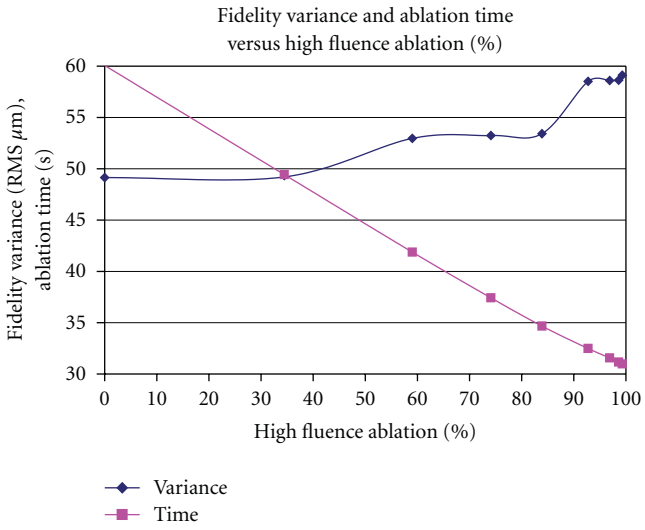

Figure 5: Dual fluence simulation results.

Table 1: AMARIS decision: single fluence concept.

Metric	High fluence	Low fluence
Fluence (pl)	220	110
Energy density (mJ/cm^2)	488	197
Ablation time (s)	31	60
Ablation time (s/D at 6 mm OZ)	2.1	4.0
Fidelity variance (μm RMS)	60	50
Ablation error (μm for each location)	0.575	0.475

aim of this work is to provide a simple and understandable theoretical frame explaining a possible method of ablation resolution optimisation.

Most of the systems available for laser refractive surgery include possibilities to customise the ablation, either based on topographical elevation or on corneal or ocular wavefront aberration.

2. Materials

To evaluate the technical capabilities to correct individual Zernike modes, and the extent to which individual Zernike modes can be corrected, the CAM software was used to plan the ablations, which were first simulated and then ablated onto flat PMMA plates with an AMARIS excimer laser (SCHWIND eye-tech-solutions GmbH, Kleinhostheim, Germany).

The AMARIS laser system works at a repetition rate of 500 Hz, produces a spot size of 0.54 mm (full width at half maximum (FWHM)) with a superGaussian ablative spot profile [16, 17]. High-speed eye-tracking with 1050 Hz acquisition rate is accomplished with 3-ms latency period [18]. The system delivers aspheric wavefront-customised profiles and including some optimisations: The aspheric

Table 2: AMARIS decision: dual fluence concept.

Metric	≈80% High fluence	+20% Low fluence
Fluence (pl)	220	110
Energy density (mJ/cm^2)	488	197
Ablation time (s)	35	
Ablation time (s/D at 6 mm OZ)	2.4	
Fidelity variance (μm RMS)	53	
Ablation error (μm for each location)	0.500	

profiles go beyond the Munnerlyn proposed profiles, and add some aspheric characteristics to balance the induction of spherical aberration (prolateness optimisation).

These particular case of aspheric profiles compensate for the aberrations induction observed with other types of profile definitions [19], some of those sources of aberrations are those ones related to the loss of efficiency of the laser ablation for nonnormal incidence [20–22].

Optimisation consisted to take into account the loss of efficiency at the periphery of the cornea in relation to the centre as there is a tangential effect of the spot in relation to the curvature of the cornea (Keratometry (K-reading)). The software provides K-reading compensation, which considers the change in spot geometry and reflection losses of ablation efficiency.

An optical zone of 6.50 mm in diameter was planned, a variable transition zone, to smooth the ablated area towards the nontreated cornea, was provided automatically by the software in relation to the refraction to be corrected.

Real ablative spot shape (volume) is considered through a self-constructing algorithm. In addition, there is a randomised flying-spot ablation pattern, and controls the local repetition rates to minimise the thermal load of the treatment [23] (smooth ablation, no risk of thermal damage). Therefore, the ablated surface after aspheric wavefront-customised profiles is very smooth, so that there are some benefits in higher order aberrations.

3. Method

Laser corneal refractive surgery is based on the use of a Laser (typically an excimer one) to change the corneal curvature to compensate for refractive errors of the eye. It has become the most successful technique, mainly due to the submicron precision and the high repeatability of the ablation of the cornea accompanied by minimal side effects. Laser refractive surgery is based upon the sequential delivery of a multiplicity of laser pulses each one removing (ablating) a small amount of corneal tissue.

From the blowoff model (derived form the Beer-Lambert's law), the real energy density absorbed at that point determines the ablation depth as

$$d_{ij} = \frac{\ln\left(I_{ij}\left(1 - R_{ij}\right)/I_{\mathrm{Th}}\right)}{\alpha_{\mathrm{Cornea}}}, \quad (1)$$

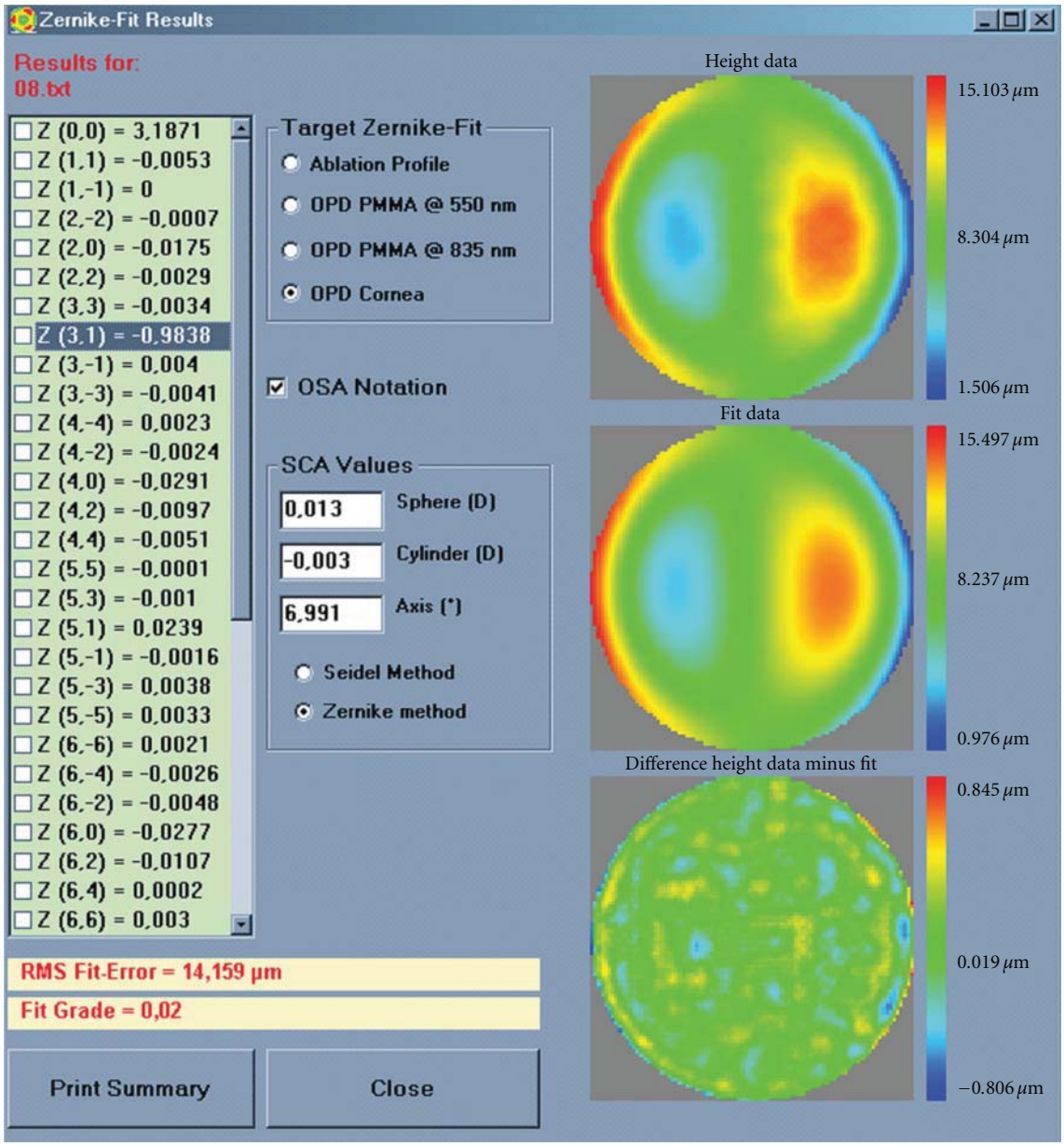

Figure 6: Ablation simulation of primary coma aberration Z[3, ±1], with 98,4% accuracy and 98% fit quality.

where d_{ij} is the actual depth per pulse at the location i, j; I_{ij} is the radiant exposure of pulse at the location i, j; R_{ij} is the reflectivity at the location i, j; I_{Th} is the corneal threshold; α_{Cornea} is the corneal absorption coefficient.

In general,

$$d(r) = \frac{\ln(I(r)(1 - R(r))/I_{\text{Th}})}{\alpha_{\text{Cornea}}}. \quad (2)$$

For different beam profiles we get different spot profiles as depicted in Figures 1 and 2.

For different radiant exposures with the same beam profiles, we get different spot profiles as displayed in Figure 3.

The problem of the spot profile and the radiant exposure of the system relies on the sequential delivery of a multiplicity of laser pulses each one ablating locally a small amount of corneal tissue, being the global process an integral effect. The higher the spot profile is, the higher the ablated volume per pulse limiting the resolution of the treatment.

There are several ways to avoid that problem.

(i) Reducing the radiant exposure improving the vertical resolution of the treatment.

(ii) Reducing the spot diameter improving the horizontal resolution of the treatment.

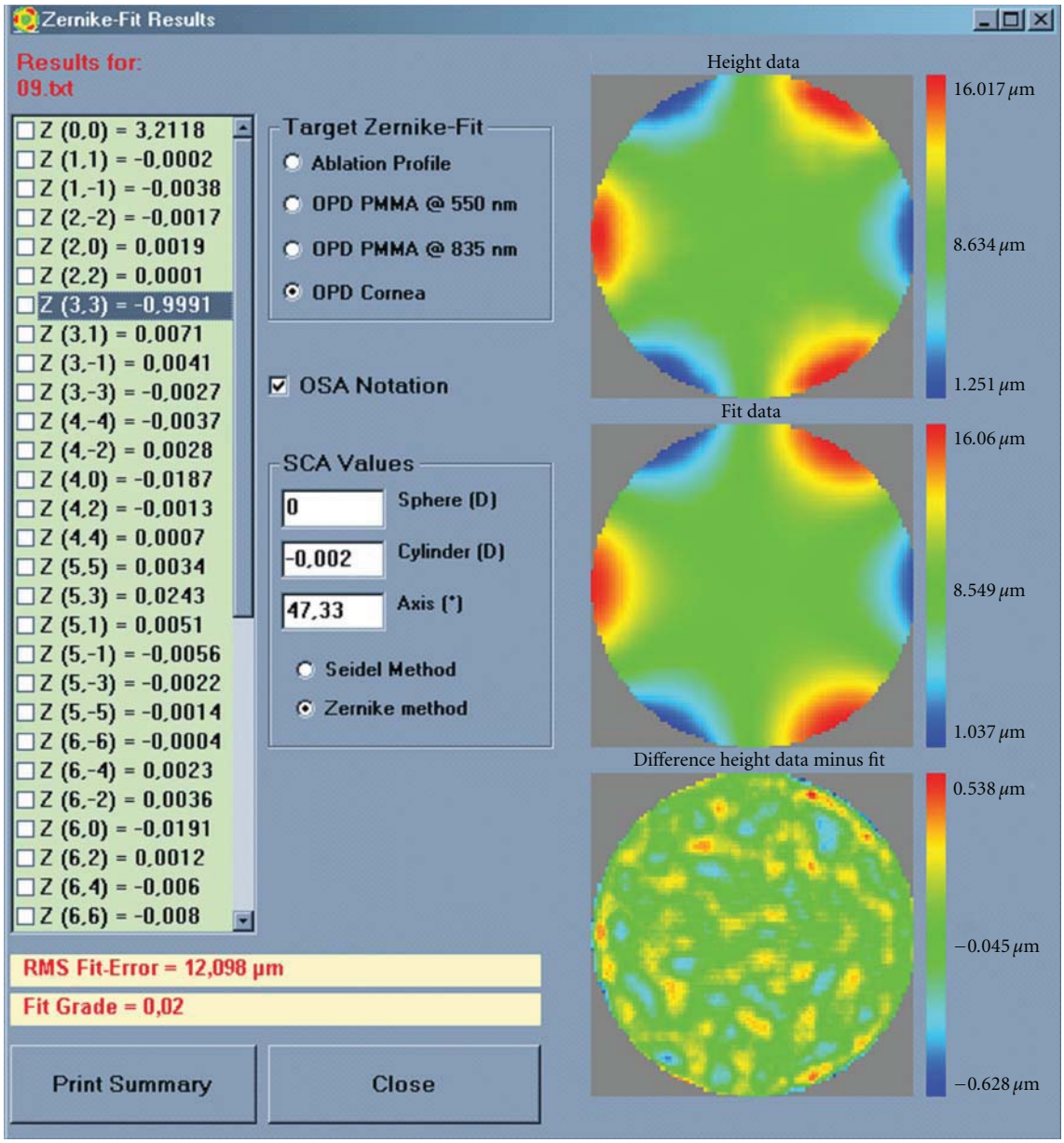

Figure 7: Ablation simulation of primary trefoil aberration Z[3, ±3], with 99,9% accuracy and 98% fit quality.

The problem of both alternatives is that they need extra time for the ablation procedure, which may produce another inconveniences.

The gained ablation volume has to be applied onto the cornea by thousands of single laser shots at different but partly repeated corneal positions, because the ablated volume of a single spot is much smaller than the ablation volume.

We have introduced as well some innovations concerning ablation shot file (sequences of pulses needed to carry out a refractive procedure) generation, in order to optimally remove the tissue corresponding to these state-of-the-art treatments, generating the sequence of laser shot coordinates in a way that

(i) guarantees a high fidelity reproduction of the given ablation volume line shape and
(ii) avoids vacancies and roughness of the cornea.

In this context, two opposed requirements define the fluence level.

(i) A short ablation time (favouring high fluence levels).

(ii) A high-fidelity ablation (favouring low fluence levels).

We have analysed ablation times and fidelity using fixed fluence levels ranging from 37 pl spot volume to 440 pl spot

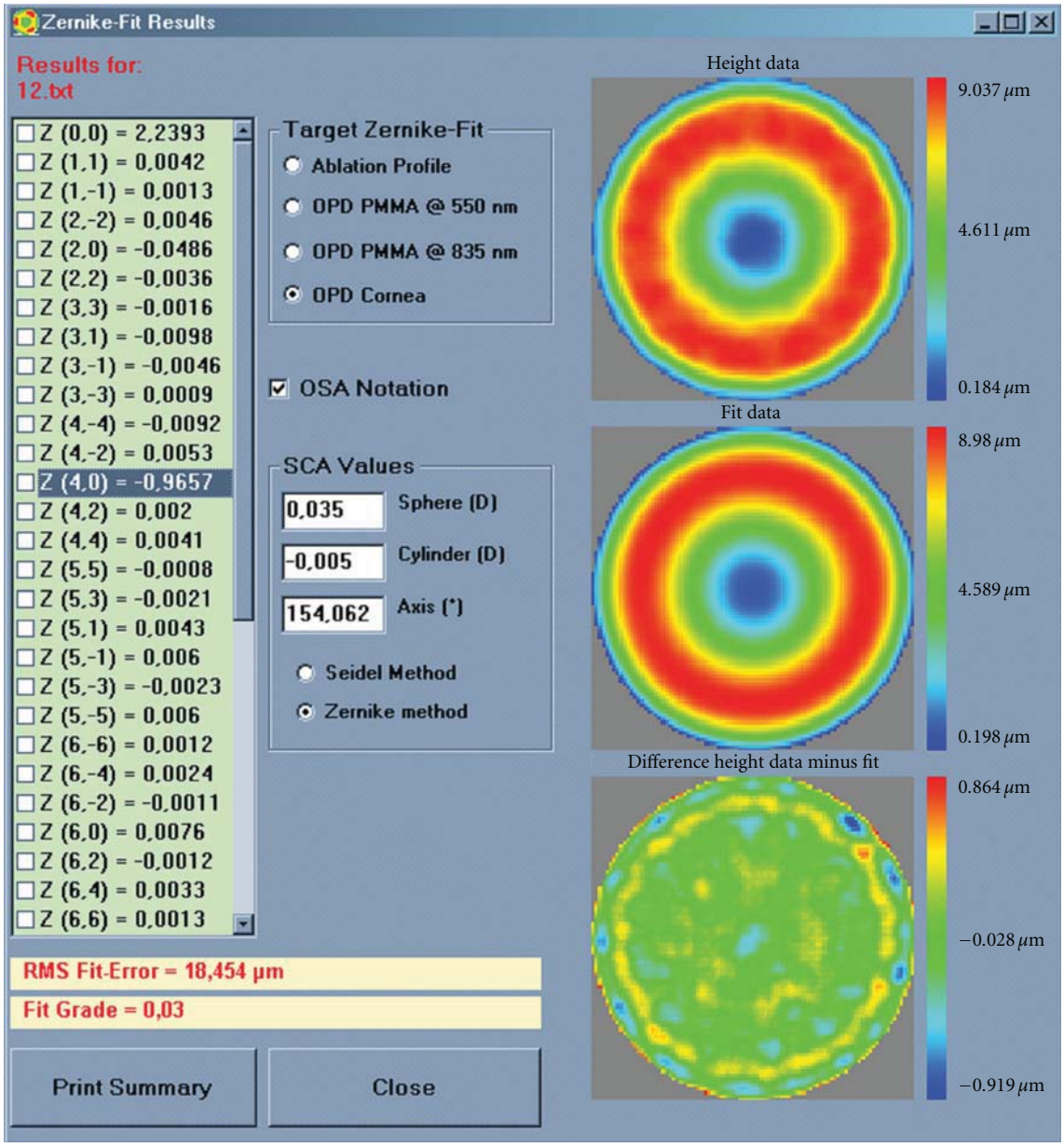

Figure 8: Ablation simulation of primary spherical aberration Z[4, 0], with 96,6% accuracy and 97% fit quality.

volume (corresponding to 90 mJ/cm^2 to 2000 mJ/cm^2 energy density, using as ablation volume the one corresponding to an aberration-free correction of −5.00 D–3.50 D × 15° at 6.50 mm OZ, 8.21 mm TAZ.

A second simulation was prepared upon the basis of a dual fluence level concept, using a variable rate from only low-fluence spots to only high-fluence spots using the same ablation volume for the correction of −5.00 D–3.50 D × 15° at 6.50 mm OZ, 8.21 mm TAZ.

With the optimal parameters we have evaluated the extent to which individual Zernike modes can be corrected, first simulated and then ablated onto flat PMMA plates.

4. Results

We have analysed ablation times and fidelity using fixed fluence levels ranging from 37 pl spot volume to 440 pl spot volume (corresponding to 90 mJ/cm^2 to 2000 mJ/cm^2 energy density, using as ablation volume the one corresponding to an aberration-free correction of −5.00 D–3.50 D × 15° at 6.50 mm OZ, 8.21 mm TAZ (Figure 4).

We have obtained as optimum fluence level a variable range from 105 pl spot volume to 240 pl spot volume, corresponding to 188 mJ/cm^2 to 565 mJ/cm^2 energy density with equivalent ablation time ranges from 60 seconds to 26 seconds, corresponding to 4.0 s/D to 1.7 s/D at 6 mm OZ and

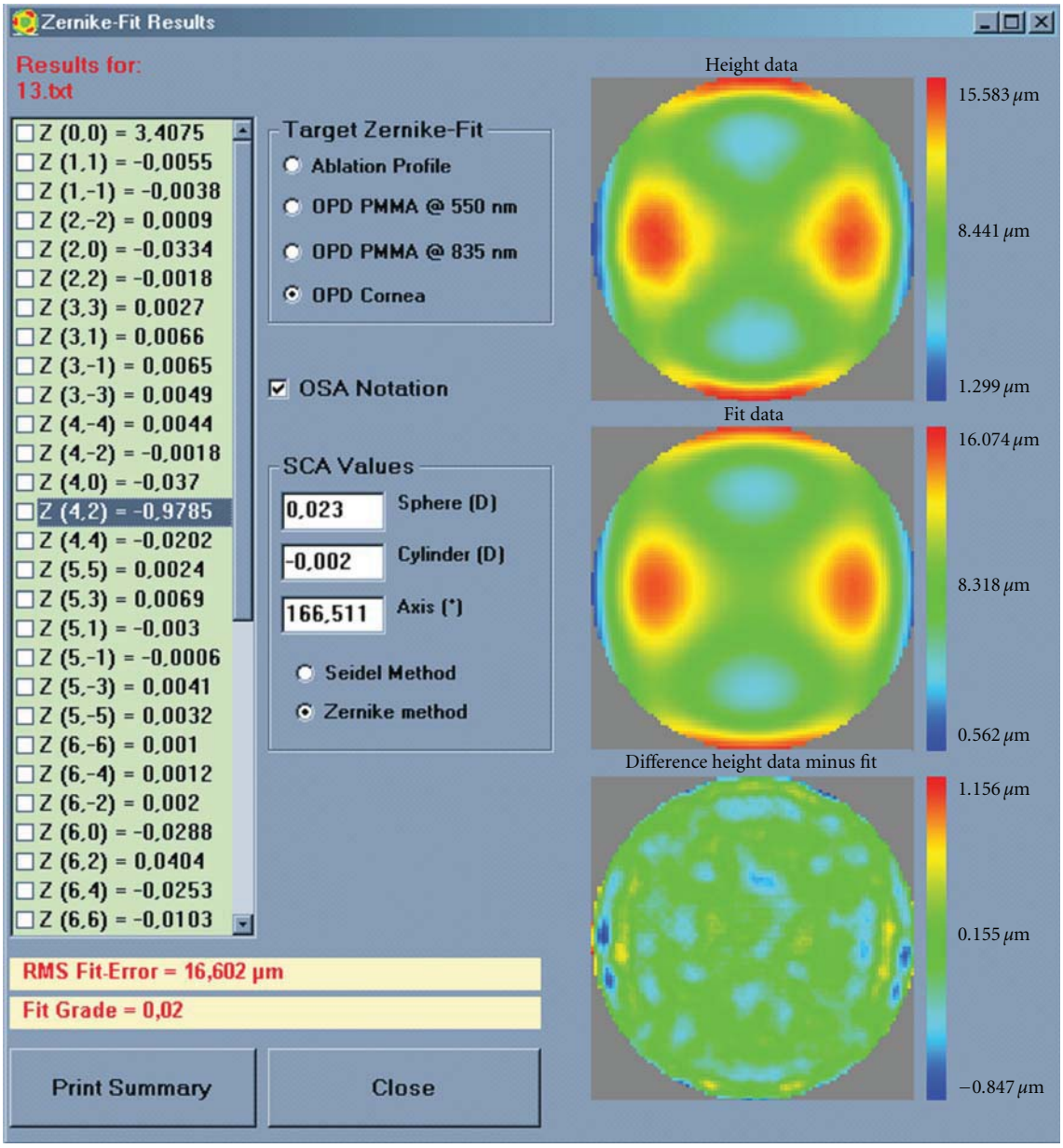

Figure 9: Ablation simulation of secondary astigmatism aberration Z[4, ±2], with 97,9% accuracy and 98% fit quality.

equivalent fidelity variance from 50 μm RMS to 60 μm RMS and average ablation error from 0.475 to 0.575 μm for each location (Table 1).

A second simulation was prepared upon the basis of a dual fluence level concept, using a variable rate from only low-fluence spots to only high-fluence spots using the same ablation volume for the correction of −5.00 D–3.50 D × 15° at 6.50 mm OZ, 8.21 mm TAZ (Figure 5).

We have obtained an optimum proportion range variable from 50% high fluence to 90% high fluence, with equivalent ablation time range from 45 seconds to 33 seconds, corresponding to 3.0 s/D to 2.2 s/D at 6 mm OZ, with equivalent fidelity variance from 52 μm RMS to 55 μm RMS, and average ablation error from 0.490 to 0.525 μm for each location (Table 2).

With the optimal parameters we have simulated the extent to which individual Zernike modes can be corrected (Figures 6, 7, 8, and 9, Table 3).

With the same parameters, we have evaluated the extent to which individual Zernike modes can be corrected, by ablating onto flat PMMA plates (Figures 10, 11, 12, and 13).

5. Discussion

We have evaluated to which extent individual Zernike terms can be corrected, by analysing ablation times and fidelity

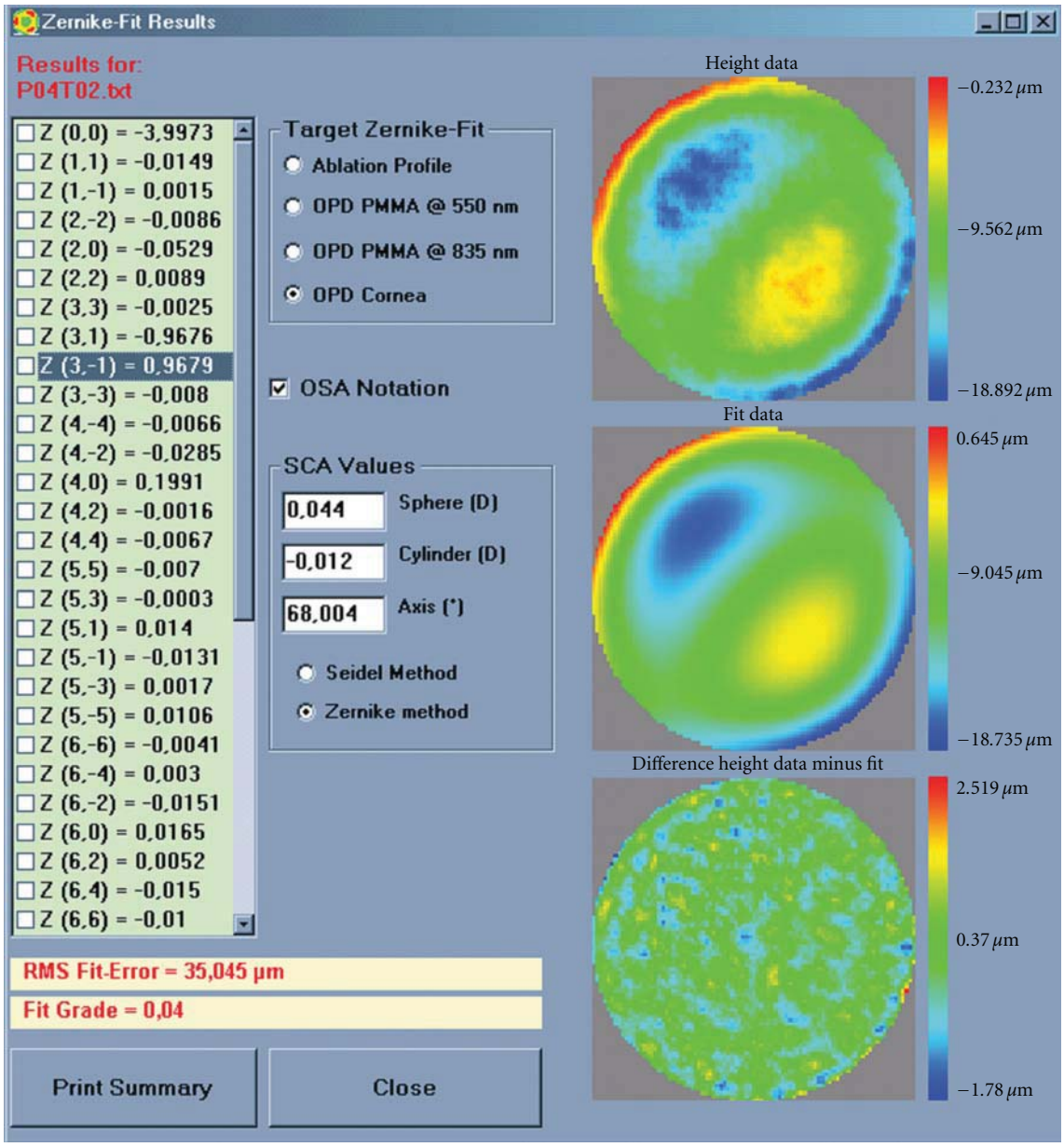

Figure 10: Ablation on a flat plate of PMMA of primary coma aberration Z[3, ±1], with 96,7% accuracy and 96% fit quality.

using different fluence levels (range 90–2000 mJ/cm^2), and aspheric ablation profiles, as well as, using a dual fluence level concept (variable rate from only low fluence to only high fluence pulses). With the optimal parameters, the extent to which individual Zernike modes can be corrected was simulated and ablated onto PMMA with a laser.

Huang and Arif [16] investigated the effect of laser spot size on the outcome of aberration correction with scanning laser corneal ablation using numerical simulation of ablation outcome of correction of wavefront aberrations of Zernike modes from second to eighth order. They modeled gaussian and top-hat beams from 0.6 to 2.0 mm full-width-half-maximum diameters, evaluated the fractional correction and secondary aberration (distortion), and used a distortion/correction ratio of less than 0.5 as a cutoff for adequate performance. The found that a 2 mm or smaller beam is adequate for spherocylindrical correction (Zernike second order), a 1 mm or smaller beam is adequate for correction of up to fourth order Zernike modes, and a 0.6 mm or smaller beam is adequate for correction of up to sixth order Zernike modes.

Guirao et al. [17] calculated that the success of a customized laser surgery attempting to correct higher order aberrations depends on using a laser beam that is small enough to produce fine ablation profiles needed to correct higher order aberrations. Simulating more than 100 theoretical customized ablations performed with beams of 0.5, 1.0, 1.5, and 2.0 mm in diameter, they calculated the

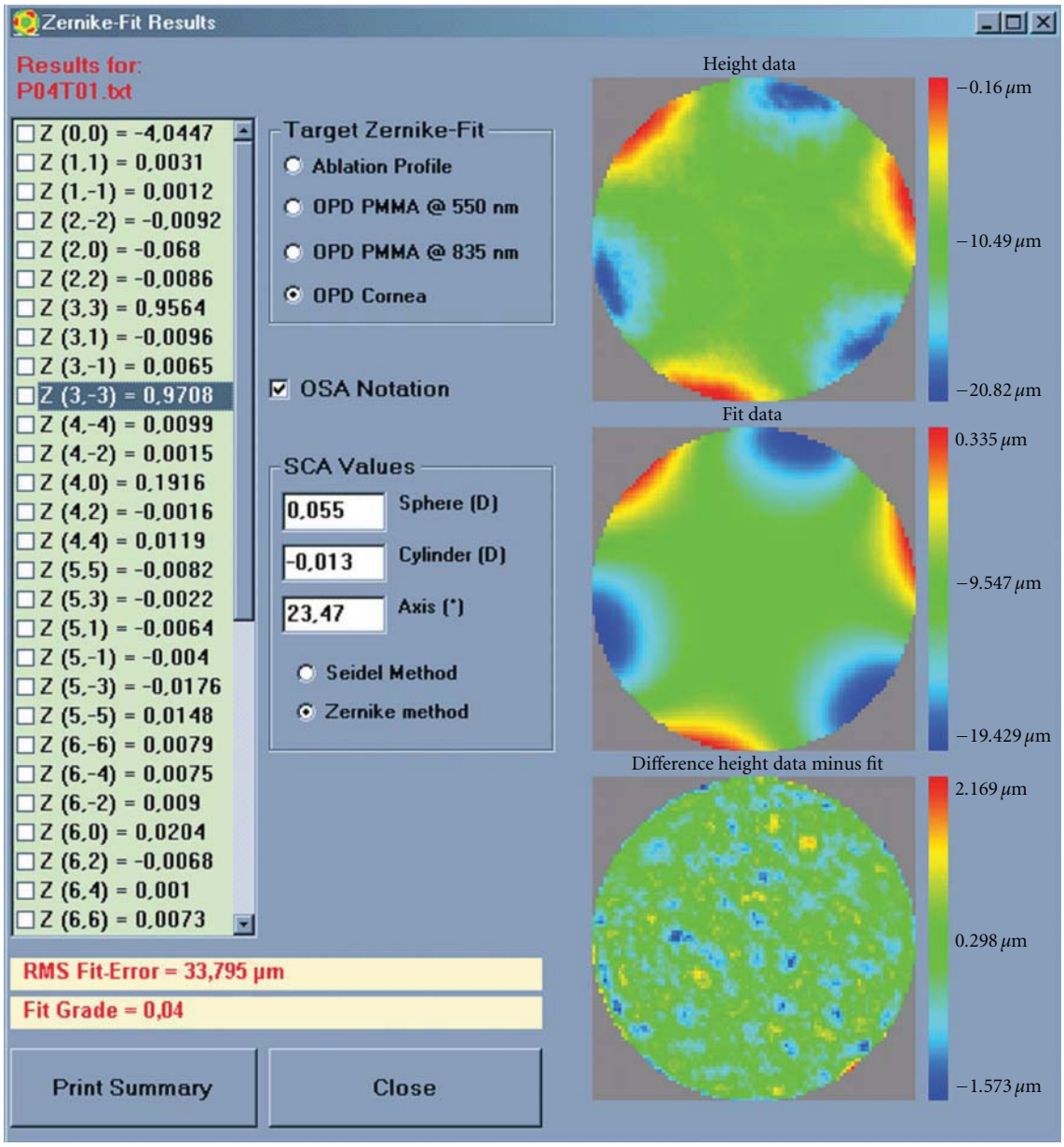

Figure 11: Ablation on a flat plate of PMMA of primary trefoil aberration Z[3, ±3], with 97,1% accuracy and 96% fit quality.

residual aberrations remaining in the eye and estimated the modulation transfer function (MTF) from the residual aberrations. They found that the laser beam acts like a spatial filter, smoothing the finest features in the ablation profile and that the quality of the correction declines steadily when the beam size increases. A beam of 2 mm was capable of correcting defocus and astigmatism. Beam diameters of 1 mm or less may effectively correct aberrations up to fifth order.

Pettit [24] claimed that the LADARVision system using a small fixed diameter excimer laser beam providing a consistent ablation per pulse, is able to ablate complex (higher order) corneal shapes accurately.

As demonstrated by Pedder et al. [25] and Jiménez et al. [26], the incorporation of models taking into account the angular dependence of laser-ablation rates as well as the effect of plume absorption can be important in efforts to improve the ablation algorithms used in refractive surgery. Differences in corneal power and corneal asphericity encountered when using this model can significantly affect the visual function of patients after LASIK. The high accuracy of determination of stroma plume absorption coefficients and the incorporation of this information in laser-ablation equations can improve the prediction of postsurgical corneal shape. More accurate values for postsurgical radius and asphericity could be achieved and thereby enhance emmetropization and correction of eye aberrations in refractive surgery. However, in case of AMARIS, the effect of the ablation plume could be not so siginificant since a debris removal system is incorporated.

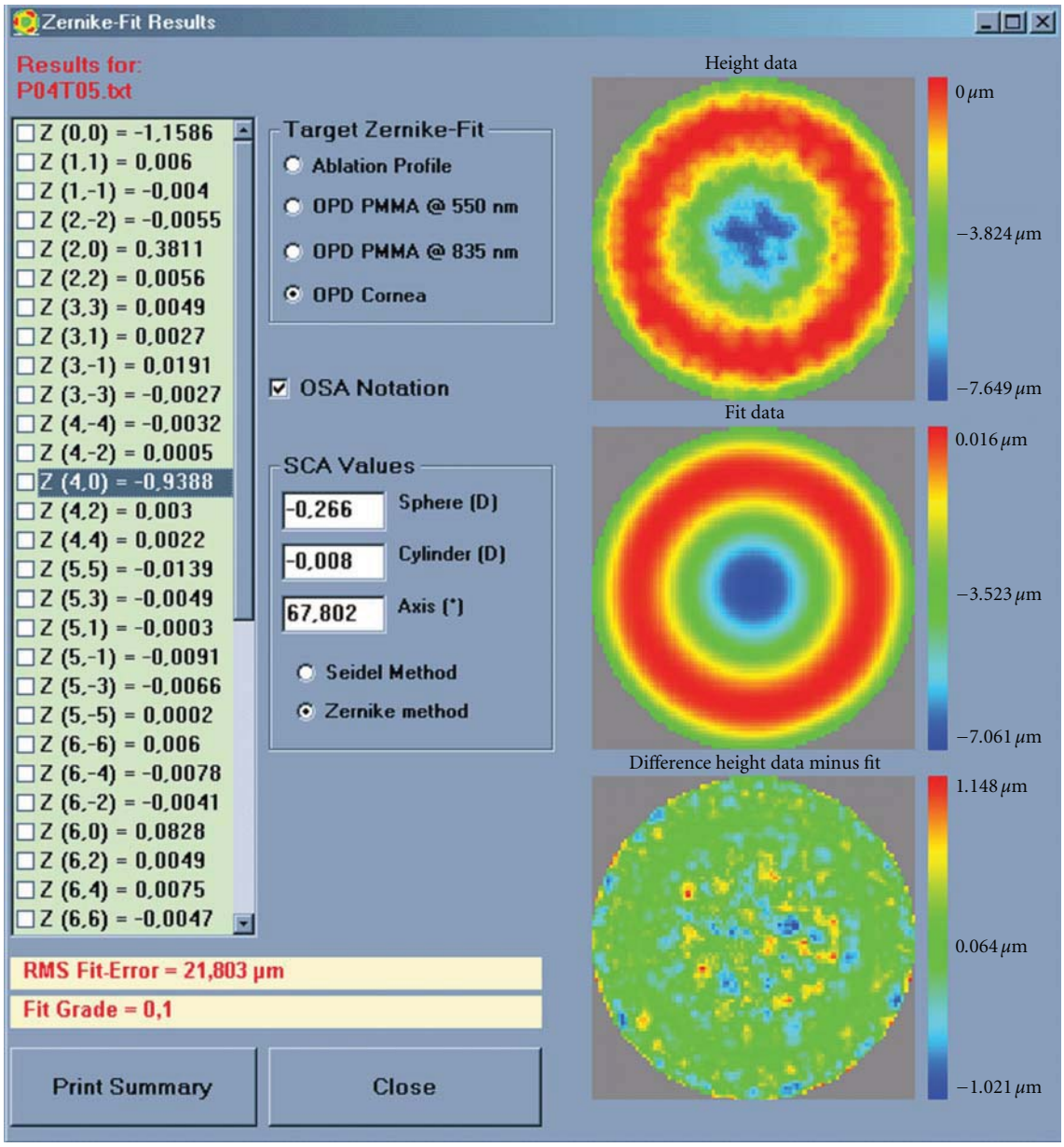

Figure 12: Ablation on a flat plate of PMMA of primary spherical aberration Z[4, 0], with 93,9% accuracy and 90% fit quality.

In our study, the range 188–565 mJ/cm^2 resulted as optimum fluence level for first simulation, and optimum proportion range 50%–90% high fluence for second one. With optimal parameters, it corresponds to 2.4 s/D at 6 mm OZ, with fidelity variance of 53 μm RMS, and average ablation error of 0.5 μm for each location.

Ablation simulation of coma Z[3, ±1], showed 98,4% accuracy, and 98% fit quality; trefoil Z[3, ±3], 99,9% accuracy and 98% fit quality; spherical aberration Z[4, 0], 96,6% accuracy and 97% fit quality; secondary astigmatism Z[4, ±2], 97,9% accuracy and 98% fit quality. Ablation on a flat plate of PMMA of coma Z[3, ±1], showed 96,7% accuracy and 96% fit quality; trefoil Z[3, ±3], 97,1% accuracy and 96% fit quality; spherical aberration Z[4, 0], with 93,9% accuracy and 90% fit quality; and secondary astigmatism Z[4, ±2], with 96,0% accuracy and 96% fit quality.

The proposed dual fluence concept uses a high-fluence "HF" and a low-fluence "LF" level. HF to speed up the treatment (minimised ablation time), LF to ensure the highest accuracy (maximised ablation smoothness). In our simulations results, HF takes out 220 pl vol per pulse (725 nm peak depth per pulse) whereas LF removes 110 pl vol per pulse (450 nm peak depth per pulse).

The amount of treatment that will receive HF pulses is optimised, to keep the overall quality of the ablation as good as possible (dynamically adjusted to speed up the treatment maintaining the highest accuracy). That means that 1 or 2 D will be made only by LF, but a higher diopter treatment

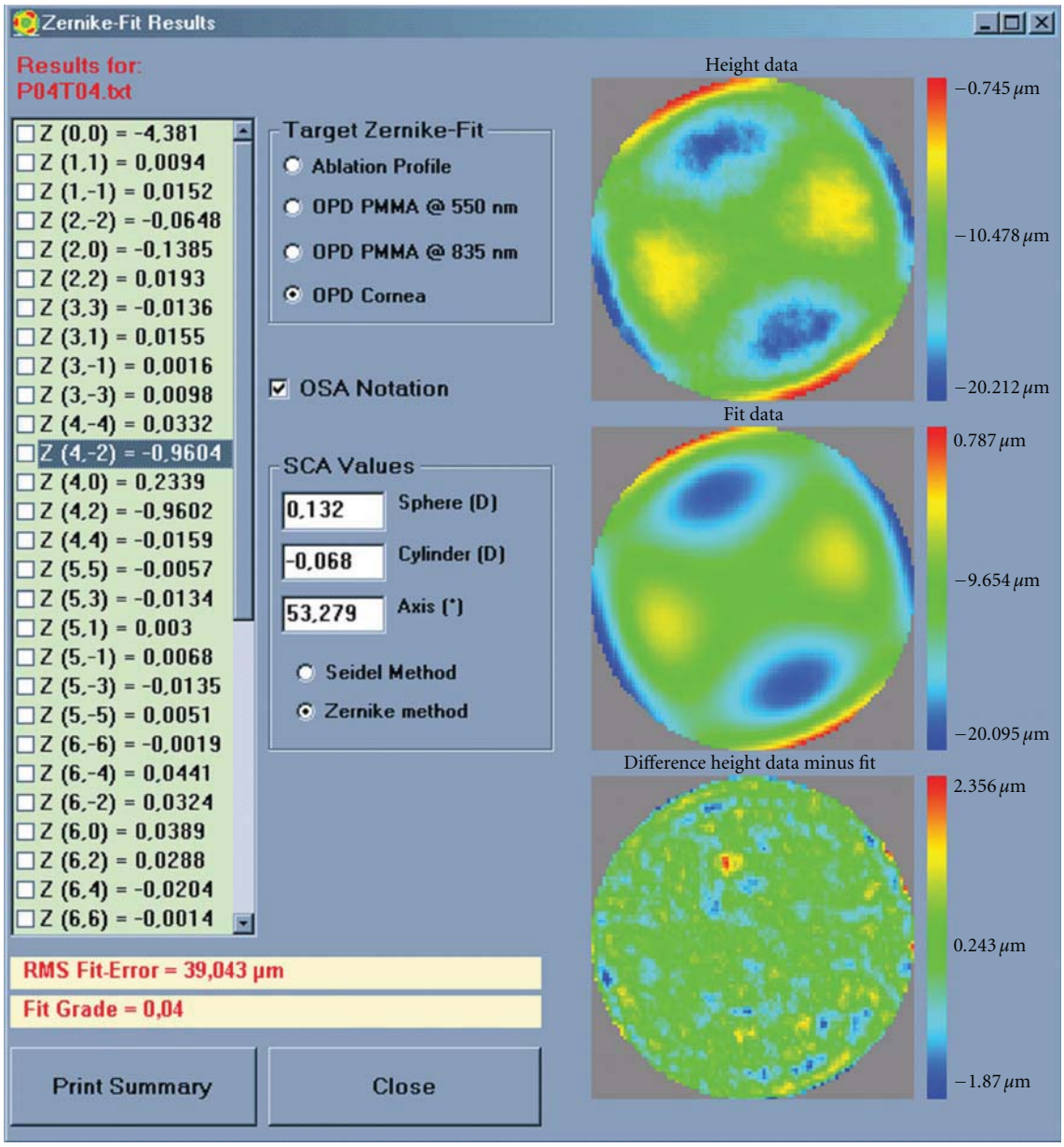

Figure 13: Ablation on a flat plate of PMMA of secondary astigmatism aberration Z[4, ±2], with 96,0% accuracy and 96% fit quality.

will be made up to 95% with HF. Typically, about 80% of the ablation will be performed at HF.

The system uses the "automatic fluence level adjustment" procedure for optimal ablation control. Depending on the planned refractive correction, about 80 percent of the corneal ablation is performed with a high fluence level speeding up the treatment. Fine correction is performed with a low fluence level improving the resolution. The advantage is that the laser treatment is significantly shortened, especially when higher refractive corrections are involved—without compromising on precision and safety.

The analysis of the clinical results specifically addressing customized treatments will show whether there are corneal discrepancies between real and expected shapes. Clinical outcomes published up to now show consistent results [27–30].

Ablation of aspherical and customised shapes based upon Zernike polynomials up the the 8th order seems accurate using the dual fluence concept implemented at the AMARIS platform.

In summary, this study demonstrated that it is possible to develop new algorithms and ablation strategies for efficiently performing laser corneal refractive surgery in a customised form. The availability of such profiles, potentially maximising visual performance without incresing the factors of risk, would be of great value for the refractive surgery community and ultimately for the health and safety of the patients.

Table 3

Zernike mode	Name	Simulation Accuracy (%)	Simulation Fit quality (%)	PMMA Accuracy (%)	PMMA Fit quality (%)
Z[3, ±1]	Primary coma	98,4	98	96,7	96
Z[3, ±3]	Primary trefoil	99,9	98	97,1	96
Z[4, 0]	Primary spherical aberration	96,6	97	93,9	90
Z[4, ±2]	Secondary astigmatism	97,9	98	96,0	96
Z[4, ±4]	Primary tetrafoil	99,4	99	97,9	96
Z[5, ±1]	Secondary coma	95,4	97	93,3	94
Z[5, ±3]	Secondary trefoil	96,7	97	94,6	94
Z[5, ±5]	Primary pentafoil	99,1	99	97,0	96
Z[6, 0]	Secondary spherical aberration	96,0	95	93,9	92
Z[6, ±2]	Tertiary astigmatism	91,3	97	89,3	94
Z[6, ±4]	Secondary tetrafoil	94,3	97	92,3	94
Z[6, ±6]	Primary hexafoil	99,0	98	96,9	95
Z[7, ±1]	Tertiary coma	83,5	94	81,7	91
Z[7, ±3]	Tertiary trefoil	86,5	95	84,6	92
Z[7, ±5]	Secondary pentafoil	93,0	96	91,0	93
Z[7, ±7]	Primary heptafoil	98,5	98	96,4	95
Z[8, 0]	Tertiary spherical aberration	76,4	89	74,8	86
Z[8, ±2]	Eighth order astigmatism	78,3	94	76,6	91
Z[8, ±4]	Tertiary tetrafoil	80,8	94	79,1	91
Z[8, ±6]	Secondary hexafoil	90,0	95	88,1	92
Z[8, ±8]	Primary octafoil	98,2	98	96,1	95

Further clinical evaluations on human eyes are needed to confirm the preliminary simulated results presented herein.

References

[1] C. R. Munnerlyn, S. J. Koons, and J. Marshall, "Photorefractive keratectomy: a technique for laser refractive surgery," *Journal of Cataract and Refractive Surgery*, vol. 14, no. 1, pp. 46–52, 1988.

[2] L. Mastropasqua, L. Toto, E. Zuppardi et al., "Photorefractive keratectomy with aspheric profile of ablation versus conventional photorefractive keratectomy for myopia correction: six-month controlled clinical trial," *Journal of Cataract and Refractive Surgery*, vol. 32, no. 1, pp. 109–116, 2006.

[3] L. Buratto, M. Ferrari, and P. Rama, "Excimer laser intrastromal keratomileusis," *American Journal of Ophthalmology*, vol. 113, no. 3, pp. 291–295, 1992.

[4] I. G. Pallikaris and D. S. Siganos, "Excimer laser in situ keratomileusis and photorefractive keratectomy for correction of high myopia," *Journal of Refractive and Corneal Surgery*, vol. 10, no. 5, pp. 498–510, 1994.

[5] K. Ditzen, H. Huschka, and S. Pieger, "Laser in situ keratomileusis for hyperopia," *Journal of Cataract and Refractive Surgery*, vol. 24, no. 1, pp. 42–47, 1998.

[6] M. A. El Danasoury, G. O. Waring III, A. El Maghraby, and K. Mehrez, "Excimer laser in situ keratomileusis to correct compound myopic astigmatism," *Journal of Refractive Surgery*, vol. 13, no. 6, pp. 511–520, 1997.

[7] E. Moreno-Barriuso, J. M. Lloves, S. Marcos, R. Navarro, L. Llorente, and S. Barbero, "Ocular aberrations before and after myopic corneal refractive surgery: LASIK-induced changes measured with laser ray tracing," *Investigative Ophthalmology and Visual Science*, vol. 42, no. 6, pp. 1396–1403, 2001.

[8] L. N. Thibos, X. Hong, A. Bradley, and R. A. Applegate, "Accuracy and precision of objective refraction from wavefront aberrations," *Journal of Vision*, vol. 4, no. 4, pp. 329–351, 2004.

[9] T. O. Salmon, *Corneal contribution to the Wavefront aberration of the eye*, PhD Dissertation, 1999.

[10] M. Mrochen, M. Jankov, M. Bueeler, and T. Seiler, "Correlation between corneal and total wavefront aberrations in myopic eyes," *Journal of Refractive Surgery*, vol. 19, no. 2, pp. 104–112, 2003.

[11] J. L. Alió, J. I. Belda, A. A. Osman, and A. M. M. Shalaby, "Topography-guided laser in situ keratomileusis (TOPOLINK) to correct irregular astigmatism after previous refractive surgery," *Journal of Refractive Surgery*, vol. 19, no. 5, pp. 516–527, 2003.

[12] M. Mrochen, M. Kaemmerer, and T. Seiler, "Clinical results of wavefront-guided laser in situ keratomileusis 3 months after surgery," *Journal of Cataract and Refractive Surgery*, vol. 27, no. 2, pp. 201–207, 2001.

[13] M. Mrochen, C. Donitzky, C. Wüllner, and J. Löffler, "Wavefront-optimized ablation profiles: theoretical background," *Journal of Cataract and Refractive Surgery*, vol. 30, no. 4, pp. 775–785, 2004.

[14] T. Koller, H. P. Iseli, F. Hafezi, M. Mrochen, and T. Seiler, "Q-factor customized ablation profile for the correction of myopic astigmatism," *Journal of Cataract and Refractive Surgery*, vol. 32, no. 4, pp. 584–589, 2006.

[15] D. Gatinel, J. Malet, T. Hoang-Xuan, and D. T. Azar, "Analysis of customized corneal ablations: theoretical limitations of

increasing negative asphericity," *Investigative Ophthalmology and Visual Science*, vol. 43, no. 4, pp. 941–948, 2002.

[16] D. Huang and M. Arif, "Spot size and quality of scanning laser correction of higher-order wavefront aberrations," *Journal of Cataract and Refractive Surgery*, vol. 28, no. 3, pp. 407–416, 2002.

[17] A. Guirao, D. R. Williams, and S. M. MacRae, "Effect of beam size on the expected benefit of customized laser refractive surgery," *Journal of Refractive Surgery*, vol. 19, no. 1, pp. 15–23, 2003.

[18] M. Bueeler and M. Mrochen, "Simulation of eye-tracker latency, spot size, and ablation pulse depth on the correction of higher order wavefront aberrations with scanning spot laser systems," *Journal of Refractive Surgery*, vol. 21, no. 1, pp. 28–36, 2005.

[19] S. Marcos, D. Cano, and S. Barbero, "Increase in corneal asphericity after standard laser in situ keratomileusis for myopia is not inherent to the Munnerlyn algorithm," *Journal of Refractive Surgery*, vol. 19, no. 5, pp. S592–S596, 2003.

[20] M. Mrochen and T. Seiler, "Influence of corneal curvature on calculation of ablation patterns used in photorefractive laser surgery," *Journal of Refractive Surgery*, vol. 17, no. 5, pp. S584–S587, 2001.

[21] J. R. Jiménez, R. G. Anera, L. Jiménez del Barco, and E. Hita, "Effect on laser-ablation algorithms of reflection losses and nonnormal incidence on the anterior cornea," *Applied Physics Letters*, vol. 81, no. 8, pp. 1521–1523, 2002.

[22] J. R. Jiménez, R. G. Anera, L. J. Del Barco, E. Hita, and F. Pérez-Ocón, "Correction factor for ablation algorithms used in corneal refractive surgery with gaussian-profile beams," *Optics Express*, vol. 13, no. 1, pp. 336–343, 2005.

[23] T. Bende, T. Seiler, and J. Wollensak, "Side effects in excimer corneal surgery. Corneal thermal gradients," *Graefe's Archive for Clinical and Experimental Ophthalmology*, vol. 226, no. 3, pp. 277–280, 1988.

[24] G. H. Pettit, "The Alcon/Summit/Autonomous perspective on fixed vs. variable spot ablation," *Journal of Refractive Surgery*, vol. 17, no. 5, pp. S592–S593, 2001.

[25] J. E. A. Pedder, A. S. Holmes, and P. E. Dyer, "Improved model for the angular dependence of excimer laser ablation rates in polymer materials," *Applied Physics Letters*, vol. 95, no. 17, Article ID 174105, 2009.

[26] J. R. Jiménez, J. J. Castro, C. Ortiz, and R. G. Anera, "Testing a model for excimer laser-ablation rates on corneal shape after refractive surgery," *Optics Letters*, vol. 35, p. 1789, 2010.

[27] M. C. Arbelaez and A. S. Mosquera, "The SCHWIND AMARIS total-tech laser as an all-rounder in refractive surgery," *Middle East African Journal of Ophthalmology*, vol. 16, no. 1, pp. 46–53, 2009.

[28] M. C. Arbelaez, I. M. Aslanides, C. Barraquer et al., "LASIK for myopia and astigmatism using the SCHWIND AMARIS excimer laser: an international multicenter trial," *Journal of Refractive Surgery*, vol. 26, no. 2, pp. 88–98, 2010.

[29] M. C. Arbelaez, T. Ewering, and S. A. Mosquera, "Decision assistant wizard to standardize optimal outcomes in excimer laser refractive corneal surgery," *Journal of Refractive Surgery*, vol. 25, pp. 1–11, 2010.

[30] M. Camellin and S. A. Mosquera, "Aspheric optical zones: the effective optical zone with the SCHWIND AMARIS," *Journal of Refractive Surgery*, vol. 19, pp. 1–12, 2010.

Topic G **METHOD TO OBJECTIVELY MINIMISE THE ABLATED TISSUE OF A CUSTOMISED ABLATION BASED ON THE ZERNIKE EXPANSION OF THE WAVEFRONT ABERRATION**

(Método para minimizar objetivamente la cantidad de tejido resecado en una ablación personalizada basada en la expansión de Zernike de la aberración del frente de onda)

13. Arba Mosquera S, de Ortueta D, Merayo-Lloves J. Tissue-Saving Zernike Terms Selection in Customized Treatments for Refractive Surgery. J Optom; 2009; 2: 182-196

AUTHOR CONTRIBUTIONS

Study concept and design (S.A.M.); data collection (D.O., M.R., C.V.); analysis and interpretation of data (S.A.M.); drafting (S.A.M.); critical revision (D.O., J.M., J.L.A., T.H., M.C.A.); statistical expertise (S.A.M.).

Tissue-Saving Zernike Terms Selection in Customized Treatments for Refractive Surgery

Samuel Arba-Mosquera[1,2], Diego de Ortueta[3] and Jesús Merayo-Lloves[1]

ABSTRACT

Purpose: To study the possibility of performing customized refractive surgery minimising the amount of ablated tissue without compromising visual quality.

Methods: A new algorithm for the selection of an optimized set of Zernike terms in customized treatments for laser corneal refractive surgery was developed. Its tissue saving attributes have been simulated on 100 different wave aberrations at 6mm diameter. Outcomes were evaluated in terms of how much depth and volume was saved for each condition (in micrometers and in percentage), whether the proposed correction consists of either a full wavefront correction or an aberration-free treatment, and whether the proposed depth or volume was less than the one required for the equivalent aberration-free treatment.

Results: Simulated outcomes showed an average saved depth of 5µm (0-16µm), and an average saved volume of 95µl (0-127µl) or 11% saved tissue (0-66% saved tissue). Proposed corrections were always less deep than full wavefront corrections and in 59% of the cases were less deep than equivalent aberration-free treatments.

Conclusions: Even though Zernike modes decomposition is a mathematical description of the aberration, it is not the aberration itself. Not all Zernike modes affect the optical quality in the same way. The eye does not see through Zernike decomposition but with its own aberration pattern. However, it seems feasible to efficiently perform laser corneal refractive surgery in a customized form minimising the amount of ablated tissue without compromising the visual quality. Further clinical evaluations on human eyes are needed to confirm the preliminary simulated results presented herein.
(J Optom 2009;2:182-196 ©2009 Spanish Council of Optometry)

Key Words: refractive surgery; visual quality; Zernike; tissue saving; wavefront; aberrations; depth; volume; time; aberration-free; free of aberrations; diffraction limited.

RESUMEN

Objetivo: Estudiar la posibilidad de realizar tratamientos personalizados de cirugía refractiva donde se minimice la cantidad de tejido ablacionado sin que por ello se vea afectada la calidad visual.

Métodos: Se ha desarrollado un nuevo algoritmo para seleccionar un conjunto optimizado de términos de Zernike para su aplicación en tratamientos personalizados de cirugía refractiva corneal. Para 100 mapas de aberración de onda corneal (para un tamaño de pupila de 6 mm de diámetro), se ha simulado la capacidad de dicho algoritmo para preservar tejido corneal. El resultado de dicha simulación se ha analizado en función de cuanto espesor (en micras) o de cuanto volumen (en %) se preserva en cada situación (respecto a otra situación de referencia): si la corrección propuesta logra corregir todo el frente de onda o sólo las aberraciones de segundo orden, y si el espesor o el volumen que hay que ablacionar con esta configuración es menor que para un tratamiento estándar equivalente, donde se traten de corregir únicamente las aberraciones de segundo orden.

Resultados: Las simulaciones arrojaron un "ahorro" promedio de tejido ablacionado igual a 5 µm en términos de espesor máximo que se ha de ablacionar (rango: 0-16 µm), igual a 95 µl en términos de volumen (rango: 0-127 µl); esto es, se preserva un 11% del tejido (rango: 0-66%) respecto al tratamiento de referencia. Las correcciones propuestas siempre requerían espesores ablacionados menores que los patrones diseñados para corregir todo el frente de onda, y en el 59% de los casos requerían incluso un espesor menor que los tratamientos estándar (aquellos en los que se pretende corregir únicamente las aberraciones de segundo orden).

Conclusiones: A pesar de que la descomposición en modos de Zernike es una descripción matemática de un patrón de aberración dado, no se corresponde exactamente con dicha aberración. No todos los modos de Zernike tienen el mismo efecto sobre la calidad óptica. El ojo no percibe su entorno "a través de" una descomposición en modos de Zernike de la aberración de onda, sino que se ve afectado por todo su propio patrón de aberración, de manera conjunta. Sin embargo, parece factible el llevar a cabo de manera eficiente tratamientos personalizados de cirugía refractiva corneal donde se minimice la cantidad de tejido ablacionado sin que por ello se vea afectada la calidad visual.

Es necesario hacer más estudios en ojos humanos reales para poder confirmar los resultados preliminares de las simulaciones que aquí se presentan.
(J Optom 2009;2:182-196 ©2009 Consejo General de Colegios de Ópticos-Optometristas de España)

Palabras Clave: cirugía refractiva; calidad visual; Zernike; preservación de tejido; frente de onda, aberraciones; espesor; volumen; tiempo; sin aberraciones (de segundo orden); libre de aberraciones (de segundo orden); limitado por difracción.

From the [1]Instituto de Oftalmobiología Aplicada, University of Valladolid, Spain. [2]Schwind eye-tech-solutions, Kleinostheim, Germany. [3]Augenzentrum Recklinghausen, Recklinghausen, Germany.

Acknowledgements: This paper is part of the Arba-Mosquera's doctoral thesis project at the Instituto Universitario de Oftalmobiología Aplicada (IOBA) in partial fulfilment of the requirements for the academic degree of Doctor of Philosophy (PhD) in Sciences of Vision, Research Group "Cirugía Refractiva y Calidad de Visión".

Received: 12 January 2009
Revised: 4 June 2009
Accepted: 25 June 2009

Corresponding author: Samuel Arba Mosquera.
Schwind eye-tech-solutions
e-mail: samuel.arba.mosquera@eye-tech.net

Introduction

With the introduction of laser technology for refractive surgery, the procedure of changing the curvature of the cornea in a controlled manner[1] to compensate for refractive errors of the eye is nowadays more accurate than ever. However, the quality of vision still deteriorates significantly, especially under mesopic and low-contrast conditions.[2]

With the LASIK (laser in-situ keratomileusis)[3] treatment, we have an accepted method for correcting refractive errors such as myopia,[4] hyperopia,[5] and astigmatism.[6] One of the

most significant side effects in myopic LASIK is the induction of spherical aberration,[7] which causes halos, and a reduction of contrast sensitivity.[2]

Although the optical quality of the eye can be described in terms of the aberration of its wavefront, it was observed that the subjects with minor aberrations in their wavefront did not always achieve the best scores in visual-quality tests.[8] Thus, the optical quality of the human eye does not determine in a one-to-one way its visual quality.

However, the induction of aberrations, such as spherical aberrations and coma, has been related to a loss of visual acuity.[9] Finally, the concept of neural compensation suggests that the neural visual system is adapted to the eye's own aberration pattern. A study by Artal et al.[10] on the effects that this neural compensation causes on the visual function indicates that the visual quality we have is somewhat superior to the optical quality that our eye provides.

To avoid inducing aberrations, as well as to eliminate the existing aberrations, "customized" treatments were developed. Customization of the ablation procedure is possible, either using wavefront measurements of the whole eye[11] (obtained, e.g., by means of Hartman-Shack wavefront sensors) or by using corneal topography-derived wavefront analyses.[12,13] Topography-guided,[14] wavefront-guided,[15] wavefront-optimized,[16] asphericity-preserving, and Q-factor profiles[17] have all been put forward as solutions. Considerations such as the duration of the treatment, removal[18] and remodelling of tissue, and, in general, the overall surgical outcome have made it difficult to establish a universal optimum profile. These considerations are interrelated in a multifactorial way, and may lead to clinical problems as corneal dehydration, ectasia or regression.

The development of new algorithms or ablation strategies for performing laser corneal refractive surgery in a customized form minimising the amount of ablated tissue without compromising the visual quality becomes an important challenge.

The availability of such profiles, potentially maximising visual performance without increasing the risk factors, would be of great value for the refractive surgery community and, ultimately, for the patients' health and safety. Therefore, the topic "Optimized Zernike Term Selection in customized treatments for laser corneal refractive surgery" (OZTS) is worth to be analysed, because its clinical implications are not yet deeply explored.

The real impact of tissue-saving algorithms in customized treatments is still discussed in a controversial way. The problem of minimising the amount of tissue that is removed is that it must be done in such a way that: a) does not compromise the refractive correction; b) does not compromise visual performance; c) is safe, reliable and reproducible.

The goal of this study is to describe in detail the theoretical framework, explaining a possible method of tissue-saving optimisation and exploring its tissue-saving capabilities.

Patients and Materials

To simulate the tissue-saving capabilities of such methods for minimising the required amount of ablated tissue, the complete records (together with their clinical data) corresponding to one-hundred eyes of fifty-five patients (39 (71%) male and 16 (29%) female) from the Augenzentrum Recklinghausen (Germany) were selected to be included in our simulation experiment. Fifty-five were right eyes (55%), and forty-five were left eyes (45%).

The mean age was 32±8 years (ranging from 19 to 54). The spherical equivalent (SE) was 1.60 D with a standard deviation (SD) of 3.44 D (range 9.75 to +7.50 D), with a mean sphere of -0.85±3.08 D (SD) (range 8.25 to +7.50 D), the mean cylinder was 1.51±1.42 D (SD) (range 5.75 to 0.00 D).

Using the Keratron-Scout videokeratoscope[19] (Optikon 2000, Rome, Italy), corneal wave aberrations were analysed up to the 7th Zernike order. Optical errors are described by means of the weight coefficients of the Zernike polynomials,[20] following the standards of the Optical society of America (OSA).[21]

For the purpose of the present work, SciLab™ was used for performing calculations and running the simulations, Microsoft™ Excel for plotting graphs, and Delphi's programming language was used for implementing the modules in the Optimized Refractive Keratectomy (ORK) and the Custom Ablation Manager (CAM). To simulate the tissue-saving capabilities of such algorithms for minimising the required amount of ablated tissue, the CAM module with a newly implemented Optimized Zernike Terms Selection (OZTS) was used.

Methods

In our study, the quadratic equivalent of a wave-aberration map was used as a relationship between wavefront-error magnitudes and classical ametropias *(Appendix 1).*That quadratic is a sphero-cylindrical surface, which approximates the wave aberration map. The idea of approximating an arbitrary surface with a quadratic equivalent is a simple extension of the ophthalmic technique of approximating a sphero-cylindrical surface with an equivalent sphere.

For this study, a variation of the objective wavefront refraction from low-order Zernike modes at a fixed subpupil diameter of 4 mm was chosen as starting point to objectively include the measured subjective manifest refraction in the wave aberration *(Appendix 2).*

The expected optical impact of high-order aberrations in the refraction is calculated and modified from the input manifest refraction. The same wave aberration is analysed for two different diameters: for the full wavefront area (6 mm in this study) and for a fixed subpupil diameter of 4 mm. The difference in refraction obtained for each of the two diameters corresponds to the manifest refraction associated to the high-order aberrations.

The condition is to re-obtain the input manifest refraction for the subpupil diameter of 4 mm. This way, the low-order parabolic terms of the modified wave aberration for the full wavefront area can be determined. An explanation of this Automatic Refraction Balance concept is provided in *figure 1.*

Figures 2 and *3* show examples of how the automatic manifest refraction balance algorithm works.

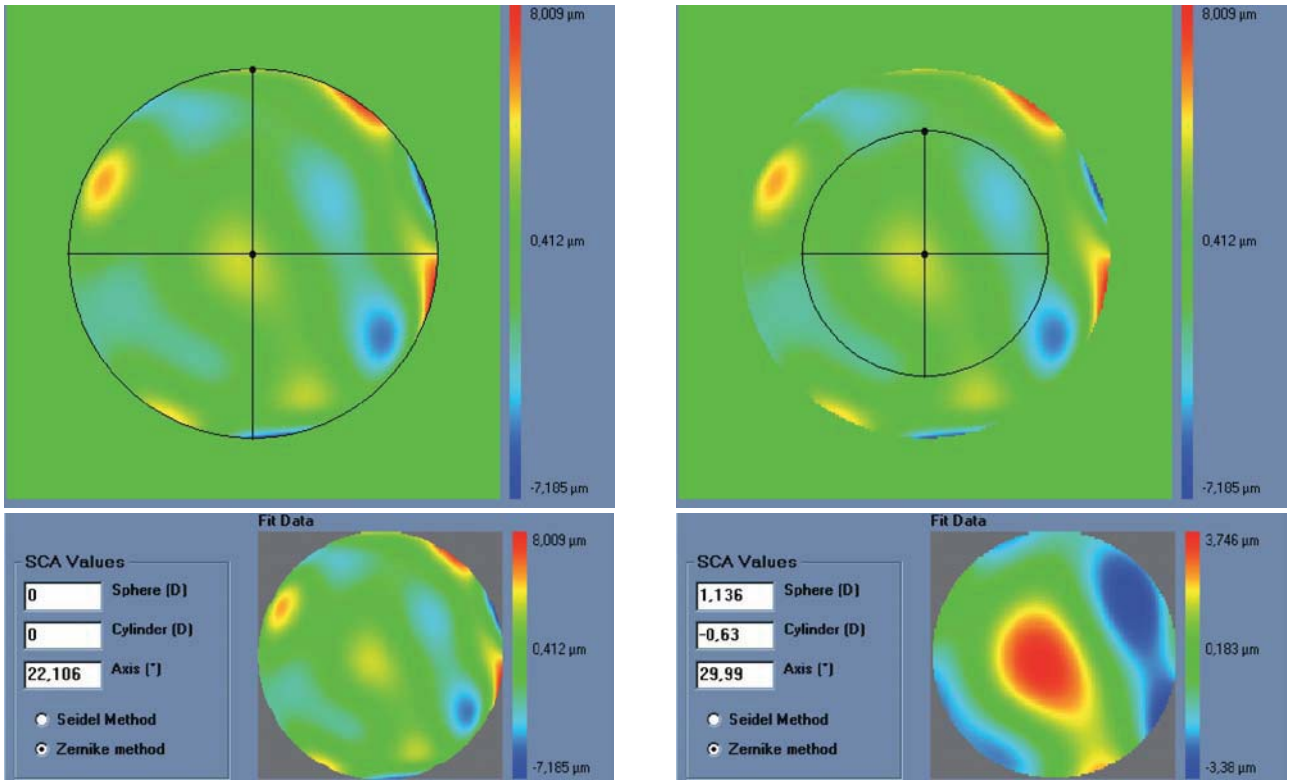

FIGURE 1
Automatic Refraction Balance. Optical impact of the HOA the refraction is calculated and balanced from input refraction. Notice that the same wave aberration is analysed for two different pupil diameters. The difference in the resulting refraction for these two diameters correspond to the manifest refraction associated to high-order aberrations.

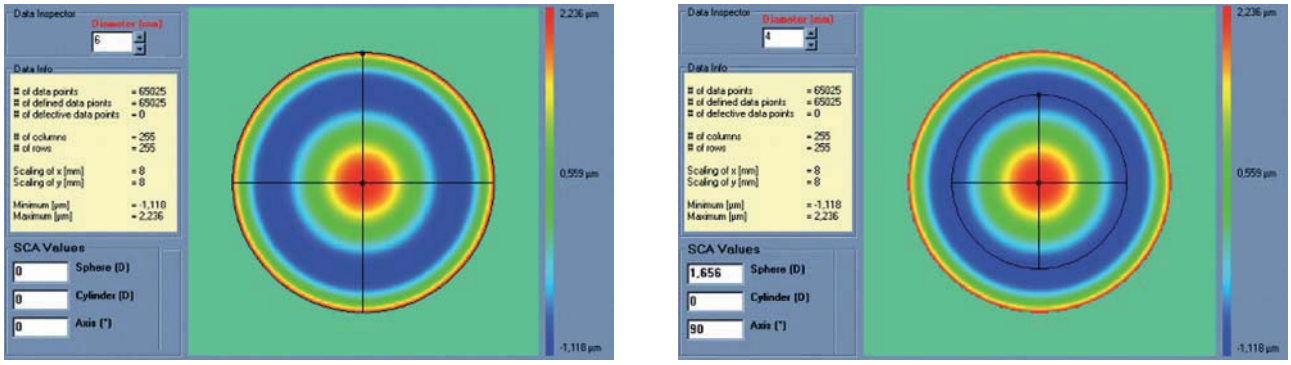

FIGURE 2
Left: Zernike refraction, for a 6 mm pupil size, of pure spherical aberration (SA). This refraction is per definition equal to 0 because SA is a high-order aberration mode. Right: Zernike refraction of the same wave aberration when analysed for a smaller pupil diameter (4 mm): SA (a high-order aberrations), when analysed for a smaller diameter, produces defocus. Explanation why a high-order aberration influences the low orders (refraction) when analysed for smaller diameters: for a full pupil (6 mm) the eye is affected by a SA producing some multifocality but without defocus; for a smaller pupil (4 mm), the optical aberration of the eye is the same but the outer ring is blocked. Thereby, the eye sees the world through the central part of a SA that resembles, in this case, a hyperopic profile producing some defocus (low-order refraction).

Objective Determination of the Actual Clinical Relevance of Each Separate Term in the Zernike Expansion of the Wave Aberration

A simple approach for the classification of the clinical relevance of individual aberration terms was proposed by Thibos et al.,[22] by introducing the concept of equivalent defocus (DEQ) as a metric to minimise the differences in the Zernike coefficients due to different pupil sizes.

Equivalent defocus is defined as the amount of defocus required to produce the same wavefront variance as found in one or more higher-order aberrations. A simple formula allows us to compute the equivalent defocus in dioptres if we

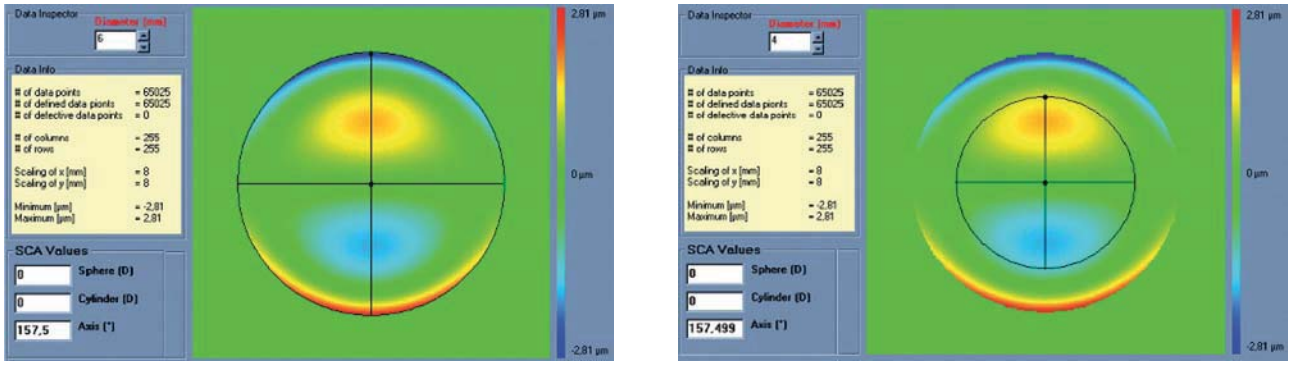

FIGURE 3
Left: Zernike refraction of pure coma (for a 6 mm pupil), which is per definition equal to 0 because coma is a high-order aberration mode. Right: Zernike refraction of the same wave aberration when analysed for a smaller pupil diameter (4 mm). Pure coma (a high-order aberration), when analysed for a smaller pupil diameter, produces only high-order coma. Notice that coma may have a "visual effect" if the visual axis changes, resulting in astigmatism.

know the total wavefront variance associated to the Zernike modes of interest:

$$M_e = \frac{16\sqrt{3}RMS}{PD^2} \qquad (1)$$

One could apply this concept of equivalent defocus to each individual Zernike mode in order to compute its clinical relevance. Of course, we must keep in mind that the kind of optical blur produced by higher-order aberrations is not the same as the blur produced by defocus. Nevertheless, this concept of equivalent defocus is helpful when it comes to interpreting the Zernike coefficients in familiar dioptric terms. The basis of the equivalent defocus concept is the notion that the imaging quality of an eye is determined primarily by wavefront variance, and that it does not matter which Zernike mode produces that variance. It is important to bear in mind that 1 dioptre of ordinary defocus does not necessarily have the same effect as 1 dioptre of equivalent defocus because different types of aberrations affect the retinal image in different ways.

Figure 4 depicts the effects on vision produced by 1 dioptre of equivalent defocus for each of the different Zernike terms, up to 7th order.

In general, for the same amount of equivalent defocus, the optical blur produced by higher-order aberrations increases with increasing radial order and decreases with increasing angular frequencies. Based on this blur effect of the individual Zernike terms we have defined a dioptric equivalent (DEq) of the form:

$$DEq_n^m = \frac{8\sqrt{2(n+1)(1+\delta_{m0})}\left|C_n^m\right|}{PD^2} \qquad (2)$$

where DEq[n,m] is the optical blur for the individual Zernike term, n is the radial order of the Zernike term, m the meridional frequency of the Zernike term, δ_{m0} a delta function, PD the analysis diameter, and C[n,m] the weight coefficient of the Zernike term.

The relative optical blur of the Zernike polynomials up to 7th order is shown in *table 1.*

This dioptric equivalent metric is identical to the power vector notation for the low orders, and makes it possible to define a general optical blur of the form:

$$U_G = \sqrt{\sum DE_q[n,m]^2} \qquad (3)$$

as a generalization of the expression proposed by Thibos et al.[23]

Using common clinician limits, the following classification is proposed:

Not clinically relevant $DEq_n^m \leq 0.25D$

Might be clinically relevant $0.25D < DEq_n^m \leq 0.50D$

Clinically relevant $DEq_n^m > 0.50D$

Objective Minimisation of the Maximum Depth of a Customized Ablation Based on the Zernike Expansion of the Wave Aberration

One of the minimisation approaches proposed in this work consists of simplifying the profile by selecting the subset of Zernike terms that minimises the necessary ablation depth while respecting the Zernike terms considered to be clinically relevant.

The "minimise depth"/"minimise depth+" function analyses the Zernike pyramid described in the previous section and evaluates the resulting ablation depth for all those possible free combinations of Zernike terms that fulfil the following conditions:

–Only 3rd- or higher-order terms can be disabled (excluded).

–Only those terms whose optical blur dioptric equivalent is less than 0.25 D can be disabled (0.50 D for "minimise depth+")

FIGURE 4
Zernike pyramid showing the effects on vision produced by 1 dioptre of equivalent defocus of each individual Zernike term, up to 7th order.

–For each subset of Zernike terms, the low-order terms are recalculated using the Automatic Refraction Balance method described above

From this evaluation, the function selects the subset of Zernike terms for which the maximum ablation depth is minimal *(Appendix 3).*

Figure 5 shows and example of the "minimise depth +" function. Notice that 8 µm of tissue are saved (16% of the ablation depth), but that the overall shape of the ablation remains.

Objective Minimisation of the Ablation Volume of a Customized Ablation Based on the Zernike Expansion of the Wave Aberration

The other minimisation approach proposed in this work consists of simplifying the profile by selecting the subset of

TABLE 1
Relative optical blur of the Zernike polynomials up to 7th order *(continued)*

j = index	n = order	m = Frequency	Relative Optical Blur (Defocus = 1)
6	3	-3	$\sqrt{\frac{2}{3}}$ =0.816
7	3	-1	$\sqrt{\frac{2}{3}}$ =0.816
8	3	1	$\sqrt{\frac{2}{3}}$ =0.816
9	3	3	$\sqrt{\frac{2}{3}}$ =0.816
10	4	-4	$\sqrt{\frac{5}{6}}$ =0.913
11	4	-2	$\sqrt{\frac{5}{6}}$ =0.913
12	4	0	$\sqrt{\frac{5}{3}}$ =1.291
13	4	2	$\sqrt{\frac{5}{6}}$ =0.913
14	4	4	$\sqrt{\frac{5}{6}}$ =0.913
15	5	-5	1
16	5	-3	1
17	5	-1	1
18	5	1	1
19	5	3	1
20	5	5	1
21	6	-6	$\sqrt{\frac{7}{6}}$ =1.080
22	6	-4	$\sqrt{\frac{7}{6}}$ =1.080
23	6	-2	$\sqrt{\frac{7}{6}}$ =1.080
24	6	0	$\sqrt{\frac{7}{3}}$ =1.528
25	6	2	$\sqrt{\frac{7}{6}}$ =1.080

(.../...)

TABLE 1
Relative optical blur of the Zernike polynomials up to 7th order

j = index	n = order	m = Frequency	Relative Optical Blur (Defocus = 1)
26	6	4	$\sqrt{\frac{7}{6}}$ =1.080
27	6	6	$\sqrt{\frac{7}{6}}$ =1.080
28	7	-7	$\frac{2}{\sqrt{3}}$ =1.155
29	7	-5	$\frac{2}{\sqrt{3}}$ =1.155
30	7	-3	$\frac{2}{\sqrt{3}}$ =1.155
31	7	-1	$\frac{2}{\sqrt{3}}$ =1.155
32	7	1	$\frac{2}{\sqrt{3}}$ =1.155
33	7	3	$\frac{2}{\sqrt{3}}$ =1.155
34	7	5	$\frac{2}{\sqrt{3}}$ =1.155
35	7	7	$\frac{2}{\sqrt{3}}$ =1.155

Zernike terms that minimises the necessary ablation volume, while respecting those Zernike terms considered to be clinically relevant.

The "minimise volume"/"minimise volume+" function analyses the Zernike pyramid described in the previous section and evaluates the required ablation volume for all those possible free combinations of Zernike terms that fulfil the following conditions:

–Only 3rd- or higher-order terms can be disabled (excluded)

–Only those terms whose optical blur dioptric equivalent is below 0.25 D can be disabled (0.50 D for "minimise volume+")

–For each combination (subset) of Zernike terms, the low-order terms are recalculated using the Automatic Refraction Balance method described above

From this evaluation, the function selects the subset of Zernike terms for which the required ablated volume is minimal *(Appendix 4).*

Figure 6 shows an example of the "minimise volume +" function.

A summary of the properties of the 4 minimisation approaches presented in this study are shown in *table 2.*

Simulation of the Tissue-saving Capabilities of These Methods for Minimising the Required amount of Ablated Tissue

For each wave aberration map, for a 6 mm pupil, it has been simulated how deep and how much volume of tissue was it necessary to ablate for 6 different scenarios:

–Correction of the full wavefront
–Minimising depth
–Minimising volume
–Minimising depth +
–Minimising volume +
–Equivalent aberration-free treatment

For each wave aberration, it has been calculated how much depth and volume of tissue was saved for each condition (in micrometers and in percentage, relative to the full wavefront correction), and it has been noted whether the proposed correction consists of either the full wavefront correction (with all Zernike terms included in the ablation) or the aberration-free treatment (without any Zernike term included in the ablation) and, finally, whether or not the proposed depth or volume was less than the one required for the equivalent aberration-free treatment.

Once the data about tissue saving was computed for each wave aberration, in order to calculate the average tis-

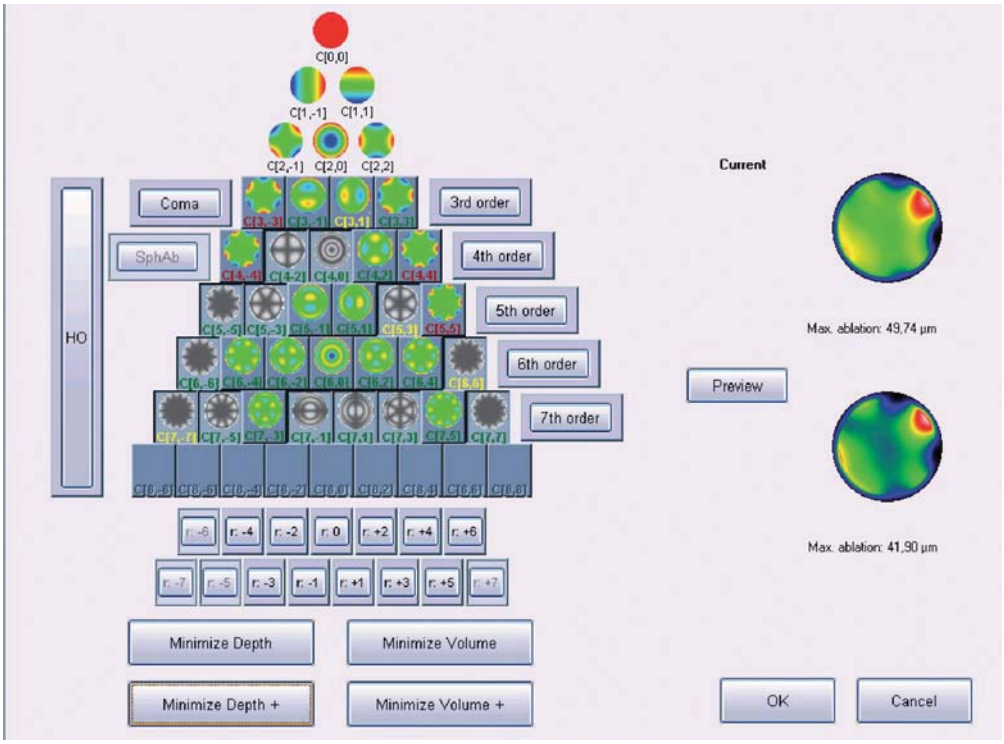

FIGURE 5
Objective analysis (Optimized Aberration-mode selection) of the optical and ablative effects of the different aberration modes for a given wavefront aberration (WFAb). Zernike terms that are considered not to be clinically relevant (DEq ≤ 0.25 D) are marked in green, Zernike terms that might be considered to be clinically relevant (0.25 D < DEq ≤ 0.50 D) are marked in yellow, and Zernike terms considered to be clinically relevant (DEq > 0.50 D) are marked in red. Note that the selection of aberration modes is not a trivial process: Not all the modes in green are unselected (not corrected) because some of them may help to save tissue. Not all aberration modes in yellow are selected (corrected) because some of them may have a low impact on vision. Notice, as well, that 8 µm of tissue are saved (16% of the ablation depth), but that the overall shape of the ablation pattern hardly changes.

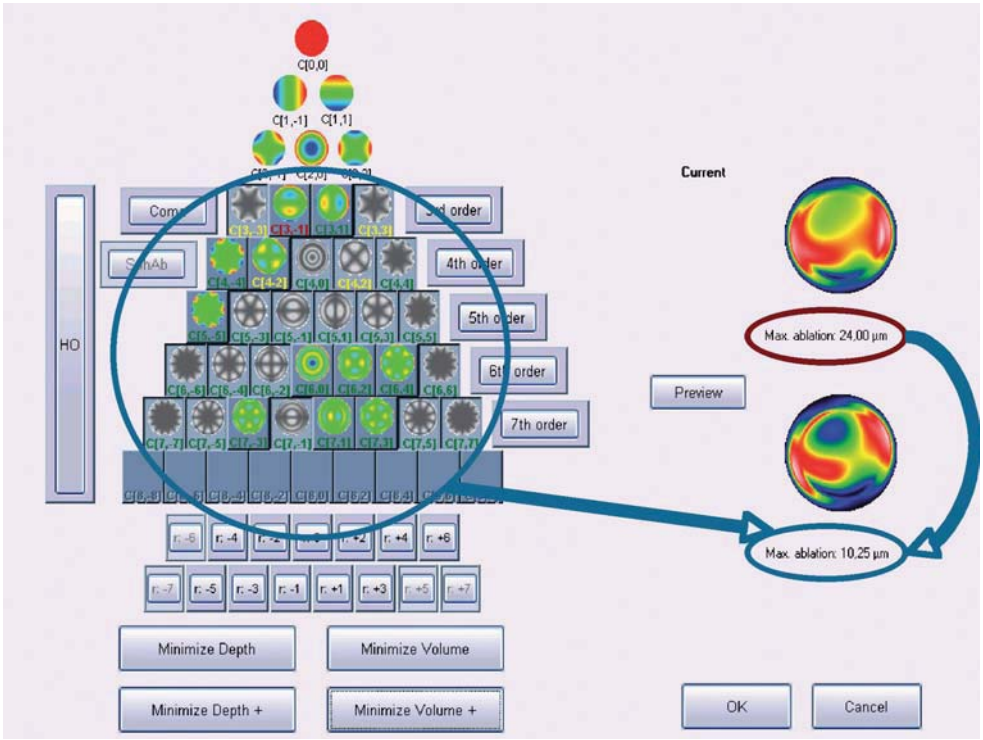

FIGURE 6
Optimized aberration-mode selection. Based on the wave aberration map, the software is able to recommend the best possible aberration-mode selection to minimise the amount of ablated tissue and time, without compromising the visual quality. Note that the wave aberration is analysed by the software showing the original ablation pattern required for a full wavefront correction and the suggested subset of aberration modes to be corrected. Notice the difference in terms of required ablated tissue, but notice as well that the most representative characteristics of the wavefront map are still present in the minimised-tissue selection.

TABLE 2
Summary properties of the 4 minimisation approaches

min Depth	min Depth +	min Vol	min Vol +
Only 3rd-or higher-order terms (HOA terms) can be disabled			
Only terms with optical blur ≤0.25 D (green) can be disabled	Only terms with optical blur ≤0.50 D (green or yellow) can be disabled	Only terms with optical blur ≤0.25 D (green) can be disabled	Only terms with optical blur ≤0.50 D (green or yellow) can be disabled
For each subset of Zernike terms, Automatic Refraction Balance is used			
The subset of Zernike terms that results in the lowest value for the maximum depth is selected		The subset of Zernike terms that results in the minimum ablation volume is selected	

sue saving for the different modalities over the sample of treatments we have used several methods: a) direct average of the saved depth or volume; b) intercept with the axis in a correlation graph; c) direct average of the percentual saved depth or volume.

Statistical Analysis

Descriptive statistics: Determination of minimum, maximum, and mean values and of the corresponding simple standard deviation. The following statistics were employed: how much tissue is saved by means of this minimisation procedure and how often this procedure results in ablated depths or volume below the amount required for the aberration-free profile. For statistical analysis, *t*-tests where used, with *P* values below 0.05 being considered to be statistically significant.

Results

Corneal Wave Aberration

The average root mean square for the high-order wave aberration (RMS_{HO}) was 0.555±0.143 µm for a 6 mm pupil (range: from 0.327 to 0.891 µm), whereas the average root mean square of the total wave aberration (RMS) was 3.955±2.715 µm also for a 6 mm pupil (range: from 0.741 to 10.920 µm).

The distribution of corneal aberration in its Zernike terms seems to be normal.

Spherical aberration was +0.107±0.205 µm (range: from -0.476 to +0.514 µm), coma aberration was 0.369±0.316 µm (range: from 0.030 to 1.628 µm), and trefoil aberration was 0.204±0.186 µm (range: from 0.022 to 1.118 µm); all of them refer to a 6 mm diameter zone.

Objective Determination of the Actual Clinical Relevance of Each Individual Term in the Zernike Expansion of the Wave Aberration

Spherical aberration was +0.184±0.136 DEq (range: from 0.000 to +0.511 DEq), coma aberration was 0.232±0.199 DEq (range: from 0.019 to 1.023 DEq), and trefoil aberration was 0.128±.117 DEq (range: from 0.014 to 0.703 DEq).

Out of all the wave aberration maps under study, 72% of them showed a spherical aberration below 0.25 DEq, 23% of them showed a spherical aberration between 0.25 DEq and 0.50 DEq, and only 5% of the maps showed a spherical aberration higher than 0.50 DEq.

Regarding coma aberration, for 68% of the wave aberration maps it was below 0.25 DEq, for 23% of them it was between 0.25 DEq and 0.50 DEq, and only for 9% of the maps was the coma aberration higher than 0.50 DEq.

Regarding trefoil aberration, for 87% of the wave aberration maps it was below 0.25 DEq, for 10% of them it was between 0.25 DEq and 0.50 DEq, and only for 3% of the maps was the trefoil aberration higher than 0.50 DEq.

Simulation of the Tissue-Saving Capabilities of these Methods for Minimising the Required amount of Ablated Tissue

Comparing the ablations planned to correct for the whole wave aberration with equivalent aberration-free ablations (designed to correct only for spherocylindrical refraction), we observed an average difference in maximum depth of +8 ± 8 µm (range: from -4 to +33 µm), and an average difference in volume of +158 ± 158 µl (range: from -127 µl to +664 µl); that is, +32% (up to +317%), indicating that more tissue was necessary to ablate to achieve full customised corrections.

In 13% of the cases the ablations designed to correct for the whole wave aberration needed to ablate less tissue than the equivalent aberration-free ablations.

Comparing the proposed "minimised-depth" ablations with the equivalent ablations designed to correct for the whole wave aberration, we observed an average difference in maximum depth of -4 ± 2 µm (range: from -10 µm to -1 µm), and an average difference in ablated volume of -64 ± 32 µl (range: from -190 µl to 0 µl); that is, -8% (up to -30%), indicating that less tissue needs to be removed for the "minimised-depth" corrections.

In 43% of the cases, the proposed "minimised-depth" ablations resulted in less ablated tissue than the equivalent aberration-free ablations. Comparing the proposed "minimised-volume" ablations with the equivalent ablations devised

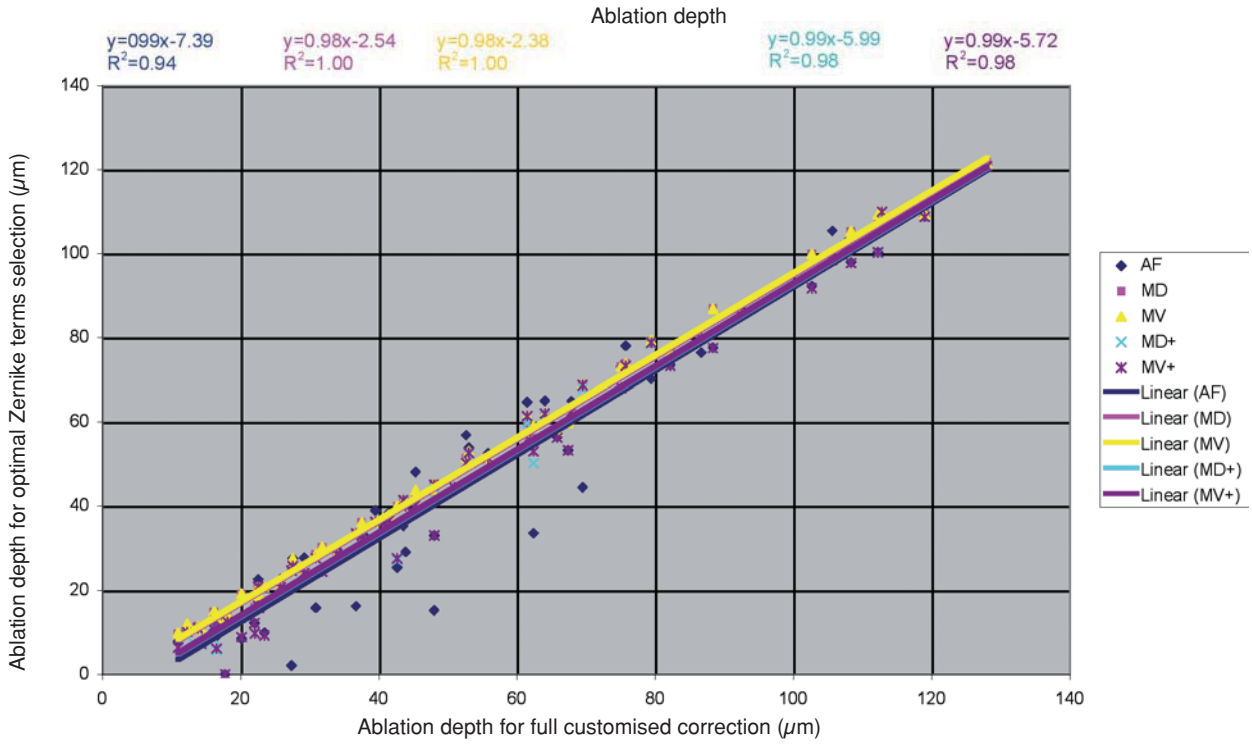

FIGURE 7
Ablation depth for the "Optimal Zernike Term Selection" method (OZTS) vs. Ablation depth for full customized correction, for the following modalities of OZTS: aberration-free correction (all HOA disabled) (AF, in blue), minimised depth (MD, in magenta), minimised volume (MV, in yellow), minimised depth+ (MD+, in cyan), and minimised volume+ (MV+, in purple).

to correct for the whole wave aberration, we observed an average difference in maximum depth of -4 ± 2 µm (range: from -10 µm to 0 µm), and an average difference in volume of -64 ± 32 µl (range: from -190 µl to 0 µl); that is -7% (up to -30%), meaning less tissue removal for the "minimised-volume" corrections.

In 39% of the cases, the proposed "minimised-volume" ablations required to remove less tissue than the equivalent aberration-free ablations (those devised to correct only for spherocylindrical refraction).

Comparing the proposed "minimised-depth+" ablations with the equivalent ablations designed to correct for the whole wave aberration, we observed an average difference in maximum depth of -6 ± 4 µm (range: from -16 µm to -1 µm), and an average difference in volume of -127 ± 95 µl (range: from -316 µl to 0 µl) or -15% (up to -66%); that is, less tissue removal was required for the "minimised-depth+" corrections.

In 80% of the cases, the proposed "minimised-depth+" ablations needed less tissue than equivalent aberration-free ablations planned to correct only spherocylindrical refraction.

Comparing the proposed "minimised-volume+" ablations with the equivalent ablations intended to correct for the whole wave aberration, we observed an average difference in maximum depth of -6 ± 4 µm (range: from -15 µm to 0 µm), and an average difference in volume of -127 ± 64 µl (range: from -316 µl to 0 µl) or -14% (up to -63%); that is, less tissue removal was needed for the "minimised-volume+" corrections.

In 75% of the cases, the proposed "minimised-volume+" ablations needed to remove less tissue than the equivalent aberration-free ablations.

Detailed results comparing the different approaches can be found in *figure 7* for the ablation-depth-analysis and in *figure 8* for the ablation-volume-and-time analysis.

Discussion

We have used the proposed dioptric equivalent applied to each individual Zernike mode in order to compute its clinical relevance. It is important to bear in mind that the orientation of the vector-like modes is not taken into account in our proposal, and 1 dioptre of cardinal astigmatism (at 0°, for example) doesn't necessarily have the same effect as 1 dioptre of oblique astigmatism (at 45°, for example). Despite this, other studies have proved this assumption to be reasonable.[24]

One could use more sophisticated equations to model the equivalences between the optical blur produced by the different Zernike terms, but we have used a relatively simple approach driven primarily by the radial order.

Different approaches have been proposed for minimising tissue ablation in refractive surgery:

In multizonal treatments, the minimisation is based on the concept of progressively decreasing corrections in different optical zones. The problem comes from the aberrations that are induced (especially spherical aberration).

In the treatments designed having a smaller optical zone combined with bigger transition zones, the minimisation is

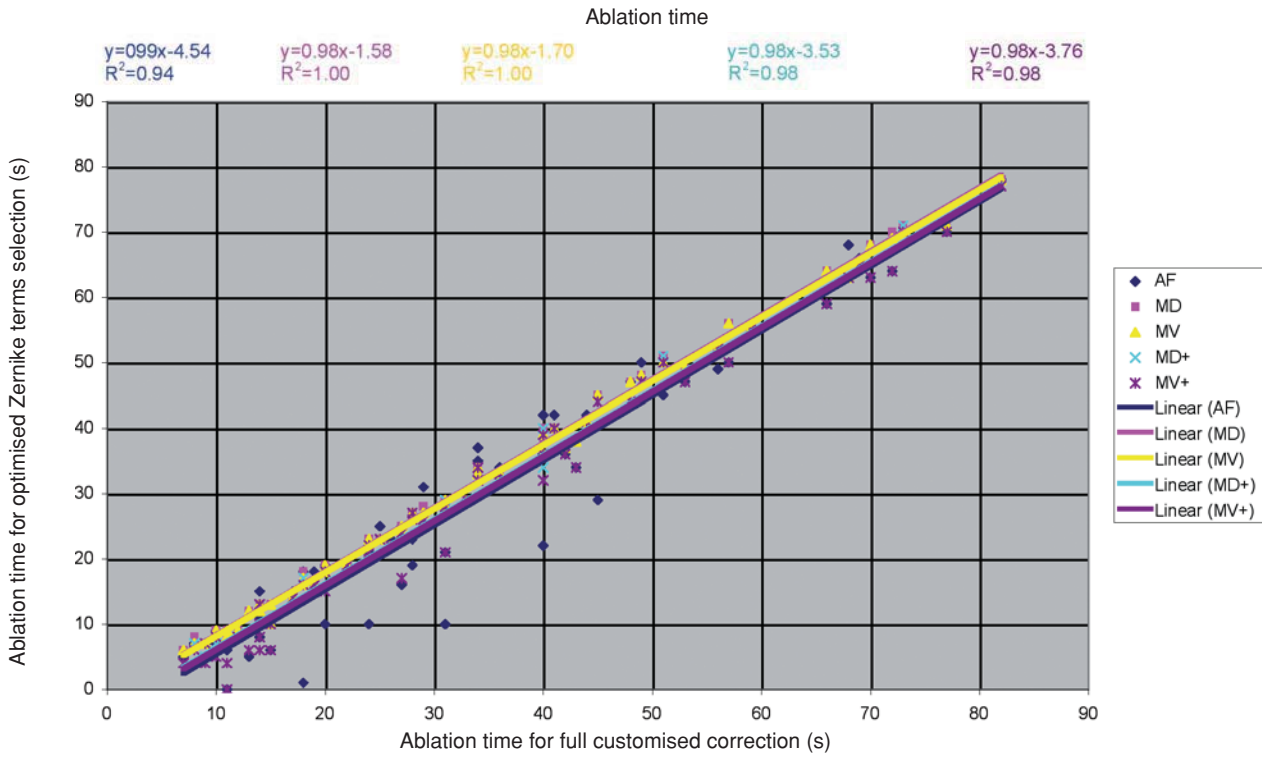

FIGURE 8
Ablation time for the "Optimal Zernike Term Selection" method (OZTS) vs. Ablation time for full customized correction, for the following modalities of OZTS: aberration-free correction (all HOA disabled) (AF, in blue), minimised depth (MD, in magenta), minimised volume (MV, in yellow), minimised depth+ (MD+, in cyan), and minimised volume+ (MV+, in purple).

a variation of the multizone concept. The problem comes, as well, from the aberrations that are induced (especially spherical aberration).

In the treatments designed having a smaller optical zone for the cylindrical component (or, in general, for the most powerful correction axis), the minimisation is based upon the concept of the maximal depth being based on the lowest meridional refraction and the selected optical zone, and the effective optical zone of the highest meridional refraction is reduced to match the same maximal depth. The problem comes again from the aberrations that are (especially high-order astigmatism).

In the boost-slider method, minimisation is achieved by means of a linear modulation of the ablated volume. The problem comes from the changes in refraction that are induced by the modulation.

In the Z-clip method, minimisation consists of defining a "saturation depth" for the ablated volume: in all those points where the ablation is designed to go deeper than the saturation value, the actual ablation depth is limited, being set to precisely that saturation value. The problem comes from the fact that this "saturation limit" may occur anywhere in the ablation area, compromising the refraction when those points are close to the ablation centre, and affecting the induction of aberrations in a complicated way.

In the Z-shift method, minimisation consists of defining a "threshold value" for the ablated volume, so that in those points where the ablated depth was designed to be less than that threshold value, no ablation is performed at all, and the rest of the points are ablated by an amount equal to the original planned ablation minus the threshold value. The problem comes from the fact that this "threshold value" may be reached anywhere in the ablation area, compromising the refraction when the below-threshold points are found close to the ablation centre, and the functional optical zone when they are found at the periphery.

Examples of each these methods can be found in *figure 9.*

The four minimisation approaches proposed in this work consists of simplifying the profile by selecting a subset of Zernike terms that minimises the necessary ablation depth or ablation volume while respecting the Zernike terms considered to be clinically relevant.

For each combination of Zernike terms, the low-order terms are recalculated using the Automatic Refraction Balance method described above, in such a way that the refractive correction is not compromised. Taking into account that the Zernike terms are either planned to be corrected or excluded, it does not compromise the visual performance because all those terms that are excluded (not planned to be corrected) are below clinical-relevance levels. The proposed approaches are safe, reliable and reproducible due to the objective foundation upon which they are based. In the same way, the selected optical zone will be used for the correction.

It is important to remark that the selection of the Zernike terms to be included in the correction is not trivial. Only those Zernike terms considered to be not clinically relevant or of minor clinical relevance can be excluded from the correction, but they don't have to be necessarily excluded. Actually,

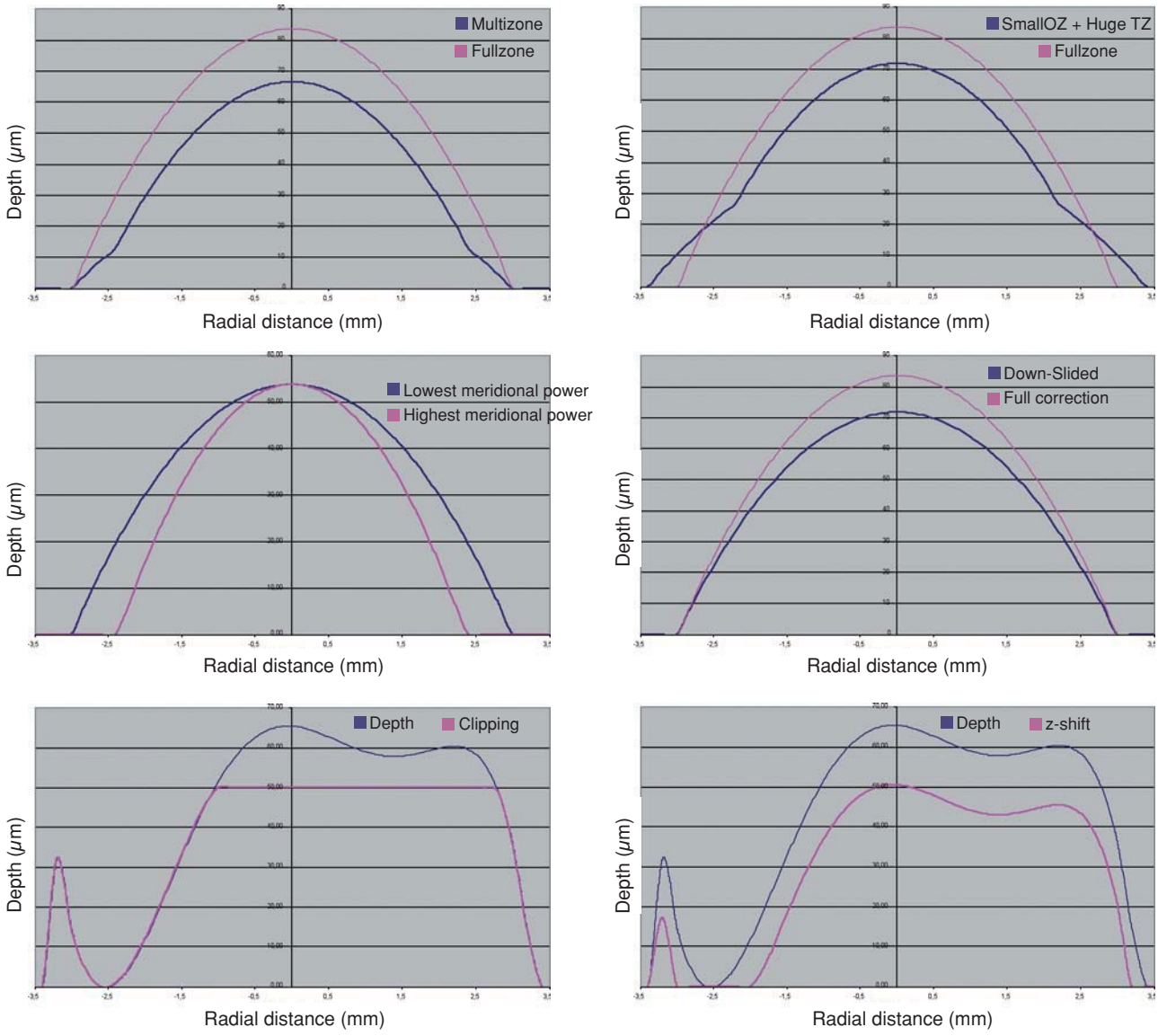

FIGURE 9
Different methods for the minimisation of the amount of ablated tissue (blue line).: by means of multizonal treatments, by means of a smaller optical zone treatments with a large transition zone, by means of a smaller optical zone for the astigmatic correction, by means of a boost slider (down-slided), by means of a Z-clip method, and by means of a Z-shift method. In all cases, the pink line indicates the required ablation profile to without minimization.

individual Zernike terms considered to be not clinically relevant will only be used (or not) when they entail an extra amount of tissue for the ablation, and they will be enabled (included) when they help to save tissue for the ablation.

In this way, particular cases are represented by the full wavefront correction, by disabling all non-clinically relevant terms, or by disabling all high-order terms.

The selection process is completely automatic and driven by a computer, ensuring systematic results and a minimisation of the amount of tissue to be ablated. This automation also simplifies the foreseeable problems of manually selecting the adequate set of terms.

A criticism to this methodology can be that fact that we are not targeting diffraction-limited optical system. That means we are reducing the ablated tissue at the cost of accepting a "trade-off" in the optical quality. However, it is still not known precisely whether an "optically perfect eye" after surgery is better than preserving the aberrations that the eye had before surgery. Although the optical quality of the eye can be described in terms of the aberration of its wavefront, it was observed that those individuals with smaller aberration in their wavefront were not always those getting the best visual-quality scores. From that, the optical quality of the human eye does not determine in a one-to-one way its visual quality. The concept of neural compensation indicates that the visual quality we have is somewhat superior to the optical quality that our eye provides, because the visual system seems to be adapted to the eye's own aberration pattern.

The optical quality in an individual can be maximized for a given wavelength by cancelling the aberration of his wavefront and optimizing his defocus (for a single distance), but this has direct and dramatically negative implications for

the optical quality for the rest of wavelengths (the greater the negative effect the more extreme is the wavelength).[25] However, the optical quality of a person showing a certain degree of aberration of his wavefront decreases, relative to the maximum obtainable quality in the absence of aberration, but it has direct positive implications in the "stability" of the optical quality for a wide range of wavelengths (which covers the spectral sensitivity of the human eye).

The implications of this concept is very interesting because, for example, a patient corrected for his wave aberration represents a case in which despite having been improved his (monochromatic) optical quality in focus, his (polychromatic) visual quality is reduced. This confirms that it is not always advantageous or advisable to correct for all aberrations of an individual aspiring to obtain a monochromatically diffraction-limited optical system, as the chromatic blur would compromise his visual quality. Another positive implication that the wave aberrations may have on the visual function is that although it produces an overall blur, the wave aberration also brings depth of focus, i.e., some stability in terms of visual quality for a range of distances that can be considered to be simultaneously "in-focus". Lastly, moderate levels of wave aberration favour the stability of the image quality for wide visual fields.[26]

This way, there are at least three criteria (chromatic blur, depth of focus, wide-field vision) favouring the option of leaving minor amounts of non-clinically-relevant aberrations.

Besides, there are no foreseeable risks derived from the proposed minimisation functions because they propose ablation profiles that are simpler than the full-wavefront corrections.

However, some drawbacks and potential improvements may be hypothesised:

There may be a sort of “edge” problem, related to the fact that a Zernike term with DEq of 0.49 D may be enabled or disabled, due to its expected minor clinical relevance, whereas a Zernike term with DEq of 0.51 D needs to be corrected (according to our selection criteria).

It is controversial, as well, whether or not one can consider the clinical relevance of every Zernike term independently. The visual effect of an aberration does not only depend on it but also on the other aberrations that are present in the full pattern; for example, a sum of small, and previously considered clinically irrelevant aberrations, could involve a clear loss of overall optical quality.

A possible improvement comes from the fact that current selection strategy consists of a binary “ON/OFF” approach for each Zernike term. However, better corrections and higher amounts of tissue saving might be obtained by using a correcting factor F[n,m] (range 0 to 1) for each Zernike correcting a wavefront of the form:

$$Abl(\rho,\theta)=\sum_{n=0}^{\infty}\sum_{m=-n}^{+n}F_n^m C_n^m Z_n^m(\rho,\vartheta) \qquad (4)$$

However, this would come to a much higher computational cost.

Another possible improvement would be to consider possible aberration couplings, at least, between Zernike modes of the same angular frequency as a new evaluation parameter.

In this work, as well, a method to objectively determine the actual clinical relevance of individual terms in a Zernike expansion of the wave aberration was described.

A method to objectively minimise the maximum depth or volume of a customised ablation based on the Zernike expansion of the wave aberration was provided in the present work.

Based upon a sample population of 100 wavefront maps, the tissues-saving capabilities of this method to minimise the amount of required ablated tissue were simulated.

The wavefront maps that were used were derived only from corneal aberrations (from which defocus, for example, cannot be determined). Moreover, correcting corneal aberrations does not imply eliminating the correspondent for the eye, as it depends also on internal aberrations. However, the proposed methods tries to minimize the amount of ablated tissue in a Zernike-based customized treatment irrespective of the origin of the wavefront map.

In summary, this study demonstrated that it is possible to develop new algorithms and ablation strategies to perform efficient laser corneal refractive surgery in a customized form, minimising the amount of ablated tissue without compromising the visual quality. The availability of such profiles, potentially maximising visual performance without increasing the risk factors, would be of great value for the refractive surgery community and, ultimately, for the patients’ health and safety.

Further clinical evaluations on human eyes are needed to confirm the preliminary simulated results presented herein.

References

1. Munnerlyn CR, Koons SJ, Marshall J. Photorefractive keratectomy: a technique for laser refractive surgery. J Cataract Refract Surg. 1988; 14:46-52.
2. Mastropasqua L, Toto L, Zuppardi E, et al. Photorefractive keratectomy with aspheric profile of ablation versus conventional photorefractive keratectomy for myopia correction: six-month controlled clinical trial. J Cataract Refract Surg. 2006;32:109-116.
3. Buratto L, Ferrari M, Rama P. Excimer laser intrastromal keratomileusis. Am J Ophthalmol. 1992;113:291-295.
4. Pallikaris IG, Siganos DS. Excimer laser in situ keratomileusis and photorefractive keratectomy for correction of high myopia. J Refract Corneal Surg. 1994;10:498-510.
5. Ditzen K, Huschka H, Pieger S. Laser in situ keratomileusis for hyperopia. J Cataract Refract Surg. 1998;24:42-47.
6. el Danasoury MA, Waring GO 3rd, el Maghraby A, Mehrez K. Excimer laser in situ keratomileusis to correct compound myopic astigmatism. J Refract Surg. 1997;13:511-520.
7. Moreno-Barriuso E, Lloves JM, Marcos S. Ocular Aberrations before and after myopic corneal refractive surgery: LASIK-induced changes measured with LASER ray tracing. Invest Ophthalmol Vis Sci. 2001; 42:1396-1403.
8. Artal P. What aberration pattern (if any) produces the best vision?, 6th International Congress of Wavefront Sensing & Optimized Refractive Corrections, Athens, Greece; February 2005.
9. Applegate RA, Howland HC. Refractive surgery, optical aberrations, and visual performance. J Refract Surg. 1997;13:295-299.
10. Artal P, Chen L, Fernandez EJ, Singer B, Manzanera S, Williams DR. Neural compensation for the eye's optical aberrations. J Vis. 2004;4: 281-287.
11. Thibos LN, Hong X, Bradley A, Applegate RA.Accuracy and precision of objective refraction from wavefront aberrations. Journal of Vision. 2004;4:329-351.
12. Salmon TO. Corneal contribution to the wavefront aberration of the eye. PhD Dissertation. 1999:70.

13. Mrochen M, Jankov M, Bueeler M, Seiler T. Correlation Between Corneal and Total Wavefront Aberrations in Myopic Eyes. J Refract Surg. 2003;19:104-112.
14. Alio JL, Belda JI, Osman AA, Shalaby AM. Topography-guided laser in situ keratomileusis (TOPOLINK) to correct irregular astigmatism after previous refractive surgery. J Refract Surg. 2003;19:516-527.
15. Mrochen M, Kaemmerer M, Seiler T. Clinical results of wavefront-guided laser in situ keratomileusis 3 months after surgery. J Cataract Refract Surg. 2001;27:201-207.
16. Mrochen M, Donetzky C, Wüllner C, Löffler J. Wavefront-optimized ablation profiles: Theoretical background. J Cataract Refract Surg. 2004;30:775-785.
17. Koller T, Iseli HP, Hafezi F, Mrochen M, Seiler T. Q-factor customized ablation profile for the correction of myopic astigmatism. J Cataract Refract Surg. 2006;32:584-589.
18. Gatinel D, Malet J, Hoang-Xuan T, Azar DT. Analysis of customized corneal ablations: theoretical limitations of increasing negative asphericity. Invest Ophthalmol Vis Sci. 2002;43:941-948.
19. Mattioli R, Tripoli NK. Corneal Geometry Reconstruction with the Keratron Videokeratographer. Optom Vis Sci. 1997;74:881-894.
20. Zernike F. Diffraction theory of the knife-edge test and its improved form, the phase-contrast method. Monthly Notices of the Royal Astronomical Society. 1934;94:377-384.
21. Thibos LN, Applegate RA, Schwiegerling JT, Webb R, VSIA Standards Taskforce Members. Standards for Reporting the Optical Aberrations of Eyes. J Refract Surg. 2002;18:S652-S660.
22. Thibos LN. Wavefront Data Reporting and Terminology. Second International Wavefront Congress in Monterey, CA. 1999. Avaliable at: http://research.opt.indiana.edu/Library/WavefrontReporting/WavefrontReporting.html. Accessed: 16 December 2008.
23. Thibos LN, Wheeler W, Horner D. A vector method for the analysis of astigmatic refractive errors. In: Vision Science and Is Applications, vol 2. 1994 OSA Technical Digest Series. Washington, DC: Optical Society of America, 1994:14-17.
24. Remón L, Tornel M, Furlan WD. Visual Acuity in Simple Myopic Astigmatism: Influence of Cylinder Axis. Optom Vis Sci. 2006;83: 311-315.
25. McLellan JS, Marcos S, Prieto PM, Burns SA. Imperfect optics may be the eye's defence against chromatic blur. Nature. 2002;417:174-176.
26. Bará S, Navarro R. Wide-field compensation of monochromatic eye aberrations: expected performance and design trade-offs. J Opt Soc Am A. 2003;20:1-10.

Appendix 1
Objective Wavefront Refraction from Low-Order Zernike Modes

A common way to fit an arbitrarily aberrated wavefront with a quadratic surface is to find the surface that minimizes the sum of the squared deviations between the two surfaces. The least-square fitting method is the basis of the Zernike wavefront expansion. Since the Zernike expansion employs an orthogonal set of basic functions, the least-square solution is simply given by the second-order Zernike coefficients of the aberrated wavefront, regardless of the values of the other coefficients. These second-order Zernike coefficients can be converted into a sphero-cylindrical prescription in power-vector notation of the form [J_0, M, J_{45}].

$$J_0 = \frac{-8\sqrt{6}C_2^{+2}}{PD^2} \quad \text{(A1.1)}$$

$$M = \frac{-16\sqrt{3}C_2^{0}}{PD^2} \quad \text{(A1.2)}$$

$$J_{45} = \frac{-8\sqrt{6}C_2^{-2}}{PD^2} \quad \text{(A1.3)}$$

Where PD is the pupil diameter, M is the spherical equivalent, J_0, the cardinal astigmatism and J_{45} the oblique astigmatism. The components J_0, M, and J_{45} represent the power of a Jackson crossed cylinder with axes at 0 and 90°, the spherical equivalent power, and the power of a Jackson crossed cylinder with axes at 45 and 135°, respectively.

The power-vector notation is a cross-cylinder convention that is easily transposed into conventional refractions in terms of sphere, cylinder, and axis in the minus-cylinder or plus-cylinder formats used by clinicians.

$$S = M - \frac{C}{2} \quad \text{(A1.4)}$$

$$C = 2\sqrt{J_0^2 + J_{45}^2} \quad \text{(A1.5)}$$

$$A = \frac{\arctan(\frac{J_{45}}{J_0})}{2} \quad \text{(A1.6)}$$

The same low-order Zernike modes can be used to calculate the refraction for any given smaller pupil size, either by refitting the raw wave-aberration data to a smaller diameter, or by mathematically performing the so-called radius transformation of the Zernike expansion to a smaller diameter.

Appendix 2
Automatic Manifest Refraction Balance

The mathematical formulation is:

$$J_{0,MR} = \frac{-C_{MR}}{2}\cos(2A_{MR}) \quad \text{(A2.1)}$$

$$M_{MR} = S_{MR} + \frac{C_{MR}}{2} \quad \text{(A2.2)}$$

$$J_{45,MR} = \frac{-C_{MR}}{2}\sin(2A_{MR}) \quad \text{(A2.3)}$$

$$J_{0,MR} = J'_{0,LOA} + J_{0,LOA(PD)\rightarrow LOA(4mm)} \quad \text{(A2.4)}$$

$$M_{MR} = M'_{LOA} + M_{HOA(PD)\rightarrow LOA(4mm)} \quad \text{(A2.5)}$$

$$J_{45,MR} = J'_{45,LOA} + J_{45,HOA(PD)\rightarrow LOA(4mm)} \quad \text{(A2.6)}$$

$$C_2^{-2}(HOA(PD) \rightarrow LOA(4mm)) = f(C_n^{-2}(PD)) \quad \text{(A2.7)}$$

$$C_2^{0}(HOA(PD) \rightarrow LOA(4mm)) = f(C_n^{0}(PD)) \quad \text{(A2.8)}$$

$$C_2^{+2}(HOA(PD) \rightarrow LOA(4mm)) = f(C_n^{+2}(PD)) \quad \text{(A2.9)}$$

$$C_2^{-2}(PD) = \frac{-J'_{45,LOA}PD^2}{8\sqrt{6}} \quad \text{(A2.10)}$$

$$C_2^{0}(PD) = \frac{-M'_{LOA}PD^2}{16\sqrt{3}} \quad \text{(A2.11)}$$

$$C_2^{+2}(PD) = \frac{-J'_{0,LOA}PD^2}{8\sqrt{6}} \quad \text{(A2.12)}$$

Appendix 3
Calculation of the Ablation Depth

Wavefront correction can be achieved by applying the reverse wavefront. Because a refractive surgery laser system can remove tissue rather than add tissue, the wavefront correction must also be taken into consideration by shifting the ablation profile from negative values to only positive values. Furthermore, the correction will be performed by modifying the anterior front surface of the cornea by means of photoablation. Thus, the change in the refractive index of air (n=1) and the cornea (n=1.376) boundary must be included. Applying these considerations, one will get:

$$Abl(\rho,\theta) = \frac{WA(\rho,\theta) - \min[WA(\rho,\theta)]}{n_{Cornea} - n_{Air}} \quad \text{(A3.1)}$$

where Abl(ρ,θ) is the ablation at a given point (in polar coordinates), WA the wave aberration, and n_{cornea} and n_{air} the refractive indices of the cornea and the air respectively.

The rigorous formulation of these minimised-depth functions is to find a vector of values E[n,m] (1 for enable, 0 for disable) that minimises the maximum ablation depth, conditioned to enabling the terms that have an optical blur dioptric equivalent above 0.25 D or 0.50 D (in yellow or red), respectively.

$$Abl(\rho,\theta) = \quad \text{(A3.2)}$$

$$= \frac{\sum_{n=0}^{\infty}\sum_{m=-n}^{+n} E_n^m C_n^m Z_n^m(\rho,\theta) - \min\left[\sum_{n=0}^{\infty}\sum_{m=-n}^{+n} E_n^m C_n^m Z_n^m(\rho,\theta)\right]}{n_{Cornea} - n_{Air}}$$

This is equivalent to minimising the peak-to-valley value of the wavefront.

$$MaxAbl = \quad \text{(A3.3)}$$

$$= \frac{\max\left[\sum_{n=0}^{\infty}\sum_{m=-n}^{+n} E_n^m C_n^m Z_n^m(\rho,\theta)\right] - \min\left[\sum_{n=0}^{\infty}\sum_{m=-n}^{+n} E_n^m C_n^m Z_n^m(\rho,\theta)\right]}{n_{Cornea} - n_{Air}}$$

Appendix 4
Calculation of the Ablation Volume

The rigorous formulation of these minimised-volume functions is, again, to find a vector of values E[n,m] (1 for enable, 0 for disable) that minimises the total ablation volume, conditioned to enabling those terms whose optical blur dioptric equivalent is above 0.25 D or 0.50 D (in yellow or red) respectively.

$$AblVol = \int_0^{2\pi}\int_0^1 Abl(\rho,\theta)\rho d\rho d\theta \quad \text{(A4.1)}$$

$$AblVol = \quad \text{(A4.2)}$$

$$\int_0^{2\pi}\int_0^1 \frac{\sum_{n=0}^{\infty}\sum_{m=-n}^{+n} E_n^m C_n^m Z_n^m(\rho,\theta) - \min\left[\sum_{n=0}^{\infty}\sum_{m=-n}^{+n} E_n^m C_n^m Z_n^m(\rho,\theta)\right]}{n_{Cornea} - n_{Air}} \rho d\rho d\theta$$

Taking into account that:

$$\int_0^{2\pi}\int_0^1 Z_n^m(\rho,\theta)\rho d\rho d\theta = 0 \quad \text{(A4.3)}$$

This leads to:

$$AblVol = \quad \text{(A4.4)}$$

$$AblVol = \int_0^{2\pi}\int_0^1 \frac{-\min\left[\sum_{n=0}^{\infty}\sum_{m=-n}^{+n} E_n^m C_n^m Z_n^m(\rho,\theta)\right]}{n_{Cornea} - n_{Air}} \rho d\rho d\theta$$

This is equivalent to maximising the minimum value of the wavefront.

$$AblVol = \pi \frac{OZ^2}{4} \frac{-\min\left[\sum_{n=0}^{\infty}\sum_{m=-n}^{+n} E_n^m C_n^m Z_n^m(\rho,\theta)\right]}{n_{Cornea} - n_{Air}} \quad \text{(A4.5)}$$